Zirconia, Sulphated Zirconia and Zirconium Phosphates as additives for membranes in PEM Fuel Cell

by

RUDZANI ANNETJIE SIGWADI

Submitted in accordance with the requirements for
the degree of

DOCTOR OF PHILOSOPHY

In the subject

PHYSICS

At the

UNIVERSITY OF SOUTH AFRICA

SUPERVISOR: PROF M S DHLAMINI

CO-SUPERVISOR: PROF T A E MOKRANI

JANUARY 2019

DECLARATION

The thesis work entitled “Zirconia, Sulphated Zirconia and Zirconium Phosphates as additives for membranes in PEM Fuel Cell” is my own work and that all sources that I have used or quoted have been indicated and acknowledged by means of complete references, under the guidance of Prof. MS Dhlamini and Prof. T Mokrani. It is being submitted for the Degree of Doctor of philosophy in Physics to the University of South Africa. The work presented in the thesis is original and not submitted for any degree or examination in any other body or organization or person outside the University.

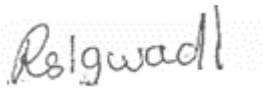

……

Signature of Candidate

……11th …day of…January…year…2019……

ABSTRACT

This research investigates the impact of zirconia nanoparticle in conductivity, water uptake, fuel crossover and fuel efficiency of modified Nafion® membranes. Synthesized water-retaining mesoporous zirconia nanoparticles (ZrO_2) were used to modify Nafion® membrane in order to enhance the thermal properties, water uptake, proton conductivity and mechanical strength of composited membrane for fuel cell applications. Recast and impregnation methods were used to prepare a nanocomposite membrane with required weight% of zirconia nanoparticles. The mechanical stability of modified membranes has become a priority for fuel cell applications as the membranes must endure all the fuel cell operations (to prevent crossover of the fuel while still conducting). Their mechanical stress and yielding stress in the recast and impregnation methods compared with the commercial Nafion® membrane were observed under tensile tests. The incorporated membrane with zirconia nanofiller shows an improvement in mechanical strength, due to the hydrophilic phase domains in the nanocomposite membrane. The water contact angle and water uptake of the composited membrane were measured. The modified membranes with zirconia nanoparticles showed a significant improvement in water uptake and contact angle leading to enhanced hydrophilicity when compared to unmodified hydrophobic Nafion® membrane. This shows the potential for use as electrolytes in fuel cell applications.

Zirconia nanoparticles were further impregnated with sulfuric acid and phosphoric acid to introduce the additional acid sites for absorption of water. In addition, zirconium phosphates (ZrP) and sulfated zirconia (S-ZrO_2) were incorporated into Nafion® 117 membrane by impregnation method to obtain a reduced methanol permeation and improved proton conductivity for fuel cell application. The mechanical properties and water uptake of Nafion® membrane incorporated with zirconium phosphates and sulfonated zirconia nanoparticles were much more improved when compared to the commercial Nafion® 117, due to the presence of acid site within the nanoparticles. Furthermore, the results showed that incorporating ZrP and S-ZrO_2 nanoparticles enhanced proton conductivity and IEC

of modified Nafion® membrane as they sustain water affinity and strong acidity. The results show that nanocomposite membranes have low water content angle, improved thermal degradation, higher conductivity and lower methanol permeability than commercial Nafion® 117 membrane, which holds great promise for fuel cell application. The Nafion®/ sulfated zirconia nanocomposite membrane obtained a higher IEC and water uptake due to the presence of SO_4^{2-} providing extra acid sites for water diffusion.

To reduce the agglomeration of ZrO_2 nanoparticles and improve the water diffusion, ZrO_2 was electrospun with polyacrylonitrile (PAN) solution to obtain a 1D morphology. The recast method was used to synthesize the high thermal and mechanical stability of Nafion® membrane incorporated with polyacrylonitrile (PAN) nanofibers. The modified Nafion® membranes exhibited improved fuel cell efficiency when tested in direct methanol fuel cells with a high proton conductivity due to incorporating PAN/Zr nanofibers that retain water within the membrane. Moreover, nanocomposite membranes achieved a reduced methanol crossover of 4.37 x 10^{-7} cm^2/s (Nafion®-PAN/ZrP nanofibers), 9.58 x 10^{-8} cm^2/s (Nafion®-PAN/ZrGO nanofibers) and 5.47 x 10^{-8} cm^2/s (Nafion®-PAN/Zr nanofibers), which is higher than 9.12 x 10^{-7} cm^2/s of recast Nafion® membrane at the higher concentration of 5M. All the blended membranes showed increase in power density at a temperature of 25 °C in comparison with pristine recast Nafion® membrane (76 $mW \cdot cm^{-2}$, 69 $mW \cdot cm^{-2}$, 44 $mW \cdot cm^{-2}$, 18 $mW \cdot cm^{-2}$). Finally, incorporating electrospun PAN/ Zr nanofibers into Nafion® membrane has successfully reduced the use of Nafion® solution that will eliminate the cost problems, while improves the protons conductivity and the methanol permeability which influence the fuel cell efficiency and long-term stability.

DEDICATION

I dedicate this work to the God Almighty, my family and friends. Specially to my husband, children, and family members for supporting and encouraging me. I also extended my dedication to my supervisors, Prof. Mokhotjwa Dhlamini and Prof Touhami Mokrani for motivating and guiding me throughout my PhD program.

ACKNOWLEDGEMENTS

At the moment, I would like to give thanks to my supervisors Prof. Mokhotjwa Dhlamini and Prof. Touhami Mokrani for their motivation, encouragement and guidance throughout my research work. I would like to thank National Research Fund (NRF) Innovation Scholarship and Academic Qualification Improvement (AQIP) University of South Africa for the funding of this research.

I would like to give the special thanks to the staff at Department of Chemical Engineering, Physics, Chemistry and Mechanical Engineering for assisting with laboratory facilities.

I would also thank Prof F. Nemavhola from the Department of Mechanical Engineering for assisting in the mechanical results under tensile stress and his assistance in identifying a suitable journal for the research work.

I would like to give thanks to Dr P. Mbule and Dr L. Mathebula from the Department of Physics (UNISA), Mrs N Mabena and Dr S Nonjola from CSIR for assisting me with for the SEM and conductivity and permeability results. I also thank Dr P Msomi (University of Johannesburg) for assisting with fuel cell efficiency. I would like to thank my friends and colleagues for their availability and their support. I would like to give thanks to all the people who helped me to accomplish my dream of achieving my PhD, by supporting me throughout my years of studies. I would like to give thanks to my mother, sisters and brothers for supporting and encouraging me.

Scientific Outputs Emanating from This Work Publication in International Journals

Published Papers

1. Sigwadi R, Dhlamini S, Mokrani T, Nonjola P. 2017. Effect of Synthesis Temperature on Particles Size and Morphology of Zirconium Oxide Nanoparticle. Journal of Nano Research 50:18-31.
2. Sigwadi R, Dhlamini S, Mokrani T, Ṇemavhola F. 2017. Wettability and mechanical strength of modified Nafion® nano-composite membrane for fuel cell. Digest Journal of Nanomaterials and Biostructures 12(4) :1137-1148.
3. Sigwadi R, Ṇemavhola F, Dhlamini S, Mokrani T. 2018. Mechanical Strength of Nafion®/ZrO_2 Nano-Composite Membrane. International Journal of Manufacturing, Materials, and Mechanical Engineering (IJMMME) 8:54-65.
4. Sigwadi R, Dhlamini S, Mokrani T, Ṇemavhola F. 2018. Effect of relative humidity on mechanical strength of zirconia/ Nafion® Nano-composite membrane. Journal of Computational and Applied Research in Mechanical Engineering 7(2): 175-187.
5. Sigwadi R, Dhlamini S, Mokrani T, Ṇemavhola F, Nonjola P. 2018. Impact of zirconia nano-rods on the methanol permeability and conductivity of Nafion®-ZrO_2 nano-composite membrane. International Journal of Microstructure and Materials Properties13(6): 381- 402.
6. Sigwadi R, Dhlamini S, Mokrani T, Ṇemavhola F. 2019. Structural morphology of blended Nafion®-Polyacrylonitrile/zirconium phosphate nanofibers. International Journal of Mechanical and Materials Engineering 14(1): 2.
7. Sigwadi R, Dhlamini S, Mokrani T, Nonjola P, Msomi Phumlani F. 2019. Nafion®/ sulphated zirconia oxide-nanocomposite membrane: the effects of ammonia sulphate on fuel permeability. Journal of Polymer Research 26: 108.
8. Sigwadi R, Dhlamini S, Mokrani T, Ṇemavhola F, Nonjola P, Msomi Phumlani F. 2019. The proton conductivity and mechanical properties of Nafion®/ ZrP nanocomposite membrane. Heliyon 5(8): p.e02240.

9. Sigwadi R, Dhlamini M, Mokrani T, Nemavhola F. 2019. Preparation of a high surface area zirconium oxide for fuel cell application. International Journal of Mechanical and Materials Engineering, 14(1): 5.
10. Sigwadi R, Dhlamini M S, Mokrani T, Nemavhola F. 2019. Enhancing the mechanical properties of zirconia/Nafion® nanocomposite membrane through carbon nanotubes for fuel cell application. Heliyon 5(7): p.e02112
11. Sigwadi R, DhIamini S, Mokrani T. 2020. The synthesis, characterization and electrochemical study of zirconia oxide nanoparticles for fuel cell application. Journal of Physica B 581:411842.

Papers to be Published

1. Sigwadi R, DhIamini S, Mokrani T, Msomi P. Nanocomposite Nafion® membranes doped with PAN/Zr nanofibers for direct methanol fuel cells efficiency.

Poster Presentations in Conferences

1. Sigwadi R, DhIamini S, Mokrani T, Nemavhola F. 2018. Route of Preparation a High Surface Area Zirconium Oxide. NanoWorld Conference, April 23-25, San Francisco, USA (NWC-2018).

TABLE OF CONTENTS

LIST OF FIGURES

LIST OF TABLES

LIST OF ABBREVIATIONS AND SYMBOLS

AFC: Alkaline fuel cell

AFM: Atomic force microscopy

$AgNO_3$: Silver nitrate

BET: Brunauer -Emmett-Teller

CV: Cyclic voltammetry

DMF: Dimethylformamide

DMFCs: Direct methanol fuel cells

DLS: Dynamic Light Scattering

DTG: Derivative thermo-gravimetric

EIS: Electrochemical impedance spectroscopy

FC: Fuel cell

FTIR: Fourier transform infrared

IEC: Ion exchange capacity

KCl: Potassium chloride

KOH: Potassium hydroxide

MCFC: Molten carbonate fuel cell

MeOH: Methanol

NaOH: Sodium hydroxide

$NaNO_3$: Sodium nitrate

PAFC: Phosphoric acid fuel cell

PEM: Proton exchange membrane

PEMFCs: Polymer electrolyte membrane fuel cells

PAA: Poly (acrylic acid)

Pd: Palladium

PEO: Poly (ethylene oxide)

PAN: Polyacrylonitrile

PVP: Poly Vinyl Pyrrolidone film

PBI: Polybenzimidazole

PETE: Polyethylene-terephthalate film

PVA: Poly (vinyl alcohol)

PZr: Phosphate zirconia

RH: Relative humidity

SEM: Scanning Electron Microscopy

SOFC: Solid oxide fuel cell

SR: Swelling ratio

S-ZrO_2: Sulfonated zirconia

TGA: Thermal Gravimetric Analysis

TEM: Transmission Electron Microscopy

Wup: Water uptake

XRD: X-ray diffraction

ZrO_2: Zirconia

ZrP: Zirconium phosphate

$ZrOCl_2 . 8H_2O$: Zirconium oxychloride hydrate

ZrO_2-CNT: Zirconia carbon nanotube

Keywords

Cubic
Dimensional swelling ratio
Electrochemical
Electrospinning
Fuel cells
Fuel cell efficiency
Methanol permeability
Mechanical properties
Monoclinic
Nafion
Nanocubes
Nanofibers
Nanoflower
Nanoparticles
Nanorods
Nanospheres
Nanocomposite
polyacrylonitrile
Proton conductivity
Stress-strain
Tensile strength
Water contact angle
Thermal stability
Water uptake

CHAPTER ONE

1. Introduction

1.1. Background of study

Energy demands increases in the day by day basis all over the world, with its production and consumption challenges facing the whole nation. The fossil fuel failed to supplement with the green energy expectation because of CO_2 emission. Therefore, the research effort has been focused into inventing the alternatives renewable energy of solar, wind, geothermal, fusion power and fuel cells. A fuel cell is an electrochemical device which directly converts chemical energy into an electrical energy, heat and water by using fuels like hydrogen, methanol, ethanol, methylene and natural gas [1]. The proton exchange membrane fuel cell (PEMFC) using fuel such as hydrogen gas has been selected as the cleanest energy technology as it maintains a high efficiency without polluting the environment [2]. Their higher efficiency makes them suitable for emergency generators in case of load shading, in warships and submarines, in automobiles and space applications [3]. However, a disadvantage of transporting and storing hydrogen gas gives a strong limitation for the hydrogen fuel cells initiation [4]. But direct methanol fuel cell (DMFC) using fuel such as methanol has been used as alternative fuel cell was compared with indirect fuel cells as it has attractive properties of higher efficiency, with a less emissions, weight and volume [5]. This advantage qualified them to be applied in the household devices. However, DMFC bring about less power energy than that of PEMFC due to its relatively stagnant oxidation and reduction reactions [6], with high methanol crossover through the membranes [6].

But their disadvantages of the highly expensive manufacturing process, with a decrease in proton conductivity at elevated temperatures due to water loss and higher in methanol crossover, limit its application in fuel cells [7-9]. Presently, the fuel cell must be designed to function at elevated temperatures due to its faster electrode kinetics, greater tolerance to impurities in the fuel such as

CO and easy to maintain thermal stability [10]. This prompts the researchers' effort to modified Nafion® membrane with metal oxides such as SiO_2, TiO_2, ZrO_2 and zeolites [11] to maintain its water content. This can also be attained by modification with solid acids such as sulfated zirconia and zirconium phosphates as it will maintain water content while increasing its acid sites [12-13]. Hence, addition of metal oxides in Nafion® membrane increases the pore size which improves the absorption and retention of water and increases the ionic conductivity at elevated temperature [10].

The introduction of zirconium phosphate (ZrP) as an inorganic filler for Nafion® membrane has increased the proton conductivity and water-retention [14-17]. Some results show a higher fuel cell performance in elevated temperature when Nafion® membranes modified with metal oxides such as zirconia or zirconium phosphate [14-19]. This may be due to high proton mobility and good water retention capabilities of zirconium phosphate and also with zirconia stability in a hydrogen/ oxygen atmosphere [20]. The results of Pt/ ZrP-Nafion® composite membrane reveals an improvement in water retention at increased cell temperatures [21-22]. The modified membrane was investigated for the aging and also its performance. This research based on the modification of Nafion® membrane which maintains high proton conductivity, less methanol permeability, less electro-osmotic drag coefficient, high chemical and thermal stability, high mechanical properties. The compositing of Nafion® membranes with metal oxide is synthesized in order to produce the nanocomposites membrane which will enable (fuel cell) to function at higher temperatures without any limitations.

1.2. Problem statement

Fuel cells are promising candidate in power-generation, stationary and vehicle application. Best preferred fuel cell is H_2PEMFC and DMFC. However, the power densities for H_2-PEMFC is higher than that of DMFC at 90 °C, but the target is to increase the power density of DMFC above 300 mW/cm^2 at higher temperature of 80 °C. The state of art membrane for fuel cell are perfloronated membranes (Nafion® series). These types of membrane cannot work more at temperature higher than 100 °C due to their depended-on water for proton conductivity. Advantages of working at high

temperatures (120 °C-150 °C): enhanced oxygen reduction reaction; CO tolerance; water management and enhanced methanol oxidation reaction in DMFC. Advantages of adding inorganic materials to organic proton conduction membranes: enhanced proton conductivity at lower humidity by reducing the diameter of the pores and ensures their hydration and reduces the methanol permeability.

1.3. Research aims and objectives

1.3.1. Research aims

The purpose of the research project is to develop a Nanocomposite membrane based on inorganic nanoparticles such as zirconia nanopowder, zirconia nanofibers, sulphated zirconia nanopowder and zirconium phosphates nanopowder that are water insoluble and that can adapt to the basic requirements of fuel cell applications.

1.3.2. Research objectives.

- To synthesize zirconia nanoparticles.
- To synthesize nanofibers.
- To prepare zirconia phosphate and sulphated zirconia nanoparticles.
- To establish the changes on chemical and mechanical properties of modified nanocomposite membrane with inorganic nanoparticles.
- To investigate the changes of the inorganic nanoparticles on the permeability of methanol.
- To evaluate the effect(s) of the nanocomposite on the water retention by the membrane.
- To investigate the effect(s) of the metal oxides on the proton conductivity at elevated temperatures.
- To measure the changes of nanocomposite on the fuel cell efficiency.

Eventually the modified Nanocomposite membranes should be able to do the following:

- Operate at elevated temperatures above 100 °C without deteriorating in chemical and mechanical durability.
- Lowering the methanol permeability.
- Increase the proton conductivity at the higher temperature;
- Decrease the operating cost.
- Reduce the platinum loading.
- Enhanced good water retention.
- Improve membrane-electrode assemblies.
- Increase the fuel cell efficiency.

1.4. Thesis overview

This dissertation is based on five papers that have been published and four papers that have been submitted to scientific journals and is comprised of the following sections: Chapter 1 gives the introduction of the fuel cell and the objectives of the research. Chapter 2 summarizes the history, the types of fuel cells and its applications. It also summarizes the types of Nafion® membrane and its modification and other types of alternative membranes. Chapter 3 gives the methods and characterizations techniques used in preparation/characterization of nanopowders and nanocomposite membranes. Chapter 4 consists of the nanopowders and nanofibers preparations with the experimental procedure and discussions of the results. It summarizes the one published paper and two submitted papers. Chapter 5 consists of the membrane preparations; their mechanical strength and thermal stabilities were investigated under Tensile Tests and TGA. Their ability to retain water, swelling stability and structural morphology were observed by Water Uptake, dimensional swelling ratio, scanning electron microscopy (SEM) and AFM. It summarizes the three published papers. Chapter 6 consists of the nanocomposite membranes. Their preparations, experimental procedure and discussions of the results. The effect of metal oxide in reduction of fuel crossover and proton conductivity were observed by methanol permeability and four-point probe conductivity cell.

It summarizes the one published paper and two submitted papers. Chapter 7 present the cell performances of modified membrane. It summarizes the one submitted paper. Chapter 8 gives summary of all the results, conclusions and recommendations for future work.

1.5. References

1. Haynes, C., Clarifying reversible efficiency misconceptions of high temperature fuel cells in relation to reversible heat engines. *Journal of Power Sources* **2001,** *92* (1-2), 199-203.
2. Hogarth, W. H.; Da Costa, J. D.; Lu, G. M., Solid acid membranes for high temperature (140° C) proton exchange membrane fuel cells. *Journal of Power Sources* **2005,** *142* (1-2), 223-237.
3. Farooque, M.; Maru, H. C., Fuel cells-the clean and efficient power generators. *Proceedings of the IEEE* **2001,** *89* (12), 1819-1829.
4. Scott, K.; Taama, W.; Argyropoulos, P., Engineering aspects of the direct methanol fuel cell system. *Journal of Power Sources* **1999,** *79* (1), 43-59.
5. Scott, K.; Taama, W.; Cruickshank, J., Performance of a direct methanol fuel cell. *Journal of Applied Electrochemistry* **1998,** *28* (3), 289-297.
6. Lufrano, F.; Baglio, V.; Staiti, P.; Antonucci, V., Performance analysis of polymer electrolyte membranes for direct methanol fuel cells. *Journal of Power Sources* **2013,** *243*, 519-534.
7. Sumner, J.; Creager, S.; Ma, J.; DesMarteau, D., Proton conductivity in Nafion® 117 and in a novel bis [(perfluoroalkyl) sulfonyl] imide ionomer membrane. *Journal of the Electrochemical Society* **1998,** *145* (1), 107-110.
8. St-Pierre, J.; Wilkinson, D. P., Fuel cells: a new, efficient and cleaner power source. *AIChE Journal* **2001,** *47* (7), 1482-1486.
9. Slade, S.; Campbell, S.; Ralph, T.; Walsh, F., Ionic conductivity of an extruded Nafion 1100 EW series of membranes. *Journal of the Electrochemical Society* **2002,** *149* (12), A1556-A1564.
10. Li, Q.; He, R.; Jensen, J. O.; Bjerrum, N. J., Approaches and recent development of polymer electrolyte membranes for fuel cells operating above 100 C. *Chemistry of Materials* **2003,** *15* (26), 4896-4915.

11. Gómez-Romero, P.; Asensio, J. A.; Borrós, S., Hybrid proton-conducting membranes for polymer electrolyte fuel cells: phosphomolybdic acid doped poly (2, 5-benzimidazole)—(ABPBI-H3PMo12O40). *Electrochimica Acta* **2005,** *50* (24), 4715-4720.
12. Thampan, T. M.; Jalani, N. H.; Choi, P.; Datta, R., Systematic approach to design higher temperature composite PEMs. *Journal of The Electrochemical Society* **2005,** *152* (2), A316-A325.
13. Choi, P.; Jalani, N. H.; Datta, R., Thermodynamics and proton transport in Nafion II. Proton diffusion mechanisms and conductivity. *Journal of the Electrochemical Society* **2005,** *152* (3), E123-E130.
14. Bauer, F.; Willert-Porada, M., Characterisation of zirconium and titanium phosphates and direct methanol fuel cell (DMFC) performance of functionally graded Nafion (R) composite membranes prepared out of them. *Journal of Power Sources* **2005,** *145* (2), 101-107.
15. Hill, M. L.; Kim, Y. S.; Einsla, B. R.; McGrath, J. E., Zirconium hydrogen phosphate/disulfonated poly (arylene ether sulfone) copolymer composite membranes for proton exchange membrane fuel cells. *Journal of Membrane Science* **2006,** *283* (1-2), 102-108.
16. Jiang, R.; Kunz, H. R.; Fenton, J. M., Influence of temperature and relative humidity on performance and CO tolerance of PEM fuel cells with Nafion®–Teflon®–Zr (HPO4) 2 higher temperature composite membranes. *Electrochimica acta* **2006,** *51* (26), 5596-5605.
17. Chen, L.-C.; Yu, T. L.; Lin, H.-L.; Yeh, S.-H., Nafion/PTFE and zirconium phosphate modified Nafion/PTFE composite membranes for direct methanol fuel cells. *Journal of Membrane Science* **2008,** *307* (1), 10-20.
18. Truffier-Boutry, D.; De Geyer, A.; Guetaz, L.; Diat, O.; Gebel, G., Structural Study of Zirconium Phosphate− Nafion Hybrid Membranes for High-Temperature Proton Exchange Membrane Fuel Cell Applications. *Macromolecules* **2007,** *40* (23), 8259-8264.
19. Krishnan, P.; Park, J.-S.; Yang, T.-H.; Lee, W.-Y.; Kim, C.-S., Sulfonated poly (ether ether ketone)-based composite membrane for polymer electrolyte membrane fuel cells. *Journal of Power Sources* **2006,** *163* (1), 2-8.

20. Vaivars, G.; Shan, J.; Gericke, G.; Linkov, V., Phosphorized zirconium oxide nanoparticles. *Applied Organometallic Chemistry* **2005,** *19* (10), 1096-1100.
21. Wasmus, S.; Küver, A., Methanol oxidation and direct methanol fuel cells: a selective review1. *Journal of Electroanalytical Chemistry* **1999,** *461* (1-2), 14-31.
22. Lee, H.-K.; Kim, J.-I.; Park, J.-H.; Lee, T.-H., A study on self-humidifying PEMFC using Pt–ZrP–Nafion composite membrane. *Electrochimica Acta* **2004,** *50* (2-3), 761-768.

CHAPTER TWO

2. Literature review

2.1. Introduction

Fuel cells (FC) will be the suitable alternatives for generating electric power on load shedding as it does not need to be recharged only refueled depending on the remaining fuel. It could also be a substitute of the cars, computer and cell phone battery due to the high energy density, high efficiency, reduced emissions and lighter than batteries as it provides longer operating life than a battery. These fuel cell also found to be the most promising agent in controlling a green-house effect when compared with the existing car battery as they don't release any toxic gases [1-2]. The main component of fuel cell is proton exchange membranes (PEM) that enable them to function without dragging the cell, allowing diffusion from the anode to the cathode. This PEM function as an electrolyte in order to prevent mixing of oxygen and hydrogen gas in fuel cell [3].

Nafion®, Aciplex and Flemion are solid polymer electrolyte which used as PEM in fuel cells due to their high mechanical, chemical and thermal stability (PEM) [4-5]. Low temperature fuel cells such as direct methanol fuel cells (DMFCs) and Polymer electrolyte membrane fuel cells (PEMFCs) are the one on board, due to their low in impact as they are low in weight but higher in energy density which makes them suitable for transportation applications [6]. DMFCs are the most preferable PEM because they use liquid methanol as fuel, which is easy to store and handle than hydrogen gas [2]. Hydrogen gas is the lightest element with low density which makes it difficult to store or transport. Moreover, it also has low ignition energy that can cause explosion. But DMFCs also have major drawbacks on its performances due to the high methanol permeability through solid polymer such as Nafion® membrane and poisoning of catalyst into the oxygen cathode in the DMFCs, which also resembles fuel loss and depolarization losses at the cathode [7-8]. Furthermore, in order to generate a mixed potential that reduces the cell voltage, DMFCs consist of cathode Pt sites for direct reaction between

methanol and oxygen [9]. Due to this cause, many researchers around the world focused on production of the PEM with a low methanol crossover and able to work at high temperature but without limitation in their performance through catalyst poisoning and conductivity [10]. Furthermore, some researchers are focused on developing new polymers or modifying the existing state of arts Nafion® membrane while exhibit high performance at low temperature of 80 °C, which consisted of hydrophobic (Teflon) and hydrophilic domain (mixture of sulphonic groups, proton and water) [5]. The modification of organic membranes such as Nafion® with inorganic nanoparticles improves PEM performance in DMFC applications [11]. PEMs are modified or blended with other electrolytes to improves their properties [12-13]. In this regard, inorganic nano-materials such as TiO_2, ZrO_2 and SiO_2 were used in modification of Nafion® membrane to enhance the operational temperature. The improves properties was due to the metal oxide that maintained the hydration of the membrane. Among the inorganic nano-materials, zirconia oxide has been used as inorganic filler for Nafion® membranes that makes them suitable used in low relative humidity and high operating temperatures fuel cells. Moreover, the incorporation of zirconia oxide decreases morphological stability and low methanol permeability [9].

ZrO_2 nanoparticles maintain the mechanical properties suitable for hydration with improvement of Nafion® membranes at high-temperature fuel cell operations. The nanometre ZrO_2 shows improvement mechanical and thermal resistance, improvement in water uptake (WU) and IEC which better than those of commercial Nafion® membrane. Furthermore, the heteropoly acids such as sulphated zirconia (S-ZrO_2) nanoparticles enhance the concentration of acid sites of Nafion® membranes while still increasing the proton conductivity [14]. Modification of Nafion® membranes with zirconium phosphate have been investigated and shown to exhibit good performance at operating temperatures up to~150 °C [15-16]. In this work, the incorporation of zirconia (Zr), sulfated zirconia (SZr), phosphate zirconia (PZr), zirconium phosphate (ZrP), zirconia carbon nanotube (ZrO_2-CNT) and nanofibers into Nafion® membrane has been studied with its proton conductivity and water retention. The aim of this research is to study the influence of zirconia nanoparticles and its acidic

groups in Nafion® membranes structure, mechanical and thermal resistance, WU, IEC, methanol permeability, proton conductivity and fuel cell efficiency. The Nafion® membrane modified by simple recast and swelling method were compared with commercials Nafion® membranes.

2.2. Fuel cells

Energy is everyday demand that bring challenges to humankind. FC is a promising energy backup for existing fossil fuels. As the consumption of fossil fuels brings some disadvantages such as environmental pollution and run-out in the near future. Researches are interested in the alternatives sustainable energy and green energy sources such as fusion power technology, wind energy, solar energy and geothermal energy. A FC is an electrochemical device that operates better than battery and combustion engine due to the reduced noise emissions when compared to combustion. It can also use fuel that has been converted or derived from natural gas, coal and alcohol fuels such as methanol from hydrogen compound and propane. Moreover, fuel sources such as landfill gas or anaerobic digester gas from wastewater, methane and biomass may be used. FC function the same as combustion engine, as they run as long as the fuel is refilled and also convert chemical energy by burning the fuel directly to electrical energy. As an electrochemical power source, fuel cells are not subject to the Carnot limitations of heat engines. A FC is a system that produces electricity directly from fuel without storing it. They only use fuel and oxygen as their energy sources, which the fuel cell then converts into electricity; only releasing water as a by-product and the heat. Unreacted oxygen and fuel can be recycled back into the fuel cell system to increase efficiency. It also functions like an engine, as it converts chemical energy from fuel into useful electricity; this is illustrated in Figure 2-1. Figure 2-1 shows that the electrolyte which separated the anode and cathode works as the barrier of electrons while allows only protons to move from anode to cathode [17]. The protons pass through the electrolyte membrane from the anode to cathode while producing heat as energy and water as by-product.

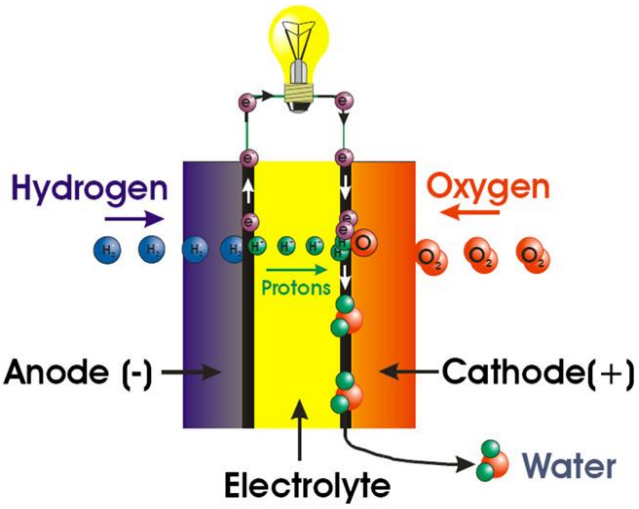

Figure 2- 1: Schematic diagram of the PEMFCs [18].

2.2.1. Types of fuel cells

Sir William Grove initially established fuel cells in 1839, by using water to produces electricity from hydrogen and oxygen using an acid electrolyte fuel cell [19-20]. Fuel cell are classified depending on how they function, on the types of electrolyte they use, operating temperature and in their structure. This also includes the type of fuels and oxidants they used, the temperature and pressure needed for operating. Fuel cells consists of five types which are alkaline fuel cells (AFC), phosphoric acid fuel cells (PAFC), proton exchange membrane (PEMFC), molten carbonate fuel cells (MCFC) and solid oxide fuel cells (SOFC). The functions and applicable properties of five main types of fuel cells are summarized in Table 2-1 [21-22].

Table 2- 1: Types of Fuel Cells

Type	Operating Temperature (°C)	Electrolyte	Fuel/Oxidant	*Efficiency (%)*	*Application Output*
Alkaline Fuel Cells (AFC)	<120	30-85% KOH	high grade H_2 /O_2	60 - 70	space 5 - 250 kW
Polymer Electrolyte Membrane Fuel Cells (PEMFC)	60-80	Polyelectro-lyte	high grade H_2 / CH_3OH / air	50-70	mobile 5 - 250 kW
Phosphoric Acid Fuel Cells (PAFC)	150-200	~100% phosphoric acid	H_2 / air	55	stationary 50 kW +
Molten Carbonate Fuel Cells (MCFC)	600-700	Na_2CO_3/K_2CO_3	CH_4, H_2 / air	60-65	stationary 100-250 kW
Solid Oxide Fuel Cells (SOFC)	800-1000	Non-porous metal oxide	CH_4, H_2 / air	65	stationary 100 kW +

2.2.1.1. Low temperature fuel cells

2.2.1.1.1. Polymer electrolyte membrane (PEM) fuel cells

PEM fuel cells has lower weight, volume, fast startup time and high-power density when compared to the other fuel cells. It consists of electrolyte and porous carbon electrodes containing a platinum alloy or platinum catalyst, which separate the protons and hydrogen's electrons. The platinum catalyst is also extremely sensitive to carbon monoxide poisoning, making it necessary to employ an additional expensive reactor to reduce carbon monoxide into the fuel gas. These PEMFCs are used as power supply for vehicular, portable and stationary applications. Moreover, it is environmentally friendly with a higher operations efficiencies, specific and volumetric energy densities than the internal-combustion engines [23]. It has a lower warm-up time, lower wear on system components and longer durability due to their ability to operate at lower temperatures of 80 °C [24-25]. Figure 2-2 presents their operating principle of PEMFCs fuel cells.

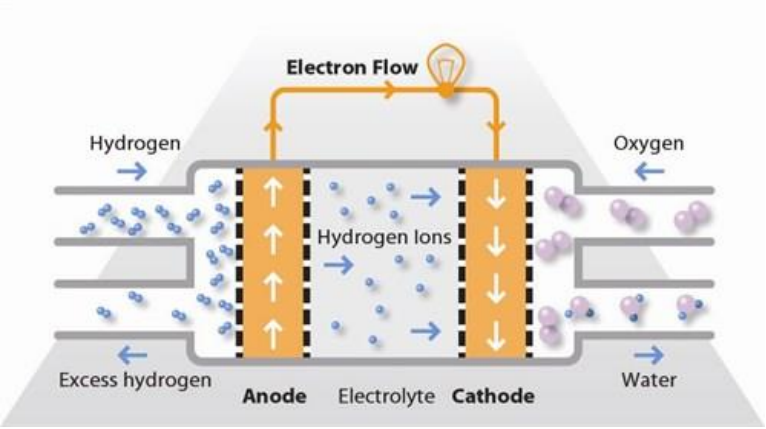

Figure 2- 2: Schematic representation of polymer electrolyte membrane fuel cell.

2.2.1.1.2. Direct methanol fuel cells (DMFCs)

DMFCs have more advantages than PEMFCs as they use methanol (MeOH) as fuel, which is easily stored and transported due to their higher energy density than hydrogen. It is high in energy density, operating at low temperature and environmentally make them preferable to use on portable portable applications such as computers, cell phones and laptop than rechargeable lithium-ion batteries [26]. These properties make them suitable replacement for rechargeable lithium-ion batteries [27]. MeOH fuel is directly fed to the anode to produce protons and electrons, which finally converted to energy [28]. These makes challenges of higher MeOH permeability, which caused the cell to deteriorate, reduced the mechanical stability and overall cell efficiency [29]. Figure 2-3 present operating principle of DMFC.

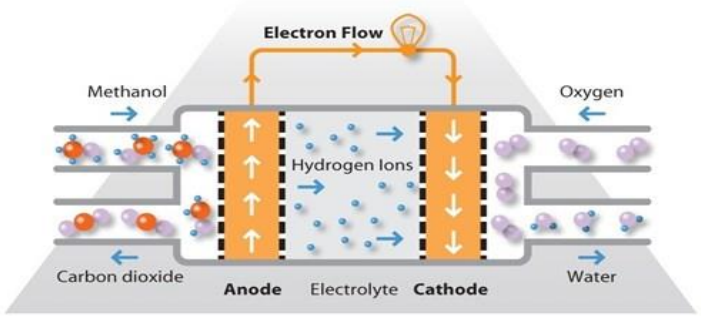

Figure 2- 3: Schematic representation of direct methanol fuel cell.

2.2.1.2. High temperature fuel cells

2.2.1.2.1. Alkaline fuel cells (AFCs)

AFCs were produced by Bacon group at Cambridge University in 1950's, which was used to generate power and water on-board spacecraft by U.S. space program [30]. It uses potassium hydroxide (KOH) solution as their electrolyte and having the higher electrical efficiency better than other fuel cells. However, it has drawbacks of using ultra-pure gases for its fuel and carbon dioxide (CO_2) poisoning and the anode and cathode consist of non-precious metals as their catalyst, which is additional cost and also affect cell performance and durability [30]. AFCs functions as PEM fuel cells but differ in their electrolyte as they utilize alkaline electrolyte rather than acid electrolyte. The alkaline electrolyte in liquid form faces some challenges due to high corrosion, difficult to control differential pressures and wettability. Nevertheless, the introduction of alkaline membrane fuel cells (AMFCs) reduces the CO_2 poisoning when compared to the liquid-electrolyte. Figure 2-4 present operating principle of AFCs.

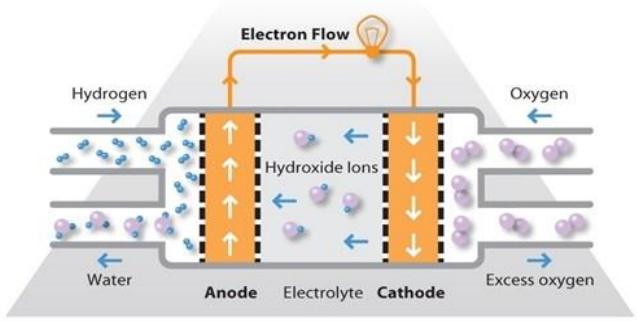

Figure 2- 4: Schematic representation of alkaline fuel cell.

2.2.1.2.2. Phosphoric acid fuel cells (PAFCs)

PAFCs uses phosphoric acid as an electrolyte. Their phosphoric acid electrolyte is chemical and thermally stable at elevated temperatures of 150-200 °C. They are the most commercially available fuel cells due to their simplicity on construction with higher efficiency when compared to that of combustion-based power plants. It was also considered as the first fuel cell to be used commercially

with a higher efficient of 85%. They used to power stationary and large vehicles as their power outputs are around 0.2 - 20 MW, which suitable to supply the electricity to hospitals and shopping malls [31]. However, having drawbacks of CO_2 poisoning the platinum catalyst at the anode which lowers the cell efficiency. PAFCs is expensive due to the higher loadings of platinum catalyst. Figure 2-5 present operating principle of PAFCs.

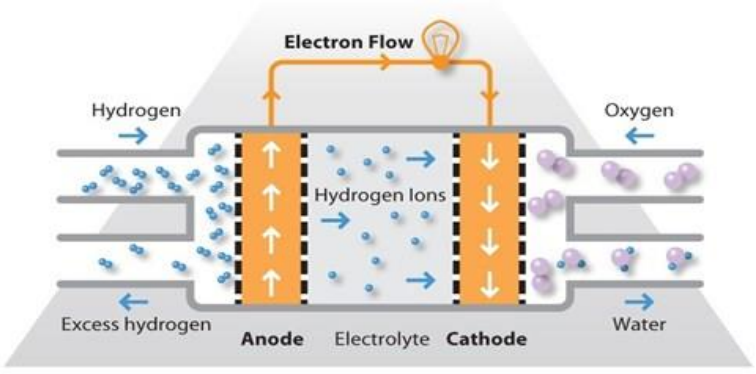

Figure 2- 5: Schematic representation of phosphoric acid fuel cell.

2.2.1.2.3. Molten carbonate fuel cells (MCFCs)

MCFCs use liquid lithium potassium or lithium sodium carbonate as their electrolyte. They used nickel as anode and cathode catalysts due to their high temperatures' operations, which lower the operational costs. MCFCs are suitable to be used for stationary power applications. They are powered by natural gas and coal-based power plants to produce electricity. When MCFCs operate at the higher temperatures, they convert the methane and other light hydrocarbons to hydrogen by using internal reforming. The process lowers the cost and improves efficiency when compared to PAFCs, PEMFCs and AFCs which use external reformer to convert fuels. However, operating at the high temperature limits the materials, safety use of cell and cell life due to the corrosion within the electrolyte. MCFCs, when coupled with a turbine, improves its efficiencies up to 65%, which is higher than that of PAFCs efficiencies (37%-42%). Furthermore, using the captured waste heat increases the fuel cell efficiencies up to 85%. Figure 2-6 present operating principle of MCFCs

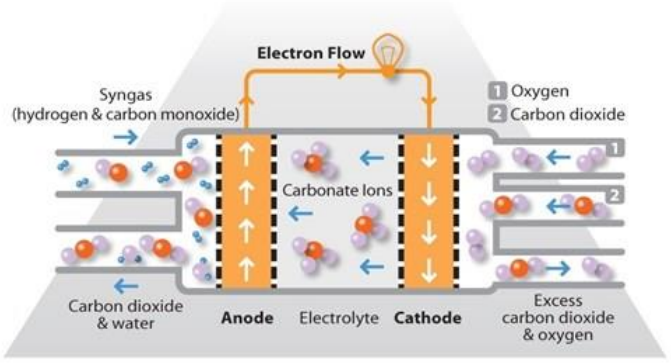

Figure 2- 6: Schematic representation of molten carbonate fuel cell.

2.2.1.2.4. Solid oxide fuel cells (SOFCs)

SOFCs uses solid electrolyte and non-porous ceramic compound. They have a higher efficiency of 60%, which increases up 85% when capture and utilize waste heat within the system. Operating the SOFCs at the higher temperatures of 1000 °C, removes the use of precious-metal catalyst and enables the use of varieties of fuels as they reform the fuels internally. These operation principles lower the cost of fuel cell. Moreover, SOFCs function better and sulfur-resistant than other fuel cell due to the solid electrolyte that removes the leaking in the system when compared to the liquid electrolyte. Furthermore, their resistance to CO_2 poisoning allows them to use gases made from coal, natural gas and biogas. Figure 2-7 present operating principle of AFCs.

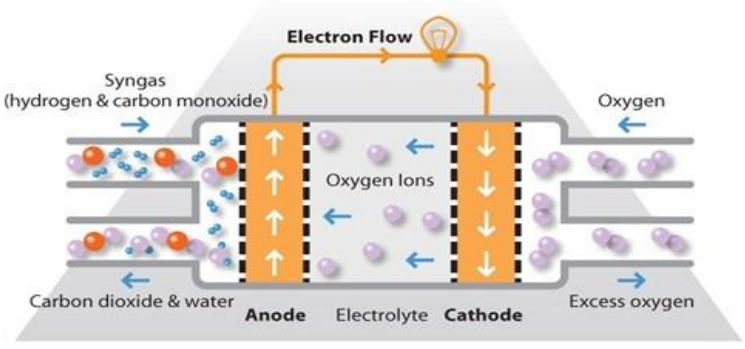

Figure 2- 7: Schematic representation of solid oxide fuel cell.

2.3. Applications of fuel cells

PEMFCs are used in variety of applications such as portable, stationary and transportation, to produce electricity without environmental pollution as there is no gas emissions only water as waste product that can be reused [32].

2.3.1. Transport

Hydrogen gas as fuel will be the upcoming suitable alternatives for fossil fuel due to their availability as they are produced from nature resources. This will also make fuel cells to be the alternatives to electricity generation technologies such as renewable energy. Some of the car manufacturing companies have already implemented a fuel cell transportation, such as fuel cell forklift that is powered by PEM fuel cells, which is used on transporting and lifting materials within the industrial premises. More than 4000 fuel cell forklifts in 2013 were manufacture in United States (US) for material transportation, as these low temperature fuel cells, generates electricity immediately upon start-up. Furthermore, these PEM fuel cells powered forklifts can operate for 8 hours shift on a single tank of hydrogen with a lifespan of eight to ten years and also environmentally friendly (no emissions) when compared to petroleum-powered forklifts. In 2011 Toyota, UTC Power, Ballard, Proton Motor and Hydrogenic produced more than 100 fuel cells buses. Many fuel cell buses were manufactured in San Francisco (US), Whistler (Canada), Shanghai (China), Hamburg (Germany), São Paulo (Brazil) and London (England). British firm Intelligent produced the hydrogen run Emission Neutral Vehicle motorcycle in 2005 (Figure 2-8(b)) [33]. The motorcycle can run for 4 hours on a single tank, in an urban area. In 2004 Honda also produced a fuel cell motorcycle [33]. The world's first fuel cell airplane was flown in 2003. The airplane which operates using lightweight lithium-ion batteries and PEM fuel cells were flight tests by Boeing researches and industry partners at Europe in 2008 (Figure 2-8(c)). Moreover, the Naval Research Laboratory's (NRL's) Ion Tiger in 2009 flew a hydrogen-powered fuel cell for 23 hours and 17 minutes. Figure 2-8(d) shows the world's first hydrogen-powered trainset that was produced by Alstom debuted the Coradia iLint in 2016,

which will be able to travel 140 km/h and travel 600-800 km on tank of hydrogen. The Hydra fuel cell boat in Figure 2-8(e) uses an Alkaline Fuel Cell system with 6.5 kW net output and reduced gas emissions.

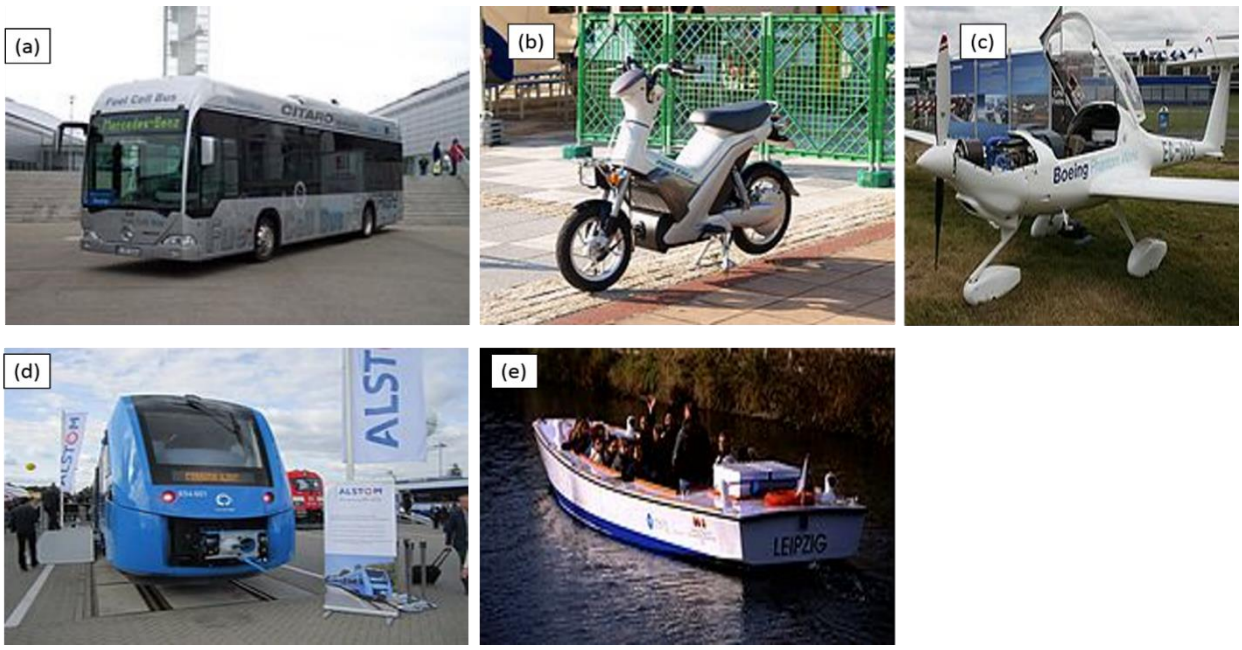

Figure 2- 8: Mercedes-Benz fuel cell bus. (a), Yamaha FC-me motorcycle (b), The Boeing Fuel Cell (c), Debut of the Alstom Coradia iLint atInnoTrans 2016 (d) and The Hydra fuel cell boat (e).

2.3.2. Stationary

Fuel cells can be used as power backup or primary source of power supply to the building, as it can generate power independent of the grid. The combined heat and power (CHP) units generate heat alongside electricity with the overall efficiencies of 80-95%, while using either PEM or SOFC fuel cells (see Figure 2- 9 and 2-10). Japan has deployed more than 10 000 residential CHP in 2010, which provides their homes with electricity. Even the South Korea also deployed CHP units for residential use.

Figure 2- 9: Pictures of installation site.

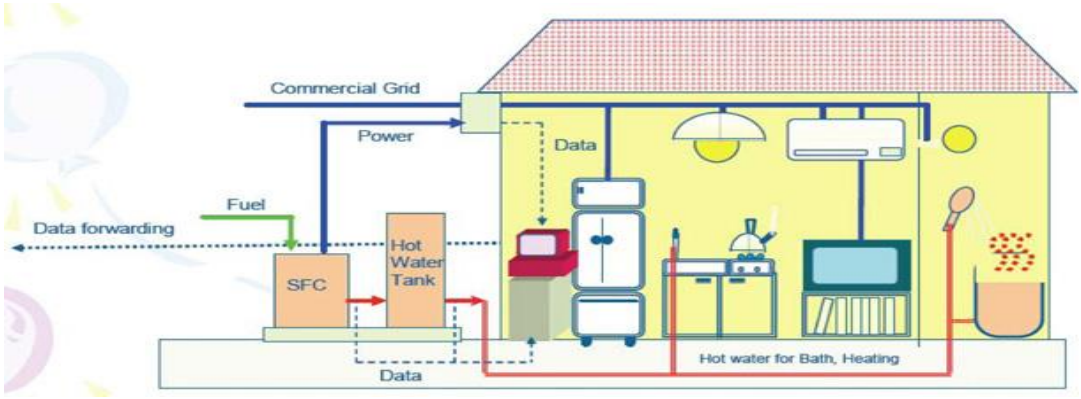

Figure 2- 10: Stationary fuel cell demonstration project.

2.3.3. Portable

Portable fuel cells used to power or recharge batteries for electronic devices, in the area without electricity. Portable fuel cells can supply energy in areas where there's no electricity. It can be used as battery substitute for portable applications such as computers, cell phones, video cameras and laptop, as prolonged used of battery may results in degradation. Figure 2-11 presents a fuel cell charger and a portable battery, which uses water and salt to provide energy.

Figure 2- 11: Charge your device via the fuel cell.

2.4. Membranes

Membranes are widely used in daily basis such as filtration in reverse osmosis or electrolyte in fuel cells. Nevertheless, lots of them faces mechanical and thermal failure under some operation conditions. As some of them can burn, shrink and has structural failure resulting from cracking, tearing, perforations and pinholes while function at low relative humidity and high temperature due to internal defects. Therefore, it is necessary to improve their thermal stability, mechanical and chemical strength in order to make them suitable for use in various conditions. The types of membrane are classified according to their performance.

2.4.1. Proton exchange membranes (PEMs)

The purpose of proton-exchange membrane (PEM) in PEMFC is to separate the fuel and oxidants while conducting electricity. The PEM must have a higher in ionic conductivity and mechanical strength to endure the start-up and shutdown process and not completed in the manufacturing, while is able to endure stress during electrode adhesion. During 1940s, researchers developed an organic ion-exchange membrane that involve the interaction between polymer and ions [34-35]. Around 1960s that PEM served at the power plants for Gemini space (GE). GE initiate prototype PEM by sulfonating of polystyrene divinyl benzene co-polymer. But PEM has some drawbacks such as cost (expensive)

and completed manufacturing process with a short lifespan which lead to the oxidation degradation of membrane [36]. This may be due to the trace amounts of CO which is poisoning the Pt catalyst [37]. These types of the membranes are Nafion® (DuPont), Flemion® (Asahi Glass), Aciplex® (Asahi Chemicals) and Dow® (Dow Chemical) [38]. Nafion® membrane is perfluorinated sulfonic acids (PFSA) which consists of a perfluorinated main chain like Teflon and with side chains containing sulfonic acid groups. Nafion® membrane when hydrated has higher thermal and mechanical stability and higher proton conductivity, which makes them suitable used as perm-selective separator in chloro-alkali electrolysis [39].

2.4.2. Nafion® membranes

The PEMs properties is to have a good proton conductivity around 10^{-2} S/cm under humidified conditions [40], which make them able to produce a high power density in fuel cells. In 1960s, DuPont Company made an effort on developing Nafion® membrane based on sulfonated polytetrafluoroethylene that is stable in chemical reaction [40]. The Nafion® membrane consists of Teflon-based backbone that is hydrophobic and offers stability and durability in the cell environment with negatively charged sulfonic acid (SO_3H) ionic groups as side chains that are hydrophilic as shown in Figure 2-12 [41]. The hydrophobic backbone is semi-crystalline and confers to its good mechanical properties [42]. The hydrophilic phase forms ionic clusters, which percolate upon hydration, forming an interconnected structure that is responsible for excellent proton conduction exhibited by Nafion® electrodes as shown in Figure 2-13 [43]. The cluster observed by small angle X-Ray (SAXS) and neuron scattering (SANS) it was composed of nanometer sized water clusters joined through narrow channels [5]. These Nafion® membrane has sustained a long lifespan when used in electrolysis, electro-synthesis, and fuel cell systems [44-45]. The Nafion® is commercially available in 120 (1200 equivalent weight (EW), 250 μm thick) which was the first membrane material to be manufactured, and then improve it to Nafion® 117 membrane (1100 EW, 175 μm thick). These Nafion® 120 membrane because of its thickness has limited use in fuel cell applications whereas Nafion® 117 membrane is suitable membrane in DMFC because of its high resistance while also

preventing the methanol crossover. These membranes have some similarity in their structure; their conductivity depends on its thicknesses of about 1100 EW with a lifetime of over 60,000 hours when operating in a fuel cell stack at 80 ºC [46].

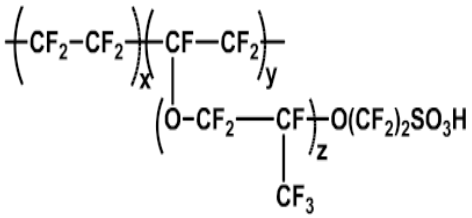

Figure 2- 12: Chemical structure of Nafion® perfluorinated membrane (x = 6 - 10; y = z=1).

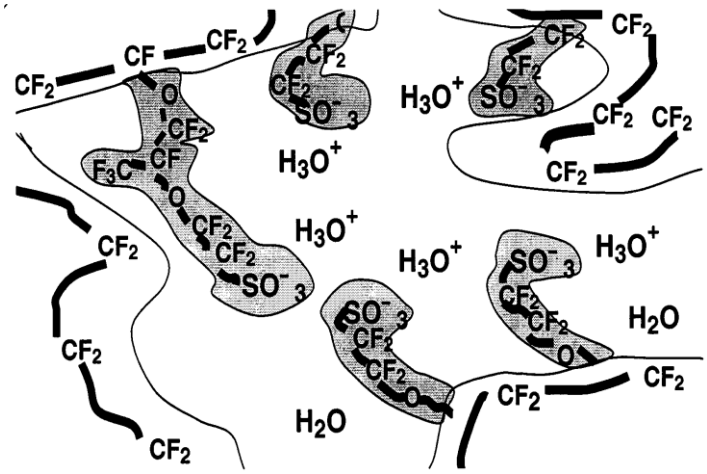

Figure 2- 13: Phenomenological sketch of the nanostructure in Nafion solid polymer electrolytes [47].

Unfortunately, as the membrane thickness decreases, its fuel crossover also increases with the reductions in their durability. This fuel crossover drawback has limitation on the oxygen cathode performance, which also decreases the electrochemical performance of the DMFCs. Most of the PEMs are more complicated to produce which resulted to an increase in manufacturing cost and environmental pollution. But Nafion® membrane still remains the main choice membrane for fuel cell applications as they possess an excellent chemical stability, good mechanical resistance and ionic conductivity [48]. Their proton transport limited them to operate in fuel cell elevated temperatures of above 90 °C with low relative humidity (RH) [49], which also changes the PEMs structure as it will

dehydrate and lose proton conductivity, and may result in irreversible mechanical damage such as fuel cells performance and degradation due to the anode of dehydration [50]. The high methanol permeability, high production cost and having a complicated and time-consuming manufacturing process has limited the Nafion® membrane to function in DMFCs [51]. It is well known that working in higher temperatures is favorable for the kinetics of Pt catalyst and may improve its tolerance to contaminants [52], improves CO tolerance, facilitates heat rejection, and improves the water management but poor mechanical stability. These limitations can be overcome through the modification of Nafion® membrane.

2.4.3. Modification of nafion® membranes

Many researchers focus their research on the blending of polymer as they produce the new ranges of polymers with the unique properties [53]. This blending method has been considered to be quick and cheaper. In the previous year's, lots of researchers have tried to initiate the new PEMs in replacement of the existing one and modify the state of art membrane. PEMs are cross-linked with other electrolyte membranes [54-55], nanofibers filler [56-57], nano-oxides filler [58-59], nonfluorinated hydrocarbon ionomers [60] and porous substrate composite membranes to overcome the temperature limitation and methanol crossover [61-62]. Moreover, fabrication of Nafion® nanofibers by electrospinning has shown a high proton conductivity which make them suitable for use in fuel cells application [63-67]. Nevertheless, electrospinning pure Nafion® solution is not possible due to low shear viscosity that makes Nafion® aggregated [68-71]. Nafion® has been electrospinning by blending with poly(acrylic acid) (PAA) [70, 72], poly(ethylene oxide) (PEO) [64, 69, 73-74], poly(vinylalcohol) (PVA) [72] and polyacrylonitrile (PAN) [75-76] to avoid aggregation. Furthermore, incorporation of inorganic materials in sub-micrometric or nanoparticles or within membranes, improves water retention, thermal and mechanical stability [16, 48, 77-78]. The state-of-the-art Nafion® membranes are faces the drawbacks of function at high temperature due to their water dependent. The polybenzimidazole (PBI) have observed and no effective polymer suitable for the replacement of Nafion® membranes as standard electrolyte of PEMFC. Watanabe et.al operate the cell at dry and 80 °C temperature [77]. Some of the

researchers found that some of metal oxide can have higher proton conductivity in its hydration states. Such as tin dioxide (SnO_2), that enhanced their proton conductivity at lower relatively humidity (RH), due to their higher water retaining [79]. Modification of membranes with SnO_2 nanopowders, let it operate operate at higher temperature of 120 °C and low relative Humidity [80-82].The working temperature of unmodified Nafion® membranes is limited at around 90 ºC with high relative humidity, which constrains the tolerance of Pt catalysts to contaminants. Modification of the Nafion® membranes with hydroscopic metal oxide was observed by some researches, as it can retain water at higher temperature [43, 83-90] and enhances reaction kinetics at both electrodes. The modification of Nafion® membrane with inorganic particles such as silicon dioxide (SiO_2), titanium dioxide (TiO_2) and zirconium oxide (ZrO_2) [37, 78, 91-99] enhanced the proton conductivity of membrane at higher temperature, improve the operating temperature, maintain water retention and also lower the methanol permeability which is the major problem in the DMFC system, due to their hydrophilic natures [50, 100-103]. The incorporation of high surface area metal oxides can increases the proton conductivity in higher temperature due to their water retention [40]. Incorporating ZrO_2 nanotubes with higher surface area, have more impact in the solid electrolytes in fuel cell [104-106]. However, modification with pure zeolites was reported to have some mechanical failure such as cracks, brittleness and fragility [107-108]. Composited membranes by moieties acids have improvement in conductivity at elevated temperatures up to 160 °C when compared with a doped membrane [109].

2.4.3.1. Silicone oxide

Incorporating metal oxides such as silicate in Nafion® membranes enhanced the water content while also improving the fuel cells performance at elevated temperatures [97, 110-112]. Nafion® / silica membrane shows the higher conductivity of 0.2 to 2 x 10^{-2} S/cm [113]. At temperature of 110 °C and relative humidity of 70%, it was observed that Nafion® / SiO_2/PWA membrane maintain a higher conductivity of 2.67 x 10^{-2} S/cm in comparison to 8.13 x 10^{-3} S/cm for Nafion® membranes [37]. This modification of membrane with inorganic particles improves the water content in the membrane, reducing the methanol crossover and the mechanical properties improvement compared to the

commercial Nafion® membranes. Nafion® membranes contains 23.3Mpa higher than 13 Mpa of silica/ Nafion® composite membrane. Recast Nafion®/ silica composite membrane [50] obtained the lower proton conductivity at low temperature [114]. But the silica/ Nafion® nanocomposite membrane prepared by plasma enhanced chemical vapour deposition (PECVD) method reduced the methanol crossover by 40% and obtained the ion conductivity that is the same as the commercial Nafion® membranes [6].

2.4.3.2. Palladium layer

Palladium (Pd) is permeable to protons while resisting methanol permeability. Nafion® membrane was modified by electrolysis plating of Pd layer [8]. The more the Pd deposited in the membrane the less the crossover while also reducing the proton conductivity. The fuel cell efficiency also depends on the thickness of Pd layer as the thin Pd layer on Nafion® membrane increases the fuel cell performance and also obtained a mechanical stability. However, modifying Nafion® membrane by sputtering, resulted in many cracks that lead to the decrease in mechanical properties [115]. The DMFC performance using Pd layer Nafion® membrane (45Mw/cm^2) was higher than 36 Mw/cm^2 of pure Nafion® membrane with a lower methanol crossover [8]. Nafion® membrane at elevated temperature is limited because of methanol attack of Nafion® impregnated membrane when it becomes thinner [114]. The impregnation of new material that bind between Nafion® and palladium membrane was shows an improvement on methanol permeability [115].

2.4.3.3. Montmorillonite (MMT)

Nafion®/ montmorillonite shows the reduction of methanol crossover of 1.6x10^{-7} cm^{-2}/s for DMFC. It also shows that those membrane delivered much higher density of 100 w/cm at concentrated 10 M methanol feed at 70 °C [116]. The modification of Nafion® membrane with sulfated montmorillonite (HSO_3-MMT) enhance the proton conductivity and decreases the methanol crossover. Montmorillonite (MMT) is cheap and easy to find with a higher surface area. (H^+-MMT) obtained an

enhanced of IEC of 0.95 meq g^{-1} and proton conductivity of 10^{-4} Scm^{-1} at room temperature [117]. When MMT grafted with organic species bearing the functionality (HSO_3-group), enhanced the acidity of montmorillonite, magadiite and kaolinite minerals [118-119].

2.4.3.4. Polyethylene-terephthalate film (PETE)

The issue of methanol permeability prompted many researchers to produce the composite membrane that will also reduce cost without decreasing conductivity. Furthermore, the permeation of methanol through anode to cathode decrease the cell efficiency which also resulted on the cathode flooding [106]. Porous PETE membranes were used in order to reduce the cost of the Nafion® membrane [114]. PETE membrane faces some drawbacks such as swelling when hydrated and distortion under pressure and little swelling after humidification. The membrane can be simple fabricated with Nafion® membrane, having the stable structurally interface bonds [114].

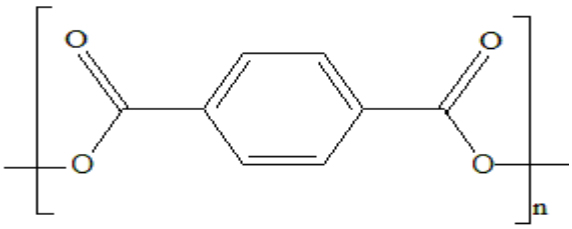

Figure 2- 14: Chemical structure of Polyethylene-terephthalate film.

2.4.3.5. Poly vinyl alcohol film (PVA)

Poly (vinyl alcohol) (PVA) membrane is a polymer that has been investigated by many researchers for its applications as blood prosthetic devices, binder, electric double layer capacitors, electrochromic windows, bio-medical fields, fuel cells and sensors, due to high tensile strength and chemical stability, biocompatibility, electrochemical stability and abrasion resistance [120-121]. PVA is an inexpensive hydrophilic polymer, easy in preparation, biodegradability, good transparency and fast charge transfer at electrode-electrolyte interface that make them useful in practical applications [122-125]. PVA polymer consists of a film-forming capacity, high density of reactive chemical functions and hydrophilic properties, that makes them easily crosslinked with other polymer through chemical,

irradiation or thermal treatments [126].These OH groups in Figure 2-15 shows that polymer blends can be easily bond through hydrogen bonding [126-127]. It has a dense structure which consists of strong intra-molecular and inter-molecular hydrogen bonding, which reduces the alcohol crossover through the membrane [127-128]. Rhim et al.(2004) used PVA as a base material for the PEMs preparation [129]. Rhim et al.(1998) also find that modification of PVA membrane by cross-linking method suppressed the permeability of alcohol in water-alcohol mixed solvent [128]. Furthermore, PVA shows an excellent methanol barrier and a good resistance to organic solvent compared to Nafion® membrane [130-131]. Moreover, modification of PVA membrane with doped inorganic acids such as H_2SO_4 or H_3PO_4 [132] or blended with other polymer such as polystyrene [133] enhance the proton conductivities and the chemical stability [134]. However, many researches they are improving the operational temperature and enhance the proton conductivity of the existing membrane, through blending of polymers [135], cross-linking [136], insertion of ceramic fillers [137] or plasticization [138] of pure PVA has highly swelling and low proton conductivity.

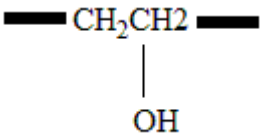

Figure 2- 15: Chemical structure of Poly Vinyl Alcohol film.

2.4.3.6. Poly vinyl pyrrolidone film (PVP)

PVP is low in chemical toxic, high in biocompatibility, good in spinnability and dissolve in many organic solvents [139], which makes it a suitable candidate in potential application such as detergents, in shielding devices, paints, adhesives, biological engineering materials and medical devices [140]. Moreover, its amorphous structure provides a low scattering loss that make it an ideal polymer for hybrid material for optical applications [141]. This vinyl polymer consists of planar and higher polar side groups due to the peptide bond in the lactam ring. The pyrrolidone rings in PVP contain a proton accepting carbonyl group as shown in Figure 2-16. When PVP is thermally cross-linked with other polymer, it shows high mechanical strength and thermal stability [142]. When PVP is used as a stabilizer

and hydrophobized, it enhances the chemical and oxidative stability of a membrane [130]. Wang et al. obtained an improvement on water flux, water adsorption and reduced water contact angle on the modified polyethersulfone (PES) with PVP than the pristine PES membrane [143]. The blending of polymer increased the attention of the researchers, due to their unique properties of material that is cheaper and quicker to synthesizes than existing Nafion® polymer. PVP blended with PVA become a favourable electrolyte due to their good compatibility, higher stability and amorphous nature.

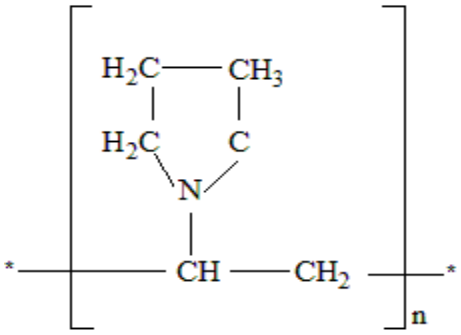

Figure 2- 16: Chemical structure of Poly Vinyl Pyrrolidone film.

2.4.3.7. Polyacrylonitrile film (PAN)

PAN has been used in producing electrospun nanofibers polymer due to their spinnability, environmentally friendly, good weatherability, commercial availability, good mechanical and chemical stability [144-146]. Moreover, electrospun PAN nanofibers obtained a higher mechanical properties [147]. It also has a good thermal stability at higher temperature of 130 °C and a good resistance to many organic solvents. When modified PAN with Li metal, used as a separator material shows a good thermal stability, an increase in ionic conductivity, good compatibility and high electrolyte uptake [148]. Electrospinning of PAN had been reported successfully and modified extensively to contain a chelating group for metal ion removal [149-150]. Such electrospun nanofiber composites may have multifaceted applications [151]. In particular, the utilisation of carbonised electrospun nanofibres as electrode materials in supercapacitors and fuel cells has been recommended in some references [152-157]. Blended membranes involving PAN for fuel cells application have been investigated by the researchers. PAN blended with sulfonated

polyphosphazene found to decrease the methanol crossover and improved mechanical properties of membrane [158]. Furthermore, the addition of PAN in another polymer lowers the methanol permeability while enhancing the mechanical properties of the mother polymer [159]. When thermal treated PAN incorporated within the membranes, it found to reduce the swelling when contact with water [160] and also increases the proton conductivity of blended membranes. The PAN structure is shown in Figure 2-17.

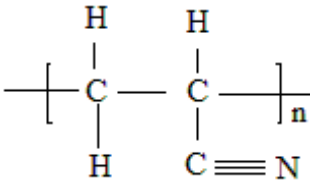

Figure 2- 17: Chemical structure of Polyacrylonitrile film.

2.4.3.8. Titanium oxide (TiO_2)

Nanocrystalline titanium oxide (TiO_2) has excellent physical and chemical properties [161]. When membrane is incorporated with inorganic filler such as TiO_2, it obtain a low glass transition while allowing the hydration [96]. The water retention of modified membrane depends at the shapes of metal oxide incorporated within the membrane, that allows them to function at higher temperature fuel cell [162]. Using nanometer TiO_2 improves the mechanical and thermal stability, water uptake and IEC of composite membrane than pristine Nafion® membrane [96]. TiO_2 nanoparticles exhibited good morphological properties with high surface area, porosity and acid character. The operation at elevated temperatures increases the performance of fuel cell, with water retention and thermal stability and with carbon monoxide (CO) tolerance [49]. At high temperature Nafion® membrane become an insulator when water is not present to promote proton dissociation [43]. TiO_2 oxide synthesised by sol-gel process has low stability in acid media that resulted on leaching out due to insufficient condensation of the hydroxides, yielded in the hydrolysis reaction at low temperature [49], but allows easy control over its thickness and porosity [6].

2.4.3.9. Zeolites

Nafion® membrane consists of fluorocarbon backbone and hydrophilic [39] that makes them commonly used as electrolyte in a fuel cell application. Its drawbacks of having higher proton conductivity only on hydrated states and high MeOH crossover limit them to function at elevated temperature [163-165]. Many of researchers have modified Nafion® membranes with metal oxides such as SiO_2 and zeolites to lower the MeOH permeability and enhance the proton conductivity while improving fuel cell operation [163-166]. Their molecular sieving and high water retention up to 200 °C, makes zeolites suitable used in selective separations [167-168]. Moreover, zeolites have 4–12 Å molecular pores sized that make them suitable in selective separations. Zeolites also used as ion exchangers, due to their higher water retention [169]. Furthermore, zeolites in micrometer-ranges have been used to modified membranes, but obtained a reduced in proton conductivity [170]. Whereas using zeolites nanofiller in nanometer-ranges shows an improvement in methanol permeability and proton conductivity, due to the compatibility with Nafion® membrane [171]. But poor compatibility of zeolites with Nafion® membrane can resulted on mechanical failure such as pinholes [172]. Moreover, membranes composited with unmodified zeolites are fragile, brittle and resulted on cracks of gaps [173]. When Nafion® membranes modified using zeolites nanofiller obtained a higher mechanical strength, thermal stability, lower methanol permeability and higher proton conductivity [174-178], due to well dispersed of zeolites with the Nafion® matrix, which provide the extra route for proton transport in the membrane.

2.4.3.10. Zirconium oxide

Zirconia (ZrO_2) has higher corrosion and wear resistance [179], higher fracture toughness and hardness lower coefficient of friction, ionic conductivity, resistance to thermal shock [180], low thermal conductivity at high temperatures, high refractoriness and catalytic properties, which make them suitable used in engineering material [181-182]. The high temperature phases of zirconia have potential applications as an oxygen sensor, in solid fuel cells, and as ceramic components [183]. PEM

membrane must have a reduction of catalyst loading, enhancing the working temperature and increasing of longevity, mechanical and chemical stability, lowering the fuel crossover and enhanced the proton conductivity at lower relative humidity [184]. Nafion® membranes is proton conductivity when fully hydrated [185]. Working at high temperature is restricted due to the dramatic water losses which lead to some physical damage. This limited the membrane to function at higher temperature of 80 ºC with a lower relative humidity. Hence, modification of Nafion® membranes by metal oxide has been prompt in order to increase the operating temperature. The organic materials such as Nafion® membranes must sustain a good proton conductivity while the inorganic material provides the improves cell performance at lower relative humidity, the higher mechanical stability and lower the fuel permeability [184]. Furthermore, the inorganic substance give the new structure arrangement that prevent the direct crossover of reaction gases [186]. Nafion® membranes incorporated with metal oxides such as ZrO_2, zeolite, TiO_2 and SiO_2 shows improvement on the mechanical strength and proton conductivity while maintaining its water management [186]. Furthermore, Nafion®/ ZrO_2 nanocomposite membranes enhance the water uptake and improves its proton conductivity than commercial Nafion® membranes at elevated working temperature above 120ºC [185]. The commercial Nafion 112 membranes also show the lower fuel cell performance on single cell fuel cell compared to Nafion®/ ZrO_2 nano-composite membranes while operating between 80-130 ºC [185].

2.4.3.11. Zirconium phosphate

DMFCs use MeOH as a fuel. DMFCs have higher energy density compared to hydrogen-based systems. But, DMFC`s face a challenge of MeOH permeability through the membrane [15]. This MeOH permeation through the membrane reduced the cell performance due to their reaction with the oxidant at the cathode. Many researcher prompt a research on decreasing the MeOH permeability [187] by producing membranes with reduced crossover and improved conductivity [188]. In addition, using lower concentration of MeOH lowers the permeation through the membranes. Zirconium phosphate (ZrP) is a proton conducting material, which is less toxic, inexpensive and stable in a hydrogen/oxygen atmosphere [189-190]. ZrP nanoparticles when composited within the Nafion®

membrane found to have a low MeOH crossover and higher proton conductivity due to good water retention capabilities while maintaining high power density [15]. Costamagna et al. obtained stable behavior on Nafion®/ zirconium phosphate membranes over time when maintained at 130 ºC while Nafion® membrane sustain an irreversible degradation under the same conditions [94]. Similarly, Alberti et al. obtained high conductivity at 140 ºC and 90% relative humidity when modified Nafion® membrane with 10wt% zirconium phosphate compared to pure recast Nafion® membrane [93]. Furthermore, the modified Nafion® membrane with ZrP obtained a decreased methanol permeability at a higher temperature of 150 ºC [191].

2.4.3.12. Sulfated zirconia oxide

The state of the art Nafion® membranes consists of sulfonic acid groups with strong ionic properties that act as proton exchange sites. Modified Nafion® membrane with sulfated zirconia (S-ZrO_2) obtained higher water uptake, proton conductivity of 14.5 mS/cm when calcined at 300 °C, with a higher IEC of 0.54 meq./g and increased water uptake property [192-194]. Furthermore, the modified Nafion® membrane with S-ZrO_2 nanoparticles has less swelling, improved mechanical properties and low methanol permeability. The S-ZrO_2/ Nafion composite membrane obtained a cell performance of 0.99 W/cm^2, which is higher than 0.75 W/cm^2 of Nafion® 112 at higher operational temperatures of 120 °C [195].

2.4.4. Effects of inorganic particles in conductivity

Nafion® Membranes have high proton conductivity in hydrated conditions. This conductivity can be obtained through the combination of charge carrier density and mobility [196]. Due to increasing demand for high-density power and energy transmission of electronic application, manufacturing a higher thermal conductivity membrane has become more important to the researchers [197-199]. The thermal conductivity of membrane enhances with the addition of inorganic material such as boron nitride, aluminum nitride, silicon nitride, alumina, silicon carbide and silica [200-206]. In 1964, the critical

breakthrough of proton conductivity in oxides was achieved [163]. The first oxide to provide the good proton conductivity was thorium oxide, at pressure and elavated temperatures of 1200 °C [207]. Iwahara et al in 1981, initial established the highest proton conductivities in cerates oxides [208]. Some increase in proton conductivity was obtained by using zirconia phosphate (ZrP) due to the high proton mobility on its surface and has good water retention capabilities. Their thermal conductivity also depends on the percentages of metal oxides incorporated in the membrane. More addition of inorganic content can form agglomerates, which induces stress concentration and decrease the tensile strength, modulus and ductility of the material [209]. Therefore, the practical application of thermal conductive polymer composites is limited.

2.4.5. Effects of inorganic particles in methanol permeability

In DMFCs application, methanol permeability limits the use of Nafion® membrane as electrolyte as it decreases its performance, as the fuel oxidized in the cathode. Furthermore, they are highly dependent on humidification that makes them function in lower temperature fuel cell. Operating at elevated temperatures of 130 °C will be beneficial in a fuel cell as it limits the oxidation of methanol, while increasing the cell efficiency. Modified membrane with metal oxides such as silica, titania, zirconia, laponite, and montmorillonite improves the methanol crossover than of pure Nafion® membrane [210]. Tricoli also reported that doping with cesium ions reduce methanol permeability [211]. Limitation of Nafion® membrane in DMFCs is methanol permeability that decreases the cell performance due to the cathode poisoning. Its further limitation is that they are highly dependent on humidification that makes them only function well below 100 °C. Operating at higher temperatures of 130 °C reduces the oxidation of methanol at the anode and obtained a higher fuel cell efficiency. Tricoli et al. obtained the decrease in fuel crossover due to incorporation of cesium ions within the membrane [211]. Moreover, using nanocrystalline oxides such as silica or titanium oxide improves the cell performance has been further improved by the [77, 212] due to water retention water.

2.4.6. Effects of inorganic particles in mechanical stability

A mechanical property is the main quality of PEMs [193, 213-225]. But changes in temperature within the operational membrane can cause mechanical damage which can be irreversible such as stress-cracking and poor compatibility with various additives which have restricted its applications [220-221]. The water content that the membranes can maintain as well as their adsorption speed depends also in the mechanical stability [226-228]. Meanwhile, water absorption in membrane in the form of swelling can drastically change its mechanical properties and durability of a membrane [3, 189]. Modifying Nafion® membranes with inorganic nanoparticles enhance the mechanical properties of the membrane which leads to better performance in fuel cells, particularly at higher temperatures and reduced humidity's [3, 189, 213, 229-230]. However, their mechanical properties strongly depend on the types of nanoparticles used, whether it is having higher surface area or low, spheres or cubes or agglomerated in the membrane. Nafion® membrane must exhibit high mechanical properties in order to perform on the methanol or hydrogen fuel cell without mechanical failure, as tough membranes improve fuel cell longevity [98, 220-221]. But the Nafion® membrane faces some challenges as the conductivity depends on the bound water within the membrane that hinders the operation in high temperatures and low relative humidity [214]. Moreover, its hydrophobic states can have effects on the mechanical properties of the membrane as it becomes swollen when in contact with water [189, 223], and also reduces the mechanical stability at elevated temperatures [231]. This is due to the diminished stability of the polymer chains at high temperatures as a result of the relatively low glass transition temperature of Nafion® membrane [48, 232]. Many researchers have enhanced the mechanical properties of commercial Nafion® membrane with inorganic materials such as zirconia, silica, titanium and clay that retain water in the Nafion® matrix and enhance thermal stability over 100 °C in order to function at high temperatures and low relative humidity [92, 230]. Furthermore, the mechanical failure of the membrane such as cracks, pinholes and tensile strength can limit its operation at fuel cell level [92, 229-230, 233]. Using the inorganic material as a nanofiller shows an improvement of the elastic modulus on the nano-composite membrane compared to the commercial membrane [234]. This may be due to the water retention of inorganic material within the membrane [235-236], as incorporation of

inorganic material within the Nafion® matrix increases the interaction between polymer matrix and filler materials [237]. The incorporation of inorganic materials improves the thermal and mechanical stability while reducing the swelling of the membrane [238].

2.4.7. Effects of inorganic particles in thermal stability

The fuel cell in its operations depends on thermal stability as it improves oxidation of fuel. Thermal stability controls the cooling system to maintain a balance of water level within the fuel cell. To operate at higher temperatures of 120 °C improves in tolerance of the electrodes to carbon monoxide, proton conductivity and kinetics of methanol oxidation. However, high operation temperatures also resulted in dehydration of the membrane due to poor water management. This makes Nafion® membranes to function under a limited range of temperatures as the higher temperature decreases its long term of functioning. A modification membrane with inorganic particles such as zeolite shows improvement in thermal stability and methanol crossover [163, 206]. In addition, silica used as filler, shows improvement thermal and mechanical stability [50, 239].

2.4.8. Effects of inorganic particles in durability (lifetime)

The electrolyte works as reactant fuel separator and their fuel cell lifetime depends on physical stability of electrolyte. However, the lifetime of the Nafion® membrane within the cell is shortened at higher temperatures because of the stress which resulted in some mechanical failure such as tears, pin-holes, cracks or punctures [50]. Some researches shows that Nafion® membrane can have a lifespan of above 50,000 hours [51] but that is limited by hydration and drying cycle on the start-up and shut-down process [50]. The benefits of using fuel cells instead of batteries are that fuel cell is refill in order to produce energy whereas battery needs to be recharge. The drawbacks of commercially membranes have limited the commercialization of fuel cell, as it degrades with the increase in temperature. The longevity of the fuel cells depends on the types of membrane and electrodes used [240]. A Nafion® membrane in DMFC has limitations that prompt a research in developing of non-

fluorinated membranes with a long lifespan [35]. A Nafion® membrane modified with inorganic particles was investigated in light of improving the durability and lifetime of PEMFCs.

2.5. References

1. Hasani-Sadrabadi, M. M.; Dashtimoghadam, E.; Majedi, F. S.; Kabiri, K.; Mokarram, N.; Solati-Hashjin, M.; Moaddel, H., Novel high-performance nanohybrid polyelectrolyte membranes based on bio-functionalized montmorillonite for fuel cell applications. *Chemical Communications* **2010,** *46* (35), 6500-6502.
2. Paturzo, L.; Basile, A.; Iulianelli, A.; Jansen, J. C.; Gatto, I.; Passalacqua, E., High temperature proton exchange membrane fuel cell using a sulfonated membrane obtained via H_2SO_4 treatment of PEEK-WC. *Catalysis Today* **2005,** *104* (2), 213-218.
3. Tang, Y.; Karlsson, A. M.; Santare, M. H.; Gilbert, M.; Cleghorn, S.; Johnson, W. B., An experimental investigation of humidity and temperature effects on the mechanical properties of perfluorosulfonic acid membrane. *Materials Science and Engineering: A* **2006,** *425* (1), 297-304.
4. Du, X.; Yu, J.; Yi, B.; Han, M.; Bi, K., Performances of proton exchange membrane fuel cells with alternate membranes. *Physical Chemistry Chemical Physics* **2001,** *3* (15), 3175-3179.
5. Tsai, C. E.; Hwang, B. J., Intermolecular interactions between methanol/water molecules and Nafion™ membrane: an infrared spectroscopy study. *Fuel Cells* **2007,** *7* (5), 408-416.
6. Liu, Z.; Guo, B.; Huang, J.; Hong, L.; Han, M.; Gan, L. M., Nano-TiO 2-coated polymer electrolyte membranes for direct methanol fuel cells. *Journal of Power Sources* **2006,** *157* (1), 207-211.
7. Kjeang, E.; Goldak, J.; Golriz, M. R.; Gu, J.; James, D.; Kordesch, K., Modeling Methanol crossover by diffusion and electro-osmosis in a flowing electrolyte direct Methanol fuel cell. *Fuel Cells* **2005,** *5* (4), 486-498.
8. Sun, H.; Sun, G.; Wang, S.; Liu, J.; Zhao, X.; Wang, G.; Xu, H.; Hou, S.; Xin, Q., Pd electroless plated Nafion® membrane for high concentration DMFCs. *Journal of Membrane Science* **2005,** *259* (1), 27-33.

9. Silva, V.; Schirmer, J.; Reissner, R.; Ruffmann, B.; Silva, H.; Mendes, A.; Madeira, L.; Nunes, S., Proton electrolyte membrane properties and direct methanol fuel cell performance: II. Fuel cell performance and membrane properties effects. *Journal of Power Sources* **2005,** *140* (1), 41-49.
10. Hejze, T.; Gollas, B.; Sauerbrey, R.; Schmied, M.; Hofer, F.; Besenhard, J., Preparation of Pd-coated polymer electrolyte membranes and their application in direct methanol fuel cells. *Journal of Power Sources* **2005,** *140* (1), 21-27.
11. Hasani-Sadrabadi, M. M.; Ghaffarian, S. R.; Mokarram-Dorri, N.; Dashtimoghadam, E.; Majedi, F. S., Characterization of nanohybrid membranes for direct methanol fuel cell applications. *Solid State Ionics* **2009,** *180* (32), 1497-1504.
12. Kerres, J., Blended and cross-linked ionomer membranes for application in membrane fuel cells. *Fuel Cells* **2005,** *5* (2), 230-247.
13. Cheng, N.; Lv, H.; Wang, W.; Mu, S.; Pan, M.; Marken, F., An ambient aqueous synthesis for highly dispersed and active Pd/C catalyst for formic acid electro-oxidation. *Journal of Power Sources* **2010,** *195* (21), 7246-7249.
14. Choi, P.; Jalani, N. H.; Datta, R., Thermodynamics and proton transport in Nafion II. Proton diffusion mechanisms and conductivity. *Journal of the Electrochemical Society* **2005,** *152* (3), E123-E130.
15. Yang, C.; Srinivasan, S.; Arico, A.; Cretı, P.; Baglio, V.; Antonucci, V., Composite Nafion/zirconium phosphate membranes for direct methanol fuel cell operation at high temperature. *Electrochemical and Solid-State Letters* **2001,** *4* (4), A31-A34.
16. Jalani, N. H.; Dunn, K.; Datta, R., Synthesis and characterization of Nafion®-MO 2 (M= Zr, Si, Ti) nanocomposite membranes for higher temperature PEM fuel cells. *Electrochimica Acta* **2005,** *51* (3), 553-560.
17. Ahmad, M.; Zaidi, S.; Rahman, S., Proton conductivity and characterization of novel composite membranes for medium-temperature fuel cells. *Desalination* **2006,** *193* (1-3), 387-397.

18. Peighambardoust, S.; Rowshanzamir, S.; Amjadi, M., Review of the proton exchange membranes for fuel cell applications. *International Journal of Hydrogen Energy* **2010,** *35* (17), 9349-9384.
19. Grove, W. R., XLII. On a small voltaic battery of great energy; some observations on voltaic combinations and forms of arrangement; and on the inactivity of a copper positive electrode in nitro-sulphuric acid. *Philosophical Magazine Series 3* **1839,** *15* (96), 287-293.
20. Grove, W. R., XXIV. On voltaic series and the combination of gases by platinum. *Philosophical Magazine Series 3* **1839,** *14* (86-87), 127-130.
21. Li, X.; Fields, L.; Way, G., Principles of fuel cells. *Platinum Metals Rev* **2006,** *50* (4), 200-1.
22. Winter, M.; Brodd, R. J., What are batteries, fuel cells, and supercapacitors? ACS Publications: 2004.
23. Gardner, T. A.; Côté, I. M.; Gill, J. A.; Grant, A.; Watkinson, A. R., Long-term region-wide declines in Caribbean corals. *Science* **2003,** *301* (5635), 958-960.
24. Springer, T. E.; Zawodzinski, T.; Gottesfeld, S., Polymer electrolyte fuel cell model. *Journal of the Electrochemical Society* **1991,** *138* (8), 2334-2342.
25. Gottesfeld, S.; Zawodzinski, T. A., Polymer electrolyte fuel cells. *Advances in Electrochemical Science and Engineering* **1997,** *5*, 195-302.
26. Service, R. F., Fuel cells. Shrinking fuel cells promise power in your pocket. *Science (New York, NY)* **2002,** *296* (5571), 1222.
27. Larminie, J.; Dicks, A.; McDonald, M. S., *Fuel cell systems explained*. J. Wiley Chichester, UK: 2003; Vol. 2.
28. Hamnett, A., Mechanism and electrocatalysis in the direct methanol fuel cell. *Catalysis Today* **1997,** *38* (4), 445-457.
29. Ravikumar, M.; Shukla, A., Effect of methanol crossover in a liquid-feed polymer-electrolyte direct methanol fuel cell. *Journal of the Electrochemical Society* **1996,** *143* (8), 2601-2606.
30. Carrette, L.; Friedrich, K.; Stimming, U., Fuel cells–fundamentals and applications. *Fuel Cells* **2001,** *1* (1), 5-39.

31. Carrette, L.; Friedrich, K. A.; Stimming, U., Fuel cells: principles, types, fuels, and applications. *ChemPhysChem* **2000,** *1* (4), 162-193.
32. Barbir, F.; Gomez, T., Efficiency and economics of proton exchange membrane (PEM) fuel cells. *International Journal of Hydrogen Energy* **1997,** *22* (10-11), 1027-1037.
33. Yildiz, F.; Baltaci, K., AC 2008-1096: Design and implementation of a hydrogen fuel cell data acquisition and monitoring scheme for educational institutions. *Age* **2008,** *13*, 1.
34. Grot, W., Discovery and development of Nafion perfluorinated membranes. *Chemistry and Industry* **1985**, 647-9.
35. Roziere, J.; Jones, D. J., Non-fluorinated polymer materials for proton exchange membrane fuel cells. *Annual Review of Materials Research* **2003,** *33* (1), 503-555.
36. Mishra, A. K.; Bose, S.; Kuila, T.; Kim, N. H.; Lee, J. H., Silicate-based polymer-nanocomposite membranes for polymer electrolyte membrane fuel cells. *Progress in Polymer Science* **2012,** *37* (6), 842-869.
37. Shao, Z.-G.; Xu, H.; Li, M.; Hsing, I.-M., Hybrid Nafion–inorganic oxides membrane doped with heteropolyacids for high temperature operation of proton exchange membrane fuel cell. *Solid State Ionics* **2006,** *177* (7), 779-785.
38. Rikukawa, M.; Sanui, K., Proton-conducting polymer electrolyte membranes based on hydrocarbon polymers. *Progress in Polymer Science* **2000,** *25* (10), 1463-1502.
39. Mauritz, K. A.; Moore, R. B., State of understanding of Nafion. *Chemical Reviews* **2004,** *104* (10), 4535-4586.
40. Sahu, A.; Pitchumani, S.; Sridhar, P.; Shukla, A., Nafion and modified-Nafion membranes for polymer electrolyte fuel cells: An overview. *Bulletin of Materials Science* **2009,** *32* (3), 285-294.
41. Hiesgen, R.; Helmly, S.; Galm, I.; Morawietz, T.; Handl, M.; Friedrich, K. A., Microscopic analysis of current and mechanical properties of Nafion® studied by atomic force microscopy. *Membranes* **2012,** *2* (4), 783-803.
42. Starkweather Jr, H. W., Crystallinity in perfluorosulfonic acid ionomers and related polymers. *Macromolecules* **1982,** *15* (2), 320-323.

43. Matos, B.; Santiago, E.; Rey, J.; Ferlauto, A.; Traversa, E.; Linardi, M.; Fonseca, F., Nafion-based composite electrolytes for proton exchange membrane fuel cells operating above 120 C with titania nanoparticles and nanotubes as fillers. *Journal of Power Sources* **2011,** *196* (3), 1061-1068.
44. Appleby, A.; Yeager, E., Solid polymer electrolyte fuel cells (SPEFCs). *Energy* **1986,** *11* (1-2), 137-52.
45. Riedinger, H.; Faul, W., The focussing of membrane R&D on areas of commercial potential. *Journal of Membrane Science* **1988,** *36*, 5-18.
46. Prater, K., The renaissance of the solid polymer fuel cell. *Journal of Power Sources* **1990,** *29* (1), 239-250.
47. Haubold, H.-G.; Vad, T.; Jungbluth, H.; Hiller, P., Nano structure of NAFION: a SAXS study. *Electrochimica Acta* **2001,** *46* (10), 1559-1563.
48. Savadogo, O., Emerging membranes for electrochemical systems: Part II. High temperature composite membranes for polymer electrolyte fuel cell (PEFC) applications. *Journal of Power Sources* **2004,** *127* (1), 135-161.
49. Santiago, E.; Isidoro, R.; Dresch, M.; Matos, B.; Linardi, M.; Fonseca, F., Nafion–TiO 2 hybrid electrolytes for stable operation of PEM fuel cells at high temperature. *Electrochimica Acta* **2009,** *54* (16), 4111-4117.
50. Zhengbang, W.; Tang, H.; Mu, P., Self-assembly of durable Nafion/TiO_2 nanowire electrolyte membranes for elevated-temperature PEM fuel cells. *Journal of Membrane Science* **2011,** *369* (1), 250-257.
51. Savadogo, O., Emerging membrane for electrochemical systems:(I) solid polymer electrolyte membranes for fuel cell systems. *Journal of New Materials for Electrochemical Systems* **1998,** *1* (1), 47-66.
52. Kong, X., Characterization of proton exchange materials for fuel cells by solid state nuclear magnetic resonance. **2010**.

53. Camposeo, A.; Mele, E.; Persano, L.; Pisignano, D.; Cingolani, R., Role of doping concentration on the competition between amplified spontaneous emission and nonradiative energy transfer in blends of conjugated polymers. *Physical Review B* **2006,** *73* (16), 165201.
54. Luu, D. X.; Kim, D., Semi-interpenetrating polymer network electrolyte membranes composed of sulfonated poly (ether ether ketone) and organosiloxane-based hybrid network. *Journal of Power Sources* **2011,** *196* (24), 10584-10590.
55. Zhang, N.; Zhang, G.; Xu, D.; Zhao, C.; Ma, W.; Li, H.; Zhang, Y.; Xu, S.; Jiang, H.; Sun, H., Cross-linked membranes based on sulfonated poly (ether ether ketone)(SPEEK)/Nafion for direct methanol fuel cells (DMFCs). *International Journal of Hydrogen Energy* **2011,** *36* (17), 11025-11033.
56. Miyatake, K.; Watanabe, M., Emerging membrane materials for high temperature polymer electrolyte fuel cells: durable hydrocarbon ionomers. *Journal of Materials Chemistry* **2006,** *16* (46), 4465-4467.
57. Liu, Y.-H.; Yi, B.; Shao, Z.-G.; Xing, D.; Zhang, H., Carbon nanotubes reinforced Nafion composite membrane for fuel cell applications. *Electrochemical and Solid-State Letters* **2006,** *9* (7), A356-A359.
58. Matos, B. R.; Santiago, E. I.; Fonseca, F. C.; Linardi, M.; Lavayen, V.; Lacerda, R. G.; Ladeira, L. O.; Ferlauto, A. S., Nafion–titanate nanotube composite membranes for PEMFC operating at high temperature. *Journal of the Electrochemical Society* **2007,** *154* (12), B1358-B1361.
59. D'Elia, D.; Beauger, C.; Hochepied, J.-F.; Rigacci, A.; Berger, M.-H.; Keller, N.; Keller-Spitzer, V.; Suzuki, Y.; Valmalette, J.-C.; Benabdesselam, M., Impact of three different TiO_2 morphologies on hydrogen evolution by methanol assisted water splitting: nanoparticles, nanotubes and aerogels. *International Journal of Hydrogen Energy* **2011,** *36* (22), 14360-14373.
60. Tang, H.; Jiang, S. P., Self-Assembled Pt/Mesoporous Silica− Carbon Electrocatalysts for Elevated-Temperature Polymer Electrolyte Membrane Fuel Cells. *The Journal of Physical Chemistry C* **2008,** *112* (49), 19748-19755.

61. Tang, H.; Wang, X.; Pan, M.; Wang, F., Fabrication and characterization of improved PFSA/ePTFE composite polymer electrolyte membranes. *Journal of Membrane Science* **2007,** *306* (1), 298-306.
62. Zhu, X.; Zhang, H.; Zhang, Y.; Liang, Y.; Wang, X.; Yi, B., An ultrathin self-humidifying membrane for PEM fuel cell application: fabrication, characterization, and experimental analysis. *The Journal of Physical Chemistry B* **2006,** *110* (29), 14240-14248.
63. Bajon, R.; Balaji, S.; Guo, S., Electrospun Nafion nanofiber for proton exchange membrane fuel cell application. *Journal of Fuel Cell Science and Technology* **2009,** *6* (3), 031004.
64. Ballengee, J.; Pintauro, P., Morphological control of electrospun Nafion nanofiber mats. *Journal of the Electrochemical Society* **2011,** *158* (5), B568-B572.
65. Burger, C.; Hsiao, B. S.; Chu, B., Nanofibrous materials and their applications. *Annu. Rev. Mater. Res.* **2006,** *36*, 333-368.
66. Wanner, M. J.; van der Haas, R. N.; de Cuba, K. R.; van Maarseveen, J. H.; Hiemstra, H., Catalytic asymmetric Pictet–Spengler reactions via sulfenyliminium ions. *Angewandte Chemie International Edition* **2007,** *46* (39), 7485-7487.
67. Chronakis, I. S., Novel nanocomposites and nanoceramics based on polymer nanofibers using electrospinning process—a review. *Journal of Materials Processing Technology* **2005,** *167* (2), 283-293.
68. Sanders, E.; McGrady, K.; Wnek, G.; Edmondson, C.; Mueller, J.; Fontanella, J.; Suarez, S.; Greenbaum, S., Characterization of electrosprayed Nafion films. *Journal of Power Sources* **2004,** *129* (1), 55-61.
69. Laforgue, A.; Robitaille, L.; Mokrini, A.; Ajji, A., Fabrication and characterization of ionic conducting nanofibers. *Macromolecular Materials and Engineering* **2007,** *292* (12), 1229-1236.
70. Chen, H.; Snyder, J. D.; Elabd, Y. A., Electrospinning and solution properties of Nafion and poly (acrylic acid). *Macromolecules* **2008,** *41* (1), 128-135.

71. Ma, C.-H.; Yu, T. L.; Lin, H.-L.; Huang, Y.-T.; Chen, Y.-L.; Jeng, U.-S.; Lai, Y.-H.; Sun, Y.-S., Morphology and properties of Nafion membranes prepared by solution casting. *Polymer* **2009,** *50* (7), 1764-1777.
72. Zhou, C.; Liu, Z.; Dai, J.; Xiao, D., Electrospun Ru (bpy) 32+-doped Nafion nanofibers for electrochemiluminescence sensing. *Analyst* **2010,** *135* (5), 1004-1009.
73. Dong, B.; Gwee, L.; Salas-de La Cruz, D.; Winey, K. I.; Elabd, Y. A., Super proton conductive high-purity Nafion nanofibers. *Nano letters* **2010,** *10* (9), 3785-3790.
74. Nah, C.; Lee, Y.-S.; Cho, B.; Yu, H.; Akle, B.; Leo, D., Preparation and properties of nanofibrous Nafion mats for ionic polymer metal composites. *Composites Science and Technology* **2008,** *68* (14), 2960-2964.
75. Tran, C.; Kalra, V., Co-continuous nanoscale assembly of Nafion–polyacrylonitrile blends within nanofibers: a facile route to fabrication of porous nanofibers. *Soft Matter* **2013,** *9* (3), 846-852.
76. Sharma, D. K.; Shen, J.; Li, F., Reinforcement of Nafion into polyacrylonitrile (PAN) to fabricate them into nanofiber mats by electrospinning: characterization of enhanced mechanical and adsorption properties. *RSC Advances* **2014,** *4* (74), 39110-39117.
77. Watanabe, M.; Uchida, H.; Seki, Y.; Emori, M.; Stonehart, P., Self-humidifying polymer electrolyte membranes for fuel cells. *Journal of the Electrochemical Society* **1996,** *143* (12), 3847-3852.
78. Adjemian, K.; Lee, S.; Srinivasan, S.; Benziger, J.; Bocarsly, A., Silicon oxide nafion composite membranes for proton-exchange membrane fuel cell operation at 80-140 C. *Journal of the electrochemical Society* **2002,** *149* (3), A256-A261.
79. Hara, S.; Takano, S.; Miyayama, M., Proton-conducting properties and microstructure of hydrated tin dioxide and hydrated zirconia. *The Journal of Physical Chemistry B* **2004,** *108* (18), 5634-5639.
80. Abbaraju, R. R.; Dasgupta, N.; Virkar, A. V., Composite Nafion Membranes Containing Nanosize TiO2⁄SnO2 for Proton Exchange Membrane Fuel Cells. *Journal of the Electrochemical Society* **2008,** *155* (12), B1307-B1313.

81. Mecheri, B.; D'Epifanio, A.; Traversa, E.; Licoccia, S., Sulfonated polyether ether ketone and hydrated tin oxide proton conducting composites for direct methanol fuel cell applications. *Journal of Power Sources* **2008,** *178* (2), 554-560.
82. Ehsani, M.; Gao, Y.; Emadi, A., *Modern electric, hybrid electric, and fuel cell vehicles: fundamentals, theory, and design*. CRC press: 2009.
83. Di Noto, V.; Lavina, S.; Negro, E.; Vittadello, M.; Conti, F.; Piga, M.; Pace, G., Hybrid inorganic–organic proton conducting membranes based on Nafion and 5wt% of M x O y (M= Ti, Zr, Hf, Ta and W). Part II: Relaxation phenomena and conductivity mechanism. *Journal of Power Sources* **2009,** *187* (1), 57-66.
84. Zou, H.; Wu, S.; Shen, J., Polymer/silica nanocomposites: preparation, characterization, properties, and applications. *Chem. Rev* **2008,** *108* (9), 3893-3957.
85. Ray, S. S.; Okamoto, M., Polymer/layered silicate nanocomposites: a review from preparation to processing. *Progress in Polymer Science* **2003,** *28* (11), 1539-1641.
86. Tripathi, B. P.; Shahi, V. K., Functionalized organic− inorganic nanostructured N-p-carboxy benzyl chitosan− silica− PVA hybrid polyelectrolyte complex as proton exchange membrane for DMFC applications. *The Journal of Physical Chemistry B* **2008,** *112* (49), 15678-15690.
87. Xing, D.; He, G.; Hou, Z.; Ming, P.; Song, S., Preparation and characterization of a modified montmorillonite/sulfonated polyphenylether sulfone/PTFE composite membrane. *International Journal of Hydrogen Energy* **2011,** *36* (3), 2177-2183.
88. Durand, N.; Gaveau, P.; Silly, G.; Améduri, B.; Boutevin, B., Radical grafting of tetrafluoroethylene and vinylidene fluoride telomers onto silica bearing vinyl groups. *Macromolecules* **2011,** *44* (16), 6249-6257.
89. Thayumanasundaram, S.; Piga, M.; Lavina, S.; Negro, E.; Jeyapandian, M.; Ghassemzadeh, L.; Müller, K.; Di Noto, V., Hybrid inorganic–organic proton conducting membranes based on Nafion, SiO 2 and triethylammonium trifluoromethanesulfonate ionic liquid. *Electrochimica Acta* **2010,** *55* (4), 1355-1365.

90. Ghassemzadeh, L.; Pace, G.; Di Noto, V.; Müller, K., Effect of SiO_2 on the dynamics of proton conducting [Nafion/(SiO_2) X] composite membranes: a solid-state 19 F NMR study. *Physical Chemistry Chemical Physics* **2011,** *13* (20), 9327-9334.
91. Adjemian, K. T.; Dominey, R.; Krishnan, L.; Ota, H.; Majsztrik, P.; Zhang, T.; Mann, J.; Kirby, B.; Gatto, L.; Velo-Simpson, M., *Chemistry of Materials* **2006,** *18* (9), 2238-2248.
92. Adjemian, K.; Srinivasan, S.; Benziger, J.; Bocarsly, A., Investigation of PEMFC operation above 100 C employing perfluorosulfonic acid silicon oxide composite membranes. *Journal of Power Sources* **2002,** *109* (2), 356-364.
93. Alberti, G.; Casciola, M.; Capitani, D.; Donnadio, A.; Narducci, R.; Pica, M.; Sganappa, M., Novel Nafion–zirconium phosphate nanocomposite membranes with enhanced stability of proton conductivity at medium temperature and high relative humidity. *Electrochimica Acta* **2007,** *52* (28), 8125-8132.
94. Costamagna, P.; Yang, C.; Bocarsly, A.; Srinivasan, S., Nafion® 115/zirconium phosphate composite membranes for operation of PEMFCs above 100 °C. *Electrochimica Acta* **2002,** *47* (7), 1023-1033.
95. Casciola, M.; Capitani, D.; Comite, A.; Donnadio, A.; Frittella, V.; Pica, M.; Sganappa, M.; Varzi, A., Nafion–zirconium phosphate nanocomposite membranes with high filler loadings: Conductivity and mechanical properties. *Fuel Cells* **2008,** *8* (3-4), 217-224.
96. Jian-hua, T.; Peng-fei, G.; Zhi-yuan, Z.; Wen-hui, L.; Zhong-qiang, S., Preparation and performance evaluation of a Nafion-TiO_2 composite membrane for PEMFCs. *International Journal of Hydrogen Energy* **2008,** *33* (20), 5686-5690.
97. Jung, D.; Cho, S.; Peck, D.; Shin, D.; Kim, J., Performance evaluation of a Nafion/silicon oxide hybrid membrane for direct methanol fuel cell. *Journal of Power Sources* **2002,** *106* (1), 173-177.
98. Dimitrova, P.; Friedrich, K.; Vogt, B.; Stimming, U., Transport properties of ionomer composite membranes for direct methanol fuel cells. *Journal of Electroanalytical Chemistry* **2002,** *532* (1), 75-83.

99. Xu, W.; Lu, T.; Liu, C.; Xing, W., Low methanol permeable composite Nafion/silica/PWA membranes for low temperature direct methanol fuel cells. *Electrochimica Acta* **2005,** *50* (16), 3280-3285.

100. Tago, T.; Kuwashiro, N.; Nishide, H., Preparation of acid-functionalized poly (phenylene oxide) s and poly (phenylene sulfone) and their proton conductivity. *Bulletin of the Chemical Society of Japan* **2007,** *80* (7), 1429-1434.

101. Cho, Y.-H.; Kim, S.-K.; Kim, T.-H.; Cho, Y.-H.; Lim, J. W.; Jung, N.; Yoon, W.-S.; Lee, J.-C.; Sung, Y.-E., Preparation of MEA with the polybenzimidazole membrane for high temperature PEM fuel cell. *Electrochemical and Solid-State Letters* **2011,** *14* (3), B38-B40.

102. Zhang, J.; Tang, Y.; Song, C.; Zhang, J., Polybenzimidazole-membrane-based PEM fuel cell in the temperature range of 120–200 C. *Journal of Power Sources* **2007,** *172* (1), 163-171.

103. Ng, F.; Péron, J.; Jones, D. J.; Rozière, J., Synthesis of novel proton-conducting highly sulfonated polybenzimidazoles for PEMFC and the effect of the type of bisphenyl bridge on polymer and membrane properties. *Journal of Polymer Science Part A: Polymer Chemistry* **2011,** *49* (10), 2107-2117.

104. Jentoft, F. C.; Hahn, A.; Kröhnert, J.; Lorenz, G.; Jentoft, R. E.; Ressler, T.; Wild, U.; Schlögl, R.; Häßner, C.; Köhler, K., Incorporation of manganese and iron into the zirconia lattice in promoted sulfated zirconia catalysts. *Journal of Catalysis* **2004,** *224* (1), 124-137.

105. Rajabbeigi, N.; Elyassi, B.; Khodadadi, A. A.; Mohajerzadeh, S.; Mortazavi, Y.; Sahimi, M., Oxygen sensor with solid-state CeO_2–ZrO_2–TiO_2 reference. *Sensors and Actuators B: Chemical* **2005,** *108* (1), 341-345.

106. Silva, V.; Ruffmann, B.; Silva, H.; Gallego, Y.; Mendes, A.; Madeira, L.; Nunes, S., Proton electrolyte membrane properties and direct methanol fuel cell performance: I. Characterization of hybrid sulfonated poly (ether ether ketone)/zirconium oxide membranes. *Journal of Power Sources* **2005,** *140* (1), 34-40.

107. Berry, M. B.; Libby, B. E.; Rose, K.; Haas, K.-H.; Thompson, R. W., Incorporation of zeolites into composite matrices. *Microporous and Mesoporous Materials* **2000,** *39* (1), 205-217.

108. Caro, J.; Noack, M.; Kölsch, P.; Schäfer, R., Zeolite membranes–state of their development and perspective. *Microporous and Mesoporous Materials* **2000,** *38* (1), 3-24.

109. Kim, D.; Scibioh, M. A.; Kwak, S.; Oh, I.-H.; Ha, H. Y., Nano-silica layered composite membranes prepared by PECVD for direct methanol fuel cells. *Electrochemistry Communications* **2004,** *6* (10), 1069-1074.

110. Miyake, N.; Wainright, J.; Savinell, R., Evaluation of a sol-gel derived Nafion/silica hybrid membrane for polymer electrolyte membrane fuel cell applications: II. Methanol uptake and methanol permeability. *Journal of the Electrochemical Society* **2001,** *148* (8), A905-A909.

111. Staiti, P.; Arico, A.; Baglio, V.; Lufrano, F.; Passalacqua, E.; Antonucci, V., Hybrid Nafion–silica membranes doped with heteropolyacids for application in direct methanol fuel cells. *Solid State Ionics* **2001,** *145* (1), 101-107.

112. Jiang, R.; Kunz, H. R.; Fenton, J. M., Composite silica/Nafion® membranes prepared by tetraethylorthosilicate sol–gel reaction and solution casting for direct methanol fuel cells. *Journal of Membrane Science* **2006,** *272* (1), 116-124.

113. Sahu, A.; Selvarani, G.; Pitchumani, S.; Sridhar, P.; Shukla, A., A sol-gel modified alternative nafion-silica composite membrane for polymer electrolyte fuel cells. *Journal of the Electrochemical Society* **2007,** *154* (2), B123-B132.

114. Shim, J.; Koo, I.; Lee, W., Nafion-impregnated polyethylene-terephthalate film used as the electrolyte for direct methanol fuel cells. *Electrochimica Acta* **2005,** *50* (12), 2385-2391.

115. Tian, A. H.; Kim, J.-Y.; Shi, J. Y.; Kim, K., Poly (1-vinylimidazole)/Pd-impregnated Nafion for direct methanol fuel cell applications. *Journal of Power Sources* **2008,** *183* (1), 1-7.

116. Yang, C.-C., Synthesis and characterization of the cross-linked PVA/TiO_2 composite polymer membrane for alkaline DMFC. *Journal of Membrane Science* **2007,** *288* (1), 51-60.

117. Palani, P. B.; Kannan, R.; Rajashabala, S.; Rajendran, S.; Velraj, G., Effect of nano-composite on polyvinyl alcohol-based proton conducting membrane for direct methanol fuel cell applications. *Ionics* **2015,** *21* (2), 507-513.

118. Tunney, J. J.; Detellier, C., Interlamellar covalent grafting of organic units on kaolinite. *Chemistry of Materials* **1993,** *5* (6), 747-748.

119. Ruiz-Hitzky, E.; Rojo, J., Intracrystalline grafting on layer silicic acids. *Nature* **1980,** *287* (5777), 28-30.

120. Merkel, T.; Bondar, V.; Nagai, K.; Freeman, B.; Pinnau, I., Gas sorption, diffusion, and permeation in poly (dimethylsiloxane). *Journal of Polymer Science Part B: Polymer Physics* **2000,** *38* (3), 415-434.

121. Kim, S. Y.; Shin, H. S.; Lee, Y. M.; Jeong, C. N., Properties of electroresponsive poly (vinyl alcohol)/poly (acrylic acid) IPN hydrogels under an electric stimulus. *Journal of Applied Polymer Science* **1999,** *73* (9), 1675-1683.

122. Lozano, K.; Bonilla-Rios, J.; Barrera, E., A study on nanofiber-reinforced thermoplastic composites (II): Investigation of the mixing rheology and conduction properties. *Journal of Applied Polymer Science* **2001,** *80* (8), 1162-1172.

123. Park, J. S.; Park, J. W.; Ruckenstein, E., A dynamic mechanical and thermal analysis of unplasticized and plasticized poly (vinyl alcohol)/methylcellulose blends. *Journal of Applied Polymer Science* **2001,** *80* (10), 1825-1834.

124. Lebrun, L.; Da Silva, E.; Metayer, M., Elaboration of ion-exchange membranes with semi-interpenetrating polymer networks containing poly (vinyl alcohol) as polymer matrix. *Journal of Applied Polymer Science* **2002,** *84* (8), 1572-1580.

125. Kim, D. S.; Park, H. B.; Rhim, J. W.; Lee, Y. M., Proton conductivity and methanol transport behavior of cross-linked PVA/PAA/silica hybrid membranes. *Solid State Ionics* **2005,** *176* (1), 117-126.

126. Lebrun, L.; Follain, N.; Metayer, M., Elaboration of a new anion-exchange membrane with semi-interpenetrating polymer networks and characterisation. *Electrochimica Acta* **2004,** *50* (4), 985-993.

127. Robeson, L.; Hale, W.; Merriam, C., Miscibility of the poly (hydroxy ether) of bisphenol A with water-soluble polyethers. *Macromolecules* **1981,** *14* (6), 1644-1650.

128. Rhim, J. W.; Yeom, C. K.; Kim, S. W., Modification of poly (vinyl alcohol) membranes using sulfur-succinic acid and its application to pervaporation separation of water–alcohol mixtures. *Journal of Applied Polymer Science* **1998,** *68* (11), 1717-1723.

129. Rhim, J.-W.; Park, H. B.; Lee, C.-S.; Jun, J.-H.; Kim, D. S.; Lee, Y. M., Crosslinked poly (vinyl alcohol) membranes containing sulfonic acid group: proton and methanol transport through membranes. *Journal of Membrane Science* **2004,** *238* (1), 143-151.

130. Qiao, J.; Hamaya, T.; Okada, T., New highly proton-conducting membrane poly (vinylpyrrolidone)(PVP) modified poly (vinyl alcohol)/2-acrylamido-2-methyl-1-propanesulfonic acid (PVA–PAMPS) for low temperature direct methanol fuel cells (DMFCs). *Polymer* **2005,** *46* (24), 10809-10816.

131. Pivovar, B. S.; Wang, Y.; Cussler, E., Pervaporation membranes in direct methanol fuel cells. *Journal of Membrane Science* **1999,** *154* (2), 155-162.

132. Vargas, R.; Zapata, V.; Matallana, E.; Vargas, M., More thermal studies on the PVOH/H_3PO_2/H_2O solid proton conductor gels. *Electrochimica Acta* **2001,** *46* (10), 1699-1702.

133. Kang, M.-S.; Choi, Y.-J.; Moon, S.-H., Water-swollen cation-exchange membranes prepared using poly (vinyl alcohol)(PVA)/poly (styrene sulfonic acid-co-maleic acid)(PSSA-MA). *Journal of Membrane Science* **2002,** *207* (2), 157-170.

134. Stevens, J.; Wieczorek, W.; Raducha, D.; Jeffrey, K., Proton conducting gel/H_3PO_4 electrolytes. *Solid State Ionics* **1997,** *97* (1), 347-358.

135. Kim, D.-W.; Park, J.-K.; Rhee, H.-W., Conductivity and thermal studies of solid polymer electrolytes prepared by blending poly (ethylene oxide), poly (oligo [oxyethylene] oxysebacoyl) and lithium perchlorate. *Solid State Ionics* **1996,** *83* (1-2), 49-56.

136. Wieczorek, W.; Stevens, J., Impedance spectroscopy and phase structure of polyether− poly (methyl methacrylate)− $LiCF_3SO_3$ blend-based electrolytes. *The Journal of Physical Chemistry B* **1997,** *101* (9), 1529-1534.

137. Przyłuski, J.; Wieczorek, W., Increasing the conductivity of polymer solid electrolytes: A review. *Solid State Ionics* **1989,** *36* (3-4), 165-169.

138. Norby, T., EMF method determination of conductivity contributions from protons and other foreign ions in oxides. *Solid State Ionics* **1988,** *28*, 1586-1591.

139. Nasouri, K.; Shoushtari, A.; Mojtahedi, M., Effects of polymer/solvent systems on electrospun polyvinylpyrrolidone nanofiber morphology and diameter. *Polymer Science--Series A* **2015,** *57* (6).

140. Nasouri, K.; Shoushtari, A. M.; Mojtahedi, M. R. M., Evaluation of effective electrospinning parameters controlling polyvinylpyrrolidone nanofibers surface morphology via response surface methodology. *Fibers and Polymers* **2015,** *16* (9), 1941-1954.

141. Zheng, M.; Gu, M.; Jin, Y.; Jin, G., Preparation, structure and properties of TiO_2–PVP hybrid films. *Materials Science and Engineering: B* **2000,** *77* (1), 55-59.

142. Zheng, M.-P.; Jin, Y.-P.; Jin, G.-L.; Gu, M.-Y., Characterization of TiO_2-PVP nanocomposites prepared by the sol-gel method. *Journal of Materials Science Letters* **2000,** *19* (5), 433-436.

143. Wang, H.; Yu, T.; Zhao, C.; Du, Q., Improvement of hydrophilicity and blood compatibility on polyethersulfone membrane by adding polyvinylpyrrolidone. *Fibers and Polymers* **2009,** *10* (1), 1-5.

144. Nataraj, S.; Yang, K.; Aminabhavi, T., Polyacrylonitrile-based nanofibers—a state-of-the-art review. *Progress in Polymer Science* **2012,** *37* (3), 487-513.

145. Nie, G.; Li, Z.; Lu, X.; Lei, J.; Zhang, C.; Wang, C., Fabrication of polyacrylonitrile/CuS composite nanofibers and their recycled application in catalysis for dye degradation. *Applied Surface Science* **2013,** *284*, 595-600.

146. Yun, K. M.; Suryamas, A. B.; Iskandar, F.; Bao, L.; Niinuma, H.; Okuyama, K., Morphology optimization of polymer nanofiber for applications in aerosol particle filtration. *Separation and Purification Technology* **2010,** *75* (3), 340-345.

147. Zhou, Z.; Lai, C.; Zhang, L.; Qian, Y.; Hou, H.; Reneker, D. H.; Fong, H., Development of carbon nanofibers from aligned electrospun polyacrylonitrile nanofiber bundles and characterization of their microstructural, electrical, and mechanical properties. *Polymer* **2009,** *50* (13), 2999-3006.

148. Gopalan, A. I.; Santhosh, P.; Manesh, K. M.; Nho, J. H.; Kim, S. H.; Hwang, C.-G.; Lee, K.-P., Development of electrospun PVdF–PAN membrane-based polymer electrolytes for lithium batteries. *Journal of Membrane Science* **2008,** *325* (2), 683-690.

149. Kampalanonwat, P.; Supaphol, P., Preparation and adsorption behavior of aminated electrospun polyacrylonitrile nanofiber mats for heavy metal ion removal. *ACS Applied Materials & Interfaces* **2010,** *2* (12), 3619-3627.

150. Saeed, K.; Haider, S.; Oh, T.-J.; Park, S.-Y., Preparation of amidoxime-modified polyacrylonitrile (PAN-oxime) nanofibers and their applications to metal ions adsorption. *Journal of Membrane Science* **2008,** *322* (2), 400-405.

151. Sahay, R.; Kumar, P. S.; Sridhar, R.; Sundaramurthy, J.; Venugopal, J.; Mhaisalkar, S. G.; Ramakrishna, S., Electrospun composite nanofibers and their multifaceted applications. *Journal of Materials Chemistry* **2012,** *22* (26), 12953-12971.

152. Kim, C.; Choi, Y.-O.; Lee, W.-J.; Yang, K.-S., Supercapacitor performances of activated carbon fiber webs prepared by electrospinning of PMDA-ODA poly (amic acid) solutions. *Electrochimica Acta* **2004,** *50* (2-3), 883-887.

153. Kim, C.; Yang, K.-S.; Lee, W.-J., The use of carbon nanofiber electrodes prepared by electrospinning for electrochemical supercapacitors. *Electrochemical and Solid-State Letters* **2004,** *7* (11), A397-A399.

154. Kim, C.; Park, S.-H.; Lee, W.-J.; Yang, K.-S., Characteristics of supercapaitor electrodes of PBI-based carbon nanofiber web prepared by electrospinning. *Electrochimica Acta* **2004,** *50* (2), 877-881.

155. Kim, C.; Yang, K., Electrochemical properties of carbon nanofiber web as an electrode for supercapacitor prepared by electrospinning. *Applied Physics Letters* **2003,** *83* (6), 1216-1218.

156. Tekmen, C.; Tsunekawa, Y.; Nakanishi, H., Electrospinning of carbon nanofiber supported Fe/Co/Ni ternary alloy nanoparticles. *Journal of Materials Processing Technology* **2010,** *210* (3), 451-455.

157. Kim, C.; Ngoc, B. T. N.; Yang, K. S.; Kojima, M.; Kim, Y. A.; Kim, Y. J.; Endo, M.; Yang, S. C., Self-Sustained Thin Webs Consisting of Porous Carbon Nanofibers for Supercapacitors via the Electrospinning of Polyacrylonitrile Solutions Containing Zinc Chloride. *Advanced Materials* **2007,** *19* (17), 2341-2346.

158. Carter, R.; Wycisk, R.; Yoo, H.; Pintauro, P., Blended polyphosphazene/polyacrylonitrile membranes for direct methanol fuel cells. *Electrochemical and Solid-State Letters* **2002,** *5* (9), A195-A197.

159. Narang, S.; Ventura, S.; Olmeijer, D. *Polymer Membrane Composition*; WO/2001/094450: 2001.

160. Wang, J.; Yue, Z.; Economy, J., Preparation of proton-conducting composite membranes from sulfonated poly (ether ether ketone) and polyacrylonitrile. *Journal of Membrane Science* **2007,** *291* (1), 210-219.

161. Yang, C.-C.; Chiu, S.-J.; Lee, K.-T.; Chien, W.-C.; Lin, C.-T.; Huang, C.-A., Study of poly (vinyl alcohol)/titanium oxide composite polymer membranes and their application on alkaline direct alcohol fuel cell. *Journal of Power Sources* **2008,** *184* (1), 44-51.

162. Chen, S.; Han, C.; Tsai, C.; Huang, J.; Chen-Yang, Y., Effect of morphological properties of ionic liquid-templated mesoporous anatase TiO2 on performance of PEMFC with Nafion/TiO2 composite membrane at elevated temperature and low relative humidity. *Journal of Power Sources* **2007,** *171* (2), 363-372.

163. Tricoli, V.; Nannetti, F., Zeolite–Nafion composites as ion conducting membrane materials. *Electrochimica Acta* **2003,** *48* (18), 2625-2633.

164. Xu, T., Ion exchange membranes: state of their development and perspective. *Journal of Membrane Science* **2005,** *263* (1), 1-29.

165. Sancho, T.; Soler, J.; Pina, M., Conductivity in zeolite–polymer composite membranes for PEMFCs. *Journal of Power Sources* **2007,** *169* (1), 92-97.

166. Li, X.; Roberts, E. P.; Holmes, S. M.; Zholobenko, V., Functionalized zeolite A–nafion composite membranes for direct methanol fuel cells. *Solid State Ionics* **2007,** *178* (19), 1248-1255.

167. Huang, A.; Lin, Y.; Yang, W., Synthesis and properties of A-type zeolite membranes by secondary growth method with vacuum seeding. *Journal of Membrane Science* **2004,** *245* (1), 41-51.

168. Libby, B.; Smyrl, W.; Cussler, E., Polymer-zeolite composite membranes for direct methanol fuel cells. *AIChE Journal* **2003,** *49* (4), 991-1001.

169. Karge, H. G.; Hunger, M.; Beyer, H. K., Characterization of Zeolites—Infrared and Nuclear Magnetic Resonance Spectroscopy and X-Ray Diffraction. In *Catalysis and Zeolites*, Springer: 1999; pp 198-326.

170. Baglio, V.; Di Blasi, A.; Aricò, A.; Antonucci, V.; Antonucci, P.; Nannetti, F.; Tricoli, V., Investigation of the electrochemical behaviour in DMFCs of chabazite and clinoptilolite-based composite membranes. *Electrochimica Acta* **2005,** *50* (25), 5181-5188.

171. Zimmerman, C. M.; Singh, A.; Koros, W. J., Tailoring mixed matrix composite membranes for gas separations. *Journal of Membrane Science* **1997,** *137* (1-2), 145-154.

172. Li, Y.; Guan, H.-M.; Chung, T.-S.; Kulprathipanja, S., Effects of novel silane modification of zeolite surface on polymer chain rigidification and partial pore blockage in polyethersulfone (PES)–zeolite A mixed matrix membranes. *Journal of Membrane Science* **2006,** *275* (1), 17-28.

173. Van Grieken, R.; Sotelo, J.; Menendez, J.; Melero, J., Anomalous crystallization mechanism in the synthesis of nanocrystalline ZSM-5. *Microporous and Mesoporous Materials* **2000,** *39* (1), 135-147.

174. Rieke, P. C.; Vanderborgh, N. E., Temperature dependence of water content and proton conductivity in polyperfluorosulfonic acid membranes. *Journal of Membrane Science* **1987,** *32* (2-3), 313-328.

175. Scibona, G.; Fabiani, C.; Scuppa, B., Electrochemical behaviour of Nafion type membrane. *Journal of Membrane Science* **1983,** *16*, 37-50.

176. Hsu, W. Y.; Barkley, J. R.; Meakin, P., Ion percolation and insulator-to-conductor transition in Nafion perfluorosulfonic acid membranes. *Macromolecules* **1980,** *13* (1), 198-200.

177. Van Nguyen, T.; Vanderborgh, N., The rate of isothermal hydration of polyperfluorosulfonic acid membranes. *Journal of Membrane Science* **1998,** *143* (1), 235-248.

178. Yeo, R.; Yeager, H. L., Structural and transport properties of perfluorinated ion-exchange membranes. *Modern Aspects of Electrochemistry* **1985,** *16*, 437-504.

179. Wang, W.; Guo, H.; Gao, J.; Dong, X.; Qin, Q., XPS, UPS and ESR studies on the interfacial interaction in Ni-ZrO_2 composite plating. *Journal of Materials Science* **2000,** *35* (6), 1495-1499.

180. Synowicki, R.; Tiwald, T. E., Optical properties of bulk c-ZrO_2, c-MgO and a-As_2 S_3 determined by variable angle spectroscopic ellipsometry. *Thin Solid Films* **2004,** *455*, 248-255.

181. Zhao, H.; Chen, J.; Sun, Y., Effect of calcination temperature on the performance of Co/ZrO_2 catalysts for fischer-tropsch synthesis. *Prepr. Pap.-Am. Chem. Soc., Div. Fuel Chem* **2003,** *48* (2), 733.

182. Davies, L.; Bonini, N.; Locatelli, S.; Gonzo, E., Characterization and catalytic activity of zirconium dioxide prepared by sol-gel. *Latin American Applied Research* **2005,** *35* (1), 23-28.

183. Maskell, W. C., Progress in the development of zirconia gas sensors. *Solid State Ionics* **2000,** *134* (1), 43-50.

184. Bauer, F.; Willert-Porada, M., Characterisation of zirconium and titanium phosphates and direct methanol fuel cell (DMFC) performance of functionally graded Nafion (R) composite membranes prepared out of them. *Journal of Power Sources* **2005,** *145* (2), 101-107.

185. Pan, J.; Zhang, H.; Chen, W.; Pan, M., Nafion–zirconia nanocomposite membranes formed via in situ sol–gel process. *International Journal of Hydrogen Energy* **2010,** *35* (7), 2796-2801.

186. Sacca, A.; Gatto, I.; Carbone, A.; Pedicini, R.; Passalacqua, E., ZrO_2 – Nafion composite membranes for polymer electrolyte fuel cells (PEFCs) at intermediate temperature. *Journal of Power Sources* **2006,** *163* (1), 47-51.

187. Wasmus, S.; Küver, A., Methanol oxidation and direct methanol fuel cells: a selective review. *Journal of Electroanalytical Chemistry* **1999,** *461* (1), 14-31.

188. Jones, D. J.; Rozière, J., Recent advances in the functionalisation of polybenzimidazole and polyetherketone for fuel cell applications. *Journal of Membrane Science* **2001,** *185* (1), 41-58.

189. Bauer, F.; Denneler, S.; Willert-Porada, M., Influence of temperature and humidity on the mechanical properties of Nafion® 117 polymer electrolyte membrane. *Journal of Polymer Science Part B: Polymer Physics* **2005,** *43* (7), 786-795.

190. Truffier-Boutry, D.; De Geyer, A.; Guetaz, L.; Diat, O.; Gebel, G., Structural Study of Zirconium Phosphate− Nafion Hybrid Membranes for High-Temperature Proton Exchange Membrane Fuel Cell Applications. *Macromolecules* **2007,** *40* (23), 8259-8264.

191. Bauer, F.; Willert-Porada, M., Microstructural characterization of Zr-phosphate–Nafion® membranes for direct methanol fuel cell (DMFC) applications. *Journal of Membrane Science* **2004,** *233* (1), 141-149.

192. Hogarth, W. H.; Da Costa, J. D.; Lu, G. M., Solid acid membranes for high temperature (^{o}C) proton exchange membrane fuel cells. *Journal of Power Sources* **2005,** *142* (1), 223-237.

193. Thampan, T. M.; Jalani, N. H.; Choi, P.; Datta, R., Systematic approach to design higher temperature composite PEMs. *Journal of The Electrochemical Society* **2005,** *152* (2), A316-A325.

194. Navarra, M.; Croce, F.; Scrosati, B., New, high temperature superacid zirconia-doped Nafion™ composite membranes. *Journal of Materials Chemistry* **2007,** *17* (30), 3210-3215.

195. Zhai, Y.; Zhang, H.; Hu, J.; Yi, B., Preparation and characterization of sulfated zirconia (SO_4^{2-}/ZrO_2)/Nafion composite membranes for PEMFC operation at high temperature/low humidity. *Journal of Membrane Science* **2006,** *280* (1), 148-155.

196. Gottesfeld, S.; Zawodzinski, T. A.; Alkire, R.; Gerischer, H.; Kolb, D.; Tobias, C. W., Advances in electrochemical science and engineering, Vol. 5. *John Wiley and Sounds, Inc., New York* **1997**, 195.

197. Zhou, W.; Qi, S.; Tu, C.; Zhao, H., Novel heat-conductive composite silicone rubber. *Journal of Applied Polymer Science* **2007,** *104* (4), 2478-2483.

198. Yu, S.; Hing, P.; Hu, X., Thermal conductivity of polystyrene–aluminum nitride composite. *Composites Part A: Applied Science and Manufacturing* **2002,** *33* (2), 289-292.

199. Lee, G.-W.; Park, M.; Kim, J.; Lee, J. I.; Yoon, H. G., Enhanced thermal conductivity of polymer composites filled with hybrid filler. *Composites Part A: Applied Science and Manufacturing* **2006,** *37* (5), 727-734.

200. Shimazaki, Y.; Hojo, F.; Takezawa, Y., Highly Thermoconductive polymer nanocomposite with a nanoporous α-Alumina sheet. *ACS applied Materials & Interfaces* **2008,** *1* (2), 225-227.

201. Zhou, W., Thermal and dielectric properties of the AlN particles reinforced linear low-density polyethylene composites. *Thermochimica Acta* **2011,** *512* (1), 183-188.

202. Zhang, H.; Shen, P. K., A brief consideration about the structural evolution of perfluorosulfonic-acid ionomer membranes. *International Journal of Hydrogen Energy* **2012,** *37* (5), 4657-4664.

203. Song, W. L.; Wang, P.; Cao, L.; Anderson, A.; Meziani, M. J.; Farr, A. J.; Sun, Y. P., Polymer/boron nitride nanocomposite materials for superior thermal transport performance. *Angewandte Chemie International Edition* **2012,** *51* (26), 6498-6501.

204. Yu, J.; Huang, X.; Wu, C.; Wu, X.; Wang, G.; Jiang, P., Interfacial modification of boron nitride nanoplatelets for epoxy composites with improved thermal properties. *Polymer* **2012,** *53* (2), 471-480.

205. Yu, J.; Huang, X.; Wang, L.; Peng, P.; Wu, C.; Wu, X.; Jiang, P., Preparation of hyperbranched aromatic polyamide grafted nanoparticles for thermal properties reinforcement of epoxy composites. *Polymer Chemistry* **2011,** *2* (6), 1380-1388.

206. Yu, J.; Duan, J.; Peng, W.; Wang, L.; Peng, P.; Jiang, P., Influence of nano-AlN particles on thermal conductivity, thermal stability and cure behavior of cycloaliphatic epoxy/trimethacrylate system. *eXPRESS Polymer Letters* **2011,** *5* (2).

207. Marnellos, G.; Zisekas, S.; Stoukides, M., Synthesis of ammonia at atmospheric pressure with the use of solid state proton conductors. *Journal of Catalysis* **2000,** *193* (1), 80-87.

208. Iwahara, H.; Esaka, T.; Uchida, H.; Maeda, N., Proton conduction in sintered oxides and its application to steam electrolysis for hydrogen production. *Solid State Ionics* **1981,** *3*, 359-363.

209. Xu, Y.; Chung, D.; Mroz, C., Thermally conducting aluminum nitride polymer-matrix composites. *Composites Part A: Applied Science and Manufacturing* **2001,** *32* (12), 1749-1757.

210. Mauritz, K.; Stefanithis, I.; Davis, S.; Scheetz, R. W.; Pope, R.; Wilkes, G. L.; Huang, H. H., Microstructural evolution of a silicon oxide phase in a perfluorosulfonic acid ionomer by an in situ sol–gel reaction. *Journal of Applied Polymer Science* **1995,** *55* (1), 181-190.

211. Tricoli, V., Proton and methanol transport in poly (perfluorosulfonate) membranes containing Cs+ and H+ cations. *Journal of the Electrochemical Society* **1998,** *145* (11), 3798-3801.

212. Zhang, Y.; Zhang, H.; Zhu, X.; Bi, C., Promotion of PEM self-humidifying effect by nanometer-sized sulfated zirconia-supported Pt catalyst hybrid with sulfonated poly (ether ether ketone). *The Journal of Physical Chemistry B* **2007,** *111* (23), 6391-6399.

213. Yang, C.; Srinivasan, S.; Bocarsly, A.; Tulyani, S.; Benziger, J., A comparison of physical properties and fuel cell performance of Nafion and zirconium phosphate/Nafion composite membranes. *Journal of Membrane Science* **2004,** *237* (1-2), 145-161.

214. Choi, P.; Jalani, N. H.; Thampan, T. M.; Datta, R., Consideration of thermodynamic, transport, and mechanical properties in the design of polymer electrolyte membranes for higher temperature fuel cell operation. *Journal of Polymer Science Part B: Polymer Physics* **2006,** *44* (16), 2183-2200.

215. Liu, D.; Kyriakides, S.; Case, S. W.; Lesko, J. J.; Li, Y.; McGrath, J. E., Tensile behavior of Nafion and sulfonated poly (arylene ether sulfone) copolymer membranes and its morphological correlations. *Journal of Polymer Science Part B: Polymer Physics* **2006,** *44* (10), 1453-1465.

216. Kundu, S.; Simon, L. C.; Fowler, M.; Grot, S., Mechanical properties of Nafion™ electrolyte membranes under hydrated conditions. *Polymer* **2005,** *46* (25), 11707-11715.

217. Rivin, D.; Kendrick, C.; Gibson, P.; Schneider, N., Solubility and transport behavior of water and alcohols in Nafion™. *Polymer* **2001,** *42* (2), 623-635.

218. Jimenez, A.; Berenguer, V.; Lopez, J.; Sanchez, A., Thermal degradation study of poly (vinyl chloride): kinetic analysis of thermogravimetric data. *Journal of Applied Polymer Science* **1993,** *50* (9), 1565-1573.

219. Takamatsu, T.; Hashiyama, M.; Eisenberg, A., Sorption phenomena in Nafion membranes. *Journal of Applied Polymer Science* **1979,** *24* (11), 2199-2220.

220. Hector, L. G.; Lai, Y.-H.; Tong, W.; Lukitsch, M. J., Strain accumulation in polymer electrolyte membrane and membrane electrode assembly materials during a single hydration/dehydration cycle. *Journal of Fuel Cell Science and Technology* **2007,** *4* (1), 19-28.

221. Huang, X.; Solasi, R.; Zou, Y.; Feshler, M.; Reifsnider, K.; Condit, D.; Burlatsky, S.; Madden, T., Mechanical endurance of polymer electrolyte membrane and PEM fuel cell durability. *Journal of Polymer Science Part B: Polymer Physics* **2006,** *44* (16), 2346-2357.

222. Benziger, J.; Chia, E.; Karnas, E.; Moxley, J.; Teuscher, C.; Kevrekidis, I., The stirred tank reactor polymer electrolyte membrane fuel cell. *AIChE Journal* **2004,** *50* (8), 1889-1900.

223. Satterfield, M. B.; Majsztrik, P. W.; Ota, H.; Benziger, J. B.; Bocarsly, A. B., Mechanical properties of Nafion and titania/Nafion composite membranes for polymer electrolyte membrane fuel cells. *Journal of Polymer Science Part B: Polymer Physics* **2006,** *44* (16), 2327-2345.

224. Bauer, F.; Willert-Porada, M., Zirconium phosphate Nafion® composites—a microstructure-based explanation of mechanical and conductivity properties. *Solid State Ionics* **2006,** *177* (26), 2391-2396.

225. Benziger, J.; Chia, E.; Moxley, J.; Kevrekidis, I., The dynamic response of PEM fuel cells to changes in load. *Chemical Engineering Science* **2005,** *60* (6), 1743-1759.

226. Newns, A., The sorption and desorption kinetics of water in a regenerated cellulose. *Transactions of the Faraday Society* **1956,** *52*, 1533-1545.

227. Krtil, P.; Trojánek, A.; Samec, Z., Kinetics of water sorption in NafionThin films− Quartz crystal microbalance study. *The Journal of Physical Chemistry B* **2001,** *105* (33), 7979-7983.

228. Bagley, E.; Long, F., Two-stage sorption and desorption of organic vapors in cellulose acetate1, 2. *Journal of the American Chemical Society* **1955,** *77* (8), 2172-2178.

229. Chalkova, E.; Pague, M. B.; Fedkin, M. V.; Wesolowski, D. J.; Lvov, S. N., Nafion/TiO_2 Proton Conductive Composite Membranes for PEMFCs Operating at Elevated Temperature and Reduced Relative Humidity. *Journal of the electrochemical Society* **2005,** *152* (6), A1035-A1040.

230. Sacca, A.; Carbone, A.; Passalacqua, E.; D'epifanio, A.; Licoccia, S.; Traversa, E.; Sala, E.; Traini, F.; Ornelas, R., Nafion–TiO 2 hybrid membranes for medium temperature polymer electrolyte fuel cells (PEFCs). *Journal of Power Sources* **2005,** *152*, 16-21.

231. Zhang, L.; Xu, J.; Hou, G.; Tang, H.; Deng, F., Interactions between Nafion resin and protonated dodecylamine modified montmorillonite: A solid state NMR study. *Journal of Colloid and Interface Science* **2007,** *311* (1), 38-44.

232. Aksoy, E. A.; Akata, B.; Bac, N.; Hasirci, N., Preparation and characterization of zeolite beta–polyurethane composite membranes. *Journal of Applied Polymer Science* **2007,** *104* (5), 3378-3387.

233. Liu, W.; Ruth, K.; Rusch, G., The membrane durability in PEM fuel cells. *Journal of New Materials for Electrochemical Systems* **2001,** *4* (4), 227-232.

234. Kumar, B.; Fellner, J., Polymer–ceramic composite protonic conductors. *Journal of Power Sources* **2003,** *123* (2), 132-136.

235. Brown, A. C.; Hargreaves, J. J., Sulfated metal oxide catalysts. Superactivity through superacidity? *Green Chemistry* **1999,** *1* (1), 17-20.

236. Lu, Y.; Yang, Y.; Sellinger, A.; Lu, M.; Huang, J.; Fan, H.; Haddad, R.; Lopez, G.; Burns, A. R.; Sasaki, D. Y., Self-assembly of mesoscopically ordered chromatic polydiacetylene/silica nanocomposites. *Nature* **2001,** *410* (6831), 913-917.

237. Wang, Z.; Tang, H.; Zhang, H.; Lei, M.; Chen, R.; Xiao, P.; Pan, M., Synthesis of Nafion/CeO_2 hybrid for chemically durable proton exchange membrane of fuel cell. *Journal of Membrane Science* **2012,** *421*, 201-210.

238. Zulfikar, M. A.; Mohammad, A. W.; Hilal, N., Preparation and characterization of novel porous PMMA-SiO2 hybrid membranes. *Desalination* **2006,** *192* (1-3), 262-270.

239. Fu, H.; Hong, R.; Zhang, Y.; Li, H.; Xu, B.; Zheng, Y.; Wei, D., Preparation and properties investigation of PMMA/silica composites derived from silicic acid. *Polymers for Advanced Technologies* **2009,** *20* (2), 84-91.

240. Cho, K.-Y.; Jung, H.-Y.; Choi, N.-S.; Sung, S.-J.; Park, J.-K.; Choi, J.-H.; Sung, Y.-E., A coated Nafion membrane with a PVdF copolymer/Nafion blend for direct methanol fuel cells (DMFCs). *Solid State Ionics* **2005,** *176* (39), 3027-3030.

CHAPTER THREE

3. Characterization techniques

This section summarizes various techniques which were used to characterized zirconium nanoparticles, nanofibers, nanotubes and nanocomposite membrane. The following techniques were used; Brunauer-Emmett-Teller (BET), X-Ray diffraction (XRD), Atomic force microscopy (AFM), Thermo-gravimetric analysis (TGA), Dynamic Light Scattering (DLS), Differential scanning calorimetry (DSC), Fourier Transform Infrared (FT-IR), Nano sizer and Zeta potential, Scanning Electron Microscopy (SEM), and Transmission electron microscopy (TEM).

3.1. Structural properties

3.1.1. The X-ray powder diffraction (XRD) analysis

X-ray diffraction provides information about the structure of the crystalline material. Since the atoms in a crystal are arranged as a regular array, so the X-ray wavelength is of the order of the spacing between the atoms and the planes. For crystals the diffraction which results from scattered x-rays by electrons is described by the Bragg's law. X-ray diffraction of a sample produces a pattern characterised by the reflections (peak intensity) at certain positions. XRD data provide information about crystalline size by using the Debye-Scherrer equation [1].

$$D = \frac{4}{3}\left(\frac{0.9\lambda}{B\cos\theta}\right) \quad (3\text{-}1)$$

D = diameter of the particle, λ = wavelength of the X-ray

B = full width of the half maximum of the peak, θ = Bragg's angle of diffraction.

3.1.2. Fourier transform infrared spectroscopy (FTIR)

Fourier transform infrared spectroscopy (FTIR) is a powerful tool used to determine the chemical structure of the sample. The sample information on FTIR is obtained by passing IR radiation through a sample and some of the FTIR radiation will be absorbed by the sample and some will be transmitted or reflected. The resulting spectrum will represent the molecular absorption and transmission, creating a molecular fingerprint of the sample. This makes FTIR spectroscopy useful for several types of analysis such as identifying unknown materials. The FTIR spectra will be obtained using a FT-IR spectroscopy (Vertex 70 Bruker FTIR instrument) as shown in Figure 3-1.

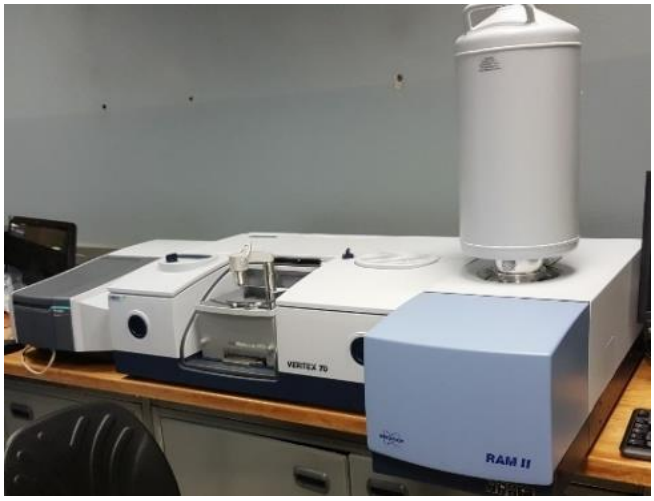

Figure 3- 1: Fourier Transform Infrared Spectroscopy.

3.1.3. Brunauer-emmett-teller (BET) surface area

The BET analysis provides precise specific surface area evaluation of materials by nitrogen multilayer adsorption measured as function of relative pressure using a fully automated analyzer. The technique encompasses external area and pore area evaluation to determine the total specific area in m^2/g yielding important in studying the effects of surface porosity and particle size in many applications. The BET analysis will be performed using Micrometrics 3-Flex instrument as shown in Figure 3-2. A dry sample will be evacuated of all gas and cooled to 77 K, using liquid nitrogen. A layer of inert gas physically adheres to the sample surface, lowering pressure in the analysis

chamber. The surface area will be calculated from the measured absorption isotherm of the experiment. Before analysis, all the samples will be out-gassed at 200-300 ^{o}C under vacuum for 2 hours. Test materials were out gassed to the pressure of 3×10^{-5} mbar for 2 hours at 470 K, prior to adsorption measurements. The measurements will be carried out on the synthesized powders. The particle size will be calculated by the Equation (3-2):

$$S = \frac{6}{\rho D_{BET}} x10^{3} \qquad (3\text{-}2)$$

Where ρ is the theoretical density of the materials which equal to 6.27 g/cm^{3} [2] and D_{BET} is the particle size in nm.

Figure 3- 2: Micrometrics 3-Flex instrument.

3.1.4. Dynamic light scattering (DLS) measurements

The dynamic light scattering was performed on the nanopowder and modified Nafion® to observe the particle-size distribution of zirconia nanoparticles.

3.2. Thermal and mechanical strength analysis

The thermal properties will be determined by Thermal gravimetric analysis (TGA) and Differential scanning calorimetry (DSC). TGA demonstrates thermal degradation of organic and inorganic components, while thermal transition behavior (glass transition) of nanocomposite membrane is obtained by DSC study. DMA and Tensile test analysis will be used to determine the mechanical stability of the membranes.

3.2.1. Thermo-gravimetric analysis (TGA)

Thermal gravimetric analysis (TGA) measurement was performed on the nanopowder, nanofibers and modified Nafion® membrane as well as on the plain Nafion® membrane to observe the weight losses due to the temperature. TGA data was obtained with PerkinElmer instrument.

3.2.2. Tensile test

The uniaxial mechanical properties of membranes were captured using a uniaxial testing system. The length, width and thickness of samples were measured using a Vernier calliper and recorded prior to testing. The testing area of the membrane samples were 4 mm x 10 mm in dimension. To allow clamping area, the samples were prepared in such a way that they will be clamped both sides and still allow the testing area to be 4 mm x 10 mm. The thicknesses of the membrane were measured with digital micrometres. Each thickness was measured in the average of 3-7 reading at different positions of the membrane and was repeated twice on each membrane in order to obtain the average value. The thickness of the nanocomposite membrane was used in analysing the stress applied to the sample. The membrane was soaked in water for 24 hours and tested as wet test. Then the membrane was dried in a vacuum oven at 80 °C for 24 hours and tested as dry test. The tensile strength of membranes was measured using CellScale Ustretch device dried at 25 °C and wet at 34 °C and actuator speed of 5 mm per min.

3.2.3. Atomic force microscopy (AFM)

AFM is a powerful technique that allows imaging of almost any type of surface. It will be used to measure and localize many different forces including adhesion strength, magnetic forces, and mechanical properties. AFM is operated in two basic modes, i.e., contact and tapping modes. In contact mode the AFM tip is in contact with the surface continuously. Whereas in tapping mode the AFM cantilever is vibrated above the sample surface so that the tip is only in contact with the surface intermittently.

3.3. The morphological properties

The morphological properties were determined by Scanning electron microscopy (SEM) and Transmission electron microscopy (TEM).

3.3.1. Scanning electron microscopy (SEM)

Scanning electron microscopy (SEM) was used to observe the morphological properties of nanocomposite membranes, nanofibers and nanoparticles. SEM samples will be prepared by placing some of the nanoparticle materials onto an aluminum stub using adhesive carbon tape. The samples were sputter-coated with gold or carbon under vacuum before SEM observations to prevent charging effects inside the microscope. The composite membranes were cut into small pieces under liquid nitrogen and their cross-section will also be sputtered with gold before analysis.

3.3.2. Transmission electron microscopy (TEM)

It makes it possible to image nanoparticles, determine their particle size, shape and statistical analysis of the size and shape distribution. The high resolution of TEM is due to use of high energy electron beam, during analysis. TEM does have some limitations such as alteration of the sample exposed to electrons, but its ability to image any kind of material and high resolution imaging, shadows this limitations when it comes to nanoparticles [3].

3.4. The membrane properties

3.4.1. Proton conductivity measurement

The conductivities of nanocomposite membranes and commercial Nafion® membrane were measured in a a four-point probe conductivity cell as shown in Figure 3-3. The ionic conductivity was determined galvanostatically with a current amplitude of 0.1 mA over frequencies ranging from 1MHz to 10Hz. Using a Bode plot, the frequency region over which the impedance had a constant value was checked and the electrical resistance was then obtained from a Nyquist plot [4]. The ionic conductivity (σ) was calculated according to the following equation:

$$K = L/RWd \qquad (3\text{-}3)$$

where R is the obtained membrane resistance, L is the distance between potential-sensing electrodes (1 cm), W and d are the width (2 cm) and thickness of the membrane respectively. For conductivity testing, the membrane was immersed in 1M sulfuric acid solution for 6 hours at room temperature. The membrane was then rinsed with deionized water several times to remove any excess H_2SO_4 and then immersed in deionized water for 6 hours at 60 °C. All membranes were kept in deionized water at room temperature before conductivity testing measurement.

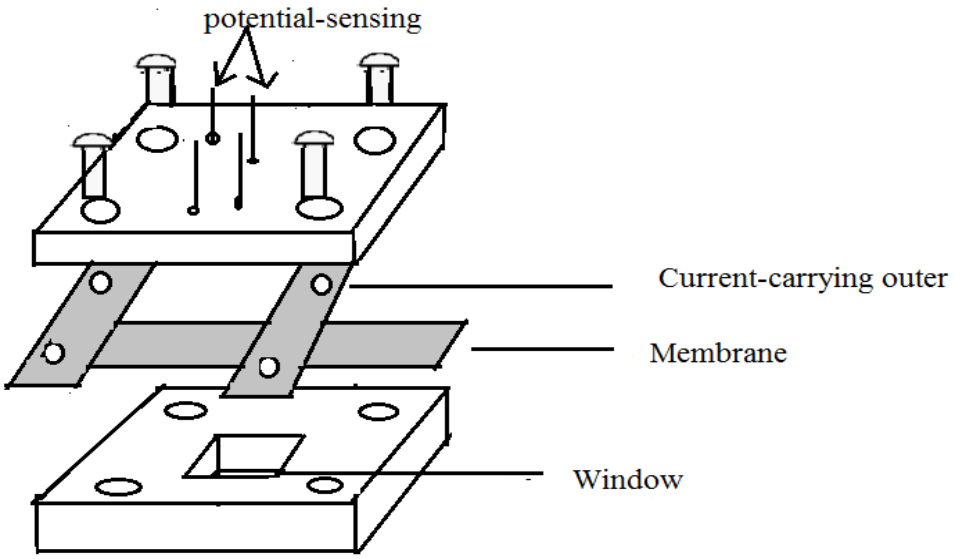

Figure 3- 3: Schematic diagram of proton conductivity cell for four-point-probe electrochemical impedance spectroscopy technique.

3.4.2. Methanol permeability

The methanol permeability was performed with a permeation-measuring cell designed in our lab that consisted of two compartments. The membrane was mounted between the two compartments and the diameter of the diffusion area was 3.5 cm. One of the compartments (A) was filled with 50 mL of methanol solution and the other compartment (B) was filled with 50 mL of distilled water as shown in Figure 3-4. The solutions were prepared in 2M and 5M methanol and the results collected at 30 ºC, 60 ºC and 80 ºC for comparison. The methanol concentration in compartment B was monitored with a methanol concentration sensor. The output signal was converted using a data module and recorded on a personal computer. Methanol permeability (P) was obtained by means of the following relationship:

$$C_B = \frac{A\,P}{V_B\,L}\,C_A\,(t - t_0) \qquad (3\text{-}4)$$

where C_A is the initial methanol concentration in compartment A; $C_B(t)$ the methanol concentration in compartment B at diffusion time t; V_B the volume of distilled water in compartment B; L the thickness of the membrane; and A is the effective permeating area.

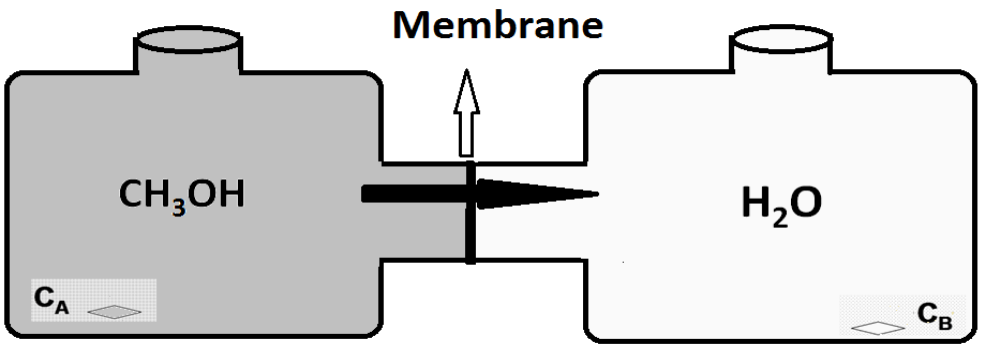

Figure 3- 4: Schematic representation of the experimental setup for the determination of the methanol permeability across the membranes.

3.4.3. Water contact angle measurements

The hydrophilicity of the membrane surfaces was performed under contact angles measurement instrument equipped with a video system. Membranes were cut into strips and mounted on glass slides for analysis. The droplet of de-ionized water (0.16 µL) was dropped onto the surface of membranes at ambient temperature by placing the tip of the syringe close to the sample surface with all the images been captured using a camera. The measurement was repeated 10 times at different surface of membrane to obtain an average value. Before the water droplet attached to the sample surface, the wetting process was recorded until no significant change at the surface was observed any more [5].

3.4.4. Water uptake measurements

The membranes were immersed in deionized water for 24 hours, blotted with a paper towel and then measured as wet mass percentage. The membranes were dried in a vacuum oven at 80°C for 24

hours and then was measured. The water uptake of the nanocomposite membranes and recast Nafion® membrane were calculated from the equation:

$$\boldsymbol{Wup}(\%) = \frac{(\boldsymbol{Mwet - Mdry})}{\boldsymbol{Mdry}} * \mathbf{100} \quad (3\text{-}5)$$

where W_{up} is the percentage of water uptake, m_{wet} is the weight of wet membrane and m_{dry} is the weight of the dried membrane.

3.4.5. Swelling measurements

The swelling of the membranes was determined by measuring changes of the membrane length upon equilibrating in water. Determination of linear expansion is an effective method to interpret the swelling [6]. Swelling ratio were calculated according to the equations below:

$$\boldsymbol{SR}(\%) = \frac{(\boldsymbol{L_w - L_d})}{\boldsymbol{L_d}} \boldsymbol{x100} \quad (3\text{-}6)$$

where L_w and L_d are the lengths of wet and dry membranes.

3.4.6. Hydration number (λ)

The water uptake of PEM is often expressed by the hydration number (λ) which is a useful parameter for conductivity and transport modelling. The hydration number is defined as the number of water molecules per conducting functional group: The number of water molecule per sulfonic acid group, λ, was calculated by following equations below [7]

$$\lambda = \frac{\boldsymbol{WU}}{\boldsymbol{IECx\ 100x18}} \quad (3\text{-}7)$$

3.4.7. Ion exchange capacity (IEC)

The ion exchange capacity (IEC) is defined as the ratio between the numbers of the surface ion organic groups (in mmol) and the weight of the dry materials [8]. The titration technique will be used to determine the IEC of the membranes. Firstly, the membrane will be dried at 60 °C for 24 hours and measure the weight. The dried membranes in the proton form (H^+) will be immersed in 60 ml of 1 M NaCl at 50-60 °C for 24 hours to exchange the H^+ ions with Na^+ ions. Then, the 60 ml of H^+ ions solution will be titrated with a 0.01 M NaOH solution using phenolphthalein as the endpoint indicator [9]. The titrated IEC of the membranes were determined by:

$$\mathbf{IEC} = \frac{\mathbf{V_{NaOH}\ X\ C_{NaOH}}}{\mathbf{W_{sample}}} \qquad (3\text{-}8)$$

where V_{NaOH} is the titrated volume of NaOH and W_{sample} is the weight of the dry membranes.

3.4.8. Preparation of membrane electrode assembly (MEA) and fuel cell testing

The MEA was prepared by using 20% Pt Vulcan XC-72R in Nafion® solutions for ink preparation and Pt in Carbon cloth. The prepared ink was brushed onto the carbon cloth on the cathode side. The 2 mg/cm^2 of catalyst was loaded onto the anode and cathodes of the Nafion®-PAN/Zr nanofiber, the Nafion®-PAN/ZrP nanofiber and the Nafion®- PAN/ZrGO nanofiber membranes without hot pressing, resulting in assembly membrane electrode assemblies (MEAs). The membrane assemblies thus obtained were tested at galvanostatically in open air to measure their cell potential as a function of current density. It was passed on 2 M of methanol solution mixed with 2 M of Potassium hydroxide (KOH).

3.5. References

1. Borchert, H.; Shevchenko, E. V.; Robert, A.; Mekis, I.; Kornowski, A.; Grübel, G.; Weller, H., Determination of nanocrystal sizes: a comparison of TEM, SAXS, and XRD studies of highly monodisperse CoPt3 particles. *Langmuir* **2005,** *21* (5), 1931-1936.
2. Reed, J. S., Principles of ceramics processing. **1995**.
3. Javadpour, F., Nanopores and apparent permeability of gas flow in mudrocks (shales and siltstone). *Journal of Canadian Petroleum Technology* **2009,** *48* (08), 16-21.
4. Wu, L.; Zhou, G.; Liu, X.; Zhang, Z.; Li, C.; Xu, T., Environmentally friendly synthesis of alkaline anion exchange membrane for fuel cells via a solvent-free strategy. *Journal of Membrane Science* **2011,** *371* (1), 155-162.
5. Yu, H.; Ziegler, C.; Oszcipok, M.; Zobel, M.; Hebling, C., Hydrophilicity and hydrophobicity study of catalyst layers in proton exchange membrane fuel cells. *Electrochimica Acta* **2006,** *51* (7), 1199-1207.
6. Affoune, A. M.; Yamada, A.; Umeda, M., Conductivity and surface morphology of Nafion membrane in water and alcohol environments. *Journal of Power Sources* **2005,** *148*, 9-17.
7. Yang, A. C.; Narimani, R.; Zhang, Z.; Frisken, B. J.; Holdcroft, S., Controlling crystallinity in graft ionomers, and its effect on morphology, water sorption, and proton conductivity of graft ionomer membranes. *Chemistry of Materials* **2013,** *25* (9), 1935-1946.
8. Fu, R.-Q.; Woo, J.-J.; Seo, S.-J.; Lee, J.-S.; Moon, S.-H., Covalent organic/inorganic hybrid proton-conductive membrane with semi-interpenetrating polymer network: preparation and characterizations. *Journal of Power Sources* **2008,** *179* (2), 458-466.
9. Dimitrova, P.; Friedrich, K.; Stimming, U.; Vogt, B., Modified Nafion®-based membranes for use in direct methanol fuel cells. *Solid State Ionics* **2002,** *150* (1), 115-122.

CHAPTER FOUR

4. Synthesis of zirconia oxide nanoparticles and Polyacrylonitrile/zirconium phosphate (PAN ZrP) nanofibers

This Chapter presents the three scientific papers summary in the following sections

Presents the results from the paper**: "Effect of synthesis temperature on particles size and morphology of zirconium oxide nanoparticle".** Journal of Nano Research 50 (2017)18.

Presents the results from the paper: "**The synthesis, characterization and electrochemical study of zirconia oxide nanoparticles for fuel cell application"**. Journal of Physica B. (Accepted 2019)

Presents the results from the paper: "**Structural morphology of blended Nafion®-Polyacrylonitrile/zirconium phosphate nanofibers**". International Journal of Mechanical and Materials Engineering 14(1) (2019) 2.

A: Effect of synthesis temperature on particles size and morphology of zirconium oxide nanoparticle

4.1. Introduction

ZrO_2 nanomaterial in the form of spheres, rods and cubes with a high specific surface area at the present time is very attractive material in many applications such as fuel cell electrolytes, catalysts, buffer layers for superconductor growth, oxygen sensor, damage resistant, optical coatings and gate dielectric [1]. The ZrO_2 nanomaterial is also known as a wide band gap p-type semiconductor that exhibits abundant oxygen vacancies on its surface [2]. Additionally, it has very good transparency on a broad spectral range [3], a great chemical stability and a threshold of resistance to high laser flow. Zirconia is known to be crystalline in three phases which crucially depend on the change of temperature; monoclinic (1170 °C), tetragonal (2370 °C) and cubic (2680 °C) [4]. Hence, these high temperature phases of cubic and tetragonal with excellent chemical resistance, mechanical and thermal stability and oxygen ion conductivity are normally found more stable at high temperatures [5].

So far, the tetragonal and cubic phases tended to transform the monoclinic phase at ambient temperature [6], which resulted in sample crack. When this phase stabilized under lower temperature, it was found to be good for applications in chemical engineering [4].

Many researchers have shown great interest in developing methods to stabilize these high-temperature phases, using dopants such as yttria (Y_2O_3), magnesia (MgO) and calcia (CaO) [7] or reducing the particle size into nanometre [8-9]. The stabilization by size reduction method has attracted many researchers due to their higher porosity and specific surface area that promotes adsorption. The room temperature thermal stabilised tetragonal ZrO_2 with excellent mechanical and electrical properties, such as fracture toughness, high strength and hardness has been used in structural ceramic [10]. However, other researchers have succeeded in preparing the tetragonal form of zirconia at low temperature, which does not transform to the monoclinic phase [11]. It has been reported that stabilised tetragonal phase was obtained at ambient temperature by aging the ZrO_2 nanoparticles in its mother liquor [12]. Furthermore, stabilised tetragonal zirconia exhibits a high toughness which makes it suitable to be used in dental and orthopaedic fields [13-14]. Similarly, stabilized cubic phase at a lower temperature has mainly been used in solid oxide fuel cells (SOFCs) applications due to high oxygen ionic conductivity and chemical stability [15]. Some researchers have found that synthesis of stabilized tetragonal and cubic phase zirconia nanoparticles in their nano-size form, play an important role in enhancing their diffusivity, strength and ductility [16], which is very important in the modification of membrane for fuel cell application. The modification of membrane with this nano-size material also has an impact on increasing its porosity with ultra-thin separation layer because of their small diameter. Depending on nano-size crystalline structure, it can be used in many zirconia-based devices [17]. Moreover, the semiconductor particles obtained in the form of nano-size, have attracted many researchers because of their atom-like size-dependent properties that make them suitable for insignificants application [18]. Many ZrO_2 applications require high surface area which should remain stable under process conditions. But it has a significant shortage as the specific surface area of ZrO_2 is usually much smaller compared to other similar catalysts, such as alumina

or silica [19], as it disappears when calcinated at high temperatures. For further enhancement of specific surface area and its crystallinity, the ZrO_2 was aged for 24 hours at varied temperatures. Numerous experiments with different temperatures were conducted in order to produce ZrO_2 nanoparticles with high specific surface area and narrow pore size distribution as it is important in the modification of Nafion® membrane, to enhance the thermal stability. The main aim of this work is to obtain zirconia nanoparticles with a high surface area and high porosity with a different morphology through simple precipitation method, which will be used in preparation of modified Nafion® nanocomposite membrane to be applied in fuel cells. The addition of zirconia oxides in the membrane has been found to improve permeability and fouling resistance by either changing the pore structure or increasing the hydrophobicity of membrane.

4.2. Experimental

4.2.1. Reagents

Zirconium oxychloride hydrate (Sigma Aldrich), sodium hydroxide pellets (Sigma Aldrich) and silver nitrate (Sigma Aldrich). All the chemicals were used as received, without any further purification.

4.2.2. Synthesis of ZrO_2 nanoparticles

The ZrO_2 nanoparticles were prepared by precipitation method where zirconium oxychloride hydrate ($ZrOCl_2 . 8H_2O$) and sodium hydroxide (NaOH) were used as starting materials. 0.2M $ZrOCl_2.8H_2O$ was prepared in a 250 ml beaker and 2N NaOH solution was added dropwise with continuous stirring for 45 minutes at room temperature (RT). Obtained precipitate was divided into six parts; one part was filtered and washed several times with distilled water until chlorine ions (Cl^-) were not detected by the silver nitrate ($AgNO_3$). The precipitate was dried at 100 °C for 24 hours, calcinated at 600 °C for 4 hours and then labelled as Zr-0. The remaining parts of the solution were aged at 50 °C, 80 °C, 100 °C, 120 °C and 150 °C temperatures respectively for 24 hours. The solution was then filtered,

washed and calcinated according to the procedure followed for part one. The samples were labelled as follows: Zr-50, Zr-80, Zr-100, Zr-120 and Zr-150.

4.2.3. Characterisation techniques

The XRD analysis was performed using a Philips X-ray automated diffract meter with a Cu K radiation source. Samples were scanned in a continuous mode from 10°-90° (2 theta) at a scanning rate of 0.026 (degree)/1 (sec). The thermal properties of the samples were studied by thermal gravimetric analysis (TGA) under nitrogen flow. TGA data was obtained with model STA (Simultaneous Thermal Analyzer) 1500 (Rheometric Scientific Ltd, UK), over nitrogen and at a heating rate of 10°C/min from 50 °C to 1000 °C. A Bruneau-Emmett-Teller (BET) surface area instrument (Micromeritics Accelerated SA and Porisimetry (ASAP) 2010 system) was used to determine information such as gas uptake, micropore volume (t–plot method), and pore size distribution via adsorption and desorption isotherms. In a BET surface area analysis, a dry sample was cleared of all gas and cooled to 77 K, using liquid nitrogen. The matrix surface and cross-section of the synthesized nanopowder morphology were investigated by means of a scanning electron microscope. SEM images were obtained on a Hitachi x650. Electronic techniques are based on the interaction of the sample with electrons, which results in a secondary effect that is detected and measured**.** TEM in a Leo 912 electron microscope was used to estimate their particle size and observe the morphology. FT-IR spectroscopy was used to determine the quality and composition of the sample. FT-IR spectra was obtained with a Perkin-Elmer Paragon 1000 FT-IR instrument over a range of 4000-500 cm^{-1} and a resolution of 4 cm.

4.3. Results and discussion

4.3.1. Structure analysis

In order to observe the effect of synthesis temperature on the phase structure of zirconia nanoparticles, the XRD measurements of Zr-0, Zr-50, Zr-80, Zr-100, Zr-120 and Zr-150 were respectively performed, as shown in Figure 4-1(a-f). The XRD results in Figure 4-1 clearly revealed the presence of monoclinic phase of zirconia that corresponds to (JCPDS card no. 00-037-1484) and cubic phase of zirconia that corresponds to (JCPDS No. 65-1022). It was also observed that all XRD patterns have broad peaks, which indicate the nanometre characteristics of zirconia particles. The XRD results of Zr-0 in Figure 4-1(a) observed to have a mixture of cubic and monoclinic phases, with diffraction angles of 30.2°, 35.2°, 50.5°, 60,1°, 74.2° and 82.5° corresponding to planes (1 1 1), (2 0 0), (2 2 0), (3 1 1), (4 0 0), (3 3 1) of the cubic phase and a diffraction angle of 31.7°, 41.5° and 45.5°corresponding to planes (1 1 1), (1 0 2), (1 1 2) of the monoclinic phase. The results that were obtained show that the reaction temperature has an effect on the crystallite phase of zirconia nanoparticles. This was observed on the XRD pattern obtained in Figure 4-1(a), which was completely different from those prepared at various temperatures as shown in Figures 4-1(b-f). Figures 4-1(b) to (e), show that when the temperature was raised from 50 °C to 120 °C, only a single cubic phase appeared, with diffraction peaks in the spectra indexed as cubic (arkelite) with lattice constants a = 0.51291 nm, b = 0.51291 nm, c = 0.51291 nm, and β = 90.0^{o}. The main peaks at 2theta are 30.2°, 35.2°, 50.6°, 60.2°,74.2°, 82.5° and 94.1°, which correspond to planes (1 1 1), (2 0 0), (2 2 0), (3 1 1), (4 0 0), (3 3 1), and (4 2 2) [20-21]. This may be due to high synthesis temperature of ZrO_2 which stabilises the high temperature phases at room temperature if the crystallite size is below a critical size [9], which is associated with reduced total energy of the system due to the inherent high surface energy of the nanoparticles [22]. In the cubic phase of zirconia, vacancies increase and improve the diffusion of oxygen ions as the primary charge carriers elevate the electrical conductivity [23]. From these results it can be deduced that increasing synthesis temperature favoured structural growth. The influence of synthesis temperature on the morphology and stabilisation of the phase

was discussed by Adamski et al. [24]. Figure 4-1(f) shows that heating Zr(OH) solution at the synthesis temperature of 150 ˚C lowers the particle size to nano-diameter with the influence of the monoclinic phase that provides a more versatile surface than the cubic and tetragonal phases due to a less symmetrical lattice [25]. The XRD pattern in Figure 4-1(f) shows the same crystalline of zirconia nanoparticle synthesis under 150 °C, which was completely transformed to a monoclinic structure with broadening sharp peaks of m-ZrO_2 at a diffraction angle of 14.2°, 23.4°, 30.4°, 35.1°, 50.6°, 60.1°,74.0° and 82.4° corresponding to planes (1 0 0), (1 1 0), (1 1 1), (0 2 0), (3 0 0), (1 3 1), (4 1 1) and (4 2 0).

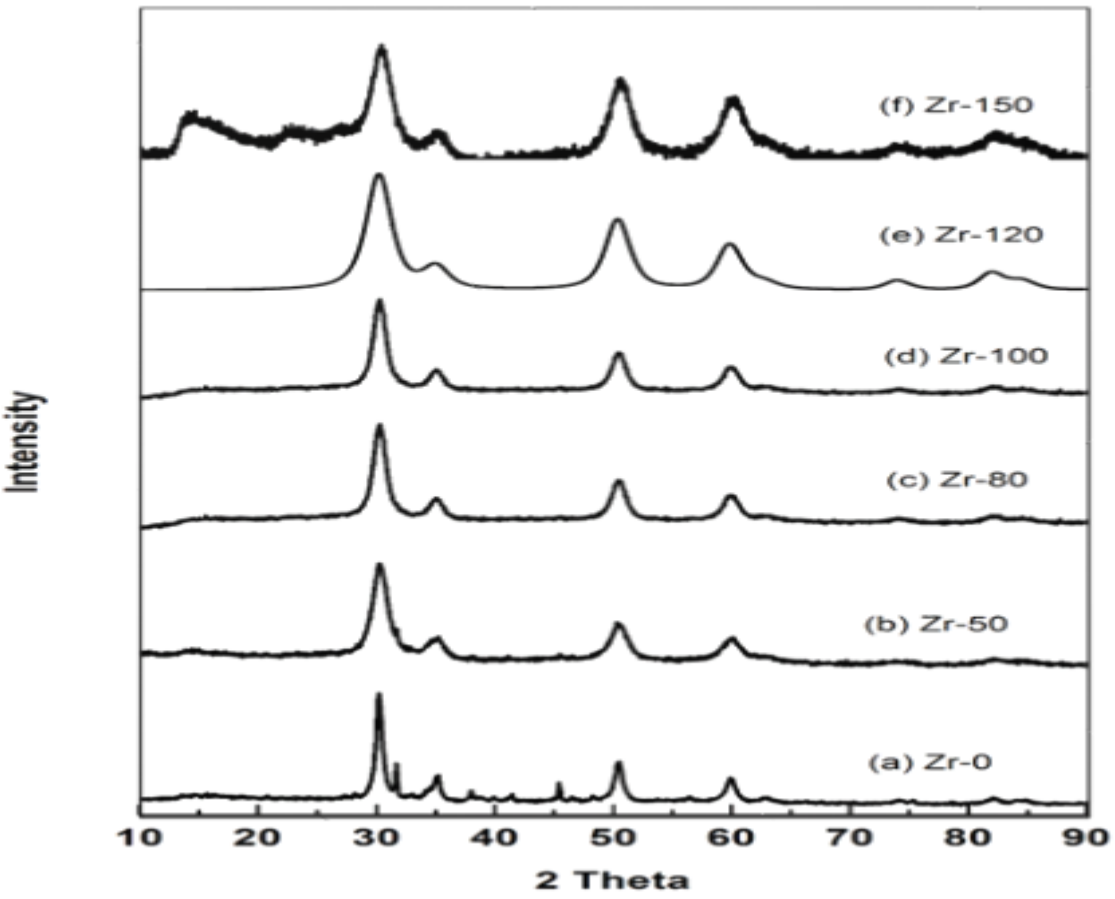

Figure 4- 1: The comparison of the XRD patterns of the ZrO_2 nanoparticles at the different temperatures of (a) Zr-0, (b) Zr-50, (c) Zr-80, (d) Zr-100, (e) Zr-120 and (f) Zr-150.

4.3.2. FTIR spectrum of ZrO_2 nanoparticles

In order to observe the effect of temperature on the molecular nature of Zr-0, Zr-50, Zr-80, Zr-100, Zr-120 and Zr-150 nanomaterial, Fourier transform infrared spectroscopic (FTIR) spectra were measured in Figure 4-2(a-f). Figure 2(a) shows vibration bands at 569 cm^{-1} and 853 cm^{-1} which are assigned to Zr-O bond vibrations [26-27]. The peaks observed at 1180 cm^{-1}, 1443 cm^{-1} and 1380 cm^{-1} are assigned to O-H stretching vibration [28]. The broad feature around 1684 cm^{-1} seems to occur due to adsorbed water deformation mode region and 3450 cm^{-1} is attributed to stretching of O-H groups, characteristic of a highly hydrated compound. It can be noted that the 569 cm^{-1} peak of Zr-O vibrations on the Zr-0 [29], has disappeared in the high temperature synthesis samples. Figure 4-2(b) shows vibration bands at 685 cm^{-1} and 863 cm^{-1} which are assigned to Zr-O [26-27] bond vibrations. The symmetric frequencies of Zr-OH were observed at 1072 cm^{-1} and 1398 cm^{-1} [28]. The characteristic peaks observed at 2962 cm^{-1} and 2462 cm^{-1} are due to the presence of inorganic ions. The frequencies observed in Figure 4-2(c) at 863 cm^{-1} and 926 cm^{-1} are due to the Zr-O vibration [27]. The peaks at 1393 cm^{-1} and 1434 cm^{-1} are assigned to O-H bonding, the peak observed at 2346 cm^{-1} is due to the presence of inorganic ions. Figure 4-2(d) shows the vibration bands at 846 cm^{-1} and 916 cm^{-1} due to the Zr-O vibrations [27]. The peaks at 1367 cm^{-1} and 1447 cm^{-1} correspond to O-H bonding. The peaks in the region of 1554 cm^{-1} and 1660 cm^{-1} may be due to the adsorbed moisture and the peak in the 3456 cm^{-1} region is attributed to O-H stretching of nanomaterials [29-30]. The FTIR-reflectance spectrum of the Zr-120 sample in Figure 4-2(e) presented cubic phase at 2338 cm^{-1}, which appears at temperatures near 600 ˚C [31]. Figure 4-2(f) shows the vibration bands at 930 cm^{-1} due to the Zr-O vibration [27], the peak of 1371 cm^{-1} corresponds to O-H bonding, peaks in the region of 1536 cm^{-1} and 1634 cm^{-1} may be due to the adsorbed moisture and in the 3390 cm^{-1} region it is attributed to O-H stretching of nanomaterials [29-30].

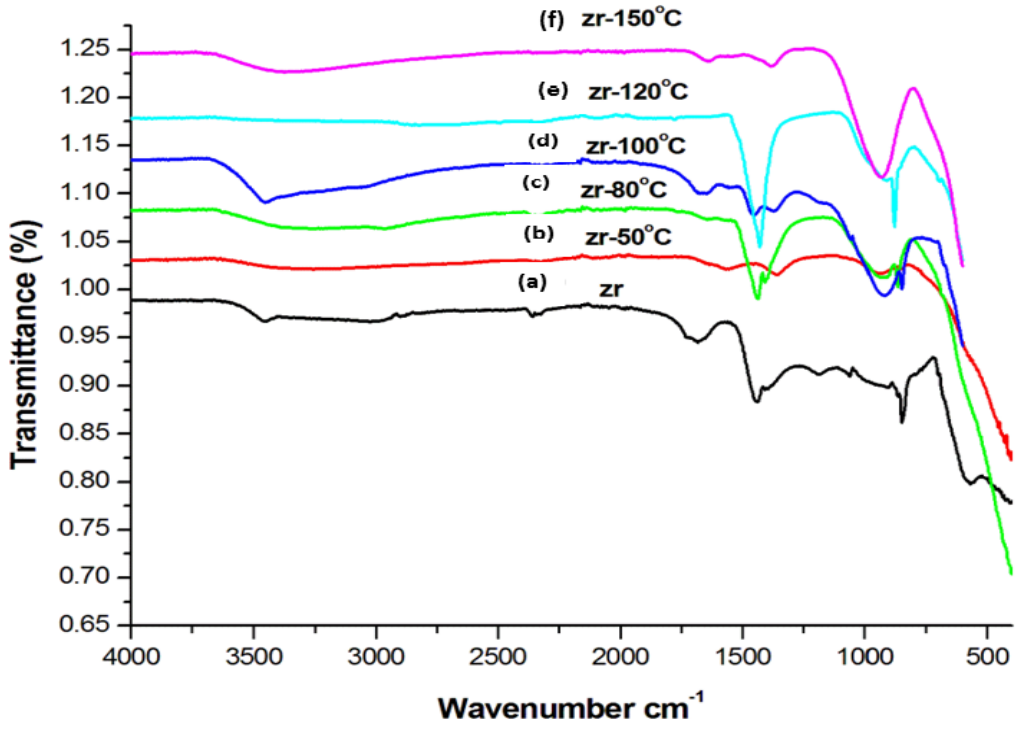

Figure 4- 2: The comparison of the FTIR curves of the ZrO_2 nanoparticles at the different temperature (a) Zr-0, (b) Zr-50, (c) Zr-80, (d) Zr-100, (e) Zr-120 and (f) Zr-150.

4.3.3. Scanning electron microscopy (SEM) analysis

In order to observe the effect of synthesis temperature on the morphology of zirconia nanoparticles, Zr-0, Zr-50, Zr-80, Zr-100, Zr-120 and Zr-150 samples were compared. In Figure 4-3, it was observed that zirconia nanoparticles prepared at different temperatures resulted in different morphologies in SEM micrographs. Figure 4-3(a-f) shows that ZrO_2 nanoparticles can resemble different shapes when the synthesis temperature is increased from room temperature to 150 °C. The SEM images were taken at a high magnification scale bar of 100 nm and 1µm of the ZrO_2 nanoparticles. It was observed in Figure 4-3(a) that many nanoparticles were aggregated in the form of irregular shaped nanoparticles and mixed with little nanorod structures. Figure 4-3(b) shows that zirconia nanoparticles consist of small particles agglomerated in the form of nanorods with irregular shapes. This agglomeration occurred due to the formation of unstable and ultrafine nuclei that have a strong

tendency to be stable when agglomerated. Figure 4-3(c) shows less agglomeration compared to Zr-0 nanoparticles. This may be due to a higher temperature reaction than at room temperature, which increases the rate of collisions between the charged particles [32]. These collisions also introduce the charge to the particles so that they repel one another. In addition, the higher temperature reaction enhances the dissolution and re-precipitation of material, which helps in strengthening the network of particles [32]. The agglomeration in the nanoparticles was assembled in the form of flower-like nanostructures composed of nanoparticles. From Figure 4-3(d), it can be seen that increasing temperature to 100 ˚C transforms the flower-like shapes into a mixture of nanorods and cube-shaped nanoparticles with narrow size distribution. It can be observed that nanocubes aggregate in one direction while the nanorods aggregate on top. These observations indicate the possibility of formation of nanorods or nanocubes shaped by increasing the reaction temperature up to 100 ˚C. The formation of the nanorods could result from the crystallographic orientations which are joined by a planar interface to form a larger particle. Therefore, to obtain an appropriate and uniform size and morphology, the optimal temperature obtained at 150 ˚C, is important. To understand the influence of temperature on the morphology, several experiments were carried out on the basis of temperature variables. When the temperature increased, homogenous nanoparticles were obtained. According to Figure 4-3(e), it was found that the sample is composed of a mixture of irregular and rod-like nanostructures. The temperature increases to 150 ˚C has major effects on the morphology and surface area of the zirconia nanostructures. Figure 4-3(f) shows the SEM images of Zr-150 composed of nanospheres that is useful in fuel cell electrolytes, oxygen sensors and gate dielectrics [33]. Generally, the SEM images indicate that the morphologies and particle sizes of zirconia nanostructures change with increases in synthesis temperatures. During higher temperature reaction, all the excess precipitate (cations and anions) dissolves and reacts with the hydrous oxides which affect the morphological properties of the material [32].

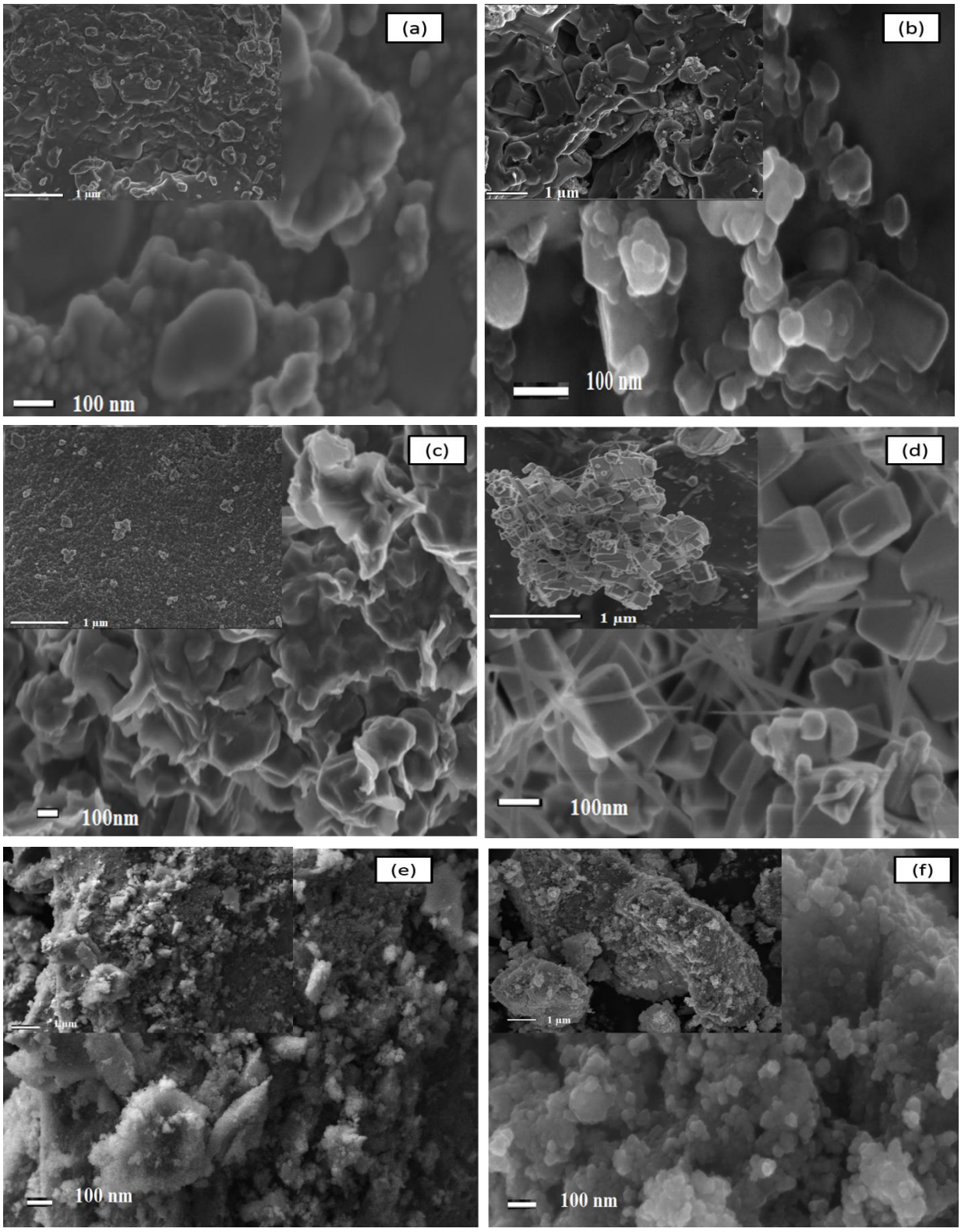

Figure 4- 3: Scanning Electron Microscopy (SEM): (a) Zr-0, (b) Zr-50, (c) Zr-80, (d) Zr-100, (e) Zr-120 and (f) Zr-150.

4.3.4. Transmission electron microscopy (TEM)

The transmission electron microscope (TEM) was used to confirm the phase structure and particle size of zirconia nanoparticles. TEM images of Zr-0, Zr-50, Zr-80, Zr-100, Zr-120 and Zr-150 as indicated (Figure 4-4), show that all the nanomaterials obtained were in nanometre size. Figure 4-4(a) shows agglomerated nanoparticles in the form of nanospheres and nanorod-like shapes with an average size of 10 nm and 20 nm, respectively. TEM analysis revealed more crystalline particles and a reduction in particle size of zirconia nanoparticles as shown in Figure 4-4 (b-f). Figure 4-4(b) shows that the particle size of zirconia nanoparticles ranges from 7-15 nm with less agglomeration. Figure 4-4(c) shows that the nanoparticles have nanospherical shapes with the particle size ranging from 5-15 nm. Figure 4-4(d-f), shows that the formation of pure nanocrystalline ZrO_2 and particle size reduction are highly affected by higher reaction temperature within the specified period. It can be observed in Figure 4-4(d-f), that increasing synthesis temperature to 100 °C, 120 °C and 150 °C can lead to very small nanoparticles of 2 nm. We have found that higher temperature reactions have an effect on the size reduction of zirconia nanoparticles, which will be a filler in Nafion membrane. This nanometer size of zirconia nanoparticles as a filler in membrane was found to have a significant effect on the proton conductivity and methanol permeability of composite membrane; more so than those having bigger nanoparticle sizes [34]. The observed crystallite size is much smaller than the reported average particle size of 4.45 nm [35]. The size reduction was also confirmed by HR-TEM atomic structure shown in Figure 4-5. Figure 4-5(a-f) shows that the HR-TEM image of Zr-0, Zr-50, Zr-80, Zr-100, Zr-120 and Zr-150 are clearly presented in well-resolved equidistant lattice fringes. The distance between the fringes was calculated to be 0.2891 nm and 0.2922 nm which can be attributed to the interplanar spacing corresponding to (111) plane of monoclinic and cubic ZrO_2 [36-37]. This HR-TEM results are in agreement with the XRD results discussed above that the monoclinic and cubic phases are attributed to the d-spacing corresponding to (111).

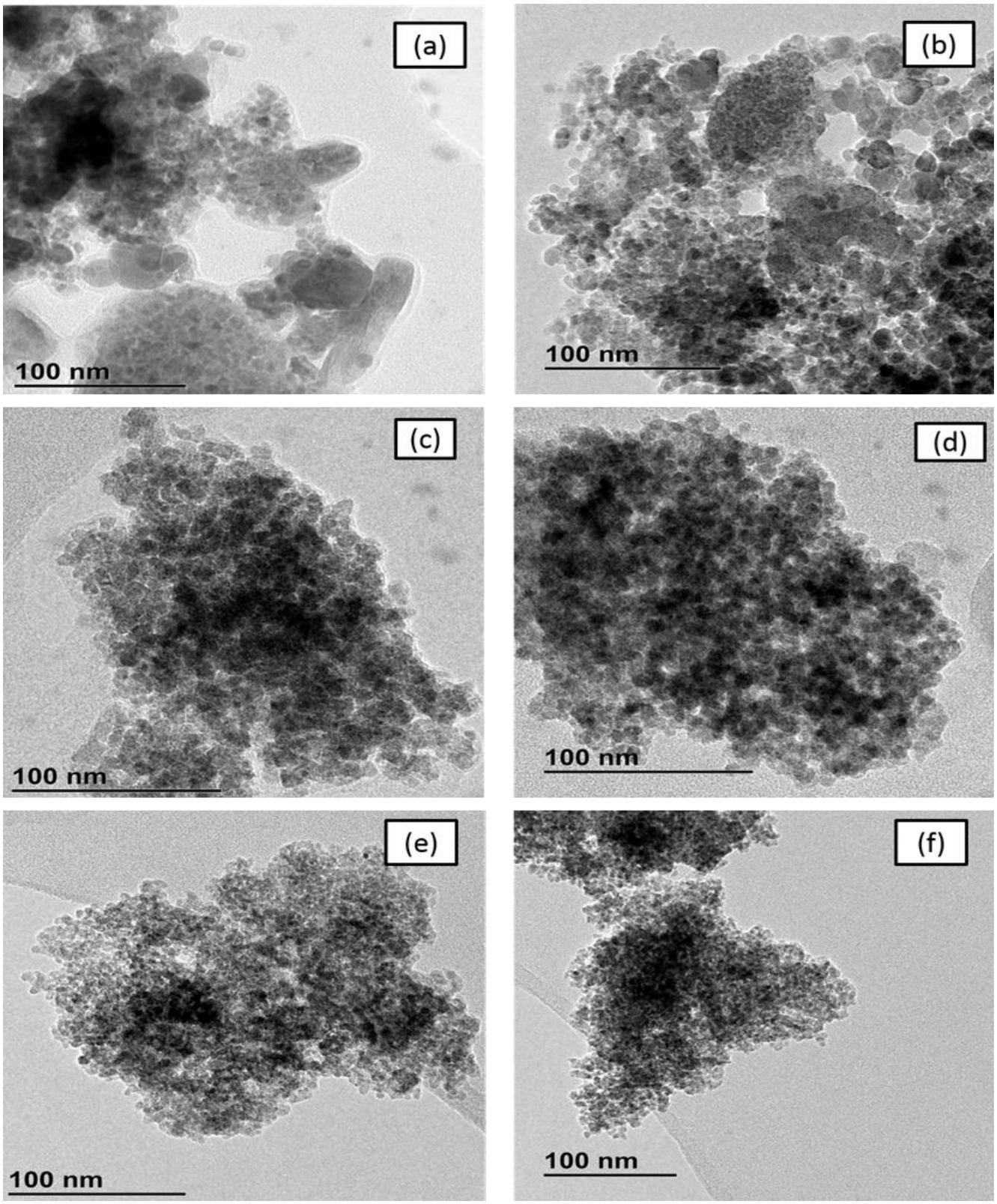

Figure 4- 4: TEM image of the ZrO_2 nanoparticles: (a) Zr-0, (b) Zr-50, (c) Zr-80, (d) Zr-100, (e) Zr-120 and (f) Zr-150.

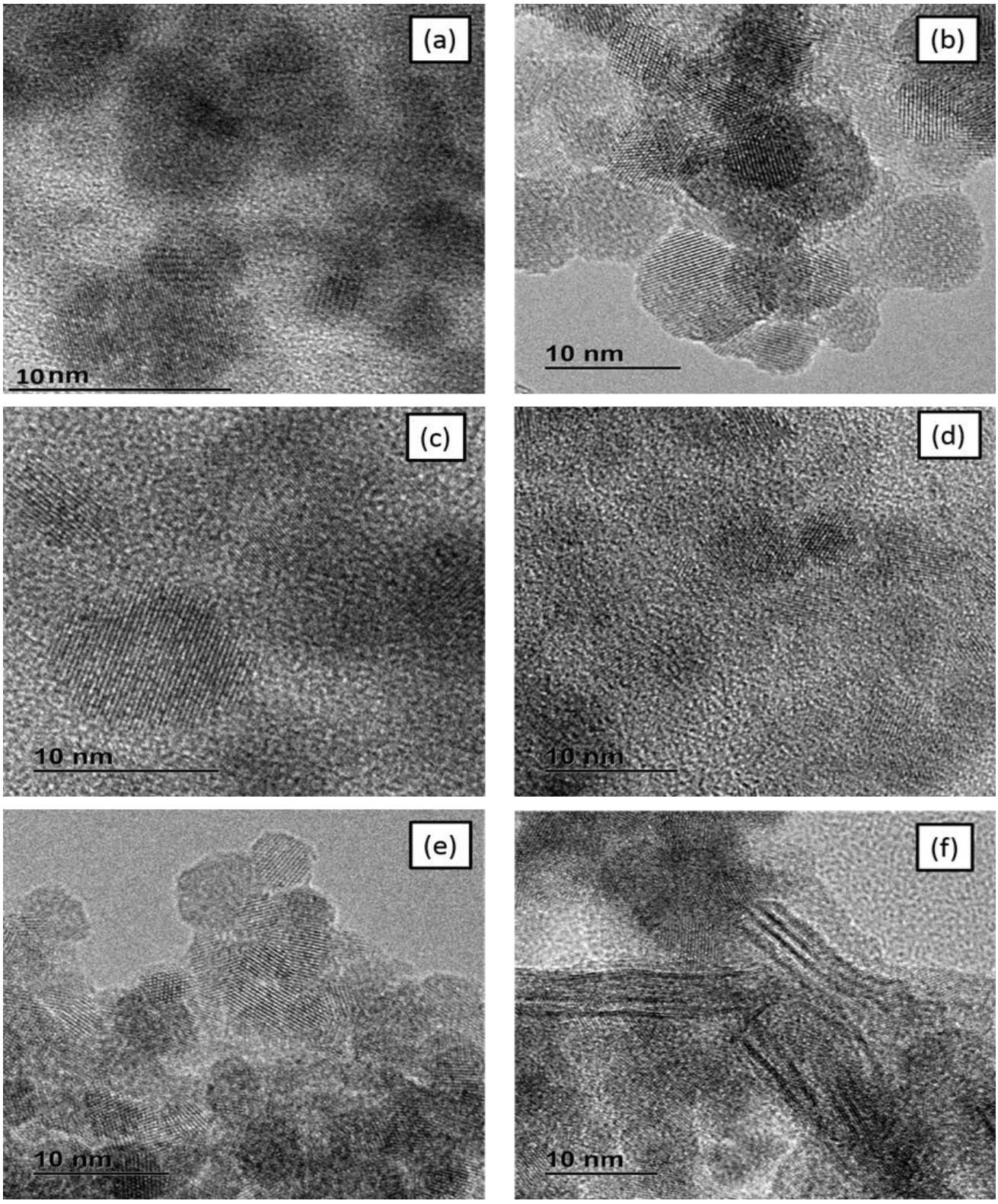

Figure 4- 5: HR-TEM image of the ZrO_2 nanoparticles: (a) Zr-0, (b) Zr-50, (c) Zr-80, (d) Zr-100, (e) Zr-120 and (f) Zr-150.

4.3.5. Thermo-gravimetric analysis (TGA)

The thermal stability of the zirconia nanoparticles was studied by thermo-gravimetric analysis (TGA) as show in Figure 4-6. Figure 4-6(a) indicates that the thermal decomposition process occurs in three stages. The TGA curve of Zr-0 results shows that the thermal decomposition occurs initially between 20 °C and 100 °C, with mass loss of 5 % associated with the removal of absorbed water. The second weight loss occurred between 100 °C and 600 °C and this is due to the removal of terminal hydroxyl groups decomposition bonded to the surface of zirconia [38]. The third stage weight loss occurred between 600 °C and 900 °C due to the degradation of material. The total weight loss of original material reaches about 19%. The TGA curves in Figure 4-6 (b-f) show the thermal stability of zirconia at the synthesis temperature ranges of 50, 80,100,120 and 150 °C, has little loss of its original weight on heating up to 100 °C. This weight loss is attributed to the removal of the adsorbed water on the surface. The behaviour up to 100 ˚C is the same for both samples. This may be due to the water desorption from the surface and pores of material. Second stage of weight loss is between 100 °C and 900 °C corresponding to the removal of terminal hydroxyl groups bonded to the surface of zirconia. The TGA curves in Figure 4-6(b-f) confirm that the samples were stable as there was less decomposition of oxide compared to the results in Figure 4-6(a). The lower degradation of zirconia oxide is very important on modification of Nafion® membrane, as it will enhance the thermal stability of membrane [39]. The Zr-50 lost only 9 % of its total weight, Zr-80 lost only 8% of its total weight, Zr-100 lost only 6% of its total weight, Zr-120 lost only 5% of its total weight and Zr-150 lost only 3% of its total weight, respectively, indicating that a large amount of organic matter was stable and that it lost less water.

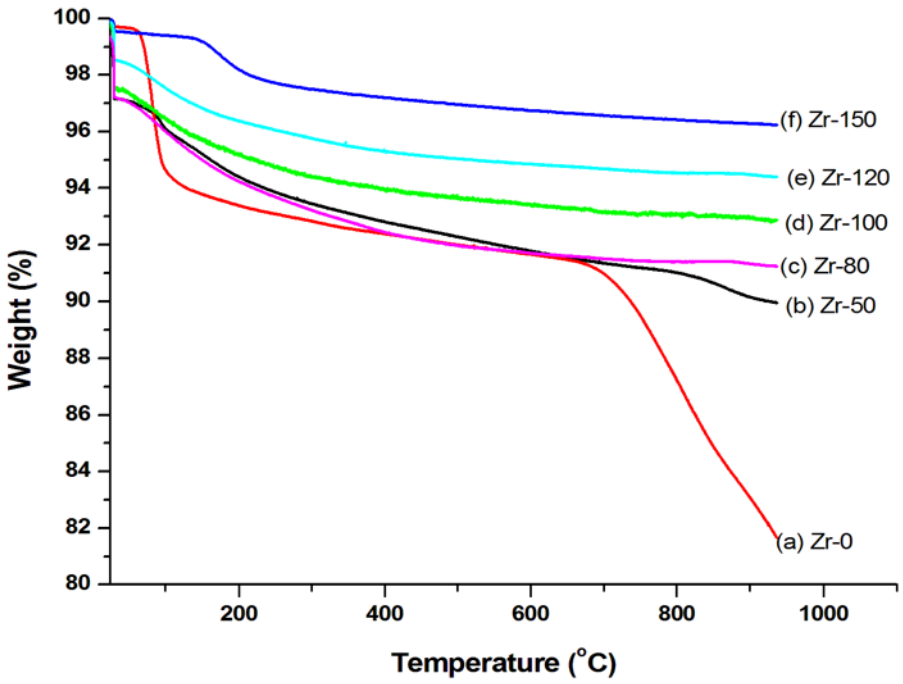

Figure 4- 6: The comparison of the TGA curves of the ZrO_2 nanoparticles at the different temperatures (a) Zr-0, (b) Zr-50, (c) Zr-80, (d) Zr-100, (e) Zr-120 and (f) Zr-150.

4.3.6. Brunauer-emmett-teller (BET)

BET of zirconia nanoparticles prepared at different temperatures are shown in Figure 4-7 (a) with the specific surface area and total pore volume. From the results tabulated in Figure 4-7 (a), it is observed that raising the reaction temperature from 50 °C to 150 °C resulted in porous texture, with a higher specific surface area that ranges from 55-162 m^2/g when calcinated at 600 °C. The result obtained in Figure 4-7 (b) shows that the pore volume of Zr-150 (0.33 cm^3/g) is much bigger than that of Zr-0 (0.09 cm^3/g) that was synthesised at room temperature. The results in Figure 4-7 (a) and (b) show that the increase in the reaction temperature results in the increase in the specific surface area and pore volume. This may be due to the fact that sintering at higher temperatures decomposes the hydrous zirconia to give a fine crystallite of zirconia. The TGA results also confirmed that higher temperature reaction had a drier hydrous zirconia than room temperature. These dry hydrous zirconia show the condensation between hydroxyl groups leading to three-dimensional structures

that enhance the porosity of zirconia nanoparticles [40]. Moreover, the zirconia nanoparticles with high porosity as inorganic filler that retains water within the membrane and increases the conductivity at a low relative humidity [41]. But Zr-100 in Figure 4-7 (a) shows the slight decrease in specific surface area with a bigger pore volume when compared to Zr-80. This may be due to their different morphological structures (cubes and nanorods) as confirmed by the SEM images in Figure 4-3.

(a)

Sample ID	Surface area (m^2/g)	Pore volume (cm^3/g)
Zr-0	55	0.09
Zr-50	77	0.16
Zr- 80	132	0.17
Zr-100	82	0.20
Zr-120	157	0.26
Zr-150	162	0.33

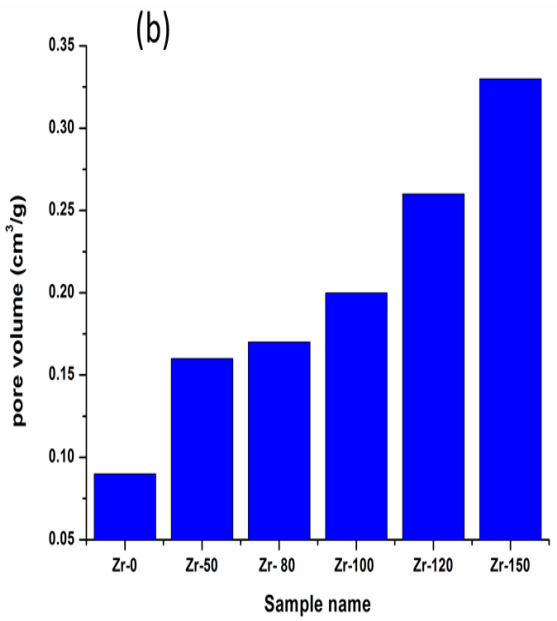

Figure 4- 7: **(**a) table of BET of ZrO_2 nanoparticles (b) pore volume of (a) Zr-0, (b) Zr-50, (c) Zr-80, (d) Zr-100, (e) Zr-120 and (f) Zr-150.

4.4. Conclusion

A simple precipitate method was used to synthesis a high surface area of zirconium oxide with a high temperature phase (cubic), stabilised at a low calcination temperature of 600 ˚C. The effect of temperature on the decomposition of nanoparticles was observed under TGA and FTIR. The cubes, rods and flower-like spheres of nanostructures were obtained at varied temperatures, which were confirmed by SEM studies. The SEM and XRD results show that the synthesis temperature has an effect on the morphology and crystallinity of ZrO_2 nanoparticles. Furthermore, it was observed that

by increasing the synthesis temperature, the surface area of zirconia nanoparticles also increased from 55 to162 m^2/g and its pore volume from 0.09 to 0.33, while the agglomeration of nanoparticles reduced. Notably, it was found that the synthesis temperature has an effect on the crystallinity and particle size of the zirconia nanoparticles, which was observed under HRTEM results with a particle size range of 2-20 nm. Monoclinic ZrO_2 nanoparticles have been obtained at the synthesis temperature of 150 °C, whereas at the lower synthesis temperatures of 50 °C, 80 °C, 100 °C and 120 °C only the pure cubic phase was present.

B: The synthesis, characterization and electrochemical study of zirconia oxide nanoparticles for fuel cell application

4.5. Introduction

Zirconia is polymorphic, as it has a different crystal structure at different temperatures [9]. The monoclinic phase is thermodynamically stable up to 1 100 °C, the tetragonal phase exists in the temperature range 1 100-2 370 °C, and the cubic phase is found above 2 370 °C [42]. Moreover, cubic zirconium oxide (ZrO_2) is a well-known material with extreme refractoriness [43], fracture toughness and high mechanical strength [44] and has been used as an ionic conductor in fuel cells and as proton transport material [45]. Furthermore, ZrO_2 maintains good electrical and mechanical properties, higher dielectric constant, chemical inertness, wide band gap, thermal stability, wear and corrosion resistance [46]. This makes it suitable for use in solid fuel cells, gas sensors, catalytic agents and high durability coating [47]. ZrO_2 is also used in catalysis as a catalyst [48] and catalyst support [49], biomaterial [50] and as coating for corrosion protection [51]. When ZrO_2 is used as a photocatalyst, it can be applied in environmental cleaning applications [52]. Its good thermal matching with other metals makes it suitable to be used in protective coatings and exhaust gas purifying devices [53] and as a constituent present in transition metal-based catalysts [54]. Moreover, when ZrO_2 is composited with other metals, it can be used in commercial applications and variety of technological such as oxygen sensors [55], catalysts [56], as gate dielectrics in metal oxide-semiconductor devices and high dielectric constant

materials for very large-scale integrated circuits [57]. The nanometre-size semiconductors have attracted significant attention because of their atom-like size-dependent properties [58]. Among the ceramic semiconductors, zirconia is the only metal oxide that has both weak base and weak acid properties [59-60]. Depending on its crystalline structure, it can be an insulator used as a higher resistance ceramic or an n-type semiconductor [61]. The morphological structure of nanoparticles has influence in their potential applications. Spherical ZrO_2 nanoparticles have been applied as oxygen sensors, fuel cell electrolytes and gate dielectrics [33]. Several studies have been carried out in order to test different synthesis possibilities due to their hardness and corrosion resistance [62]. The ZrO_2 reactions resulted into the formation of mixed phases that makes not easy to obtain a pure cubic ZrO_2 nanoparticles. Here we report the cubic (Arkelite) and monoclinic (baddeleyite) zirconia nanoparticles synthesized by a simple precipitation method with control of morphology and crystallinity. The influence of temperature on the lattice fringes and size reduction of zirconia oxide nanoparticles was observed under high-resolution transmission electronic microscopy (HRTEM). The reaction temperature we used to obtain cubic ZrO_2 nanoparticles was low (50 °C and 120 °C). The effect of temperature on the morphology and crystal shape of ZrO_2 was observed under scanning electron microscopy (SEM) and X-ray powder diffraction (XRD). The performance of electrochemical was investigated under potential dynamic polarisation techniques (Autolab PGSTAT302). Nafion® solution, when used as a binding material of ZrO_2 nanoparticles, obtained a high specific capacitance and good reversible redox reactions.

4.6. Experimental

4.6.1. Materials

Zirconium oxychloride hydrate (Sigma Aldrich), sodium hydroxide pellets (Sigma Aldrich), sodium nitrate (Sigma Aldrich), ethanol (Sigma Aldrich), potassium chloride (Sigma Aldrich), Nafion solution (Sigma Aldrich) and silver nitrate ($AgNO_3$) (Sigma Aldrich). All the chemicals were used as received.

4.6.2. Synthesis of ZrO_2 nanoparticles

The ZrO_2 nanoparticles were prepared by the precipitation method. $ZrOCl_2.8H_2O$ and NaOH were used as starting materials. 0.2M $ZrOCl_2.8H_2O$ was prepared in a 250 ml beaker and 2N NaOH solution was added dropwise with continuous stirring for 45 minutes. The precipitate obtained was divided into three parts, and then aged at 50 °C, 120 °C and 150 °C for 24 hours, after which it was filtered and washed several times with distilled water until chlorine ions (Cl^-) were not detected by the $AgNO_3$ [63]. The precipitate was dried at 100 °C for 24 hours, which was calcinated at 600 °C for 4 hours and labelled as follows: ZrO_2-1 (50 °C), ZrO_2-2 (120 °C) and $Zr0_2$-3 (150 °C). Figure 4-8 shows the schematic diagram of the synthesis method.

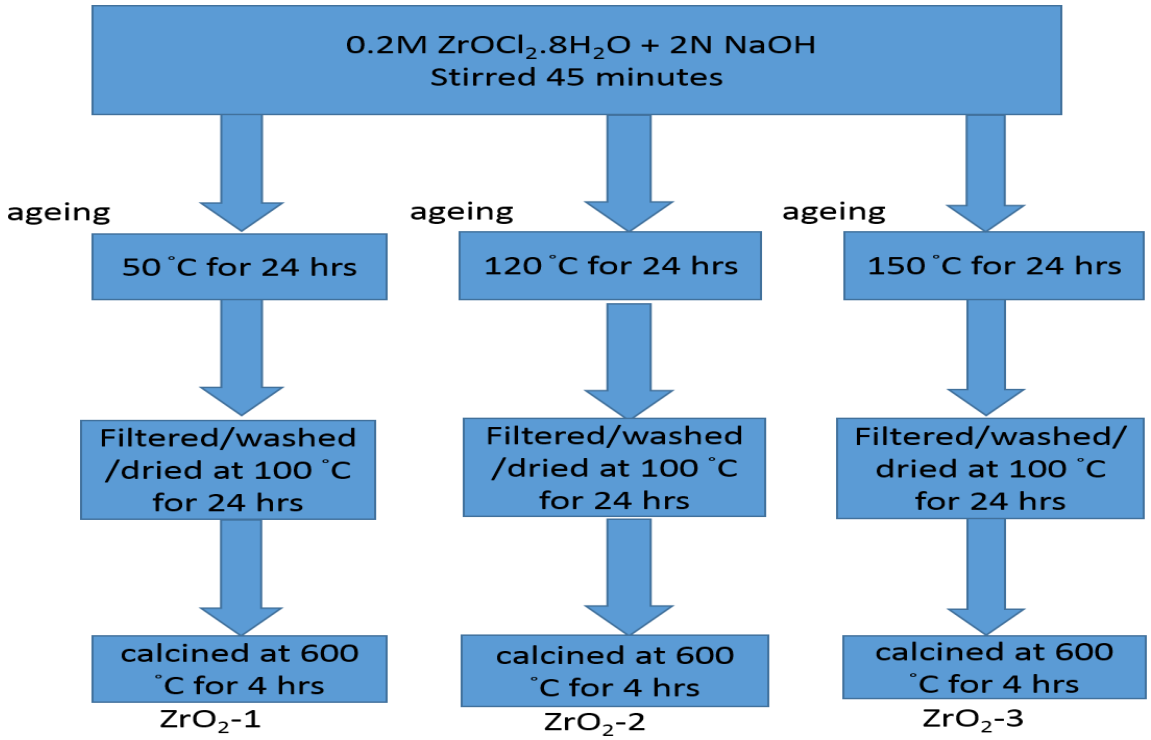

Figure 4- 8: Synthesis of zirconium oxide.

4.6.3. Characterisation

The X-ray diffraction (XRD) analysis was performed through X-ray diffraction with Cu K radiation source and the samples were scanned in a continuous mode from 5°–90° with a scanning rate of

0.026 (degree) / 1 (sec). The surface morphologies of all the membrane were studied using Scanning Electron Microscopy (SEM). Fourier-transform infrared spectroscopy (FTIR) was employed to investigate the changes in the chemical structure of the membrane. The thermal properties and the characteristics of the samples were studied by thermal gravimetric analysis (TGA) under nitrogen flow. TGA data was obtained using TGA instrument (PerkinElmer) over nitrogen and at a heating rate of 10° C/min from 28° C to 1000° C. A Brunauer-Emmett-Teller (BET) was used to determine pore size distribution via adsorption, micropore volume (t-plot method) and desorption isotherms. In a BET surface area analysis, a dry sample was evacuated of all gas and cooled to 77 K, using liquid nitrogen.

4.6.4. Electrochemical studies

Electrochemical measurements were observed under three electrodes. While silver-silver chloride (Ag/AgCl) electrode was used as the reference electrode, zirconia nanoparticles coated on glassy carbon were used as a working electrode and Pt wire was used as a counter electrode. 0.03 g of ZrO_2-1, ZrO_2-2 and ZrO_2-3 were ultra-sonicated in 0.5 ml 1 wt% Nafion in absolute ethanol for 30 minutes, and pipetted a 0.05 ml suspension onto the glassy carbon electrode and dried at ambient temperature [64]. Cyclic voltammetry (CV) and electrochemical impedance spectroscopy (EIS) were observed under 2M of KCl and $NaNO_3$ electrolytes. The scan rates used were 10 mV s^{-1}, 20 mV s^{-1}, 30 mV s^{-1}, 50 mV s^{-1} and 100 mV s^{-1} with the CV test ranging from -0.15 V to 0.55 V vs. EIS measurements were obtained under the frequency range of 100 kHz to 0.01 Hz.

4.7. Results and discussion

4.7.1. Transmission electron microscopy (TEM)

The sizes and morphology of ZrO_2-1, ZrO_2-2 and ZrO_2-3 nanoparticles were observed under TEM in high-resolution mode as shown in Figure 4-9. Figure 4-9 (a) shows that the TEM micrographs of ZrO_2-1 are less agglomerated with very small particle sizes of 10-20 nm, in the form of nanospheres

and a nanorod-like shape. TEM micrographs of ZrO_2-2 nanoparticles show a spherical phase of ZrO_2 nanoparticles with less agglomeration in the size range of 2-10 nm as shown in Figure 4-9 (b). Figure 4-9 (c) shows that TEM analysis revealed more crystalline particles and a reduction in particle size of zirconia nanoparticles. The nanoparticles have a nanospherical shape with the particle size ranging from 2-5 nm as shown in Figure 4-9 (c). It also shows that the formation of pure nanocrystalline ZrO_2 and particle size reduction are highly affected by higher reaction temperatures within the specified period. It is observable in Figure 4-9 (c) that increasing the synthesis temperature to 150 °C led to very small nanoparticles of 2 nm. We found that higher temperature reactions have an effect on the size reduction of zirconia nanoparticles, which will be a filler in Nafion membranes. This nanometer size of zirconia nanoparticles as a filler in membranes has been found to have a significant effect on the methanol permeability and proton conductivity of composite membrane than those with bigger nanoparticle sizes [34]. The observed crystallite size is much smaller than the reported average particle size of 4.45 nm [35]. The selected area electron diffraction (SAED) pattern of ZrO_2-1, ZrO_2-2 and ZrO_2-3 nanoparticles is presented in Figure 4-10. Figure 4-10 (a) shows the detectable rings that are indexed to DB card number: 5000038 for the standard cubic phase. It indicates that the nanocrystals obtained were cubic phases. The corresponding diffraction pattern shows the presence of a few clear spots together with connecting diffraction rings as shown in Figure 4-10 (a). The presence of the streaks and spots represent the crystallization of reasonably sufficient sizes to diffract. The short-range order indicated by connecting streaks, which is due to the presence of some smaller size particles. The clarity in the fringe patterns inside the crystallite indicates the formation of single-phase ZrO_2 with the long-range order in the structure. When the crystallites are of large size, the SAED pattern show the clear spots without the rings. The HRTEM results of ZrO_2-2 nanoparticles is clearly presented in well-resolved equidistant lattice fringes as shown in Figure 4-10 (b). The distance between the fringes was calculated to be 0.2928 nm and 0.2927 nm, which can be attributed to the interplanar spacing corresponding to (1 1 1) plane of cubic ZrO_2 [36-37]. These HRTEM results correspond well with the XRD results. The lattice fringes are equidistant and clear, all along the length of the nanorods and width of the nanoparticle, without any lattice mismatch,

hence depicting a single crystalline-like structure. Figure 4-10 (c) shows the HRTEM image of a single zirconia nanoparticle with the electron diffraction pattern of (1 1 1) planes of the cubic structure. Figure 4-11 shows the lattice spacing of ZrO_2-1, ZrO_2-2 and ZrO_2-3 nanoparticles observed under HRTEM. The ZrO_2-1, ZrO_2-2 and ZrO_2-3 nanoparticles obtained a lower lattice spacing of 0.2485, 0.2891 nm, 0.2998 nm, 0.2928 nm and 2927 nm for the (1 1 1) plane of the cubic and monoclinic ZrO_2 structure as shown in Figure 4-11 (a-f). Figure 4-11 (a-f) show clear lattice images, indicating the high crystallinity and single crystalline nature of ZrO_2 nanoparticles.

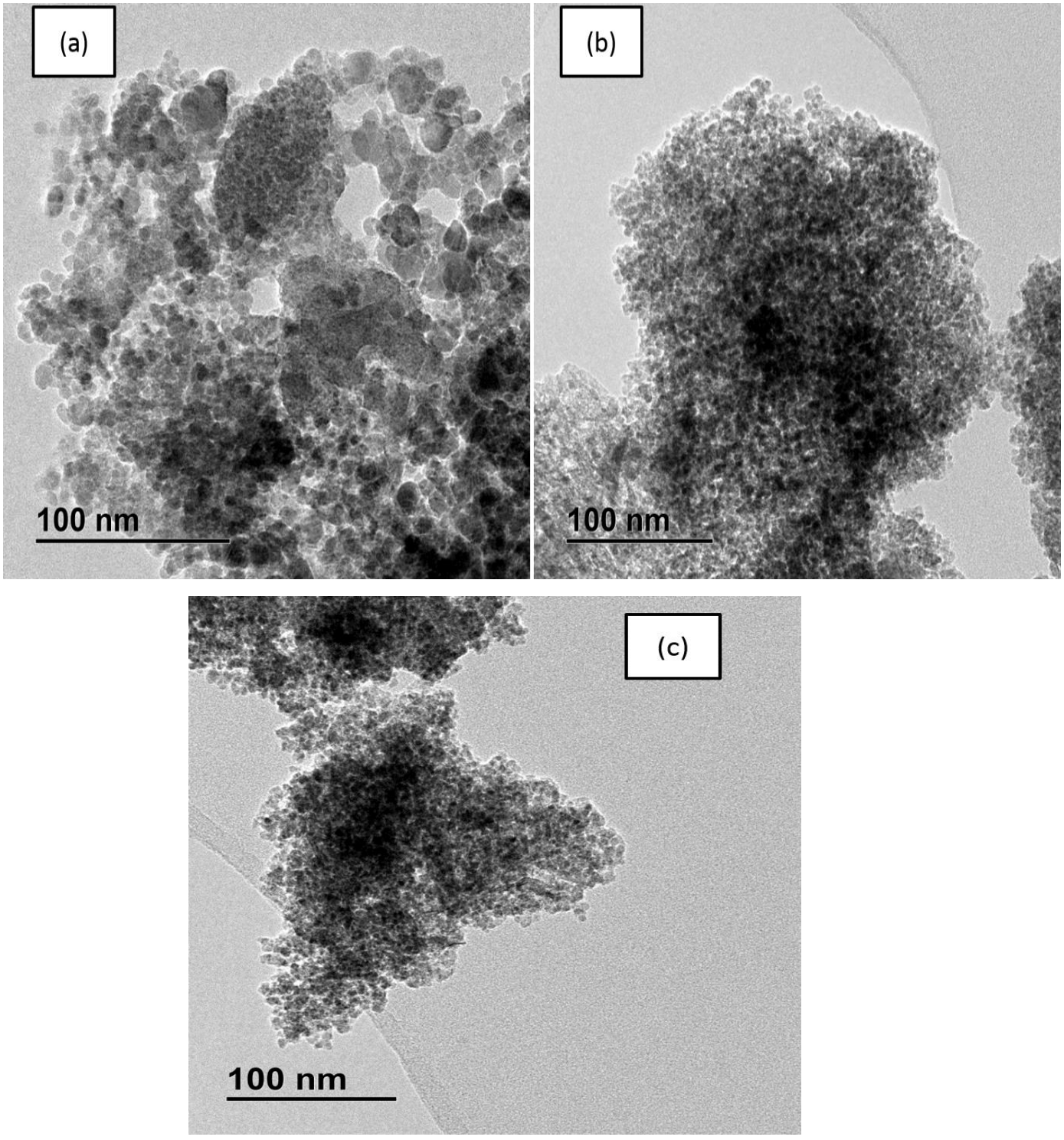

Figure 4- 9: TEM image of ZrO_2 nanoparticles: (a) ZrO_2-1, (b) ZrO_2-2 and (c) ZrO_2-3.

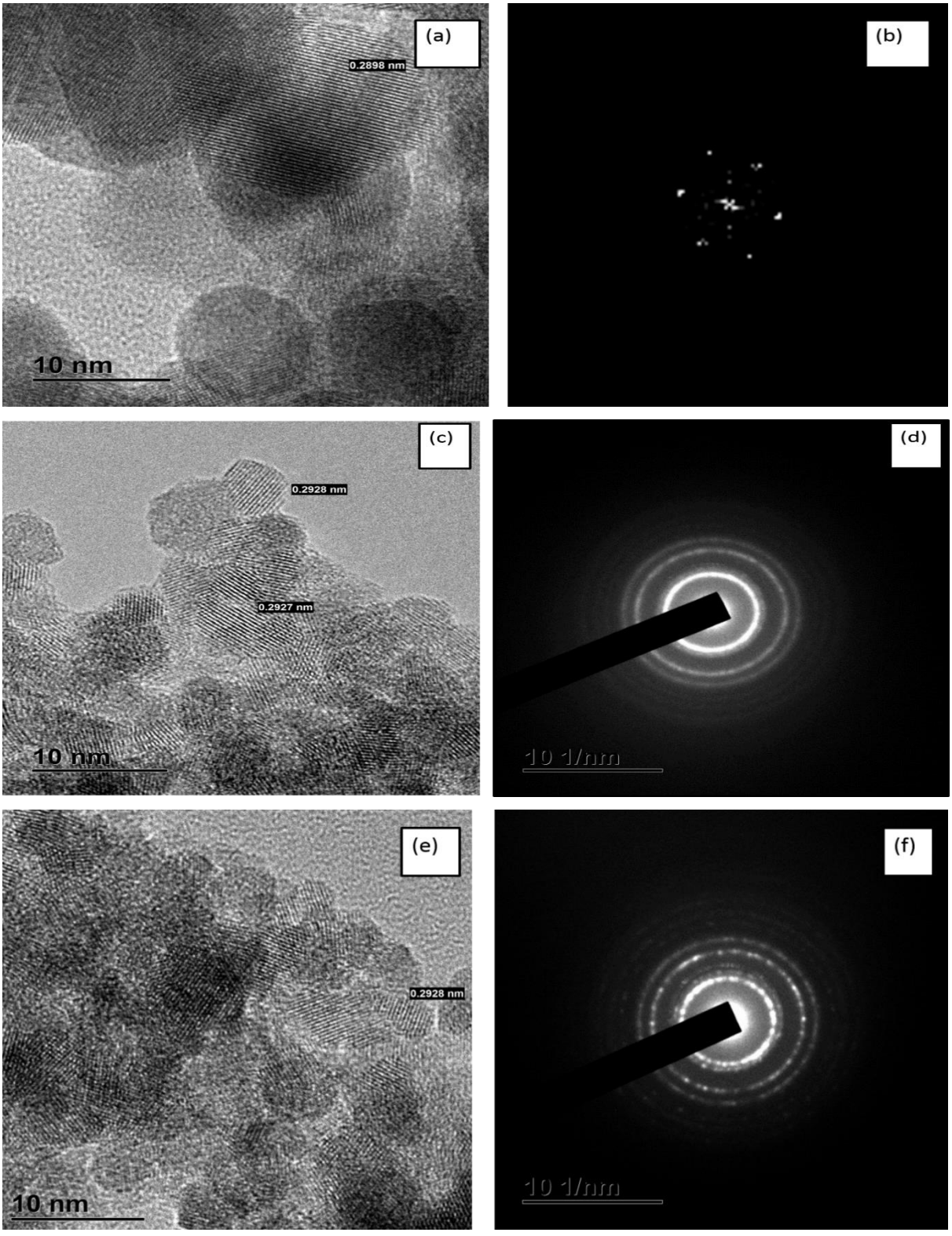

Figure 4- 10: HRTEM image of ZrO_2 nanoparticles at higher magnification: (a) Zr- ZrO_2-1, (b) SAED, Zr-ZrO_2-1, (c) ZrO_2-2, (d) SAED, ZrO_2-2, (e) ZrO_2-3 and (f) SAED, ZrO_2-3.

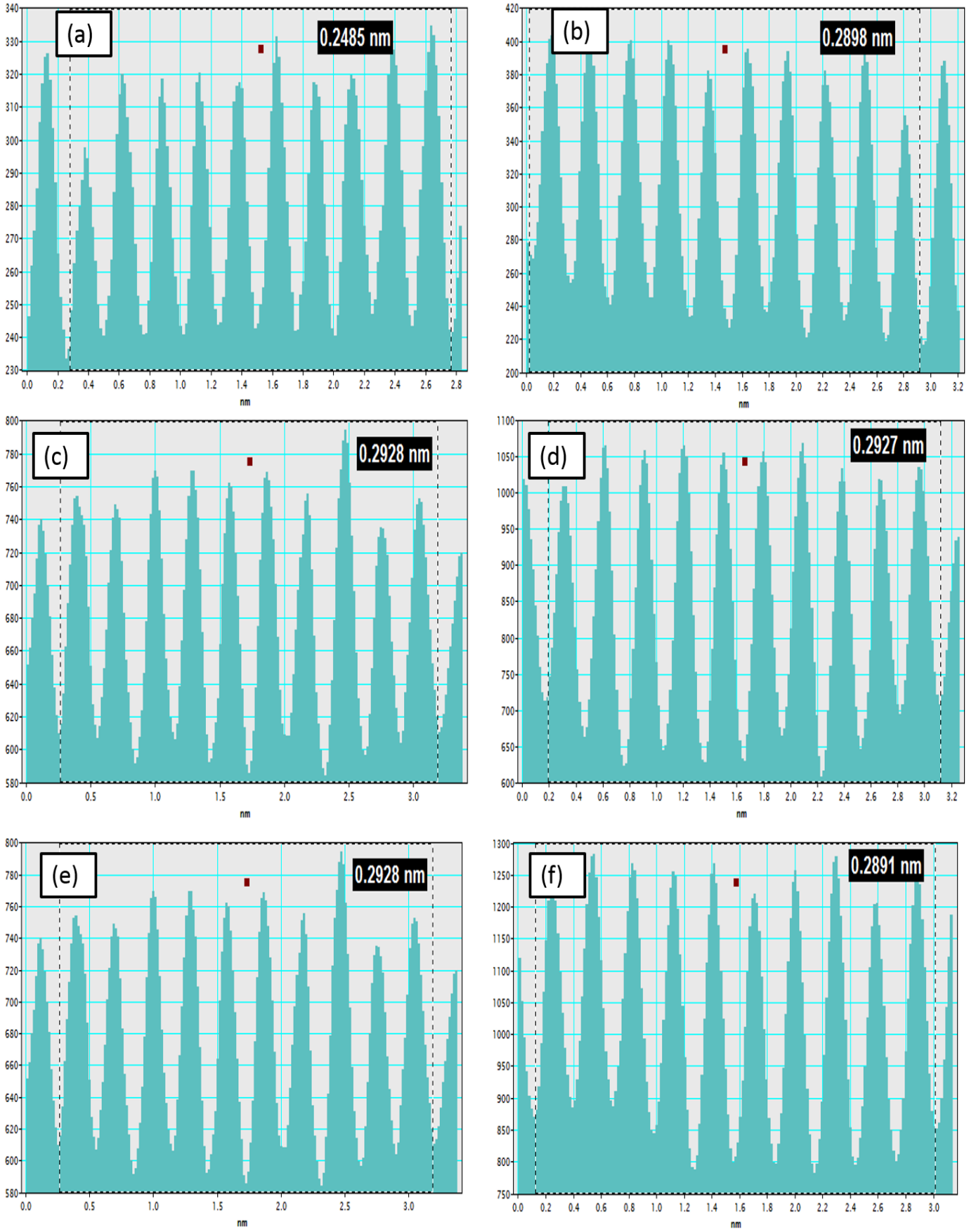

Figure 4- 11: HRTEM lattice fringes of ZrO_2 nanoparticles: (a-b) ZrO_2-1, (c-d) Zr- ZrO_2-2, (e-f) ZrO_2-3.

4.7.2. Structure analysis

The XRD pattern of ZrO_2-1, ZrO_2-2 and ZrO_2-3 is shown in Figure 4-12. The XRD results in Figure 4-12 clearly reveal the presence of the monoclinic crystallite phase of zirconia corresponding to (JCPDS card no. 00-037-1484) and the cubic crystallite phase of zirconia corresponding to (JCPDS No. 65-1022). It was also observed in all XRD patterns that they have broad peaks, which indicates the nanometer characteristics of zirconia particles. Figure 4-12(a-b) show only broad reflections originating from cubic ZrO_2 nanoparticles, with diffraction peaks in the spectra indexed as cubic with lattice constants a = 0.51291 nm, b = 0.51291 nm, c = 0.51291 nm and β = 90.0°. The main peaks at 2 theta are 30.2°, 35.2°, 50.6°, 60.2°,74.2°, 82.5° and 94.1°, which correspond to the planes (1 1 1), (2 0 0), (2 2 0), (3 1 1), (4 0 0), (3 3 1), (4 2 2) [20-21] as shown in Table 4-1. The results show that when zirconium oxychloride hydrate is hydrolysed directly using concentrated sodium hydroxide solution, the particle size and the crystallinity remain almost unchanged, but the product shows a higher degree of agglomeration. This may be due to a high synthesis temperature of ZrO_2 which stabilises the high temperature phases at room temperature if the crystallite size is below a critical size [9]. This is associated with reduced total energy of the system due to the inherent high surface energy of the nanoparticles [22]. In the cubic phase of zirconia, vacancies increase, improving the diffusion of oxygen ions as the primary charge carriers elevate electrical conductivity [23]. From these results it can be deduced that increasing synthesis temperature favours structural growth. The influence of synthesis temperature on the morphology and stabilisation of the phase was discussed by Adamski et al. [24]. Figure 4-12 (c) illustrates the monoclinic phase, which may be due to ageing at a temperature of 150 °C that lowers the particle size to nano-diameter, with the influence of the monoclinic phase which provides a more versatile surface than the cubic and tetragonal phases due to a less symmetrical lattice [25]. The XRD pattern in Figure 4-12 (c) shows the same crystalline of zirconia nanoparticle synthesis under 150 °C, which was completely transformed to a baddeleyite structure, with diffraction peaks in the spectra indexed a = 0.49920 nm, b = 0.52290 nm, c = 0.50460 nm and β = 90.0°. The main peaks at 2 theta are 14.2°, 23.4°, 30.4°, 35.1°, 50.6°, 60.1°,74.0° , 82.4° and 95.1° corresponding to the planes (1 0 0), (1 1 0), (1 1 1), (0 2 0), (3 0 0), (1 3 1), (4 1 1), (4 2 0) and (5 1 1) as shown in Table 4-2.

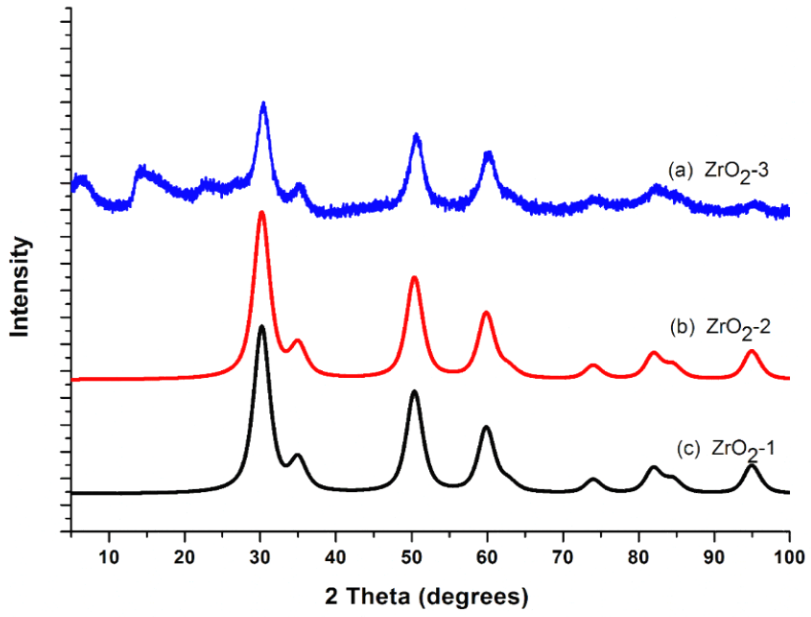

Figure 4- 12: XRD patterns of ZrO2 nanoparticles: (a) ZrO_2-3, (b) ZrO_2-2 and (c) ZrO_2-1.

Table 4- 1: XRD data of ZrO_2-1 and ZrO_2-2 nanoparticles

No.	2theta (deg)	d (ang.)	Height (cps)	FWHM (deg)	Size (ang.)	Phase name	Chemical formula	DB card number
1	13.81(3)	6.409(16)	3353(169)	2.45(7)	34.1(10)	Unknown	Unknown	0
2	16.6(6)	5.3(2)	4491(195)	5.7(4)	14.6(9)	Unknown	Unknown	0
3	23.35(13)	3.81(2)	16443(373)	14.3(3)	5.6(9)	Unknown	Unknown	0
4	24.518(11)	3.6278(16)	3732(178)	0.183(18)	463(45)	Unknown	Unknown	0
5	30.224(6)	2.9546(6)	28738(493)	2.359(15)	36.4(2)	Arkelite(1,1,1)	O_2 Zr	5000038
6	34.98(2)	2.5631(14)	7192(247)	2.37(4)	36.7(7)	Arkelite(2,0,0)	O_2 Zr	5000038
7	43.28(2)	2.0887(9)	813(83)	0.77(6)	116(9)	Unknown	Unknown	0
8	50.345(12)	1.8110(4)	11738(315)	2.490(12)	36.8(18)	Arkelite(2,2,0)	O_2 Zr	5000038
9	60.035(18)	1.5398(4)	8699(271)	3.07(3)	31.2(3)	Arkelite(3,1,1)	O_2 Zr	5000038
10	74.15(15)	1.278(2)	1151(99)	3.18(13)	32.7(13)	Arkelite(4,0,0)	O_2 Zr	5000038
11	82.54(9)	1.1679(11)	2155(135)	5.50(15)	20.1(6)	Arkelite(3,3,1	O_2 Zr	5000038
12	94.71(11)	1.0473(9)	1225(102)	3.5(2)	35(2)	Arkelite(4,2,2)	O_2 Zr	5000038

Table 4- 2: XRD data of ZrO_2-3

No.	2theta) (deg)	d (ang.)	Height (cps)	F(deg) WHM	Size (ang.)	Phase name	Chemical formula	DB card number
1	6.53(7)	13.53(14)	3604(175)	4.0(5)	21(3)	Unknown	Unknown	0
2	14.170(16)	6.245(7)	3088(162)	4.33(7)	19.3(3)	Baddeleyite (1,0,0)	O_2 Zr	9005835
3	23.42(10)	3.795(16)	2627(149)	10.0(6)	8.5(5)	Baddeleyite (1,1,0)	O_2 Zr	9005835
4	30.388(13)	2.9390(12)	12222(322)	2.05(2)	41.9(4)	Baddeleyite (1,1,1)	O_2 Zr	9005835
5	35.142(16)	2.5516(12)	2225(137)	1.96(5)	44.3(11)	Baddeleyite (0,2,0)	O_2 Zr	9005835
6	50.610(17)	1.8021(6)	9169(279)	2.20(2)	41.8(4)	Baddeleyite (3,0,0)	O_2 Zr	9005835
7	60.12(2)	1.5377(5)	7027(244)	2.54(4)	37.8(5)	Baddeleyite (1,3,1)	O_2 Zr	9005835
8	73.99(6)	1.2801(8)	902(87)	3.3(2)	32(2)	Baddeleyite (4,1,1)	O_2 Zr	9005835
9	82.37(4)	1.1698(5)	2394(142)	5.84(17)	18.9(5)	Baddeleyite (4,2,0)	O_2 Zr	9005835
10	95.14(16)	1.0436(13)	723(78)	2.45(15)	50(3)	Baddeleyite (5,1,1)	O_2 Zr	9005835

4.7.3. SEM analysis

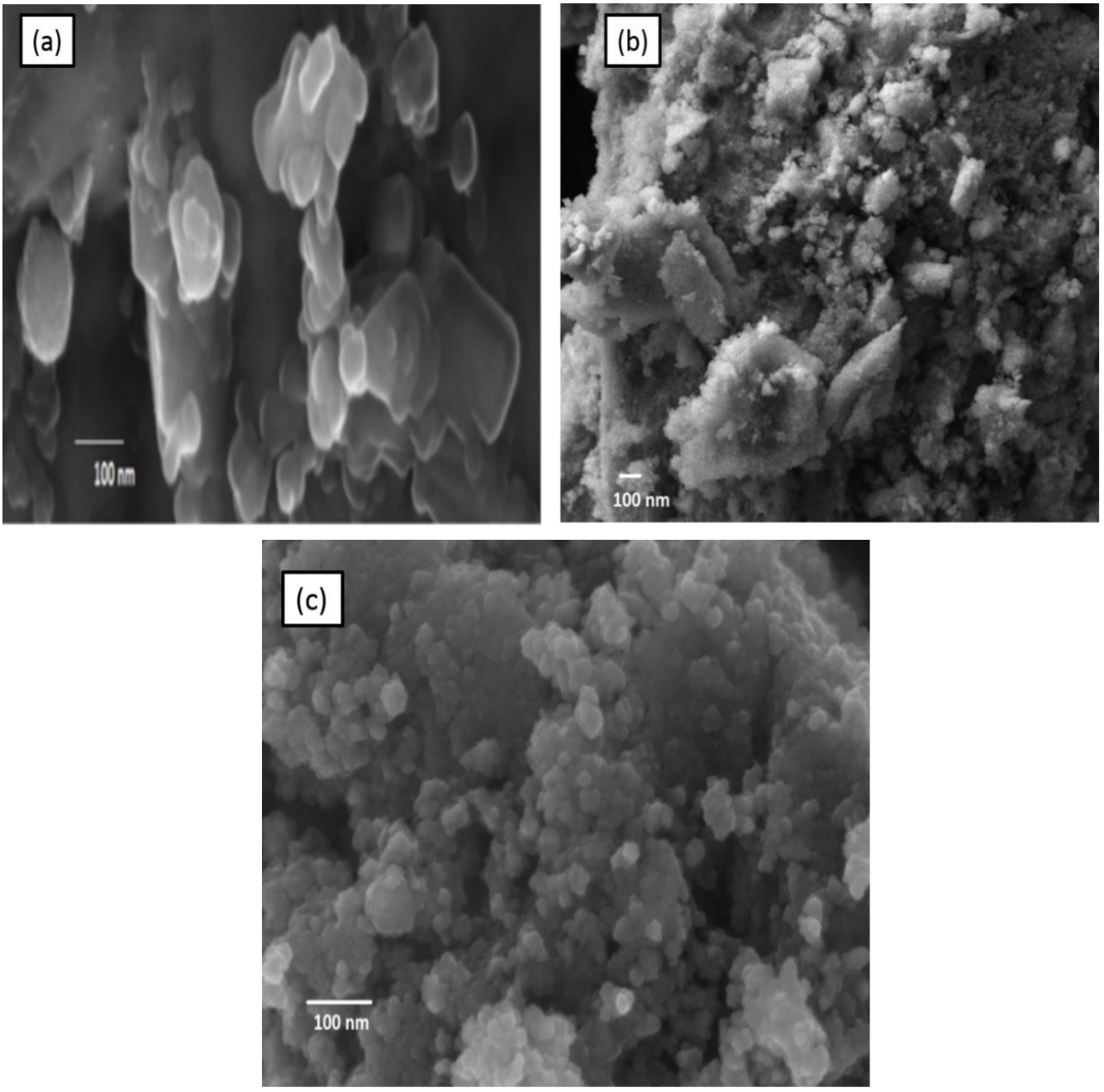

Figure 4- 13: SEM micrographs: (a) ZrO_2-1, (b) ZrO_2-2 and (c) ZrO_2-3.

Figure 4-13 shows the SEM images of ZrO_2-1, ZrO_2-2 and ZrO_2-3 nanoparticles. Figure 4-13(a) shows that zirconia nanoparticles consist of small particles agglomerated in the form of nanorods and with an irregular shape. This agglomeration occurs due to the formation of unstable and ultrafine nuclei that have a strong tendency to be stable when agglomerated. Figure 4-13 (b and c) show less agglomeration compared to ZrO_2-1 nanoparticles. This may be due to a higher temperature reaction which increases the rate of collision

between the charged particles compared to room temperature [32]. This collision also introduces a charge to the particles so that they repel one another. In addition, the higher temperature reaction enhances the dissolution and re-precipitation of material, which helps strengthen the network of particles [32]. As seen in Figure 4-13 (b), it was found that the sample is composed of a mixture of irregular and rod-like nanostructures. Figure 4-13 (c) shows the SEM images of ZrO_2-3 composed of nanospheres that are useful in fuel cell electrolytes, oxygen sensors and gate dielectrics [33]. Generally, the SEM images indicate that the morphologies and particle sizes of zirconia nanostructures change with an increase in synthesis temperature. During a higher temperature reaction, all the excess precipitate (cations and anions) dissolves and reacts with the hydrous oxides, which affects the morphological properties of the material [32].

4.7.4. TGA and derivative thermo-gravimetric (DTG)

The thermal stability of the zirconia nanoparticles was studied by thermo-gravimetric analysis (TGA/ DTG) as shown in Figure 4-14. Figure 4-14 (a) indicates that the thermal decomposition process occurs in three stages. The TGA curves from Figure 4-14 (a) show the thermal stability of zirconia at the synthesis temperature ranges of ZrO_2-1, ZrO_2-2 and ZrO_2-3, and that it has little loss of its original weight on heating up to 100 ˚C. This weight loss is attributed to the removal of the adsorbed water on the surface. The behaviour up to 100 ˚C is the same for both samples, which may be due to the water desorption from the surface and pores of material. The second stage of weight loss is between 100 °C and 900 °C, corresponding to the removal of terminal hydroxyl groups bonded to the surface of zirconia [38]. The TGA curve of Figure 4-14 (a) confirms that the samples were stable as there was less decomposition of oxide. Moreover, we find that the lesser degradation of zirconia oxide is very important in the modification of the Nafion membrane for fuel cell application, as it will enhance the thermal stability of the membrane [39]. The ZrO_2-1 lost only 9% of its total weight, Zr- ZrO_2-2 lost only 5% of its total weight and ZrO_2-3 lost only 3% of its total weight, indicating that a large amount of organic matter was stabilised and lost less water. Figure 4-14 (b) shows the DTG curves of ZrO_2-1, ZrO_2-2 and ZrO_2-3. ZrO_2-1 shows the two transition peaks, which are associated with the first and second stages of weight loss within the nanoparticles. ZrO_2-2 and ZrO_2-3 undergo only one stage of weight loss due to the removal of adsorbed water on the nanoparticles.

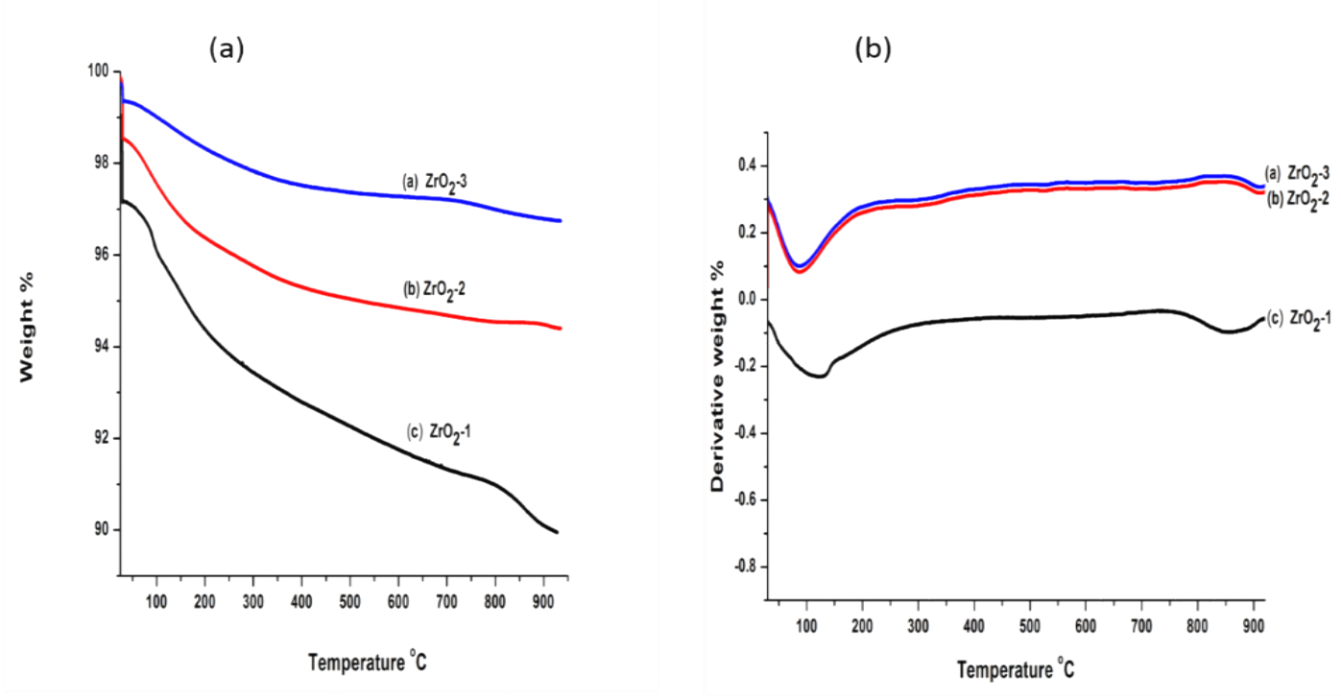

Figure 4- 14: (a) TGA of the (a) ZrO_2-3, (b) ZrO_2-2, (c) ZrO_2-1; (b) DTG of (a) ZrO_2-3, (b) ZrO_2-2, (c) ZrO_2-1.

4.7.5. FTIR spectrum of ZrO_2 nanoparticles

In order to ascertain the molecular nature of ZrO_2-1, ZrO_2-2 and ZrO_2-3 nanoparticles, FTIR spectroscopic spectra were measured as shown in Figure 8. The vibration bands at 685 cm^{-1} and 863 cm^{-1} are due to Zr-O-Zr asymmetric and Zr-O stretching modes, respectively, confirming the formation of C-ZrO_2 phases as shown in Figure 4-15 (a) [26-27]. The symmetric frequencies of Zr-OH were observed at 1 072 cm^{-1} and 1 398 cm^{-1} [28]. The characteristic peaks observed at 2 962 cm^{-1} and 2 462 cm^{-1} are due to the presence of inorganic ions. Figure 4-15 (b) shows the vibration band in the region of 685 and 875 cm^{-1} due to the vibration of the Zr-O-Zr and Zr-0 groups, confirming the formation of C-ZrO_2 phases which correspond to the crystalline zirconia [65]. The weak band at 2 338 cm^{-1} which appears at temperatures near to 600 ˚C [31] was attributed to vibration modes of the cubic phase. Figure 4-15 (c) shows the vibration bands at 930 cm^{-1} due to the Zr-O vibration [27]. The peak of 1 371 cm^{-1} corresponds to O-H bonding, and the peaks in the region of 1 536 cm^{-1} and 1 634 cm^{-1} may be due to the adsorbed moisture. The peak in the 3 390 cm^{-1} region is attributed to O-H stretching of nanomaterials [29-30]. The slight shift of the Zr-O vibration peak and disappearance of the Zr-O-Zr vibration peak may be due to the high synthesis temperature.

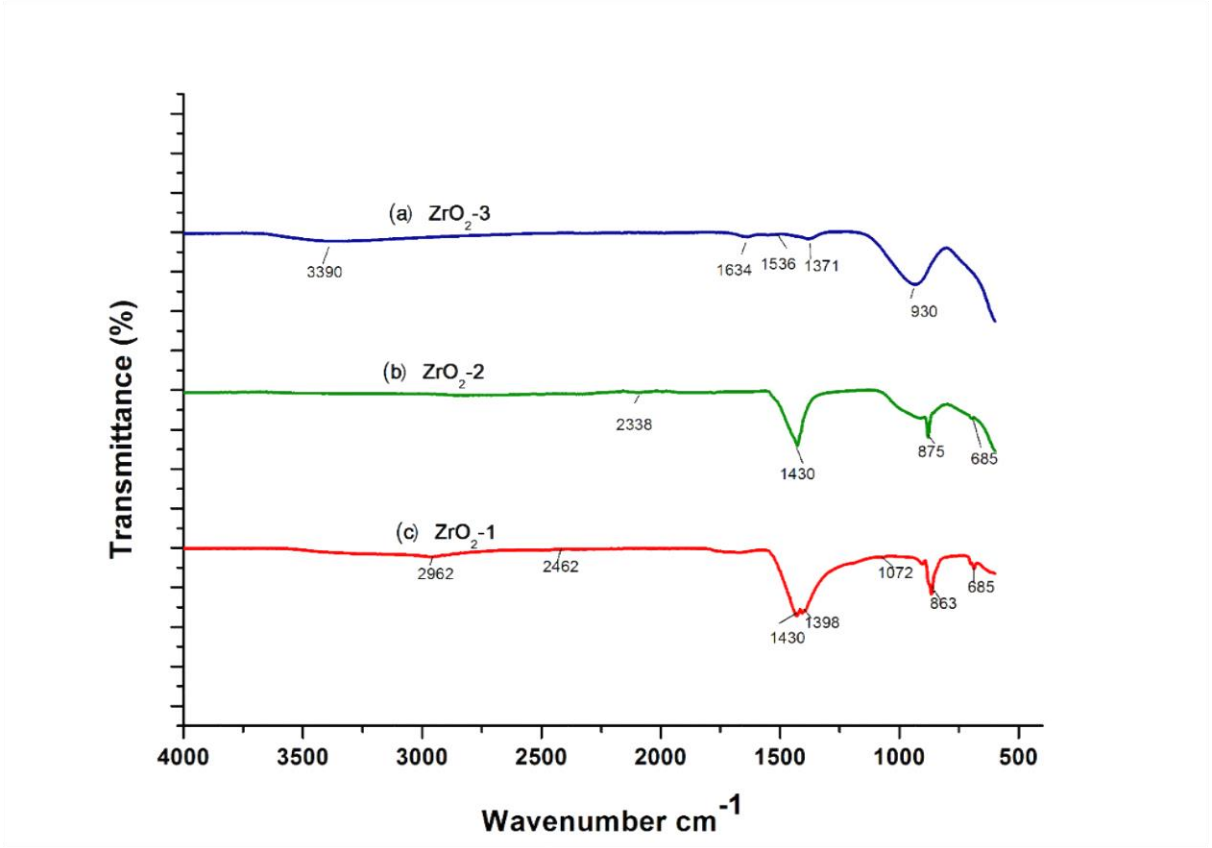

Figure 4- 15: Comparison of FTIR curves of ZrO_2 nanoparticles at different temperature (a) ZrO_2-3, (b) ZrO_2-2 and (c) ZrO_2-1.

4.7.6. Nitrogen adsorption-desorption

Figure 4-16 shows the nitrogen adsorption-desorption isotherms and pore size distribution curve of ZrO_2-1, ZrO_2-2 and ZrO_2-3 nanoparticles. Nitrogen adsorption-desorption isotherm patterns of ZrO_2-1, ZrO_2-2 and ZrO_2-3 nanoparticles correspond to the type IV isotherm, indicating typical mesoporous materials. Figure 4-16(a) shows a very narrow pore size distribution in both samples; this may be due to the synthesis temperature which promotes the growth of zirconia powder. The hysteresis does not exhibit any limiting adsorption at high P/P0 and contains a steep region associated with a closure of the hysteresis loop due to the tensile strength effect [66]. The pore width range of ZrO_2-1 nanoparticles is between 109 A and 48 A, and the small pores width range is 27 A-18 A due to thermal collapse of the pore structure of the calcined samples. Figure 4-16 (b) shows that the pore size distribution of ZrO_2-2 and ZrO_2-3 was narrower and there was only one pore size distribution when compared to ZrO_2-1; this may be due to the difference in synthesis temperature. The pore distribution results show that aging temperature has an effect on the porosity of zirconia nanoparticles. As can be seen, the pore size distribution for the ZrO_2-3 that was aged at 150 ^oC was narrower than ZrO_2-1 and ZrO_2-2, which were aged at 50 ^oC and 120 ^oC for 24 hours. This may be due to the varying synthesis temperature. The specific surface area of ZrO_2-1, ZrO_2-2 and ZrO_2-3 nanoparticles calcined at 600 °C are 77 m^2/g, 157 m^2/g, 162 m^2/g and a pore volume of 0.16 cm^3/g, 0.26

cm^3/g and 0.33 cm^3/g, respectively, as shown in Table 4-3, which are bigger than 72 m^2/g obtained when aged at 48hrs without temperature [12]. Table 4-3 shows that the increase in the reaction temperature results in an increase in the specific surface area and pore volume. This may be due to the fact that sintering at higher temperatures decomposes the hydrous zirconia to give fine crystallites of zirconia. Also, as confirmed by TGA results, higher temperature reaction has dry hydrous zirconia than at room temperature. The dry hydrous zirconia shows the condensation between hydroxyl groups, which leads to three-dimensional structures that enhance the porosity of zirconia nanoparticles [40]. Moreover, the zirconia nanoparticles with high porosity as inorganic filler retain water within the membrane, which increases conductivity at a low relative humidity [41].

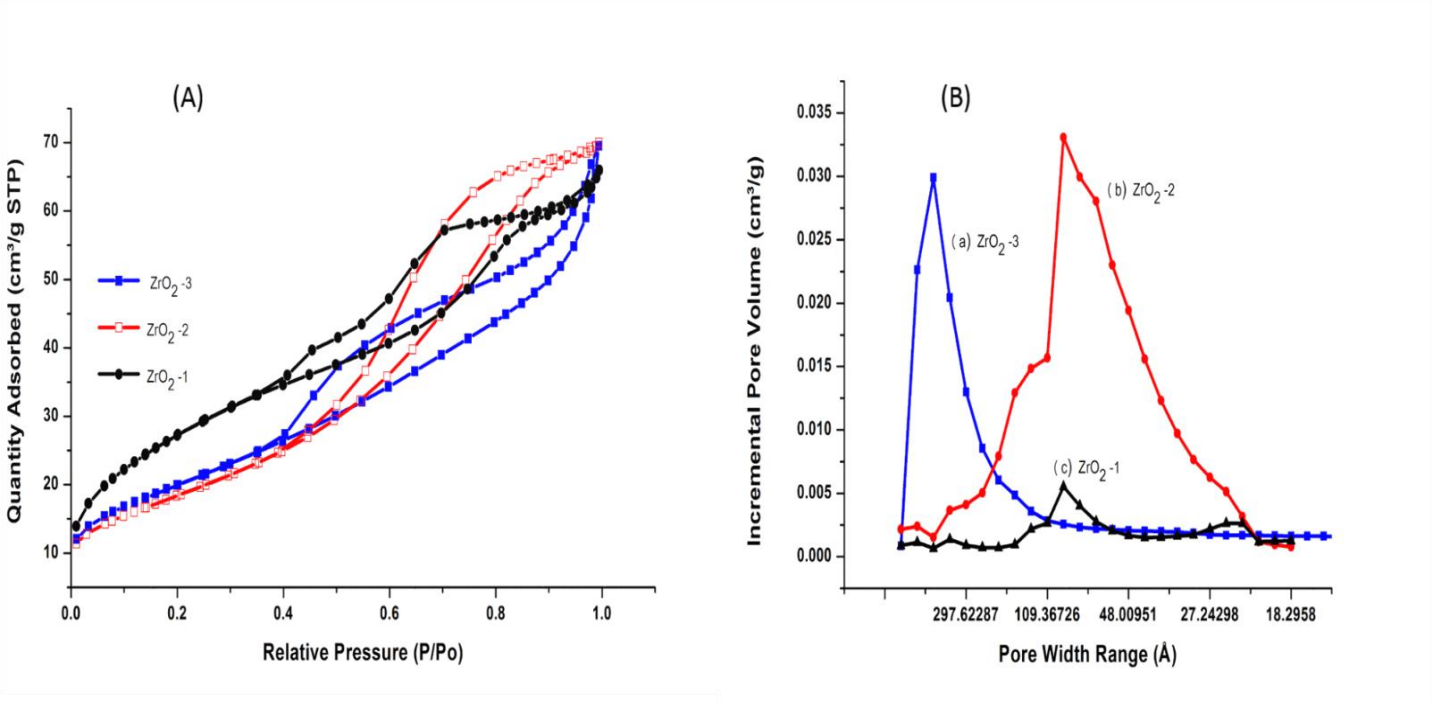

Figure 4- 16: (a) N_2 adsorption-desorption isotherm of ZrO_2-1(a), ZrO_2-2 (b) and ZrO_2-3 (c) nanoparticles; (b) Pore size distribution curves of ZrO_2-1(a), ZrO_2-2 (b) and ZrO_2-3 (c) nanoparticles.

Table 4- 3: BET of ZrO_2 nanoparticles: (a) ZrO_2-1, (b) ZrO_2-2 and (c) ZrO_2-3.

Sample ID	Surface area (m^2/g)	Pore volume (cm^3/g)
ZrO_2-1	77	0.16
ZrO_2-2	157	0.26
ZrO_2-3	162	0.33

4.7.7. CV behaviour of zirconia nanoparticles

The electrochemical behaviour of zirconia nanoparticles was observed under CV and EIS using KCl as shown in Figure 4-17. Figure 4-17(a) shows the CV behaviours of ZrO_2-1, ZrO_2-2 and ZrO_2-3 in KCl electrodes at scan rates of 10 mV s^{-1}. As shown in Figure 4-17, CVs of ZrO_2-1, ZrO_2-2 and ZrO_2-3 modified with Nafion solution resulted in a rectangular shape, which shows the ideal capacitive behaviour [67], with the increased redox peak current; this may be due to the transfer of electrons. Figure 4-17(b-c) show that when the scan rate is increased to 20 mV s^{-1} and 30 mV s^{-1}, this also increases the current, expected for a pure capacitor due to the resistance effects down the pores [68]. At higher scan rates of 50 mV s^{-1} and 100 mV s^{-1}, the volumetric cycle is higher and faster to complete compared to the lower scan rates as shown in Figure 4-17(d-e). ZrO_2-1 shows that the capacitance decreases when the scan rate increases, due to difficulty of the formation of the electrochemical layer at high scan rates as shown in Figure 4-17(a-e). ZrO_2-2 and ZrO_2-3 become stable in all the scan rates, which may be due to their high specific surface area and porosities that enhance the diffusion of ions within the pores [69]. Figure 4-18 shows the CVs of ZrO_2-1, ZrO_2-2 and ZrO_2-3 in $NaNO_3$ electrodes at scan rates of 10 mV s^{-1}, 20 mV s^{-1}, 30 mV s^{-1},50 mV s^{-1} and 100 mV s^{-1}. ZrO_2-1, ZrO_2-2 and ZrO_2-3 represent the redox transitions (anodic and cathodic) between semiconducting states. ZrO_2-1, ZrO_2-2 and ZrO_2-3 were more stable at a scan rate of 10 mV s^{-1}, 20 mV s^{-1}, 30 mV s^{-1} and 50 mV s^{-1} with a sharp peak current and the sharp peak that represents higher voltage and current values. Moreover, the CV of the $NaNO_3$ electrolyte shows a higher electrochemical reaction than the KCl electrolyte as shown in Figures 4-17 and 4-18, due to the higher redox peak [70]. Figure 4-18 (e) shows that ZrO_2-3 obtained a higher current response and higher charge transfer resistance compared to ZrO_2-1 and ZrO_2-2 at a scan rate of 100 mV s^{-1}. This may be due to the high pore size of ZrO_2-3 which increases the porosity of Nafion. However, the increases in ionic resistivity of ZrO_2-1, ZrO_2-2 and ZrO_2-3 at the higher scan rate of 100 mV s^{-1} decrease the capacitance of the electrode. This may be due to the slower transfer rate of ions, which leads to either depletion or saturation of protons in the electrolytes inside the electrode during the redox process as shown in Figures 4-17(e) and 4-18(e). Furthermore, the CV of KCl and $NaNO_3$ electrolyte shows that the capacitance increases in higher surface area and smallest particle size with a small distance between the fringes and a lower surface area than zirconia nanoparticles, as confirmed by the BET and HRTEM results.

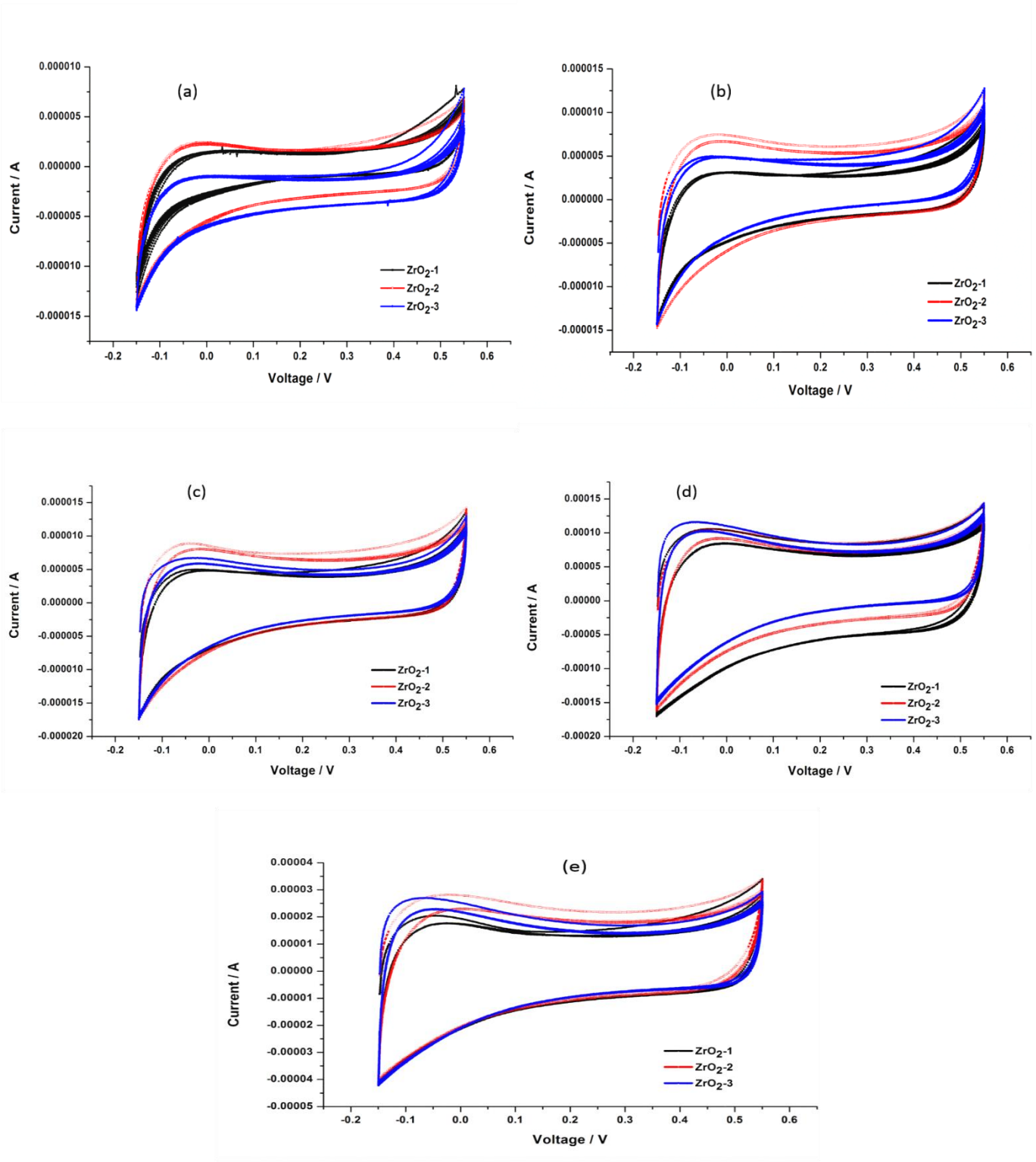

Figure 4- 17: CV of ZrO_2-1, ZrO_2-2 and ZrO_2-3 in KCl electrodes at scanning rate of (a) 10 mV s^{-1}, (b) 20 mV s^{-1}, (c) 30 mV s^{-1}, (d) 50 mV s^{-1} and (e) 100 mV s^{-1}.

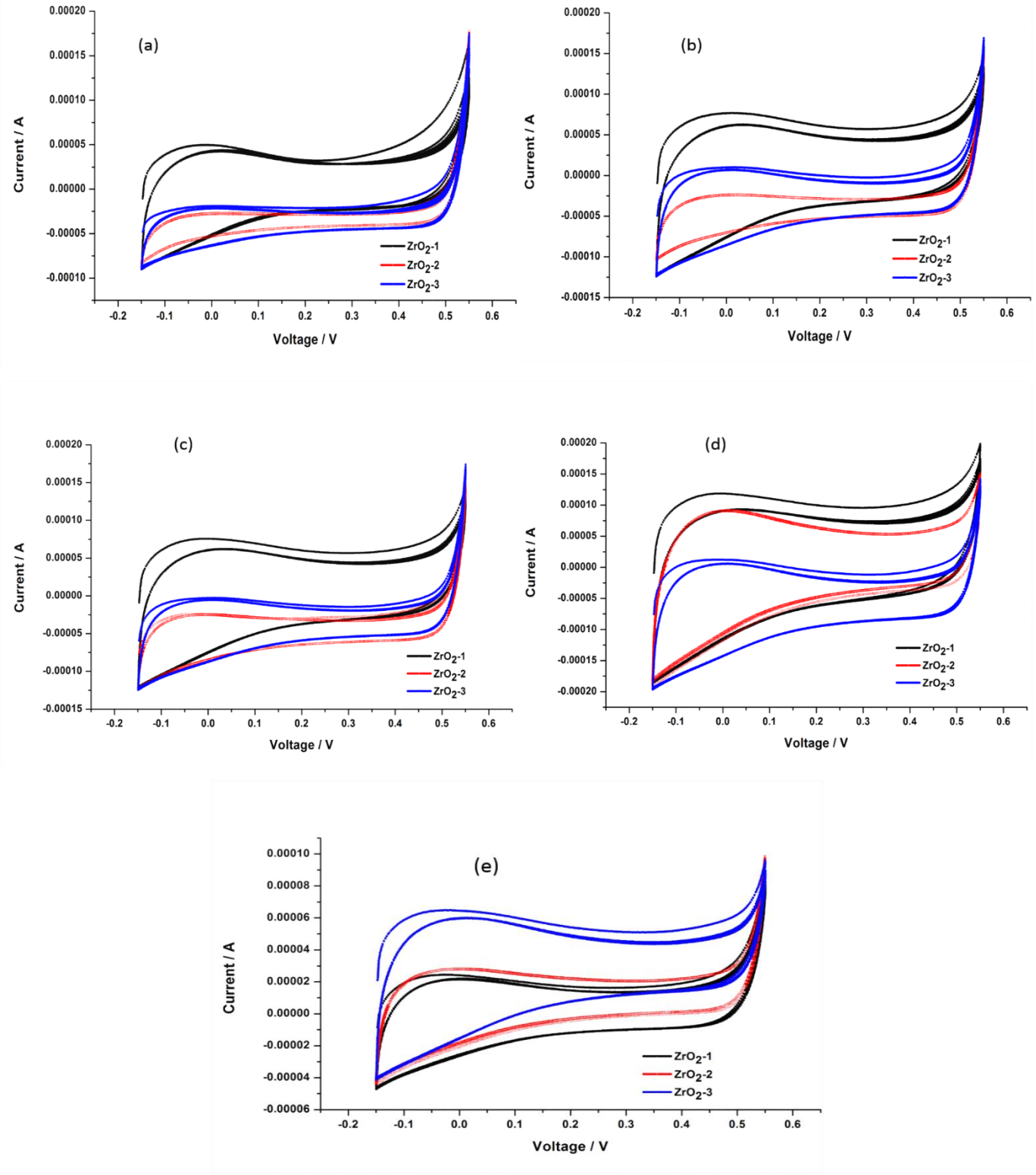

Figure 4- 18: CV of ZrO_2-1, ZrO_2-2 and ZrO_2-3 in $NaNO_3$ electrolytes at scanning rate of (a) 10 mV s^{-1}, (b) 20 mV s^{-1}, (c) 30 mV s^{-1}, (d) 50 mV s^{-1} and (e) 100 mV s^{-1}.

Figure 4-19 represents the Nyquist plot measurements performed to investigate the charge kinetic properties of ZrO_2-1, ZrO_2-2 and ZrO_2-3 in 2M KCl and $NaNO_3$ electrolyte. Figure 4-19(a-b) shows the Nyquist plots obtained for these cells in the frequency range from 100 kHz to 0.01 Hz. ZrO_2-1 shows a curved region of a 45^o slope at a low frequency side, which may be due to weak electrical conductivity. ZrO_2-2 and ZrO_2-3 have vertical Nyquist plots without a curve region as shown in Figure 4-19(a) insert due to the electrons transfer through their porous structure of nanoparticles. Figure 4-19(b) and insert show only the vertical plots without any curves with a high charge transfer resistance in 2M KCl solution. KCl electrolytes show a higher charge transfer resistance than $NaNO_3$, indicating good capacitive behaviour without diffusion limitation. Figure 4-19(a-b) show that ZrO_2-1, ZrO_2-2 and ZrO_2-3 exhibit typical characteristics of porous nanoparticles [69]. This shows that zirconia nanoparticles can increase the conductivity of the Nafion® membrane, which will be used as an electrolyte of fuel cells. The result in Figure 4-19(a-b) shows that ZrO_2-2 and ZrO_2-3 have a rapid charge transportation as electrode material in all the electrolyte solution due to high porosity. Moreover, the vertical slope indicates the ion diffusion through the composite; this indicates that zirconia nanoparticles with a controlled nanocrystal shape and small distance between lattice fringes can increase conductivity, which makes them suitable for use in fuel cell applications.

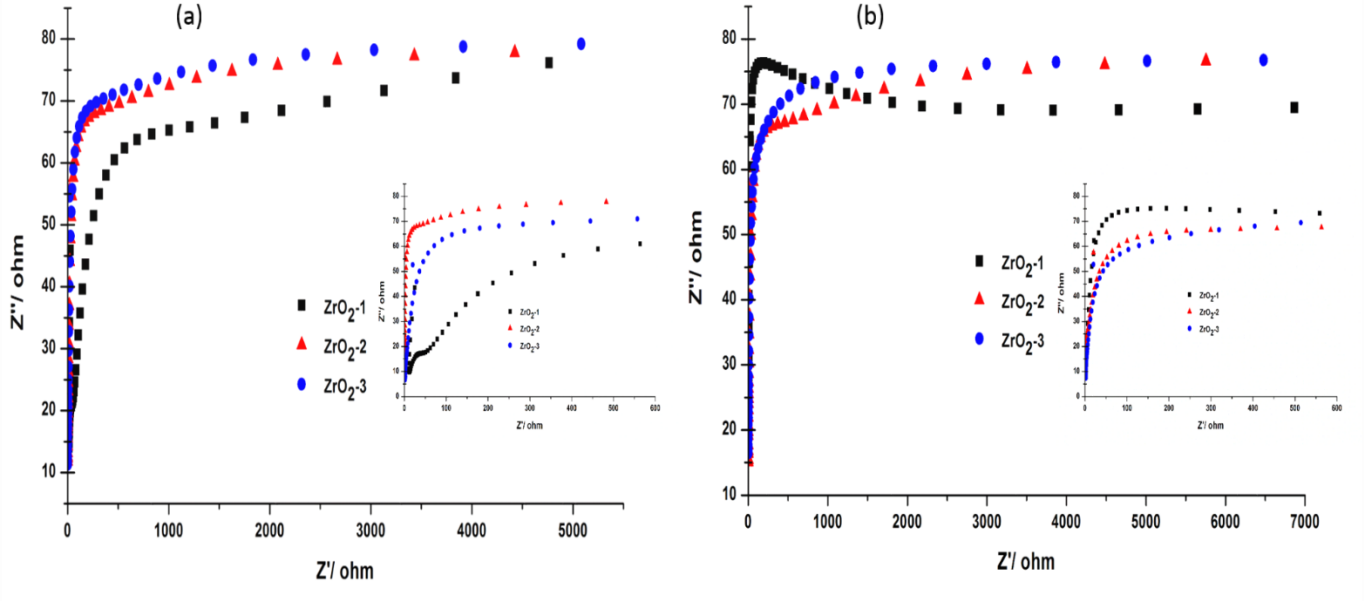

Figure 4- 19: Nyquist plots of ZrO_2-1, ZrO_2-2 and ZrO_2-3 in (a) $NaNO_3$ and (b) KCl electrolytes at a range of 10 kHz–1Hz.

4.8. Conclusion

The HRTEM results show that the lattice fringes of nanoparticles become smaller as their size decreases. The lattice fringes are equidistant and clear, all along the length of the nanorods and width of the nanoparticle, without any lattice mismatch, hence depicting a single crystalline-like structure. The HRTEM image of a single zirconia nanoparticle with the electron diffraction pattern of (1 1 1) planes of the cubic and monoclinic structure were obtained. It was observed that synthesis temperature has an effect on porosity and nanoparticle sizes, as all the nanoparticles were smaller than 20 nm as confirmed by powder HRTEM results. The XRD results confirm the formation of single-phase c-ZrO_2 and m-ZrO_2 and crystallinity. The TGA results show that the higher temperature degradation of ZrO_2 nanoparticles was stable due to synthesis temperature. It was observed in FTIR results that the slight shift of the Zr-O vibration peak and the disappearance of the Zr-O-Zr vibration peak on ZrO_2-3 nanoparticles may be due to the high synthesis temperature. The porosity of zirconia nanoparticles was observed under BET. The synthesis temperature of zirconia nanoparticles shows an effect in electrochemical tests. ZrO_2-2 and ZrO_2-3 obtained good electrochemical performance, good stability and good ion flow compared to ZrO_2-1. This good electrochemical performance is due to the higher surface area and pore volume, which promotes the transfer of electrons. The Nyquist plot of ZrO_2-1, ZrO_2-2 and ZrO_2-3 in the $NaNO_3$ and KCl electrolytes exhibited typical characteristics of porous nanoparticles. A KCl electrolyte shows a higher charge transfer resistance than $NaNO_3$, indicating good capacitive behaviour without diffusion limitation. These results show that zirconia nanoparticles can increase the conductivity of the Nafion® membrane, which will be used as an electrolyte of fuel cells.

C: Structural morphology of blended Nafion®-Polyacrylonitrile/zirconium phosphate nanofibers

4.9. Introduction

Polymer nanofibers are prepared by electrospinning a polymer solution, with a high-voltage electric field applied to a polymer solution ejected from a metal syringe needle. Electrospinning is when the electric forces are utilised within the polymer solution to produce the varied morphology. Moreover, by varying viscosity, surface tension, molecular structure, molecular weight, solution concentration, solvent structure, additive and operational conditions such as rotating speed, spinning head diameter, nozzle diameter and nozzle-collector distance of the same solution may produce a nanofiber web with the various fineness, orientation and surface morphology [71]. Many researchers focus on how to synthesise high surface area nanofibers (less than 1 000 nm), which make them useful in fuel cell membranes, tissue engineering, catalysis, sensors, separations, electrochemical cells, drug delivery and chemical filtration [2]. Some of the researchers also focus on the proton conductivity of electrospun nanofibrous mats [72]. Nafion® membrane is a perfluorinated state-of-the-art polymer developed by DuPont in the 1970s. Nafion® at low temperature maintained a high proton conductivity and chemical resistance due to its hydrophobic tetrafluoroethylene backbone and sulfonate groups. Electrospinning Nafion® solution increases the proton conductivity of nanofibers with the reduced nanometer scale [73]. Electrospinning the plain Nafion® solution is impossible due to the low shear viscosity that makes Nafion® aggregates in the solution [74-75]. Nafion® solution was blended with other polymers such as poly(ethylene oxide) (PEO) [76], poly(acrylic) (PAA) [77], or poly(vinylalcohol) (PVA) [7] and polyacrylonitrile (PAN) [74, 78] in order to enhance the mechanical properties and electrospinning. Furthermore, blending Nafion® solution with electron-conducting polymers may enhance their protons' conductivity and their electrons. PAN is mostly the chosen copolymer for the preparation of fibrous filter media as it can be fabricated easily into nanofibers by electrospinning due to their superior mechanical properties, excellent weatherability and chemical stability [79]. Moreover, PAN also maintains a good thermal stability at a higher temperature of 130 °C and has a good resistance to many organic solvents. PAN has been studied as a separator material and PAN-based separators show promising properties, including high ionic conductivity, good thermal stability, high electrolyte uptake and good compatibility, with lithium metal [80]. Electrospinning of composited PAN nanofibers has been found to have multifaceted applications [81], such as electrode materials in supercapacitors and fuel cells [82]. Zirconium oxide (ZrO_2) has several properties that make it a useful material. These properties include high density, hardness, electrical conductivity, wear resistance, high fracture toughness, low thermal conductivity, and relatively high dielectric constant. Because of its high refractive index and high oxygen-ion conduction, ZrO_2 has been applied as resistive heating elements, oxygen sensors, catalysts and fuel

cells [42]. The use of totally stabilised zirconia in fuel-cell technology obtain a good ionic conductivity of cubic zirconia at medium and high temperatures [12]. Zirconium phosphates (ZrP) are inorganic cation exchange material with high thermal stability. Zirconium phosphate has the features of increasing conductivity due to high proton mobility on the surface of its particles, and good water retention. The reduced methanol permeability of the polymer membrane while maintaining a high power density is obtained by impregnating it with zirconium phosphate [83-84]. In this work, we study the effect of ZrP nanofillers on the improvement of the morphological and conductivity of blended Nafion®-PAN nanofibers compared with pure PAN nanofibers, which can be fabricated by electrospinning into nanofiber mats.

4.10. Experimental

4.10.1. Materials

Nafion® solution D521 (Ion Power) was purchased from Ion Power. Polyacrylonitrile (PAN), average Mw 150,000 g/mol, was purchased from Sigma-Aldrich. N, N-dimethylformamide (DMF) (99.8%) (Merck), sodium hydroxide (Merck), N, N-dimethylformade (Merck), phosphoric acid (Merck), sulfuric acid (Merck), zirconium oxychloride hydrate (Merck), were obtained and used as received.

4.10.2. Preparation of electrospinning solutions

Plain Polyacrylonitrile (PAN) nanofiber solutions were obtained by dissolving PAN (1g) in DMF (6g) solution and a magnetic mixer stirred the solutions for three hours at 80 °C [85].The obtained solution was divided into three parts. One part was for plain PAN, and other parts for the PAN/ ZrP and Nafion®-PAN/ ZrP nanofibers. In order to prepare the PAN/ ZrP nanofibers, 0.1 wt% ZrP nanoparticles were added to the obtained solution and sonicated for 30 min to obtain a homogenous solution and magnetically stirred for three hours at 80 °C. Moreover, the third part 5:5 Nafion®/PAN and 0.1 wt% ZrP nanoparticles were added and magnetically stirred for three hours at 80 °C. The obtained solution was spun by an electrospinning system perpendicularly aligned to the target collector. The electrospinning solution was fed by using a syringe of 10 mL through a capillary tip with a diameter of 1.25 mm. A voltage of 16 kV and a syringe pump were used to feed the electrospinning solution at a constant rate of 0.5 mL/h. The distance between the nozzle and the collector was set as 10 cm. The collector plate was covered with aluminium foil to gather the resultant nanofibers at a specified distance as shown in Figure 4-20.

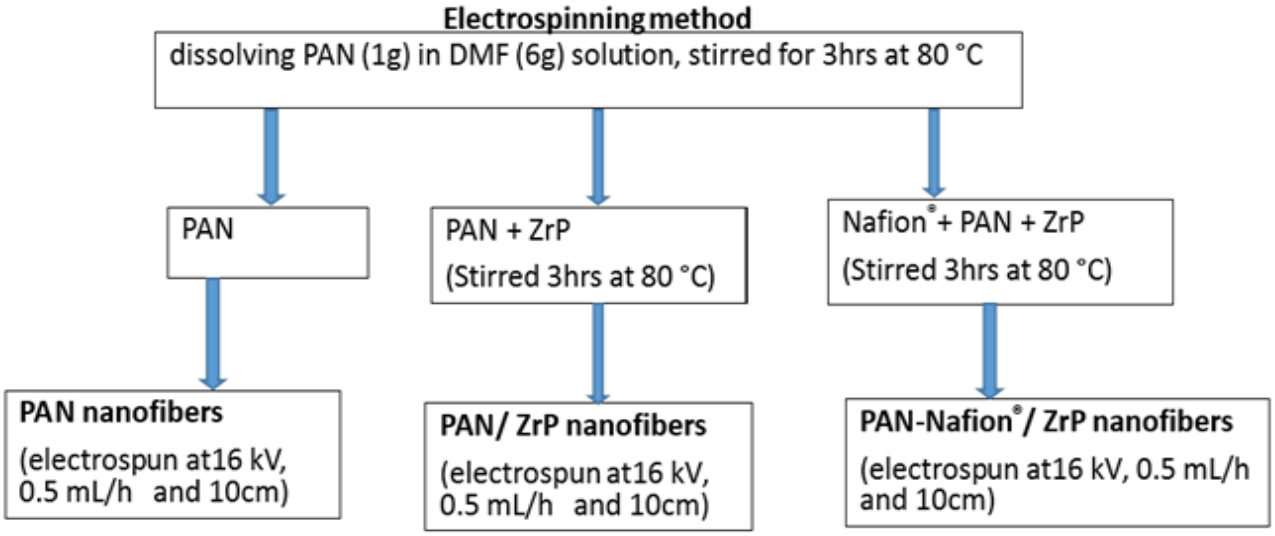

Figure 4- 20: Electrospinning process.

4.10.3. Characterisation

The X-ray diffraction (XRD) analysis was performed using a Philips X-ray automated diffractometer, with a Cu K radiation source. Samples were scanned in continuous mode, from 5° to 90° (2 theta). The thermal properties of the samples and their characteristics were studied by thermal gravimetric analysis (TGA) under nitrogen flow. TGA data was obtained with the PerkinElmer instrument, over nitrogen and at a heating rate of 10 °C/min from 50 °C to 1 000 °C. Fourier transform infrared (FTIR) spectroscopy was used to determine the quality and composition of the sample. FTIR spectra were obtained with a (Vertex 70 Bruker) FTIR instrument over a range of 4 000–400 cm^{-1} and a resolution of 4 cm^{-1}. The surface morphology of the nanofibers was analysed by atomic force microscopy (AFM) and Scanning Electron Microscopy (SEM).

4.10.4. **Electrochemical studies**

Electrochemical measurements were observed under three electrodes. While a silver-silver chloride (Ag/AgCl) electrode was used as the reference electrode, zirconium nanoparticles coated on glassy carbon were used as a working electrode, and Pt wire was used as a counter electrode. 0.03 g of PAN, PAN/ ZrP and Nafion®-PAN/ZrP nanofibers were ultra-sonicated in 0.5 ml of 1 wt% Nafion® in absolute ethanol for 30 minutes, and pipetted a 0.05 ml suspension onto the glassy carbon electrode and dried at ambient temperature [64]. Cyclic voltammetry (CV) and electrochemical impedance spectroscopy (EIS) were observed under 2M of KCl electrolyte. The scan rates used were 10 mV s^{-1}, 20 mV s^{-1}, 30 mV s^{-1}, 50 mV

s^{-1} and 100 mV s^{-1} with the CV test ranging from -0.15 V to 0.55 V vs. EIS measurements were obtained under the frequency range of 100 kHz to 0.01 Hz.

4.11. Results and discussion

4.11.1. **Morphologies and structures**

The effect of zirconium phosphate nanoparticles on nanofibers were confirmed under SEM micrographs of PAN, PAN/ZrP and PAN-Nafion®/ ZrP nanofibers electrospun on the same conditions (voltage 16 kV, distance 10 mm) as presented in Figure 4-21. It was observable in Figure 4-21(a-b) and 4-22(a(II)) that nanofibers are smooth, uniform in morphologies and uniformly arranged on top of each other with average diameters of 100–200 nm. The modified PAN nanofibers with zirconium phosphate nanoparticles showed the surface smoothness with the reduced diameters of 100–150 nm as presented in Figure 4-21 (c-d). These may be due to the increase of conductivity within the composited solution with zirconium phosphates ions, which reduced the diameter of the nanofibers [86]. At a lower magnification of 100 nm, PAN/ ZrP nanofibers present smooth and overlaying on top of each other; this could be due to the presence of zirconium phosphate nanoparticles within the nanofibers as shown in Figure 4-21(d) and 4-22(b II). Figure 4-21(e-f) shows that PAN-Nafion®/ ZrP nanofibers obtained a different morphology with the rougher surface without beads and slightly increases diameters of 150–300 nm whereas the PAN nanofibers obtained a uniform morphology and relatively smoother surface [87]. That surface roughness and slightly increased diameter may be due to the addition of a Nafion® solution [78]. Furthermore, the addition of ZrP nanoparticles in the PAN-Nafion® solution reduces the diameters as presented in Figure 4-21(e-f) and 4-22(c II). Topography images measured in tapping mode of PAN, PAN/ ZrP and PAN-Nafion®/ ZrP nanofibers are shown in Figure 4-22. Figure 4-22(c II) shows that the PAN-Nafion® solution modified with ZrP nanoparticles has roughness in all the area, when compared with PAN/ ZrP (Figure 4-22(b II) and PAN (Figure 4-22(a II) nanofibers, which shows less roughness in all the dark (hydrophilic) and light (hydrophobic) sections [88]. This may be due to the Nafion® solution that introduced the surface roughness of nanofibers. Moreover, PAN-Nafion®/ ZrP nanofibers have more darkness than the lighter surface; these may be due to the enhanced water within the nanofibers.

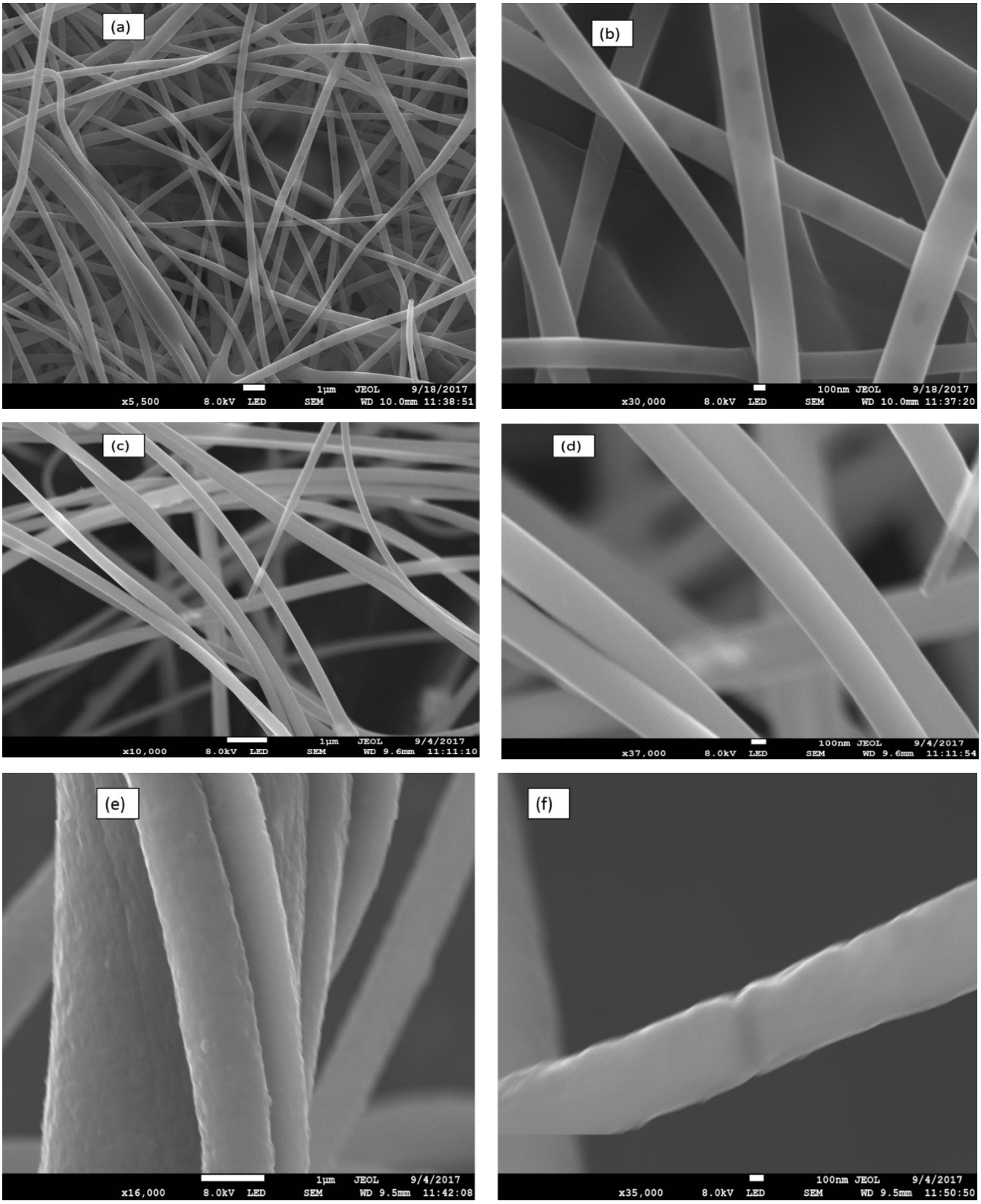

Figure 4- 21: Scanning electron microscopy (SEM) (a) and (b) SEM micrographs of PAN nanofibres. (c) and (d) micrographs of PAN/ZrP nanofibers and (e) and (f) micrographs of PAN-Nafion/ZrP nanofibres at low and high magnification.

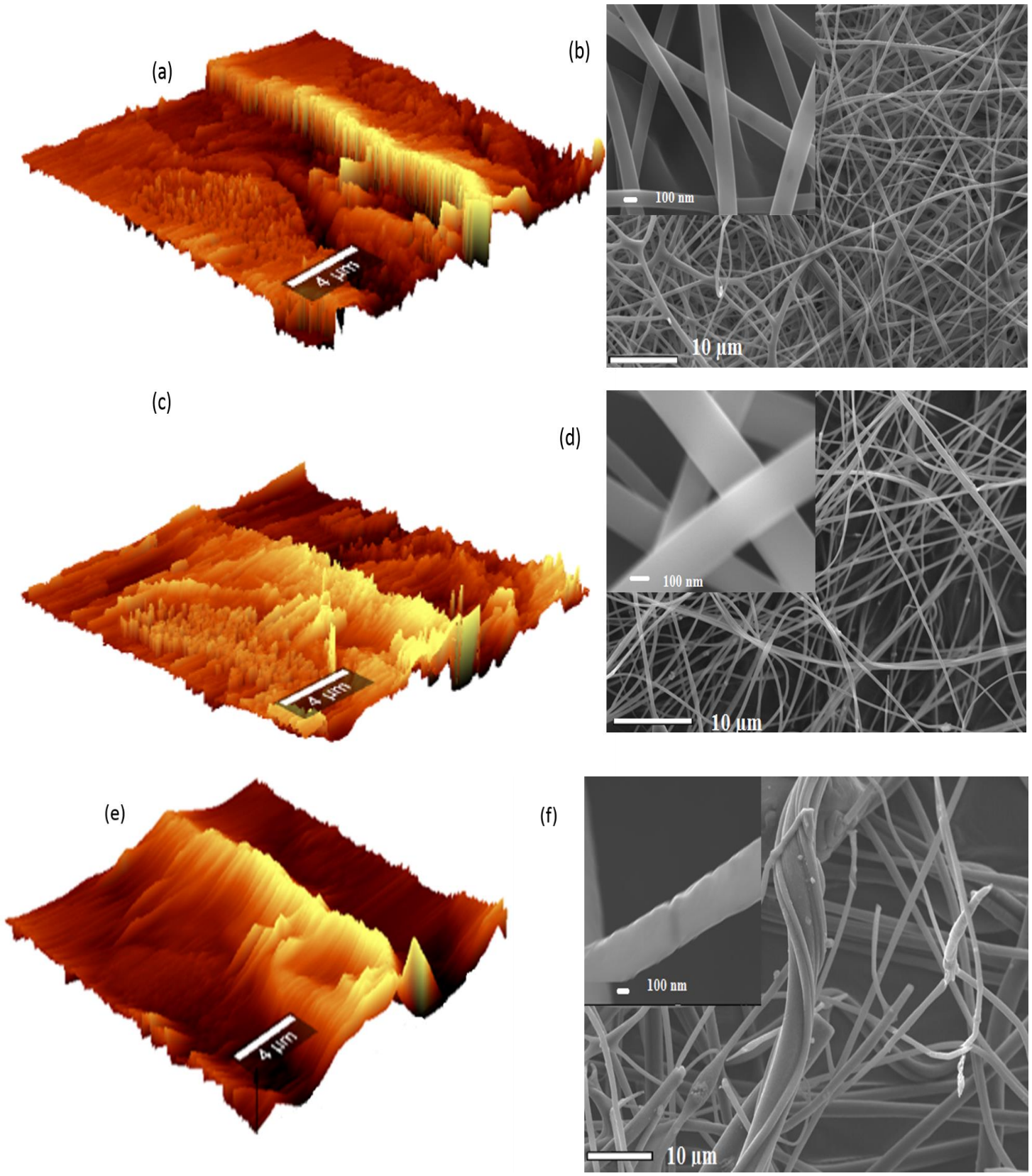

Figure 4- 22: Atomic force microscope images SEM images at scale bars of 10 µm and 100 nm of (a-b) PAN nanofibers, (c-d) PAN/ZrP nanofibers and (e-f) PAN Nafion/ZrP nanofibers.

4.11.2. The X-ray diffraction (XRD) analysis

Figure 4-23 shows the X-ray diffraction pattern of PAN, PAN/ ZrP and PAN-Nafion®/ ZrP nanofibers. The weak peak at 2theta = 17.6 °, 2theta = 24.9 °, 2theta = 37.1 °, 2theta = 50.4 °, 2theta = 55.4 ° and 2theta = 59.1 °, with a strong peak of 2theta = 39.2 °, indicated the crystalline peaks of ZrP as shown in Figure 4-23(a). This PAN-Nafion®/ ZrP nanofibers show peaks at 2theta are 21.5 °, 26.8 °, 30.8 °, 36.4 °, 49.4 °, 54.5 ° and 58.1 ° which correspond to planes (2 0 0), (2 1 1), (2 2 0), (3 1 1), (4 2 0) as shown in figure 4-23(b) [89-90]. XRD patterns in Figure 4-23(b) show only the crystalline peak of ZrP nanoparticles without reflecting the peak of electrospun Nafion® and PAN. Appearance of ZrP crystalline peaks indicates that the metal oxide was successfully composited within the electrospun nanofibers. The PAN nanofibers are amorphous with the strong peak at 2theta = 17.6 °, that assigned to crystal planes of PAN as shown in Figure 4-23(c) [91].

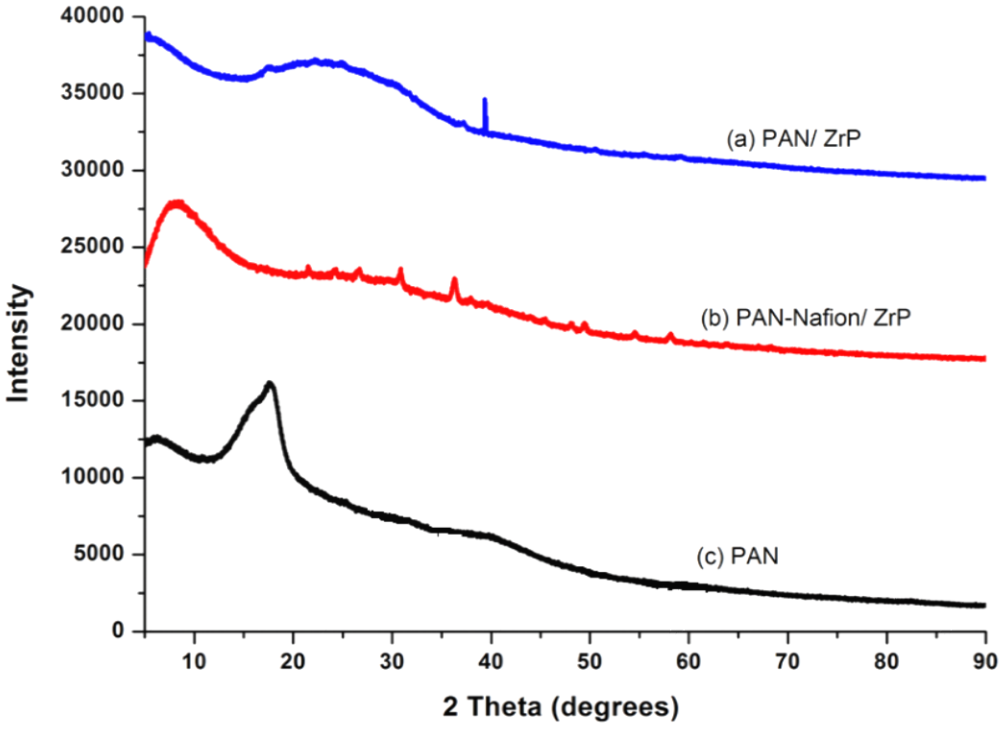

Figure 4- 23: The comparison of the XRD patterns of the (a) PAN/ZrP nanofibers, (b) PAN-Nafion®/ ZrP nanofibres and (c) PAN nanofibers.

4.11.3. **Fourier transform infrared spectroscopy (FTIR)**

FTIR spectra analysis of PAN, PAN/ ZrP and PAN-Nafion/ ZrP nanofibers are presented in Figure 4-24. Figure 4-24(a-c) show the vibration peak at 2933 cm^{-1} (CH stretching) and 1456 cm^{-1} (CH bending) which

can be assigned to vibrations of the CH and CH_2 group of PAN [92]. Also the peaks at 2246 cm^{-1}, 1673 cm^{-1} and 1630 cm^{-1} related to the stretching vibration of nitrile groups C≡N and C= O stretching vibrations of the acrylonitrile [93]. Figure 4-24 (a) shows the vibration peaks of 1097 cm^{-1} and 658 cm^{-1} that are assigned to Zr-O vibration and P-O_4 stretching due to the present of ZrP nanoparticles within the PAN nanofibers and 978 cm^{-1} which correspond to the C-O-C stretching [27]. FTIR spectrum of the composite PAN-Nafion/ ZrP nanofibers shows the presence of Nafion polymer [94] as shown in figure 4-24(b), with the strong bands at 1233 cm^{-1} and 1149 cm^{-1}, which correspond to the -C-F- stretching [95-96]. Figure 4-24(a-b) shows the disappearing of vibrational structures at 1742 cm^{-1} for C= O stretching vibration of the PAN backbone [97]. This may be due to the incorporation of ZrP nanoparticles that reduced some of the vibration peaks of PAN polymer. Figure 4-24(a-b), shows vibration bands at 2361 cm^{-1} are assigned to O-H bonding, the peak observed at 2335 cm^{-1} is due to the presence of inorganic ions. Therefore, the appearance of Zr-O groups at the PAN nanofibers was caused by the zirconium phosphates composited within the electrospun solution.

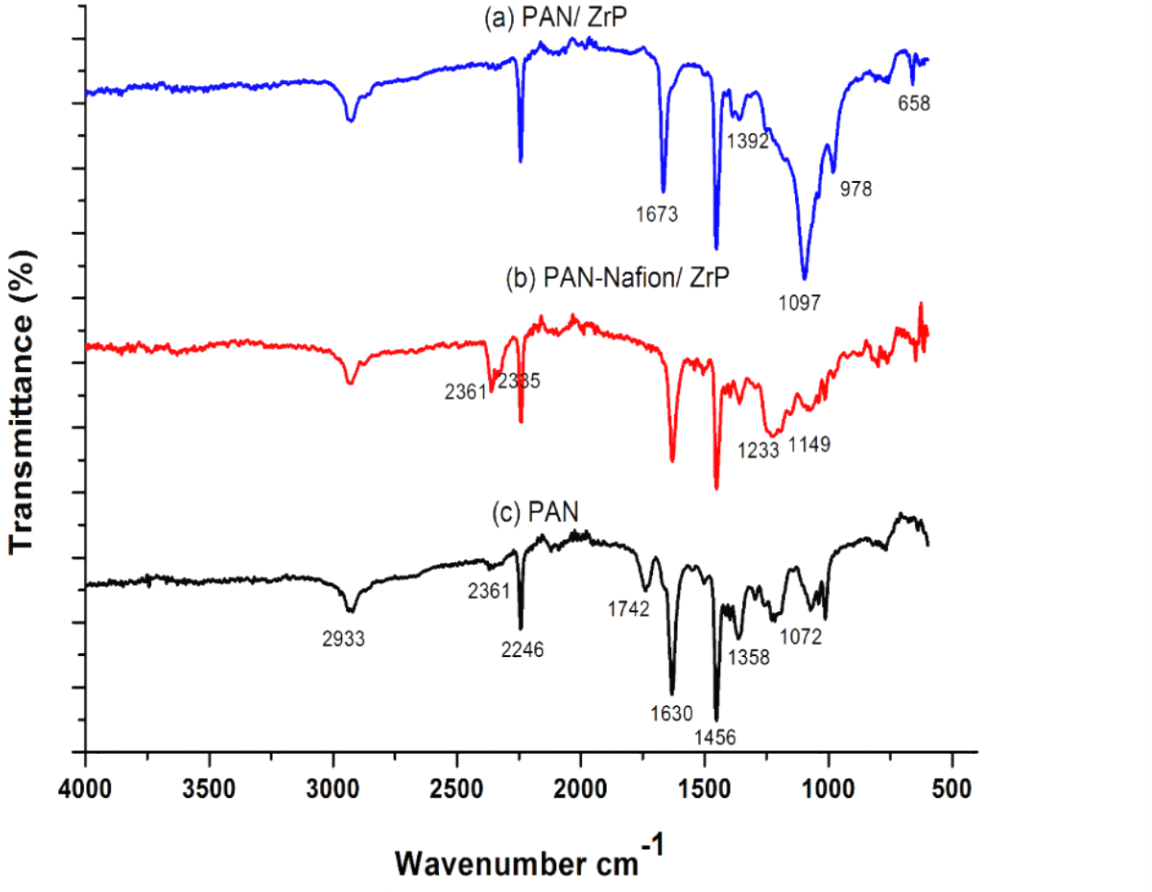

Figure 4- 24: FTIR spectra of (a) PAN/ZrP nanofibers, (b) PAN-Nafion/ZrP nanofibers and (c) PAN nanofibres.

4.11.4. Thermo-gravimetric analysis (TGA)

Figure 4-25 shows the TGA curve of PAN nanofibers. The TGA results show that the initial weight loss occurred at 300 °C in PAN, PAN/ ZrP and PAN-Nafion/ ZrP nanofibers, with a little weight loss as shown in Figure 4-25(a-c) due to dehydration. The second weight loss occurs at 333 °C, due to the release of the volatile gases. The third weight loss occurs at 565 °C, due to partial evaporation of NH_3 and HCN [98]. In addition, the final weight loss stage is at 882 °C, due to the total evaporation of polymer chain fragments from the PAN nanofibers. Figure 4-25(a) shows that PAN-Nafion/ ZrP nanofibers are thermally more stable than PAN and PAN/ ZrP nanofibers as they have a higher decomposition temperature. These may be due to thermal decomposition of composited Nafion polymer that occurs in three stages, and the incorporation of ZrP nanoparticles that presented the interactions between ZrP and Nafion-PAN nanofibers.

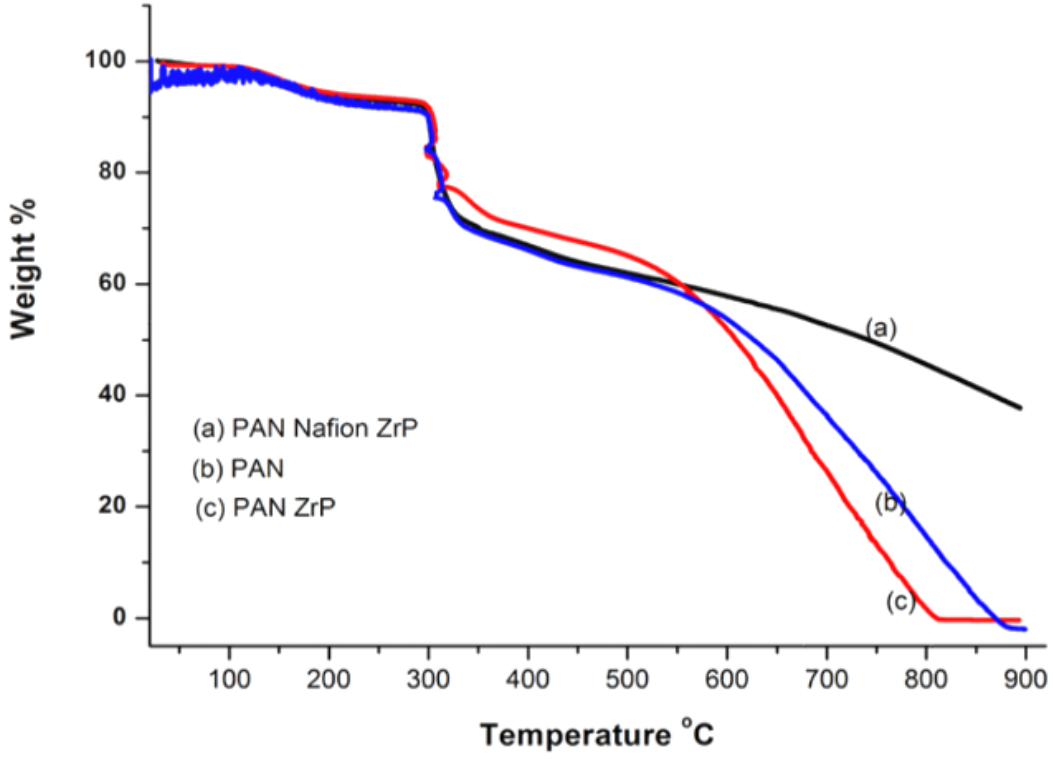

Figure 4- 25: Thermal gravimetric analysis (TGA) and derivative thermogravimetric of (a) PAN-Nafion/ZrP nanofibers, (b) PAN nanofibers and (c) PAN/ZrP nanofibers.

4.11.5. Electrochemical properties

Figure 4-26 shows the cyclic voltammograms (CV) of PAN, PAN/ ZrP and PAN-Nafion/ ZrP nanofibers at a scan rate of 10 mV s^{-1}, 20 mV s^{-1}, 30 mV s^{-1}, 50 mV s^{-1} and 100 mV s^{-1}. The CV of modified PAN shows a higher current response and less estimated charge transfer resistance in all the scanning rates as shown in Figure 4-26 (a-f). In Figure 4-26(a-f), it is observed that the current is directly proportional to the scan

rates of CV, as when the scan rate increases, the current also increases [99]. This may be due to the higher response of redox peak in all the nanofibers. Figure 4-26(f) shows the electrochemical stability of all the nanofibers at the scan rate of 100 mV s^{-1} and 5 cycles, with CV test ranging from -0.15 V to 1.0 V, as it has obtained a rectangular curve at high electronic conductivity and good charge dissemination [100]. This indicates that these nanofibers can be suitable materials to be used as electrolytes or the modification of electrolytes for the application of supercapacitors or fuel cells due to their fast charge and discharge behaviour. However, the CV reduction of PAN-Nafion/ ZrP nanofibers at a scan rate of 10 mV s^{-1}, 20 mV s^{-1}, 30 mV s^{-1}, 50 mV s^{-1} and 100 mV s^{-1} may be due to the conductivity as confirmed by Nyquist plots below. Figure 4-27 shows the Nyquist plots of PAN, PAN/ ZrP and PAN-Nafion/ ZrP nanofibers. It can be observed in Figure 4-27 that PAN-Nafion/ ZrP nanofibers obtained a nearly straight line without a semicircle in the high-frequency region. This indicates the ultralow charge transfer resistance during the electro-catalytic process in the composite nanofibers. The Figure 4-27 insert shows that PAN/ ZrP and PAN-Nafion/ ZrP nanofibers obtained a smaller resistance when compared with that of plain PAN nanofibers. These may be due to the incorporation of ZrP nanoparticle, which has high proton mobility. However, PAN-Nafion/ ZrP nanofibers show as highly conductive as they can be observed on Nyquist plots as show in Figure 4-27, which obtained a very steep line that shows how fast the charge transfers. PAN/ ZrP nanofibers show steep linear slopes at high frequencies as presented in Figure 4-27. It is observable that the conductivity for PAN-Nafion/ ZrP and PAN/ ZrP nanofibers is more improved than the plain PAN nanofibers. This shows that the addition of the ZrP nanoparticle has an impact on increasing electro-catalytic resistance. Furthermore, the plain PAN nanofibers show a long arc in the high-frequency region and a relatively flat curve in the low-frequency region, due to its poor electroactivity in charge transport, compared with the modified PAN nanofibers as shown in Figure 4-27 (insert).

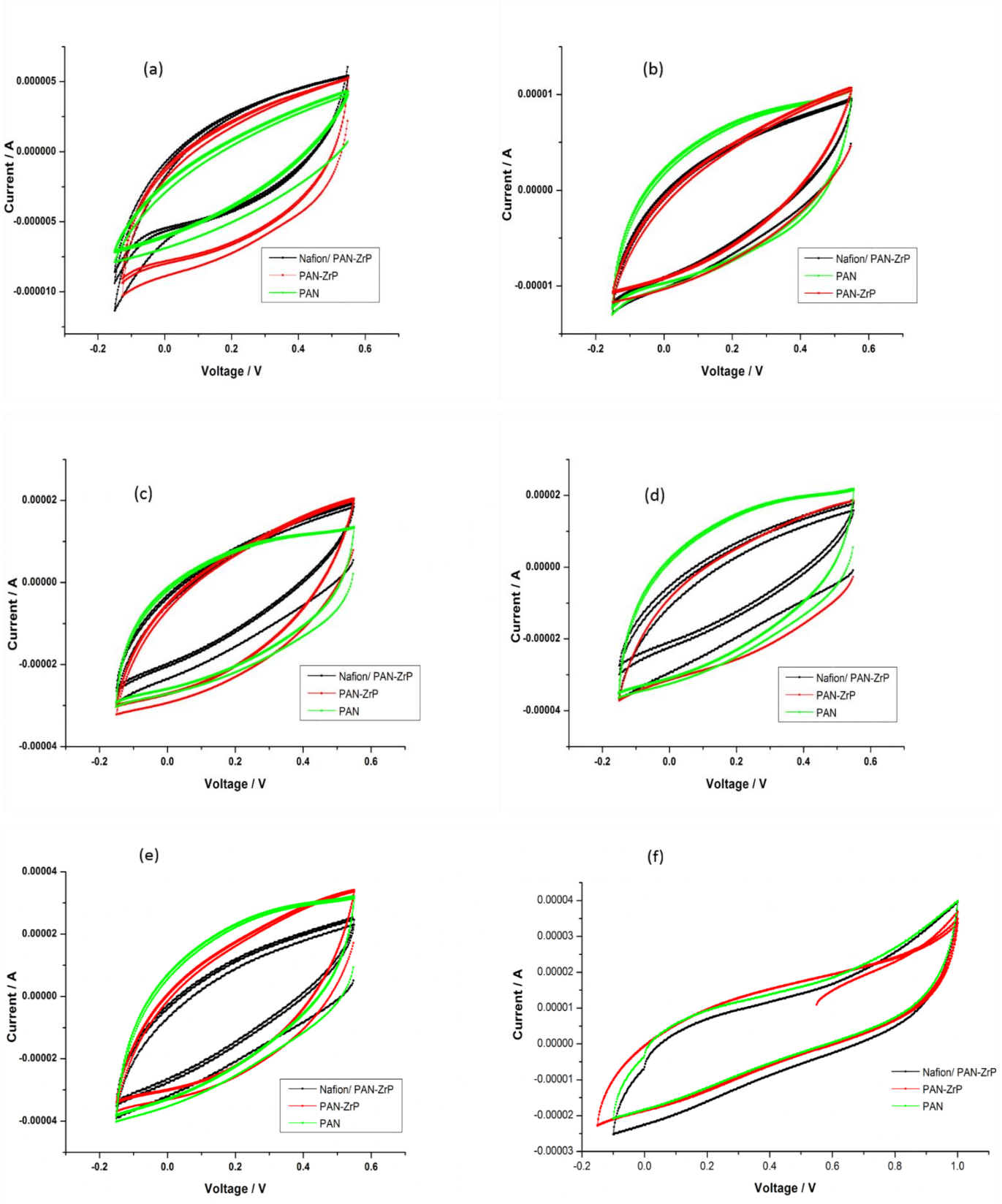

Figure 4- 26: Cyclic voltammograms of PAN, PAN/ ZrP and PAN-Nafion/ ZrP nanofibers at (a) 10 mV s^{-1}, (b) 20 mV s^{-1}, (c) 30 mV s^{-1}, (d) 50 mV s^{-1}, (e) 100 mV $s^{-1}$and (f) 100 mV s^{-1} and CV test ranging from -0.15 V to 1.0 V.

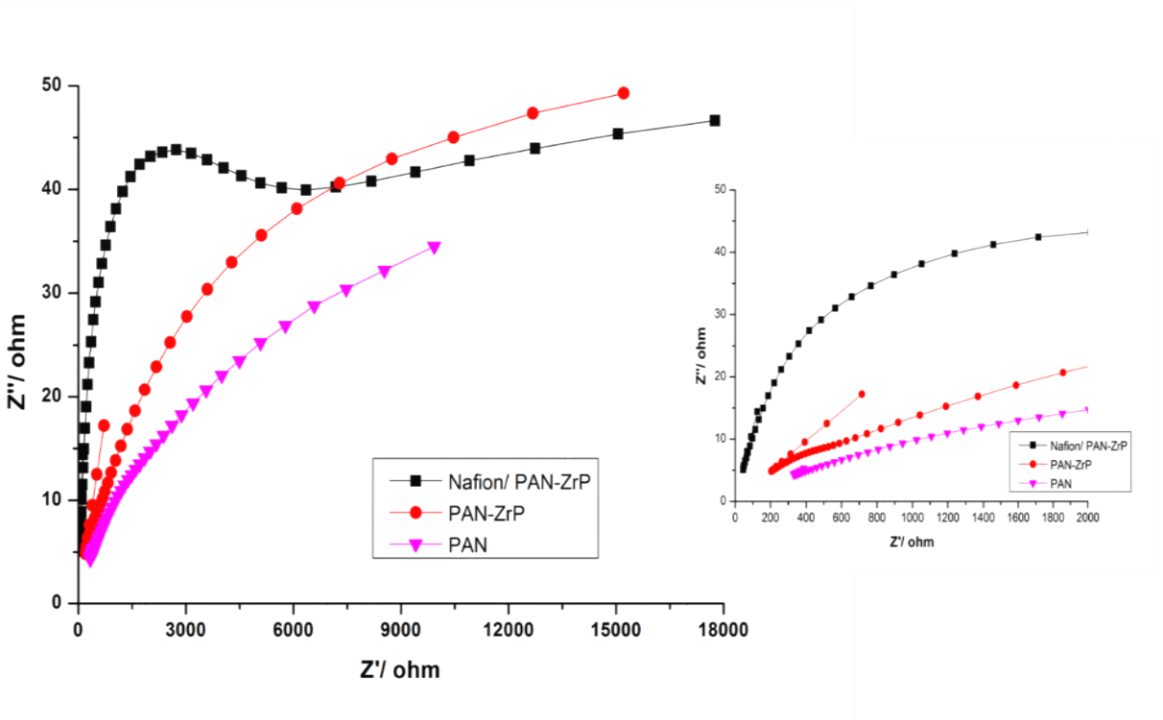

Figure 4- 27: Nyquist plots for PAN, PAN/ ZrP and PAN-Nafion/ ZrP nanofibers.

4.12. Conclusion

The SEM images show that the electrospun PAN-Nafion nanofibers modified by ZrP nanoparticles obtained a reduced diameter and roughness without formation of beads. In addition, PAN shows a more reduced diameter of 100 nm due to the ZrP nanoparticles being well distributed within the nanofibers. The XRD results also show well-crystallised zirconium phosphates within the modified PAN nanofibers. Moreover, the obtained results show that the thermal degradation properties of PAN-Nafion/ZrP nanofibers improve at a high temperature of 500 °C, with a high conductivity under CV and Nyquist plots. It can be concluded that the addition of ZrP nanoparticles within PAN and PAN/ Nafion nanofibers can reduce the diameter while improving the conductivity. When PAN blended with Nafion solution it stabilised the high decomposition temperature of Nafion. Furthermore, PAN-Nafion/ZrP nanofibers show a high stability in Nyquist plots due to the incorporation of zirconium phosphate nanoparticles that allow improved electrode surface accessibility. The plots obtained rectangular curves at high electronic conductivity and good charge dissemination. This makes composited nanofibers with ZrP nanoparticles suitable to be used as the electrolyte of a promising fuel cell application.

4.13. References

1. Arantes, T. M.; Mambrini, G. P.; Stroppa, D. G.; Leite, E. R.; Longo, E.; Ramirez, A. J.; Camargo, E. R., Stable colloidal suspensions of nanostructured zirconium oxide synthesized by hydrothermal process. *Journal of Nanoparticle Research* **2010,** *12* (8), 3105-3110.
2. Keiteb, A. S.; Saion, E.; Zakaria, A.; Soltani, N., Structural and optical properties of zirconia nanoparticles by thermal treatment synthesis. *Journal of Nanomaterials* **2016,** *2016*.
3. Harrison, D.; Melamed, N.; Subbarao, E., A New Family of Self-Activated Phosphors. *Journal of the Electrochemical Society* **1963,** *110* (1), 23-28.
4. Wang, H.; Li, G.; Xue, Y.; Li, L., Hydrated surface structure and its impacts on the stabilization of t-ZrO_2. *Journal of Solid State Chemistry* **2007,** *180* (10), 2790-2797.
5. Jayakumar, S.; Ananthapadmanabhan, P.; Thiyagarajan, T.; Perumal, K.; Mishra, S.; Suresh, G.; Su, L.; Tok, A., Nanosize stabilization of cubic and tetragonal phases in reactive plasma synthesized zirconia powders. *Materials Chemistry and Physics* **2013,** *140* (1), 176-182.
6. Manivasakan, P.; Rajendran, V.; Ranjan Rauta, P.; Bandhu Sahu, B.; Krushna Panda, B., Synthesis of monoclinic and cubic ZrO2 nanoparticles from zircon. *Journal of the American Ceramic Society* **2011,** *94* (5), 1410-1420.
7. Kim, J.-R.; Myeong, W.-J.; Ihm, S.-K., Characteristics in oxygen storage capacity of ceria–zirconia mixed oxides prepared by continuous hydrothermal synthesis in supercritical water. *Applied Catalysis B: Environmental* **2007,** *71* (1), 57-63.
8. Gateshki, M.; Petkov, V.; Hyeon, T.; Joo, J.; Niederberger, M.; Ren, Y., Interplay between the local structural disorder and the length of structural coherence in stabilizing the cubic phase in nanocrystalline ZrO_2. *Solid State Communications* **2006,** *138* (6), 279-284.
9. Garvie, R., Stabilization of the tetragonal structure in zirconia microcrystals. *The Journal of Physical Chemistry* **1978,** *82* (2), 218-224.
10. Vasylkiv, O.; Sakka, Y., Synthesis and colloidal processing of zirconia nanopowder. *Journal of the American Ceramic Society* **2001,** *84* (11), 2489-2494.
11. Chen, L.; Mashimo, T.; Omurzak, E.; Okudera, H.; Iwamoto, C.; Yoshiasa, A., Pure tetragonal ZrO_2 nanoparticles synthesized by pulsed plasma in liquid. *The Journal of Physical Chemistry C* **2011,** *115* (19), 9370-9375.
12. Sigwadi, R. A.; Mavundla, S. E.; Moloto, N.; Mokrani, T., Synthesis of zirconia-based solid acid nanoparticles for fuel cell application. *Journal of Energy in Southern Africa* **2016,** *27* (2), 60-67.
13. Bocanegra-Bernal, M.; De La Torre, S. D., Phase transitions in zirconium dioxide and related materials for high performance engineering ceramics. *Journal of Materials Science* **2002,** *37* (23), 4947-4971.
14. Piconi, C.; Maccauro, G., Zirconia as a ceramic biomaterial. *Biomaterials* **1999,** *20* (1), 1-25.

15. Tan, D.; Lin, G.; Liu, Y.; Teng, Y.; Zhuang, Y.; Zhu, B.; Zhao, Q.; Qiu, J., Synthesis of nanocrystalline cubic zirconia using femtosecond laser ablation. *Journal of Nanoparticle Research* **2011,** *13* (3), 1183-1190.
16. Cong, Y.; Li, B.; Yue, S.; Fan, D.; Wang, X.-j., Effect of oxygen vacancy on phase transition and photoluminescence properties of nanocrystalline zirconia synthesized by the one-pot reaction. *The Journal of Physical Chemistry C* **2009,** *113* (31), 13974-13978.
17. Xu, X.; Wang, X., Fine tuning of the sizes and phases of ZrO2 nanocrystals. *Nano Research* **2009,** *2* (11), 891-902.
18. Rajh, T.; Peterson, M.; Turner, J.; Nozik, A., Size quantization in small colloidal CdS particles studied with stopped flow spectrometry. *Journal of Electroanalytical Chemistry and Interfacial Electrochemistry* **1987,** *228* (1-2), 55-68.
19. Rezaei, M.; Alavi, S.; Sahebdelfar, S.; Yan, Z.-F.; Teunissen, H.; Jacobsen, J.; Sehested, J., Synthesis of pure tetragonal zirconium oxide with high surface area. *Journal of Materials Science* **2007,** *42* (4), 1228-1237.
20. Tahmasebpour, M.; Babaluo, A.; Aghjeh, M. R., Synthesis of zirconia nanopowders from various zirconium salts via polyacrylamide gel method. *Journal of the European Ceramic Society* **2008,** *28* (4), 773-778.
21. Davar, F.; Hassankhani, A.; Loghman-Estarki, M. R., Controllable synthesis of metastable tetragonal zirconia nanocrystals using citric acid assisted sol–gel method. *Ceramics International* **2013,** *39* (3), 2933-2941.
22. Navrotsky, A., Energetic clues to pathways to biomineralization: Precursors, clusters, and nanoparticles. *Proceedings of the National Academy of Sciences of the United States of America* **2004,** *101* (33), 12096-12101.
23. Indarto, A.; Choi, J.-W.; Lee, H.; Song, H. K., A review of C1 chemistry synthesis using yttrium-stabilized zirconia catalyst. *Journal of Rare Earths* **2008,** *26* (1), 1-6.
24. Adamski, A.; Jakubus, P.; Sojka, Z., Synthesis of nanostructured tetragonal ZrO_2 of enhanced thermal stability. *Nukleonika* **2006,** *51*, 27-33.
25. Christensen, A.; Carter, E. A., First-principles study of the surfaces of zirconia. *Physical Review B* **1998,** *58* (12), 8050.
26. Pérez-Maqueda, L. A.; Matijević, E., Preparation and characterization of nanosized zirconium (hydrous) oxide particles. *Journal of Materials Research* **1997,** *12* (12), 3286-3292.
27. Jansen, M.; Guenther, E., Oxide gels and ceramics prepared by a nonhydrolytic sol-gel process. *Chemistry of materials* **1995,** *7* (11), 2110-2114.
28. Tai, C. Y.; Hsiao, B.-Y.; Chiu, H.-Y., Preparation of spherical hydrous-zirconia nanoparticles by low temperature hydrolysis in a reverse microemulsion. *Colloids and Surfaces A: Physicochemical and Engineering Aspects* **2004,** *237* (1), 105-111.

29. Piszczek, P.; Radtke, A.; Grodzicki, A.; Wojtczak, A.; Chojnacki, J., The new type of [Zr_6 (μ_3-O)$_4$ (μ_3-OH)$_4$] cluster core: Crystal structure and spectral characterization of [Zr_6O_4 (OH)$_4$ (OOCR)$_{12}$](R= Bu t, C (CH_3)$_2$ Et). *Polyhedron* **2007,** *26* (3), 679-685.
30. Yashima, M.; Kato, T.-a.; Kakihana, M.; Gulgun, M. A.; Matsuo, Y.; Yoshimura, M., Crystallization of hafnia and zirconia during the pyrolysis of acetate gels. *Journal of Materials Research* **1997,** *12* (10), 2575-2583.
31. Manrıquez, M.; López, T.; Gómez, R.; Navarrete, J., Preparation of TiO_2–ZrO_2 mixed oxides with controlled acid–basic properties. *Journal of Molecular Catalysis A: Chemical* **2004,** *220* (2), 229-237.
32. Chuah, G.; Jaenicke, S.; Pong, B., The preparation of high-surface-area zirconia: II. Influence of precipitating agent and digestion on the morphology and microstructure of hydrous zirconia. *Journal of Catalysis* **1998,** *175* (1), 80-92.
33. Noh, H.-J.; Seo, D.-S.; Kim, H.; Lee, J.-K., Synthesis and crystallization of anisotropic shaped ZrO_2 nanocrystalline powders by hydrothermal process. *Materials Letters* **2003,** *57* (16), 2425-2431.
34. Zimmerman, C. M.; Singh, A.; Koros, W. J., Tailoring mixed matrix composite membranes for gas separations. *Journal of Membrane Science* **1997,** *137* (1-2), 145-154.
35. Alaei, M.; Rashidi, A. M.; Bakhtiari, I., Preparation of High Surface Area ZrO_2 Nanoparticles. *Iranian Journal of Chemistry and Chemical Engineering (IJCCE)* **2014,** *33* (2), 47-53.
36. Basahel, S. N.; Ali, T. T.; Mokhtar, M.; Narasimharao, K., Influence of crystal structure of nanosized ZrO2 on photocatalytic degradation of methyl orange. *Nanoscale Research Letters* **2015,** *10* (1), 1-13.
37. Zhao, N.; Pan, D.; Nie, W.; Ji, X., Two-phase synthesis of shape-controlled colloidal zirconia nanocrystals and their characterization. *Journal of the American Chemical Society* **2006,** *128* (31), 10118-10124.
38. Gil, E.; Mas, Á.; Lerma, C.; Vercher, J., Exposure factors influence stone deterioration by crystallization of soluble salts. *Advances in Materials Science and Engineering* **2015,** *2015*.
39. Wang, S.; Tan, Z.; Li, Y.; Sun, L.; Zhang, T., Synthesis, characterization and thermal analysis of polyaniline/ZrO 2 composites. *Thermochimica Acta* **2006,** *441* (2), 191-194.
40. Clearfield, A., Structural aspects of zirconium chemistry. *Reviews of Pure and Applied Chemistry (Australia)* **1964,** *14*.
41. Navarra, M.; Abbati, C.; Scrosati, B., Properties and fuel cell performance of a Nafion-based, sulfated zirconia-added, composite membrane. *Journal of Power Sources* **2008,** *183* (1), 109-113.
42. Chraska, T.; King, A. H.; Berndt, C. C., On the size-dependent phase transformation in nanoparticulate zirconia. *Materials Science and Engineering: A* **2000,** *286* (1), 169-178.
43. Synowicki, R.; Tiwald, T. E., Optical properties of bulk c-ZrO 2, c-MgO and a-As 2 S 3 determined by variable angle spectroscopic ellipsometry. *Thin Solid Films* **2004,** *455*, 248-255.
44. Lukin, E.; Anufrieva, E.; Makarov, N.; Popova, N.; Kuteinikova, A., Dense and durable ceramics based on alumina and zirconia. *Refractories and Industrial Ceramics* **2004,** *45* (6), 421-423.

45. Kowalski, D.; Aoki, Y.; Habazaki, H., High proton conductivity in anodic ZrO_2/WO_3 nanofilms. *Angewandte Chemie International Edition* **2009,** *48* (41), 7582-7585.
46. Wang, W.; Guo, H.; Gao, J.; Dong, X.; Qin, Q., XPS, UPS and ESR studies on the interfacial interaction in Ni-ZrO_2 composite plating. *Journal of Materials Science* **2000,** *35* (6), 1495-1499.
47. Maskell, W. C., Progress in the development of zirconia gas sensors. *Solid State Ionics* **2000,** *134* (1), 43-50.
48. Khaodee, W.; Jongsomjit, B.; Praserthdam, P.; Goto, S.; Assabumrungrat, S., Impact of temperature ramping rate during calcination on characteristics of nano-ZrO_2 and its catalytic activity for isosynthesis. *Journal of Molecular Catalysis A: Chemical* **2008,** *280* (1), 35-42.
49. Davies, L.; Bonini, N.; Locatelli, S.; Gonzo, E., Characterization and catalytic activity of zirconium dioxide prepared by sol-gel. *Latin American Applied Research* **2005,** *35* (1), 23-28.
50. Kim, H.-W.; Lee, S.-Y.; Bae, C.-J.; Noh, Y.-J.; Kim, H.-E.; Kim, H.-M.; Ko, J. S., Porous ZrO_2 bone scaffold coated with hydroxyapatite with fluorapatite intermediate layer. *Biomaterials* **2003,** *24* (19), 3277-3284.
51. Surviliene, S.; Lisowska-Oleksiak, A.; Češuniene, A., Effect of ZrO_2 on corrosion behaviour of chromium coatings. *Corrosion Science* **2008,** *50* (2), 338-344.
52. Karunakaran, C.; Senthilvelan, S., Photocatalysis with ZrO_2: oxidation of aniline. *Journal of Molecular Catalysis A: Chemical* **2005,** *233* (1), 1-8.
53. Setare, E.; Raeissi, K.; Golozar, M.; Fathi, M., The structure and corrosion barrier performance of nanocrystalline zirconia electrodeposited coating. *Corrosion Science* **2009,** *51* (8), 1802-1808.
54. Stoychev, D.; Ikonomov, J.; Robinson, K.; Stefanov, P.; Stoycheva, M.; Marinova, T., Surface modification of porous zirconia layers by electrochemical deposition of small amounts of Cu or Co and Co+ Cu. *Surface and Interface Analysis* **2000,** *30* (1), 69-73.
55. Hobbs, L. W., *Science and Technology of Zircona: Proceedings of the 1a International Conference on the Science and Technology of Zircona: Held at the Case Institute of Technology, Case Western Reserve University, Cleveland, Ohio, June 16-18, 1980*. American Ceramic Society: 1981.
56. Shchukin, D. G.; Caruso, R. A., Inorganic macroporous films from preformed nanoparticles and membrane templates: synthesis and investigation of photocatalytic and photoelectrochemical properties. *Advanced Functional Materials* **2003,** *13* (10), 789-794.
57. Wilk, G.; Wallace, R., Stable zirconium silicate gate dielectrics deposited directly on silicon. *Applied Physics Letters* **2000,** *76* (1), 112-114.
58. Pelskov, Y. V.; Sakharova, A. Y.; Krotova, M.; Bouilov, L.; Spitsyn, B., Photoelectrochemical properties of semiconductor diamond. *Journal of Electroanalytical Chemistry and Interfacial Electrochemistry* **1987,** *228* (1-2), 19-27.
59. Su, C.; Li, J.; He, D.; Cheng, Z.; Zhu, Q., Synthesis of isobutene from synthesis gas over nanosize zirconia catalysts. *Applied Catalysis A: General* **2000,** *202* (1), 81-89.

60. Wong, M. S.; Antonelli, D. M.; Ying, J. Y., Synthesis and characterization of phosphated mesoporous zirconium oxide. *Nanostructured Materials* **1997,** *9* (1-8), 165-168.
61. Valov, I.; Stoychev, D.; Marinova, T., Study of the kinetics of processes during electrochemical deposition of zirconia from nonaqueous electrolytes. *Electrochimica Acta* **2002,** *47* (28), 4419-4431.
62. Fortulan, C. A.; de Souza, D. P., Microstructural evolution of the al2o3-zro2 composite and its correlation with electrical conductivity. *Materials Research* **1999,** *2* (3), 205-210.
63. Sigwadi R.; Dhlamini s.; Mokrani T.; Nonjola P., Effect of Synthesis Temperature on Particles Size and Morphology of Zirconium Oxide Nanoparticle. *Journal of Nano Research* **2017,** *50*, 8-31.
64. Dong, W.-S.; Lin, F.-Q.; Liu, C.-L.; Li, M.-Y., Synthesis of ZrO_2 nanowires by ionic-liquid route. *Journal of colloid and Interface Science* **2009,** *333* (2), 734-740.
65. Rashad, M.; Baioumy, H., Effect of thermal treatment on the crystal structure and morphology of zirconia nanopowders produced by three different routes. *Journal of Materials Processing Technology* **2008,** *195* (1), 178-185.
66. Sonwane, C.; Bhatia, S., Analysis of criticality and isotherm reversibility in regular mesoporous materials. *Langmuir* **1999,** *15* (16), 5347-5354.
67. Tran, C.; Kalra, V., Fabrication of porous carbon nanofibers with adjustable pore sizes as electrodes for supercapacitors. *Journal of power sources* **2013,** *235*, 289-296.
68. Nasibi, M.; Golozar, M. A.; Rashed, G., Nano zirconium oxide/carbon black as a new electrode material for electrochemical double layer capacitors. *Journal of power sources* **2012,** *206*, 108-110.
69. Cai, F.; Jiang, C.; Zhang, Z.; Muttini, E.; Fu, P.; Zhao, Y.; Ji, V., Fabrication and characterization of Ni–Zr composite coatings using electrodepositing technique. *Journal of Alloys and Compounds* **2015,** *635*, 73-81.
70. Mudila, H.; Joshi, V.; Rana, S.; Zaidi, M. G. H.; Alam, S., Enhanced electrocapacitive performance and high power density of polypyrrole/graphene oxide nanocomposites prepared at reduced temperature. *Carbon letters* **2014,** *15* (3), 171-179.
71. Zhang, X.; Lu, Y., Centrifugal spinning: an alternative approach to fabricate nanofibers at high speed and low cost. *Polymer Reviews* **2014,** *54* (4), 677-701.
72. Choi, J.; Lee, K. M.; Wycisk, R.; Pintauro, P. N.; Mather, P. T., Nanofiber network ion-exchange membranes. *Macromolecules* **2008,** *41* (13), 4569-4572.
73. Dong, B.; Gwee, L.; Salas-de La Cruz, D.; Winey, K. I.; Elabd, Y. A., Super proton conductive high-purity Nafion nanofibers. *Nano Letters* **2010,** *10* (9), 3785-3790.
74. Tran, C.; Kalra, V., Co-continuous nanoscale assembly of Nafion–polyacrylonitrile blends within nanofibers: a facile route to fabrication of porous nanofibers. *Soft Matter* **2013,** *9* (3), 846-852.
75. Zhou, C.; Liu, Z.; Dai, J.; Xiao, D., Electrospun Ru (bpy) 32^{+}-doped Nafion nanofibers for electrochemiluminescence sensing. *Analyst* **2010,** *135* (5), 1004-1009.

76. Ballengee, J.; Pintauro, P., Morphological control of electrospun Nafion nanofiber mats. *Journal of the Electrochemical Society* **2011,** *158* (5), B568-B572.
77. Mauritz, K. A.; Moore, R. B., State of understanding of Nafion. *Chemical Reviews* **2004,** *104* (10), 4535-4586.
78. Sharma, D. K.; Shen, J.; Li, F., Reinforcement of Nafion into polyacrylonitrile (PAN) to fabricate them into nanofiber mats by electrospinning: characterization of enhanced mechanical and adsorption properties. *RSC Advances* **2014,** *4* (74), 39110-39117.
79. Nie, G.; Li, Z.; Lu, X.; Lei, J.; Zhang, C.; Wang, C., Fabrication of polyacrylonitrile/CuS composite nanofibers and their recycled application in catalysis for dye degradation. *Applied Surface Science* **2013,** *284*, 595-600.
80. Gopalan, A. I.; Santhosh, P.; Manesh, K. M.; Nho, J. H.; Kim, S. H.; Hwang, C.-G.; Lee, K.-P., Development of electrospun PVdF–PAN membrane-based polymer electrolytes for lithium batteries. *Journal of Membrane Science* **2008,** *325* (2), 683-690.
81. Sahay, R.; Kumar, P. S.; Sridhar, R.; Sundaramurthy, J.; Venugopal, J.; Mhaisalkar, S. G.; Ramakrishna, S., Electrospun composite nanofibers and their multifaceted applications. *Journal of Materials Chemistry* **2012,** *22* (26), 12953-12971.
82. Kim, C.; Choi, Y.-O.; Lee, W.-J.; Yang, K.-S., Supercapacitor performances of activated carbon fiber webs prepared by electrospinning of PMDA-ODA poly (amic acid) solutions. *Electrochimica Acta* **2004,** *50* (2-3), 883-887.
83. Jones, D. J.; Rozière, J., Recent advances in the functionalisation of polybenzimidazole and polyetherketone for fuel cell applications. *Journal of membrane science* **2001,** *185* (1), 41-58.
84. Carriere, D.; Moreau, M.; Lhalil, K.; Barboux, P.; Boilot, J., Proton conductivity of colloidal nanometric zirconium phosphates. *Solid State Ionics* **2003,** *162*, 185-190.
85. Pilehrood, M. K.; Heikkilä, P.; Harlin, A., Preparation of carbon nanotube embedded in polyacrylonitrile (pan) nanofibre composites by electrospinning process. *AUTEX Research Journal* **2012,** *12* (1), 1-6.
86. Nayak, R.; Padhye, R.; Kyratzis, I. L.; Truong, Y. B.; Arnold, L., Recent advances in nanofibre fabrication techniques. *Textile Research Journal* **2012,** *82* (2), 129-147.
87. Fong, H.; Chun, I.; Reneker, D., Beaded nanofibers formed during electrospinning. *Polymer* **1999,** *40* (16), 4585-4592.
88. Shin, D. W.; Lee, S. Y.; Kang, N. R.; Lee, K. H.; Cho, D. H.; Lee, M. J.; Lee, Y. M.; Do Suh, K., Effect of crosslinking on the durability and electrochemical performance of sulfonated aromatic polymer membranes at elevated temperatures. *International Journal of Hydrogen Energy* **2014,** *39* (9), 4459-4467.
89. Trobajo, C.; Khainakov, S. A.; Espina, A.; García, J. R., On the synthesis of α-zirconium phosphate. *Chemistry of Materials* **2000,** *12* (6), 1787-1790.

90. Zhao, G.; Yuan, Z.; Chen, T., Synthesis of amorphous supermicroporous zirconium phosphate materials by nonionic surfactant templating. *Materials Research Bulletin* **2005,** *40* (11), 1922-1928.
91. Mathur, R.; Bahl, O.; Mittal, J.; Nagpal, K., Structure of thermally stabilized PAN fibers. *Carbon* **1991,** *29* (7), 1059-1061.
92. Zhang, C.; Yang, Q.; Zhan, N.; Sun, L.; Wang, H.; Song, Y.; Li, Y., Silver nanoparticles grown on the surface of PAN nanofiber: Preparation, characterization and catalytic performance. *Colloids and Surfaces A: Physicochemical and Engineering Aspects* **2010,** *362* (1), 58-64.
93. Neghlani, P. K.; Rafizadeh, M.; Taromi, F. A., Preparation of aminated-polyacrylonitrile nanofiber membranes for the adsorption of metal ions: comparison with microfibers. *Journal of Hazardous Materials* **2011,** *186* (1), 182-189.
94. Salavati-Niasari, M.; Dadkhah, M.; Davar, F., Pure cubic ZrO_2 nanoparticles by thermolysis of a new precursor. *Polyhedron* **2009,** *28* (14), 3005-3009.
95. Ostrowska, J.; Narebska, A., Infrared study of hydration and association of functional groups in a perfluorinated Nafion membrane, Part 1. *Colloid and Polymer Science* **1983,** *261* (2), 93-98.
96. Zhai, Y.; Zhang, H.; Hu, J.; Yi, B., Preparation and characterization of sulfated zirconia (SO42−/ZrO2)/Nafion composite membranes for PEMFC operation at high temperature/low humidity. *Journal of Membrane Science* **2006,** *280* (1), 148-155.
97. Di Noto, V.; Gliubizzi, R.; Negro, E.; Pace, G., Effect of SiO_2 on relaxation phenomena and mechanism of ion conductivity of [Nafion/$(SiO_2)_x$] composite membranes. *The Journal of Physical Chemistry B* **2006,** *110* (49), 24972-24986.
98. Ouyang, Q.; Cheng, L.; Wang, H.; Li, K., Mechanism and kinetics of the stabilization reactions of itaconic acid-modified polyacrylonitrile. *Polymer Degradation and Stability* **2008,** *93* (8), 1415-1421.
99. Nguyen, T.; Carmezim, M. J.; Boudard, M.; Montemor, M. F., Cathodic electrodeposition and electrochemical response of manganese oxide pseudocapacitor electrodes. *International Journal of Hydrogen Energy* **2015,** *40* (46), 16355-16364.
100. Babakhani, B.; Ivey, D. G., Anodic deposition of manganese oxide electrodes with rod-like structures for application as electrochemical capacitors. *Journal of Power Sources* **2010,** *195* (7), 2110-2117.

CHAPTER FIVE

5. Modification of Nafion® membrane and their mechanical properties

This chapter presents the three scientific papers summary in the following sections:
Presents the results from the paper: "**Effect of relative humidity on mechanical strength of zirconia/ Nafion® Nano-composite membrane"** Journal of Computational and Applied Research in Mechanical Engineering 7(2) (2018) 175.
Presents the results from the paper: "**Wettability and mechanical strength of modified Nafion® nano-composite membrane for fuel cell**" Digest Journal of Nanomaterials and Biostructures 12(4) (2017) 1137.
Presents the results from the paper: "**Mechanical strength of Nafion®/ZrO_2 nanocomposite membrane**" International Journal of Manufacturing, Materials, and Mechanical Engineering 8(1) (2018) 54.

A: Effect of relative humidity on mechanical strength of zirconia/ Nafion® Nano-composite membrane

5.1. Introduction

Proton exchange membrane fuel cells (PEMFCs) are used in variety of applications such as stationary, automotive and mobile [1] due to their high efficiency of electrical conversion. PEMFCs uses hydrogen or methanol as their fuel to produce electricity without environmental pollution as there is no gas emissions only water as waste product that can be reused [2]. The PEMFCs heart is a proton conducting membrane. As this proton conducting membrane conduct protons from the anode electrode to the cathode electrode, without allowing the oxygen and hydrogen gas crossover. Moreover, the fuel cell longevity depends on the mechanical strength of proton conducting membrane, as it must endures any operational changes such a water content and temperature without any operation failure [3-4]. Nafion® membrane when operates at lower temperature maintain a high ionic conductivity and mechanical, thermal and chemical stability [5-6]. It consists of hydrophobic polytrafluoroethylene (PTFE) backbone and hydrophilic perfluorinated pendant side chains ending with sulfonic groups SO_3H^+ (acid form) [7]. When in contact with water the sulfonic swell and form hydrophilic domain. Critical characteristics of a good polymer electrolyte membrane (PEM) are fast friction conduction, good water transport, thermo-mechanical stability and sustained durability under various operating conditions [7]. Furthermore, the Nafion® membrane because of its chemical structure function well in its hydrated state, with the proton conductivity decreasing with the increase of temperature and lower relative humidity [8]. But this Nafion® membrane dehydrates at the temperature above 80 ˚C and starts to shrink which leads to the development of cracks, and with a high methanol permeability.

Incorporating various nanoparticles can improve membrane conductivity, water management, mechanical properties, and bring changes to pore and channel structure [9-13]. Zirconium oxide (ZrO_2) has been used in fuel cell, thermal barrier coating and refractory materials due to its high thermal, chemical and mechanical stability [14]. Nafion® membrane was modified with inorganics fillers such as ZrO_2 to introduce the hydrophilic side of the membrane and enhance the mechanical strength with higher ionic conductivity in order to function on the methanol or hydrogen fuel cell at higher temperature [15-17]. To function at higher temperature improves the carbon monoxide (CO) tolerance and reaction kinetics with reduction of catalyst loading on the membrane electrode assembly of fuel cell [18-20]. This eliminate the properties of fuel cell gas; the findings prompt the research on fuel cell working on high temperature. In this paper, we investigate the mechanical properties of modified nanocomposite membrane using tensile modulus measurement when dry and wet state compared with that of recast Nafion® membrane as these wet-up and dry-out can cause significant stresses in membrane.

5.2. Experimental

5.2.1. Materials

Sodium hydroxide, silver nitrate, N, N-dimethylformade (Merck), Sulfuric Acid (Merck), Zirconium oxychloride hydrate (Merck), Iso-propanol (Merck) and Nafion® solution (Sigma) was obtained and was used as received.

5.2.2. Synthesis of ZrO_2 nanoparticles

The ZrO_2 nanoparticles were prepared by precipitation method. Zirconium oxychloride hydrate ($ZrOCl_2.8H_2O$) and sodium hydroxide (NaOH) were used as starting materials. 0.2M $ZrOCl_2.8H_2O$ was prepared in 250ml beaker and 2N NaOH solution was added drop wise with continuous stirring for 45 minutes. Obtained precipitate was divided into six parts, one parts was filtered and washed several times with distilled water until chlorine ions (Cl^-) were not detected by the silver nitrate ($AgNO_3$). The precipitate was dried at 100 °C for 24 hours, which was calcinated at 600 °C for 4 hours and labelled as Zr-0. Whereas the remaining parts of the solution were covered with a foil and put in an oven at 50 °C, 80 °C and 100 °C temperatures for 24 hours, after which they were filtered, then washed and calcinated according to the Zr-0 procedure and then stored for analysis. Then the samples were labelled as follows Zr-50, Zr-80 and Zr-100.

5.2.3. Preparation of nanocomposite membranes

The nanocomposite membranes were prepared using 5 % Nafion® solution as the standard material for reference. Nafion® solution (10ml) with N, N-dimethylformade **(**DMF) (20ml) was mixed to replace solvents.

10wt % of Zr, Zr-50, Zr-80 and Zr-100 nanoparticles (obtained by using method in 4.2.2) were added to the Nafion®/ DMF solution and stirred at room temperature for 2 hours, then ultrasonizing for 30 minutes [21]. The resulting solution was poured onto a piece of flat glass and placed into an oven at 80 °C for 12 hours to remove solvent, and finally heated up to 160 °C for 30 minutes. The membranes were then removed by peeling off from the glass plate. Before conducting any measurement, all membranes were kept at deionized water for 12 hours. The thicknesses of the membrane were measured with digital micrometre (0.18 cm). Each thickness was measured in the average of 3-7 reading at different position of membrane and was repeated twice on each membrane in order to obtain the average value.

5.2.4. Water Uptake (%) of nano-composite membranes

The membrane was soaked in distilled water for one day. Then was removed, wiped and weighed on the micro-balance. Water uptake was calculated according to the following equation:

$$W_{up}(\%) = \frac{(m_{wet} - m_{dry})}{m_{dry}} X100 \qquad (5\text{-}1)$$

Where W_{up} is the percentage of water uptake, m_{wet} is the weight of a wet membrane immediately and m_{dry} is the weight of the dry membrane.

5.2.5. Tensile test

The uniaxial mechanical properties of nano-composite membranes and recast membrane were captured using a uniaxial testing system. The length, width and thickness of samples were measured using a Vernier caliper and recorded prior to testing. The testing area of the membrane samples were 4 mm x 10 mm in dimension. To allow clamping area, the sample were prepared in such a way that they will be clamped both sides and still allow the testing area to be 4 mm x1 0 mm. The thicknesses of the membrane were measured with digital micrometer (0.18 cm). Each thickness was measured in the average of 3-7 reading at different position of membrane and was repeated twice on each membrane in order to obtain the average value. The thickness of 0.18 cm of the nanocomposite membrane was used in analysing the stress applied to the sample. The membrane was soaked in water for 24 hours and tested as wet test. Then the membrane was dried in a vacuum oven at 80 °C for 24 hours and tested as dry test. The tensile strength of modified Nafion membranes were measured using CellScale Ustretch device dried at 25 °C and wet at 34 °C and actuator speed of 5 mm per min.

5.2.6. Characterization

The XRD analysis was performed using a Philips X-ray diffraction with Cu K radiation source. The analyzed material is finely ground, homogenized, and average bulk composition is determined. Samples are scanned in a continuous mode from 10° - 90°. The thermal properties of the samples and its characteristics were studied by thermal gravimetric analysis (TGA) under nitrogen flow. TGA data was obtained with model STA (Simultaneous Thermal Analyzer) 1500 (supplied by Rheometric Scientific Ltd, UK), over nitrogen and at a heating rate of 10 °C/min from 28 °C to 1000 °C. Scanning Electron Microscopy (SEM) images were obtained on a Hitachi x650. Electronic techniques are based on the interaction of the sample with electrons, which results in a secondary effect that is detected and measured.

5.3. Results and discussion

5.3.1. The X-ray diffraction (XRD) analysis

The modified membrane was characterized by XRD to observe the effect of the zirconia nanoparticles on their crystallinity. The XRD results of modified Nafion® and pristine membrane are shown in Figures 5-1. Figure 5-1(a) shows that the pristine recast membrane have only two reflections peaks at 17.5° and 39° 2thetha which resemble the crystallinity within the per-fluorocarbon chains of the ionomer [22]. Figure 5-1(b) shows the peaks corresponding to the cubic and monoclinic phase of zirconia oxide nanoparticles, also the Nafion® peaks which associated with crystallinity within the per-fluorocarbon chains. However, Figure 5-1(c-e) reflect only the broad diffraction peaks of zirconia cubic phase in the nanosized range without any Nafion® peaks detected. With diffraction peaks at 2theta are 30.2°, 35.2°, 50.6°, 60.2°,74.2°and 82.5° which corresponding to the planes (1 1 1), (2 0 0), (2 2 0), (3 1 1), (4 0 0), (3 3 1), (4 2 0) [23-24]. In comparison, it is noted that modified membrane obtains the more crystallite and bigger than the pristine Nafion® membrane, this may be due to the crystallites of zirconia nanoparticles that have been distributed within the membrane. Furthermore, it was observable on Figure 5-1 (c-e) that only the crystalline peak of zirconia nanoparticles appeared while Nafion® peak disappeared.

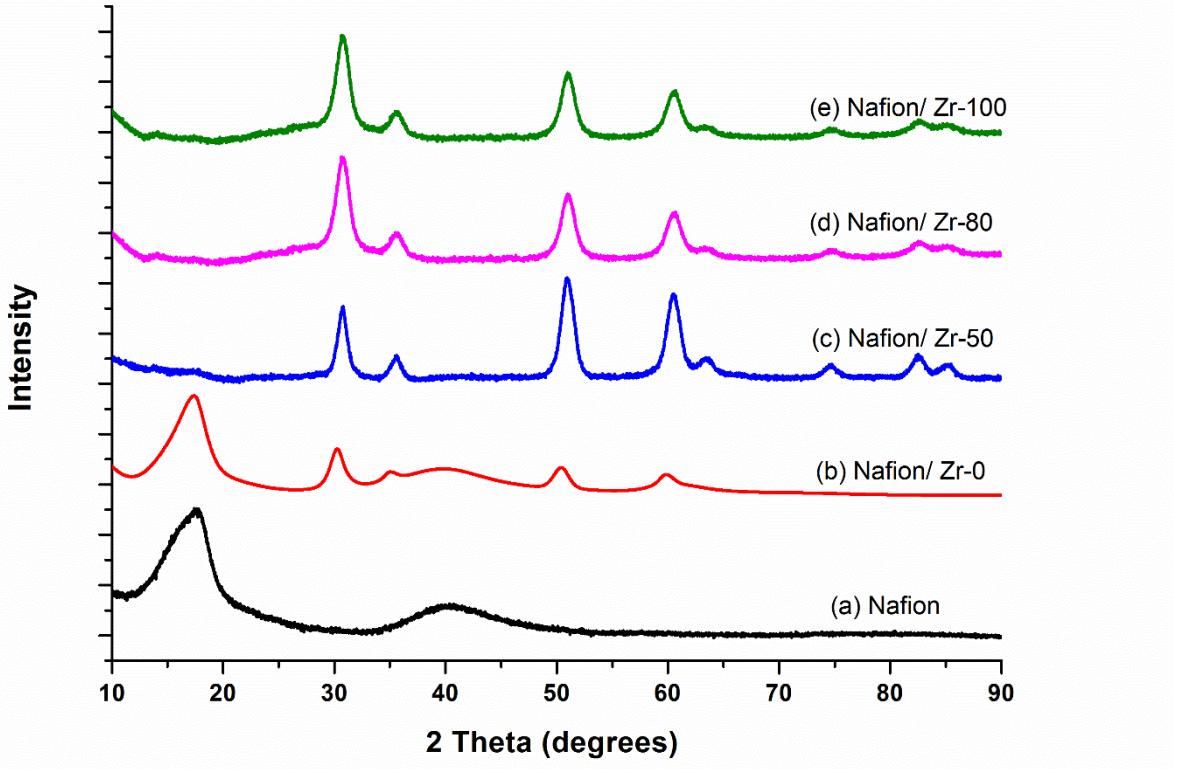

Figure 5- 1: The comparison of the XRD patterns of the (a) Nafion/ Zr-0, (b) Nafion/ Zr-50, (c) Nafion/ Zr-80, (d) Nafion®/ Zr 100 nanocomposite membrane and (e) Nafion® membrane.

5.3.2. Thermo-gravimetric analysis (TGA) and Derivative thermo-gravimetric (DTG)

The Thermo-gravimetric analysis and the derivative (DTG) of nanocomposite membrane and pristine Nafion® membrane were conducted in order to observe weight loss and thermal stability as displayed in Figure 5-2. In Figure 5-2 (b-e), modified nanocomposite membrane showed three weight loss up to 900 °C due to decomposition of membrane, with a total loss of 75-94 wt %. Figure 5-2 (b-e), shows an initial weight loss of about 2% of the original weight below 530 °C, due to the evaporation of hydrated water, and the second weight loss is attributable to the decomposition of the sulfonic acid groups of Nafion® membrane around 550 °C [25]. The third degradation step over 550 °C was assigned to degradation of the polymer main chain [21, 26-27]. Furthermore, the modified Nafion® membrane with zirconia nanoparticles as a filler have a shift in decomposition temperature, Nafion® / Zr, Nafion® / Zr-50, Nafion® / Zr-80 and Nafion® / Zr-100 nanocomposite membranes retain their weight up to 510 °C, which shows thermal degradation improvement compared to pristine Nafion® membranes. The modified Nafion® nanocomposite membrane was found to maintain water up to 530 °C, respectively, corresponding to desorption of water from membranes. This result in Figure 5-2 (b-e), confirmed that the modification of Nafion® membrane by zirconia nanoparticles can improve water retention ability and accelerate the decomposition process of the

membrane. Addition of Zirconium oxide shows the improvement of thermal stability [28] as zirconia nanoparticles were well distributed between Nafion® matrix, as confirm by XRD and SEM results. Because water is proton transporting medium for PEMs, the water retention ability above 100 °C is one of the important parameters for fuel cell applications. The pristine Nafion® membranes as shown in Figure 5-2(a), were found to be less stable compared to the modified membrane in Figure 5-2 (b-e) as they have started to decompose at a lower temperature of 360 °C. It is observable in Figure 5-2(a), as shows that pristine Nafion® membranes has three weight loss from 50 °C to 360 °C due to the evaporation of hydrated water, and the second weight loss is attributable to the decomposition of the sulfonic acid groups of Nafion® membrane [25]. The third degradation step over 550 °C was assigned to degradation and combustion of the polymer main chain [21, 26-27]. The DTG curves of modified Nafion® and Nafion® membrane obtained the same two transition peaks which associated with the second and third decomposition stage of a membrane as shown in Figure 5-3.

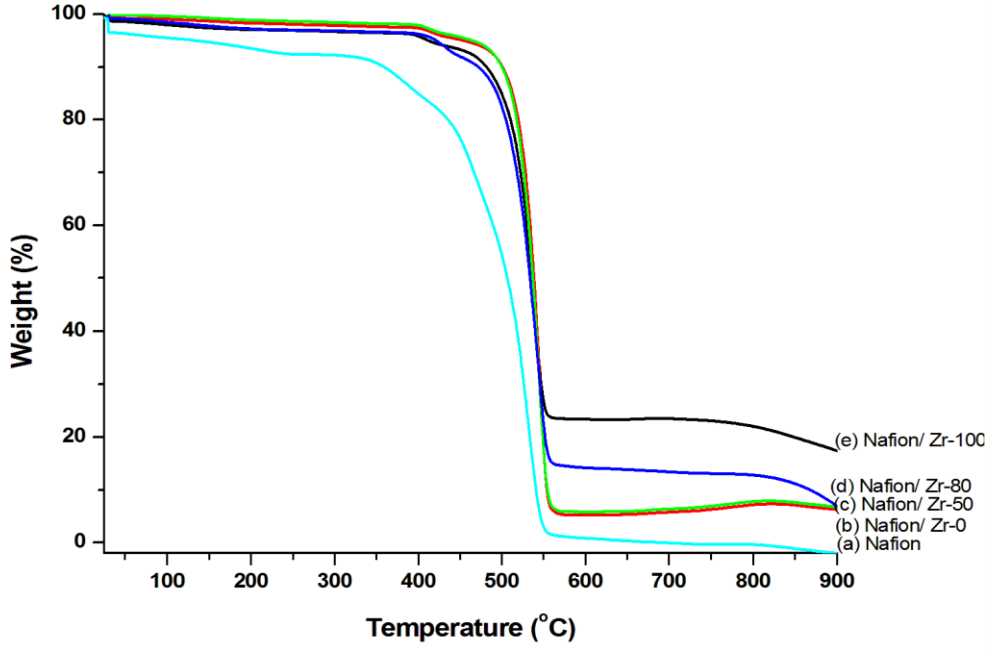

Figure 5- 2: The comparison of the TGA curves of the (a) Nafion® membrane, (b) Nafion®/ Zr-0, (c) Nafion®/ Z r-50, (d) Nafion®/ Zr-80 and (e) Nafion®/ Zr 100 nanocomposite membrane.

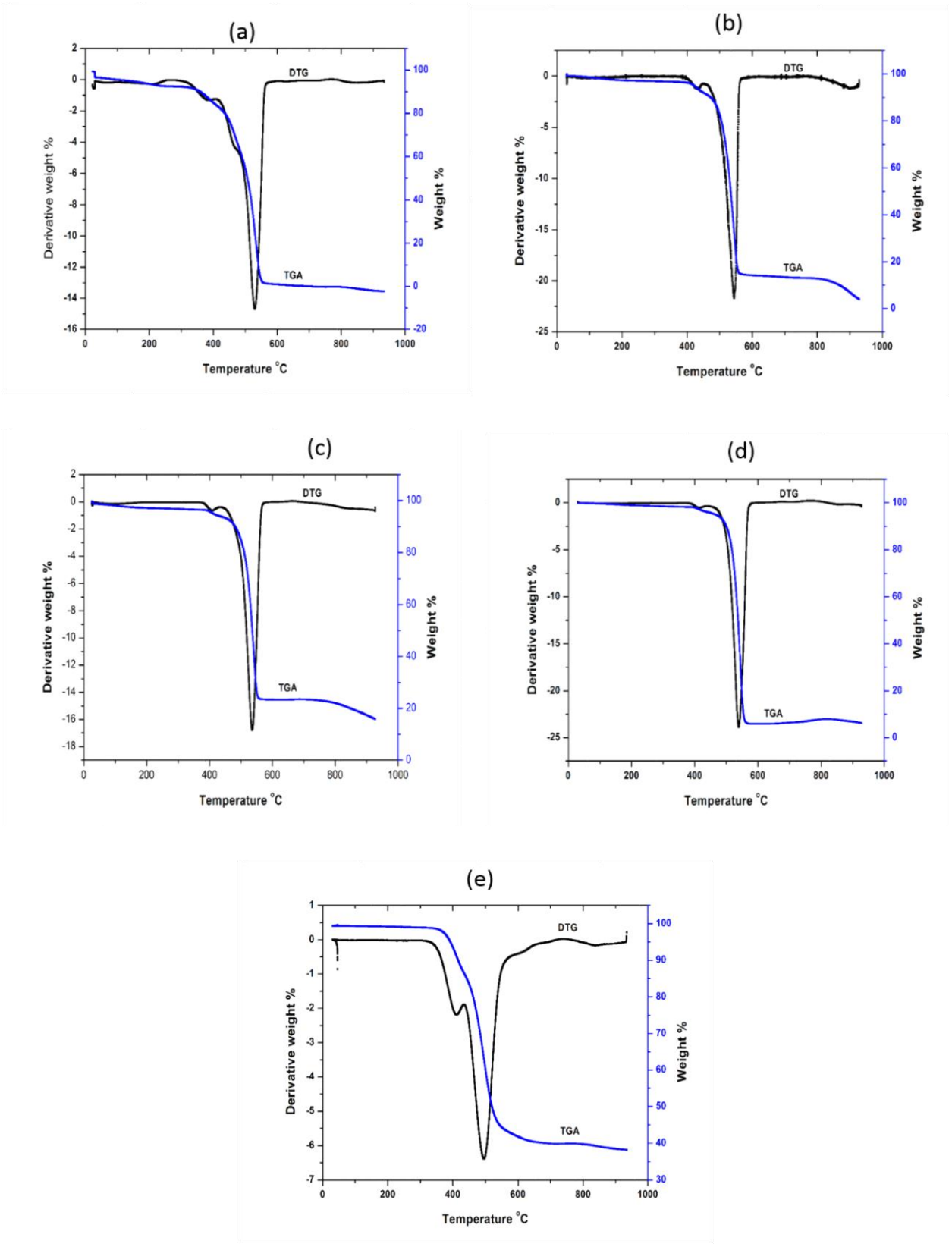

Figure 5- 3: The comparison of the TGA/ DTG curves of the (a) Nafion® membrane, (b) Nafion®/ Zr-0, (c) Nafion®/ Z r-50, (d) Nafion®/ Zr-80 and (e Nafion®/ Zr 100 nanocomposite membrane.

5.3.3. Tensile test

Force and displacement data were collected at a rate of 5 Hz. The cross-sectional area of the samples was calculated based on membrane thickness and the initial distance between membranes after preloading but prior to testing. Axial force measurements and cross-sectional areas were used to determine stress experienced by the samples in each direction (See Figure 5-4). Sample strains in each direction were determined using axial displacements measured by the UniStrecher. One stress strain relationship was plotted for each sample (See Figure 5-4 (a, c, e, g and i)). One force displacement relationship was also plotted for each sample of the membrane. The stiffness of each membrane was determined by identifying a linear region where their slopes are calculated as shown in Figure 5-4. The linear regions of these plots were identified and their slopes were calculated to generate a corresponding elastic modulus or stiffness (See Figure 5-4 (a-j)). All resultant data was examined and a common linear region, between 0% and 15%, was found. Linear regressions between 0% and 15% were taken for each plot and an R^2 value of at least 0.9 was required to confirm linearity. A typical stress strain plot with an applied linear regression is shown in Figure 5-4 (a-j).

The data collected were used to calculate the stress and strain for each of five tests using the force and displacement. The stress-strain of the modified nanocomposite membranes and recast membrane in their wet and dry state were presented in Figure 5-4(b, d, f, h and j). To verify the strain values, the motions of the nanocomposite membranes and Nafion® membrane were analysed using the image analysis toolkit. The image analysis resulted in lower strains than the actuator displacement- based strain data. This is not surprising since some of the actuator displacement could have resulted in system deflection and or specimen slippage. When looking at wet membranes, all samples have failed at approximately 0.6 strains. When looking at the dry nanocomposite membranes, Zr-100 and Zr-0 did not fail at 0.6 strain. The highest stress was recorded on the Nafion® / Zr-100 of approximately 720 kPa (See Figure 5-4(h)), with the more improvement of the yield strength and the elastic modulus thus demonstrating the close bonding between the zirconia nanoparticles and Nafion® membrane through self-assembly [29]. This improvement of the membrane rigidity demonstrates that the zirconia nanoparticles stabilized the structure of modified membrane and give a potential restriction to the humidity-generated stress when the membrane is used as an electrolyte membrane in the fuel cells application. Nafion®/ Zr-80 membrane (see Figure 5-4(a-b)) in its dry state shows improvement in stiffness (secant modulus) when compared to recast membrane, this may be due to Zr-80 nanoparticles incorporated in the Nafion which retains water to enhance mechanical strength of Nafion® membranes.

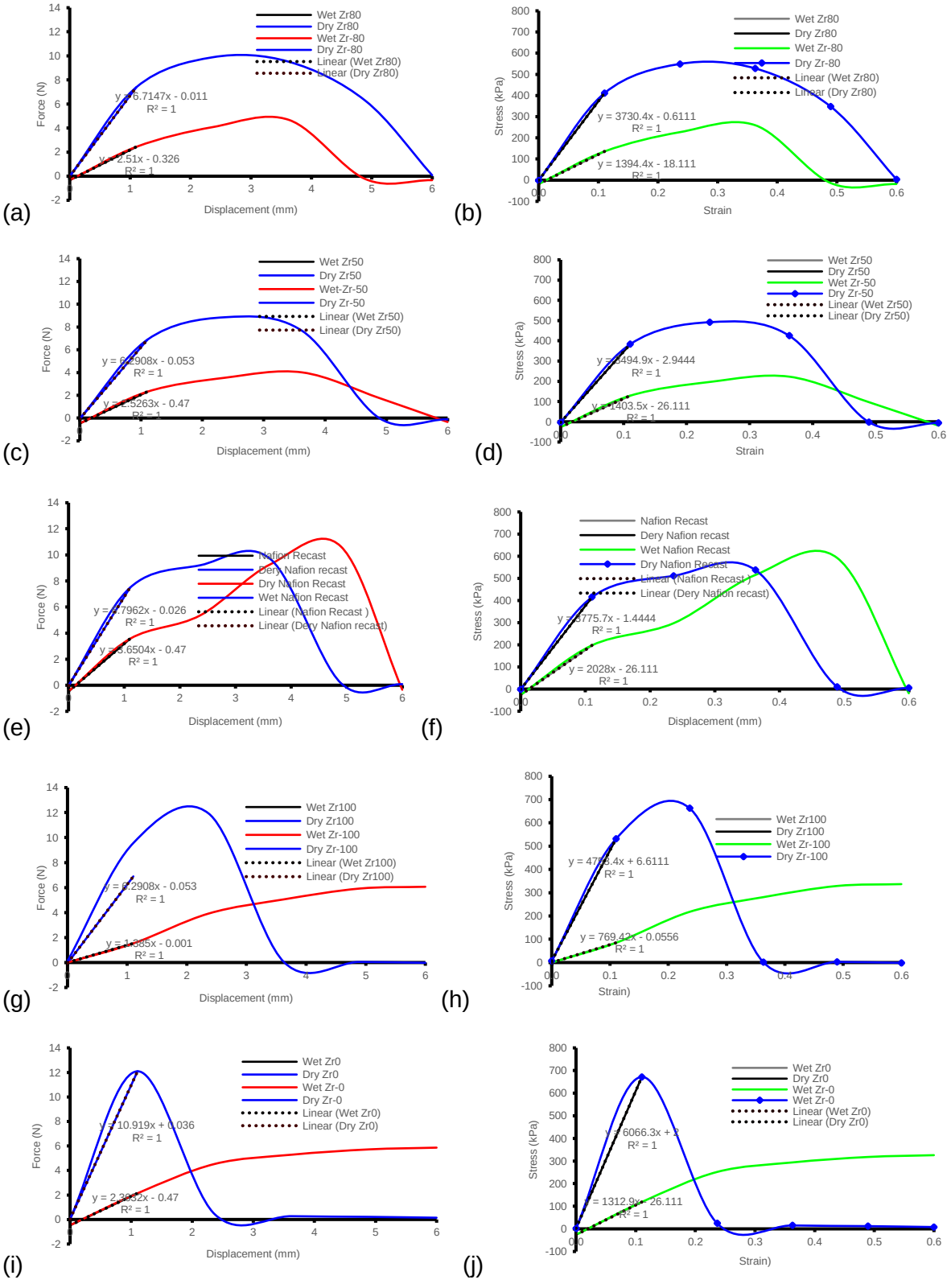

Figure 5- 4: Mechanical loading response (force-displacement curves) of wet and dry (a) Nafion®/Zr-80, (c) Nafion®/Zr-50, (e) Nafion® recast, (g) Nafion®/Zr-100 and (i) Nafion®/Zr-0 nanocomposite membranes and Stress-Strain curves of wet and dry (b) Nafion®/Zr-80, (d) Nafion®/Zr-50, (f) Nafion® recast, (h) Nafion®/Zr-100 and (j) Nafion®/Zr-0 nanocomposite membranes. Stress-strain and force-displacement curves showing the region where the membrane stiffness was determined (force-displacement region is between 0-1.2mm and Stress-strain region is between 0 %-15% strains).

The method for determining the elastic modulus and stiffness of wet and dry nanocomposite membranes and Nafion® membrane are shown in Figure 5-5. The region selected for determining stiffness is between 0.0 mm and 0.15 mm strain and similarly the region selected for determining stiffness is between 0mm and 1.3 mm. When comparing the elastic modulus of wet Nafion® recast membrane with wet Nafion®/Zirconia, it was found that Nafion® recast is 62.06 %, 35.26 %, 30.79 % and 35.26 % higher than Nafion®/Zr-100, Nafion®/Zr-80, Nafion®/Zr-50 and Nafion®/Zr-0, respectively (See Figure 5-5(a)). The elastic modulus of dry Nafion® recast membrane were found to be 1.20% and 7.44 % higher than Zr-80 and Zr-50, respectively. The elastic modulus of dry Nafion® recast membrane was found to be -25.89 % and -60.67 % lower than Zr-100 and Zr-0, respectively. The elastic modulus of dry Nafion® recast, Nafion®/Zr-100, Nafion/Zr-80, Nafion/Zr-50 and Nafion/Zr-0 membranes are 46.29 %, 83.31 %, 64.81%, 59.84 % and 78.36 % higher than wet recast Nafion®, Nafion®/Zr-100, Nafion®/Zr-80, Nafion®/Zr-50 and Nafion®/Zr-0 membranes, respectively (See Figure 5-5). The percentage differences of the elastic modulus of wet and dry membranes are similar to the percentage difference of the stiffness. Generally, the elastic moduli of dry membrane are higher than the wet membranes. Similarly, the stiffnesses of dry membrane are higher than the wet membranes.

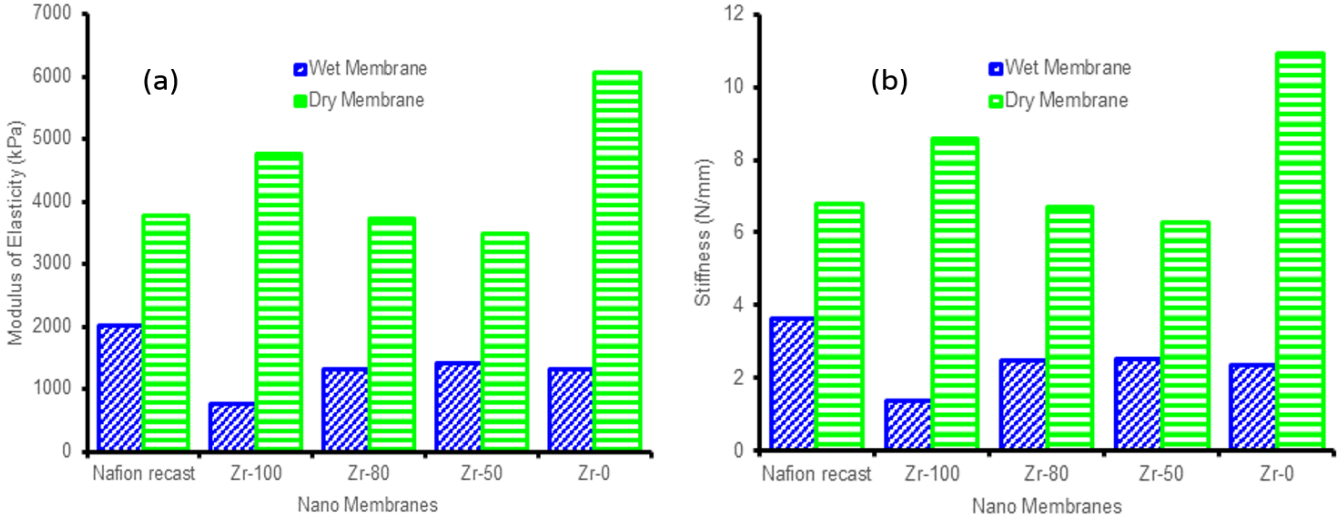

Figure 5-5: Modulus of elasticity of dry and wet Nafion® and Zirconia nanocomposite membrane determined at selected region (see Figure 5-5 (a) and (b) Stiffness of dry and wet Nafion® and Zirconia nanocomposite membrane determined at selected region (see Figure 5-5).

The highest stress is recorded on the original Nafion® when compared nanocomposites membranes (see Figure 5-6). It was observed that the dry nanocomposite membrane has higher modulus of elasticity when comparing to wet nanocomposite membrane. The opposite is observed when comparing Nafion®/Zr-0, Nafion®/Zr-50, Nafion®/Zr-80 and Nafion®/Zr-100 since in this category, the modulus of elasticity of dry nanomembrane is lower than the wet nanocomposite membrane (see Figure 5-6). The tensile strength of the wet recast Nafion® and Nafion®/Zr-0 membranes is higher than of the dry membranes (see Figure 5-

6). The modulus of elasticity of wet membrane of recast Nafion® is 53.8%, 45.6%, 39.6% and 56.8% higher than the Nafion/Zr-0, Nafion®/Zr-50, Nafion®/Zr-80 and Nafion®/Zr-100, respectively. The modulus of elasticity of dry membrane of recast Nafion is 72.5%, 20.6% and 1.8% higher than the Nafion®/Zr-0, Nafion®/Zr-50 and Nafion®/Zr-80, respectively. Ironically, the modulus of elasticity of dry membrane of Nafion is 1.2% lower than the Nafion/Zr-100 (see Figure 5-6). When comparing the wet membrane of recast Nafion®, it was observed that recast Nafion® is 45.3%, 62.4%, 56.1% and 59.3% higher than the Nafion®/Zr-0, Nafion®/Zr-50, Nafion®/Zr-80 and Nafion/Zr-100, respectively.

The tensile strength of dry membrane of recast Nafion® membrane is -25.0%, 20.9%,1.7% and 1.2% higher than the Nafion®/Zr-0, Nafion®/Zr-50, Nafion®/Zr-80 and Nafion®/Zr-100, respectively (see Figure 5-7(a-b). Generally, it was found that the recast Nafion® membrane in wet state has higher modulus of elasticity and tensile strength when compared to Nafion®/Zr-0, Nafion®/Zr-50, Nafion®/Zr-80 and Nafion®/Zr-100 due to its hydrophobic nature as their tensile strength and tensile modulus increase with increasing water content in the membranes. Moreover, the obtained results show that modified Nafion® nano-composite membranes can maintain the mechanical strength when operating in higher temperature fuel cell, as their elongation at break is higher at dry state than wet state. The incorporation of ZrO_2 nanoparticles within Nafion® membrane has resulted in an increase in tensile strength and tensile modulus. This may be due to the free motion within the membrane chains that was slightly restricted by the intermolecular forces between the membrane chains and the inorganic oxide nanoparticles; the tensile strength of membranes is sequentially enhanced [29].

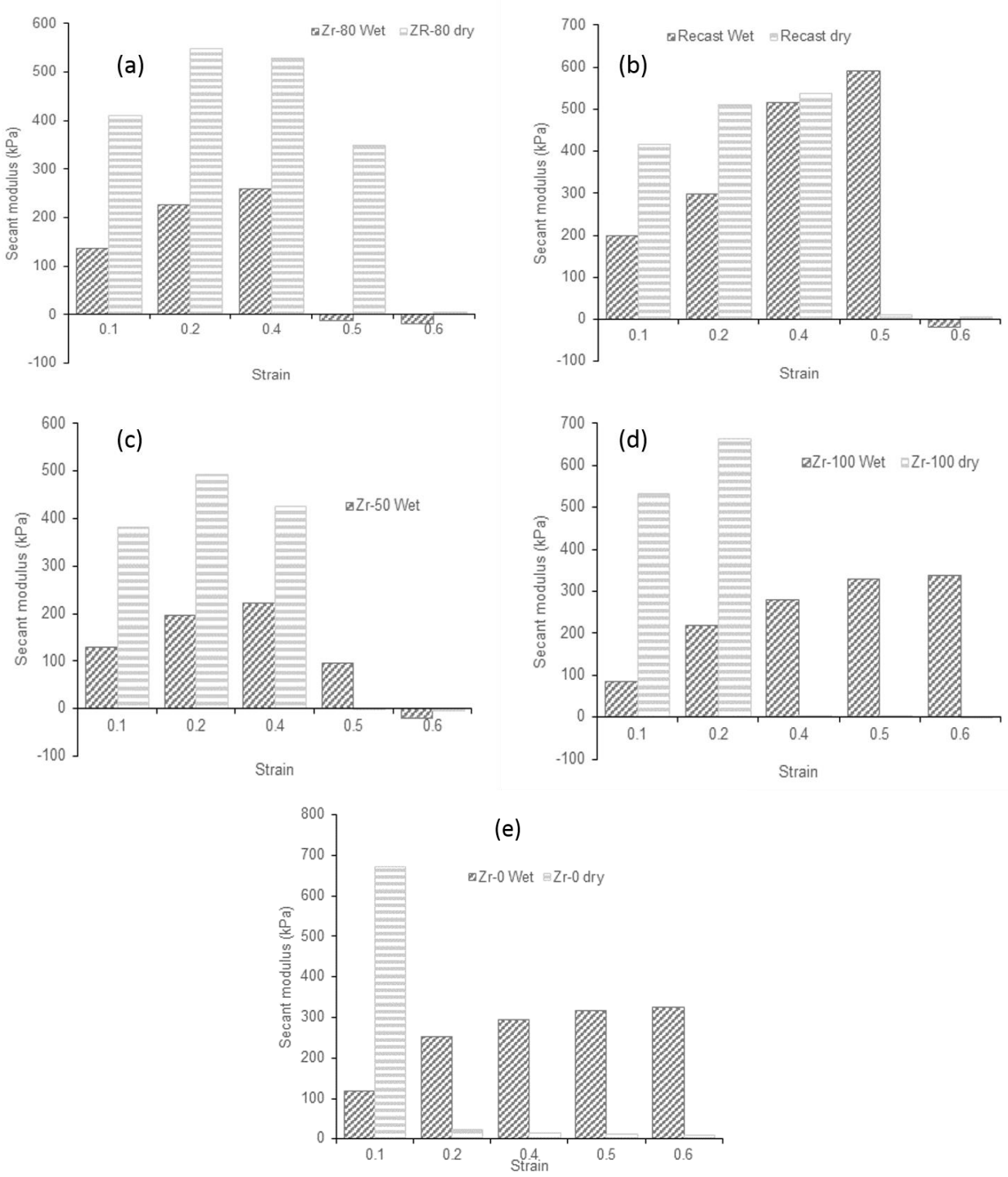

Figure 5- 6: Secant modulus of dry and wet (a) Nafion®/Zr-80, (b) Recast-Nafion®, (c) Nafion®/Zr-50, (d) Nafion®/Zr-100 and (e) Nafion®/Zr-0, membranes.

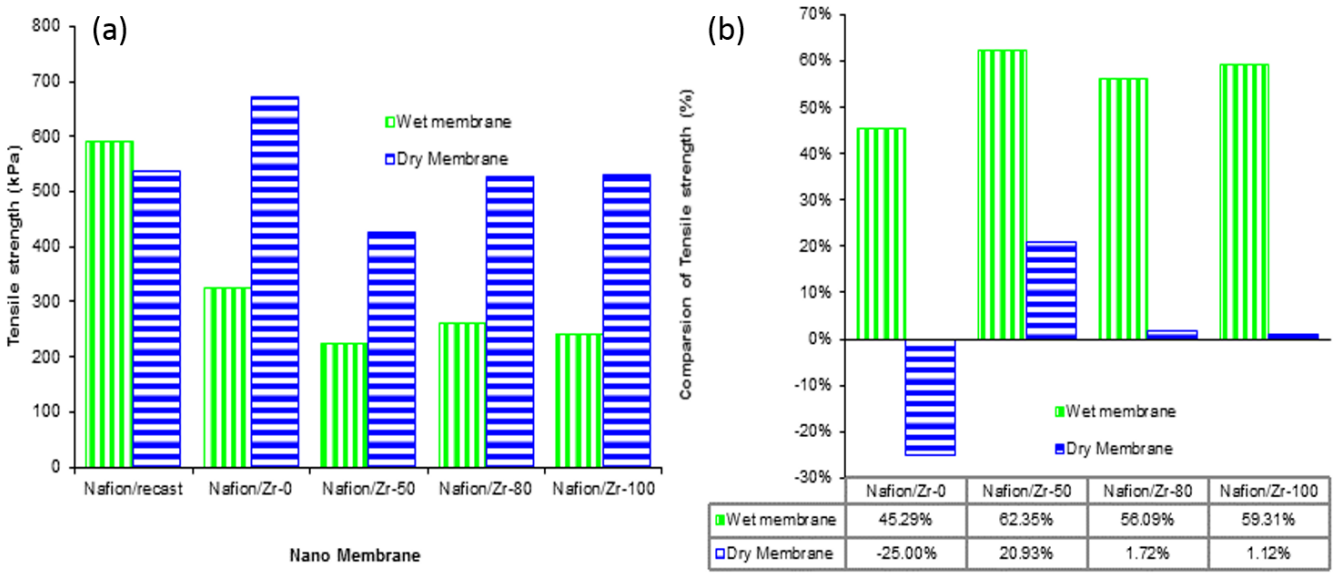

Figure 5- 7: Tensile strength of modified Nafion® membranes and Comparison of modulus of elasticity.

5.3.4. Scanning electron microscopy (SEM)

The scanning electrons microscopic of the modified and recast membranes in cross-sections are displayed in Figure 5-8. Figure 5-8(a) presents the micrographs of Nafion® /Zr-0 nano-composite membrane with 10wt.% of zirconia nanoparticles impregnated within the ionomer of Nafion® membrane. It is observable that the nanoparticles were homogenously distributed within the membrane. Figure 5-8(b) presents the cross-section of Nafion® /Zr-50 nano-composite membrane with well distributed and consistent small particles of Zr-50 nanoparticle. Results in Figure 5-8(c-d) show that zirconia nanoparticles consist of sub-micrometric particles with the similar morphology which is well dispersed within the ionomer matrix [30].

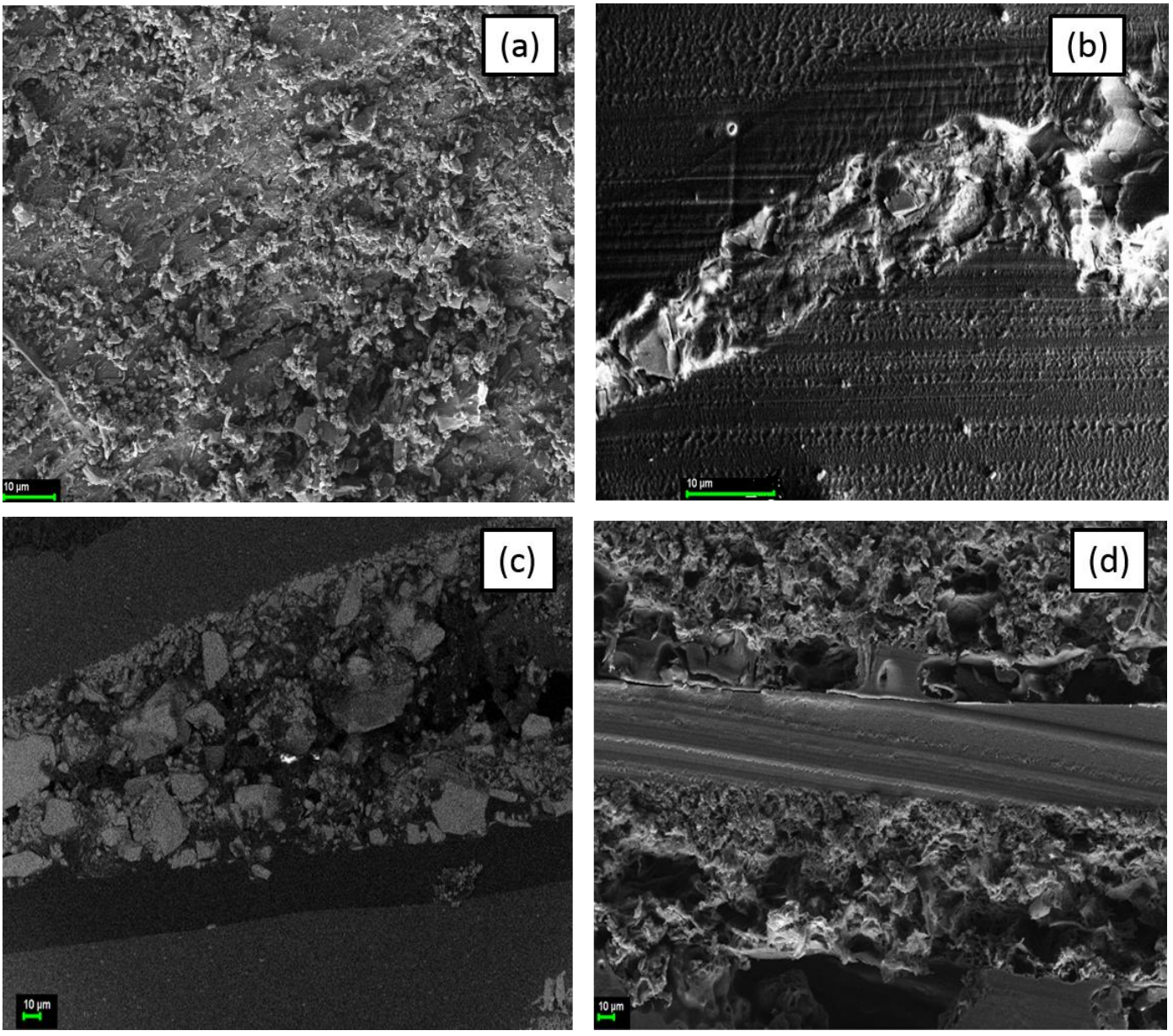

Figure 5- 8: Scanning Electron Microscopy (SEM) micrographs (a) Nafion® /Zr-0, (b) Nafion® /Zr-50, (c) Nafion® /Zr-80 and (d) Nafion® /Zr-100 nano-composite membranes.

5.3.5. Water uptake % (Wup %)

Figure 5-9(a) presents the W_{up} % of modified membrane and recast membrane. The results show that the modified Nafion membrane by incorporating inorganic nanoparticles retain more water (34-35 %) compared to plain recast Nafion membrane (30 %), this may be due to inorganic fillers distributed on the pores of swollen membrane to increase the hydrophilic nature of Nafion [31]. In Figure 5-9(b), the graph also confirms that the modified membrane with Zr-100 has about 5% higher water-uptake than un-modified membrane. Furthermore, zirconia nanoparticles having a higher porosity increases the water retention within the nanocomposite membranes which resulted also in increasing the proton conductivity, due to the

increases of exchange sites available per cluster which is an important parameter of fuel cells in order to operate on higher temperature [32].

(a)

Membrane	Water Uptake %
Nafion/ Zr-0	34
Nafion/ Zr-50	34
Nafion/ Zr-80	34
Nafion/ Zr-100	35
Nafion	30

(b)

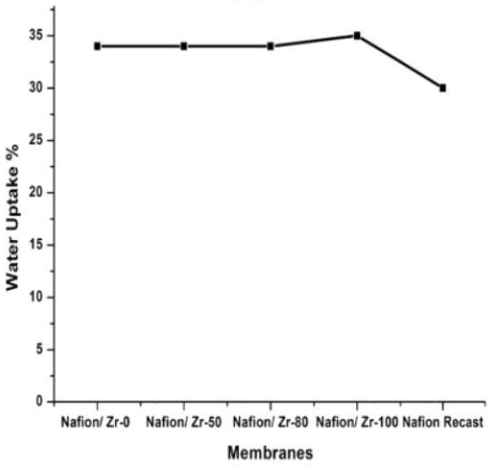

Figure 5- 9: **(a)** Water uptake data and (b) image of Nafion® /Zr-0, Nafion® /Zr-50, Nafion® /Zr-80, Nafion® /Zr-100 nano-composite membranes and Nafion® membrane.

5.4. Conclusion

Modified Nafion® membranes were analysed under the following techniques XRD, TGA, SEM and its mechanical properties under Tensile test was observed. The results obtained under XRD shows that the zirconia nanoparticles are well dispersed within the Nafion® membrane as only the monoclinic and cubic phase appears which increase the crystallinity and compatibility properties of Nafion® membrane. TGA results of modified Nafion® membrane have more thermal stability compared to recast Nafion® membrane which was completely burn. The mechanical properties of modified and recast Nafion® membranes have been also observed at dry and wet conditions. The results show that the percentage difference of the elastic modulus of wet and dry membranes are similar to the percentage difference of the stiffness. Generally, the elastic modulus and the stiffness of dry membrane are higher than the wet membranes of the modified membrane. This may be due to the ZrO_2 nano-fillers which enhance water affinity within the Nafion® membranes, as it promotes the ionic channels that increase in the storage modulus of the composite membrane. This obtained results show that the modified Nafion® membrane can function well as electrolytes in fuel cell.

B: Wettability and mechanical strength of modified Nafion® nano-composite membrane for fuel cell

5.5. Introduction

Fuel cell is an environmentally friendly energy resource, which generates electricity while removing water as bi product. It can operate using hydrogen and methanol as its fuel. This make them have some limitations, as they will need electrolyte that will be conducting while blocking some fuel to pass through. Proton exchange membrane fuel cells (PEMFCs) has been recognizes as the most promising power sources for electric vehicles because they have no carbon dioxide (CO_2) emissions and relatively high power generation efficiency [33]. Nafion® membrane is currently the most popular membrane for its superior mechanical and chemical stability and good electrochemical performances [34], robust structure and excellent proton conductivity in the hydrated state [35]. The microstructure of Nafion® membrane consists of three regions: the hydrophobic fluorocarbon backbone, hydrophilic ionic clusters of sulfonic acid groups (proton exchange sites) and an interfacial region [36-37]. The super selectivity of Nafion® and its chemical and thermal stability are ascribed to the structure [38]. The proton migration within the Nafion® membrane depends on the amount of absorbed water [33]. Application of pristine Nafion® membrane in high temperature fuel cells faces many challenges such as loses its water by evaporation that resulted in irreversible mechanical damages, lowering its proton conductivity at low relative humidity due to the lower-water content, which will hinder its operation in high temperature. However, Nafion® membrane also suffers from methanol permeability, which has limited its application in methanol fuel cell, as it releases CO that damage the catalytic side of fuel cell. The high temperature operation is performed in order to maintain reasonable proton conductivity, good mechanical stability, enhances reaction kinetics at both electrodes, improves the carbon monoxide tolerance of platinum catalyst at anode and simplifies heat and humidity management of polymer electrolyte membrane (PEM) [39]. It increases the biding energy of water [40]. Nafion® tends to shrink when relative humidity decrease and swells in contact with water due to its molecular structure [41]. Moreover, the mechanical properties of the membrane affected by changes of temperature and water content [42]. The researches has put efforts on developing modified Nafion® membrane with inorganic filler, as this inorganic nanomaterials act as water storage in the membrane which does not evaporate at a temperature higher temperature because of electrostatic attraction within the electrical double layer [43], anti-swelling and hydrophilicity properties [44-47]. Furthermore, the membrane strength and performance increased, as the organic polymer formed strong interaction with the inorganic component having large specific area [48]. The inorganic materials in the nanometer scale have been used in many applications with the improvement of the electrical, mechanical, and optical properties of any compound due to the increase in surface area [49]. Modified membrane with inorganic filler such as silica (SiO_2) [26, 43], titanium dioxide (TiO_2) [26, 50], zirconium oxide (ZrO_2) [26, 50], heteropolyacids [51] and zeolites [52]were used to facilitate proton conductivity at high temperature and a low Relative Humidity (RH) performance, water management, mechanical properties, and bring changes to pore and channel structure.[10-12, 53]. As it

restructured hydrophilic channels composed of the pendant sulfonic acid groups that retention water , this may due to the degree of acidity of the nanofiller [54]. Furthermore, when membrane modified by inorganic particles improves the mechanical properties such as the tensile strength, modulus or stiffness [55-56]. Zirconia oxide (ZrO_2) is a metal oxide that is stable at high temperatures and also has high mechanical properties [57]. ZrO_2 obtained in three different crystal phases at ambient pressure, monoclinic, tetragonal and cubic, that strongly influence the catalyst's activities and selectivity [58-59]. In this paper, the incorporation of zirconia nanoparticles within Nafion® membrane was prepared by recast method, in order to enhance the wettability and mechanical strength of electrolytes for Proton exchange membrane fuel cells. The effects of ZrO_2 nanoparticles on the recast membrane in the hydrophilicity and mechanical properties under tensile test and water contact angle was observed.

5.6. Method

5.6.1. Preparation of ZrO_2 nanoparticles

The ZrO_2 nanoparticles was prepared by precipitation method, zirconium oxychloride hydrate ($ZrOCl_2.8H_2O$) and sodium hydroxide (NaOH) were used as starting materials. 0.2M $ZrOCl_2.8H_2O$ has been dissolved in 50 ml de-ionised water. NaOH [2N] solution has been added dropwise to the $ZrOCl_2.8H_2O$ (50 ml) solution and stirred continuously for 45 minutes. The precipitate was covered with a foil and put in an oven at 80 ^oC temperatures for 24 hours, after which it was then centrifuge and wash many times with de-ionized water until Cl^- not detected and dried at 80 ^oC and then calcinated it at 600 ^oC for 4 hours and labelled as Zr-80.

5.6.2. Preparation of nanocomposite membranes.

The nanocomposite membranes were prepared using 5 % Nafion® solution as the standard material for reference. Nafion® solution (10ml) with N, N-dimethylformade **(**DMF) (20ml) was mixed to replace solvents. 10wt % of Zr-80 nanoparticles were added to the Nafion®/ DMF solution and stirred at room temperature for 2 hours, then ultrasonizing for 30 minutes [21]. The resulting solution was poured onto a piece of flat glass and placed into an oven at 80 ˚C for 12 hours to remove solvent, and finally heated up to 160 ˚C for 30 minutes. The membranes were then removed by peeling off from the glass plate. Before conducting any measurement, all membranes were kept at deionized water for 12 hours. The thicknesses of the membrane were measured with digital micrometer (0.18 cm). Each thickness was measured in the average of 3-7 reading at different position of membrane and was repeated twice on each membrane in order to obtain the average value.

5.6.3. Characterizations

The X-ray diffraction (XRD) analysis was performed using a Philips X-ray diffraction with Cu K radiation source. The analyzed material is finely ground, homogenized, and average bulk composition is determined. Samples are scanned in a continuous mode from 10° - 90° with a scanning rate of 0.026 (degree) / 1 (sec). The thermal properties of the samples and its characteristics were studied by thermal gravimetric analysis (TGA) under nitrogen flow. TGA data was obtained with model STA (Simultaneous Thermal Analyzer) 1500 (supplied by Rheometric Scientific Ltd, UK), over nitrogen and at a heating rate of 10 ˚C/min from 28 ˚C to 1000 ˚C. Fourier Transform Infrared (FTIR) investigated the changes in the chemical structure of the membrane. Scanning Electron Microscopy (SEM) images were obtained on a Hitachi x650. Electronic techniques were based on the interaction of the sample with electrons which results in a secondary effect that is detected and measured. Dynamic Light Scattering (DLS) measurements and Transmission electron microscopy (TEM) were used to observe the surface area. The surface morphology of nanocomposite membranes and roughness analysis was measured by Atomic force microscopy (AFM).

5.6.4. Tensile Test

The uniaxial mechanical properties of nano-composite membranes and recast membrane were captured using a uniaxial testing system. The length, width and thickness of samples were measured using a Vernier caliper and recorded prior to testing. The testing area of the membrane samples were 4 mm x 10 mm in dimension. To allow clamping area, the sample were prepared in such a way that they will be clamped both sides and still allow the testing area to be 4 mm x1 0 mm. The length, width and thickness of samples were measured using a Vernier calliper and recorded prior to testing. The thickness of 0.18 cm of the nanocomposite membrane was used in analyzing the stress applied to the sample. The membrane was soaked in water for 24 hours and tested as wet test. Then the membrane was dried in a vacuum oven at 80 ˚C for 24 hours and tested as dry test. The tensile strength of modified Nafion membranes were measured using CellScale Ustretch device dried at 25 ˚C and wet at 34 ˚C and actuator speed of 5 mm per min.

5.6.5. Water Contact Angle Measurements

The hydrophilicity of the membrane surfaces was performed under contact angles measurement (Phoenix 300 contact angle analyser (Surface Electro Optics Co., Korea) instrument equipped with a video system. Membranes were cut into strips and mounted on glass slides for analysis. The droplet of de-ionized water (0.16 µL) was drop onto the surface of membranes at ambient temperature by placing the tip of the syringe close to the sample surface with all the images been captured using a camera. The measurement was repeated 10 times at different surface of membrane to obtain an average value. Before the water droplet

attached to the sample surface, the wetting process was recorded until no significant change at the surface was observed any more [60].

5.6.6. Water uptake measurements

The membranes were immersed in deionized water for 24 hours, blotted with a paper towel and then measured as wet mass percentage. The membranes were dried in a vacuum oven at 80°C for 24 hours and then was measured. The water uptakes of the nano-composite membranes and recast Nafion® membrane were calculated from the equation:

$$Wup(\%) = \frac{(mwet - mdry)}{mdry} \mathrm{X}\, 100 \qquad (5\text{-}1)$$

Where W_{wet} and W_{dry} are the weights of the fully hydrated and the anhydrous membranes, respectively.

5.7. Results and discussion

5.7.1. Dynamic light scattering (DLS) measurements

The resulting particle size distribution is shown in Figure 5-10. As illustrated in Figure 5-10, DLS measurements of a sample synthesized at 80 °C for 24 hours agree with TEM about the particles size distribution. TEM measurements (insert) in Figure 5-10 show the real particle size while DLS measures the hydrodynamic radius of the particles, the synthesized particles [61]. From Figure 5-10 (a) insert picture, shows that the nanoparticles aggregate in the form of 10-20 nm diameter. Results from light scattering measurements in Figure 5-10 show that the average particle size is 345 nm and that the particle size distribution is narrow. The mean particle in Figure 5-10 (b) is also 3.40 µm, respectively, with a slightly broadened particle size distribution. The nanocomposite mean particle size is bigger than the zirconia nanoparticles on the surface area, which resulted in a slightly broadened particle size distribution in Figure 5-10 (b). This result indicates that the nanocomposite was slightly agglomerated, which may result from synthesis procedure.

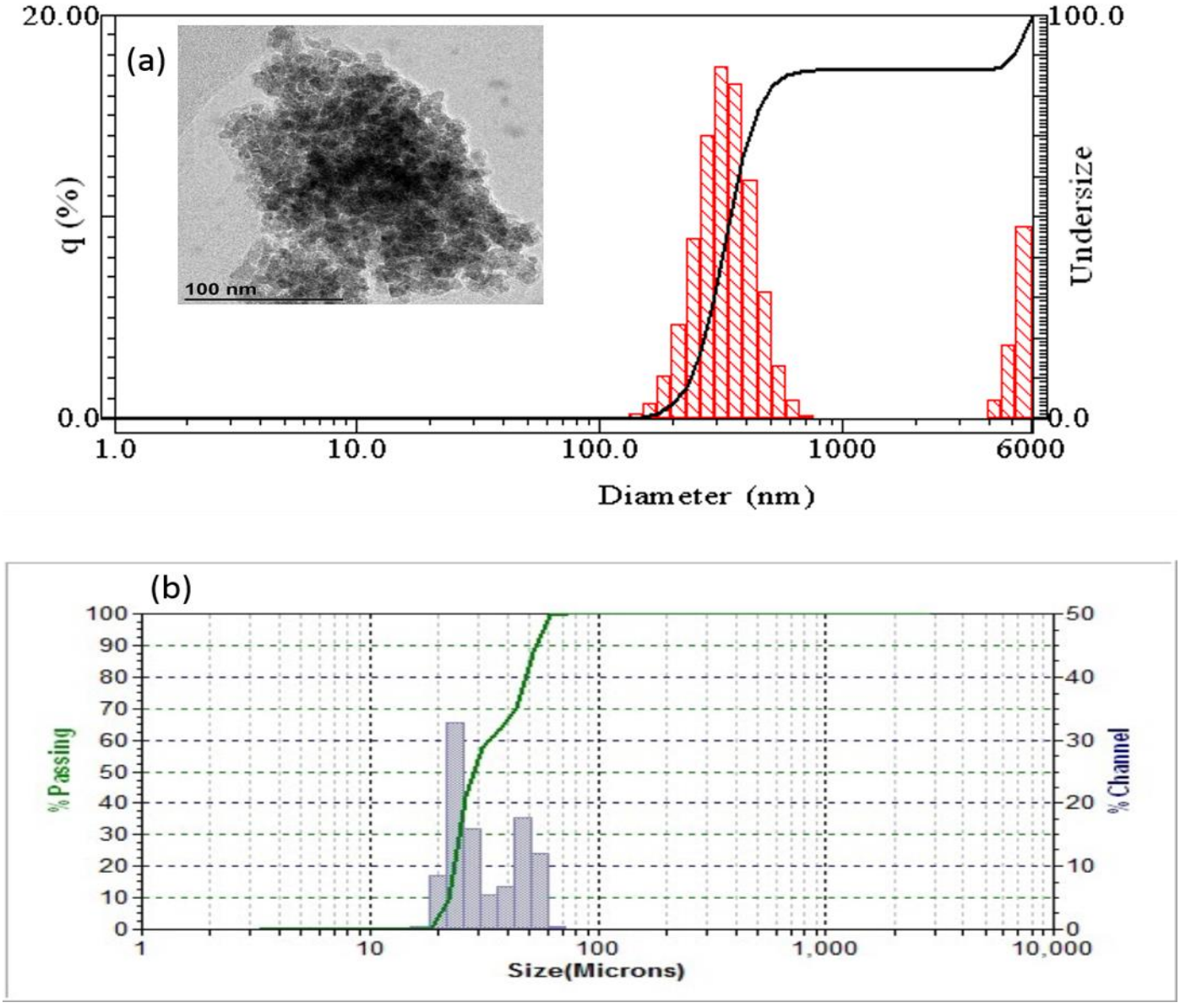

Figure 5- 10: Dynamic Light Scattering (DLS) of (a) Zr-80 nanoparticles, (insert) TEM micrograph of Zr-80 nanoparticles. (b)Nafion®/Zirconia nanocomposite.

5.7.2. Morphology

The SEM image of the Nafion®/ Zr-80 nanocomposite membrane and Zr-80 nanoparticles (insert) are shown in Figure 5-11. The cross-section and surface morphologies of modified membrane shows that the zirconia nanoparticles are well distributed within the membrane matrix that confirms by XRD results. Figure 5-11 clearly shows the white particles within the Nafion® membrane, which indicate that zirconia nanoparticles have successfully dispersed by recast method without any aggregation due to their good compatibility. The cross-section of nanocomposite membranes shows the zirconia nanoparticles is good dispersion across the thickness of the membrane without macroscopic void space and cracks. The red

arrow in Figure 5-11 shows the microscopic porosity within the modified membrane with inorganic nanoparticles that enhanced the water uptake of membrane [62]. It is notable in the Figure 5-11 (yellow circles and arrow) that zirconia nanoparticles was uniformly distributed through the whole membrane with the coarser pores in the interlayer membrane [63]. The insert image shows the nanoparticles aggregated in the form of nano-flowers having a diameter of less than 100 nm. Moreover, the distribution of inorganic filler within the modified membrane have been identified by tapping mode atomic force microscopy [64]. The amplitude and topography images measured in tapping mode of Nafion®/ Zr-80 nanocomposites membranes were shown in Figure 5-12. The modified membranes show that the presents of ZrO_2 nanoparticles in the surface of Nafion® membrane shows the roughness of 60.8 nm. In Figure 5-12(b), the nodules structure on the membrane's surface can be seen. From the topography and amplitude images, we can clearly see significant changes in the surface morphology with the addition of ZrO_2, which indicates the strong interaction of filler material within the Nafion® matrix [65]. The more the roughness on modified Nafion® nanocomposite membranes improves the contact between the electrodes [66].

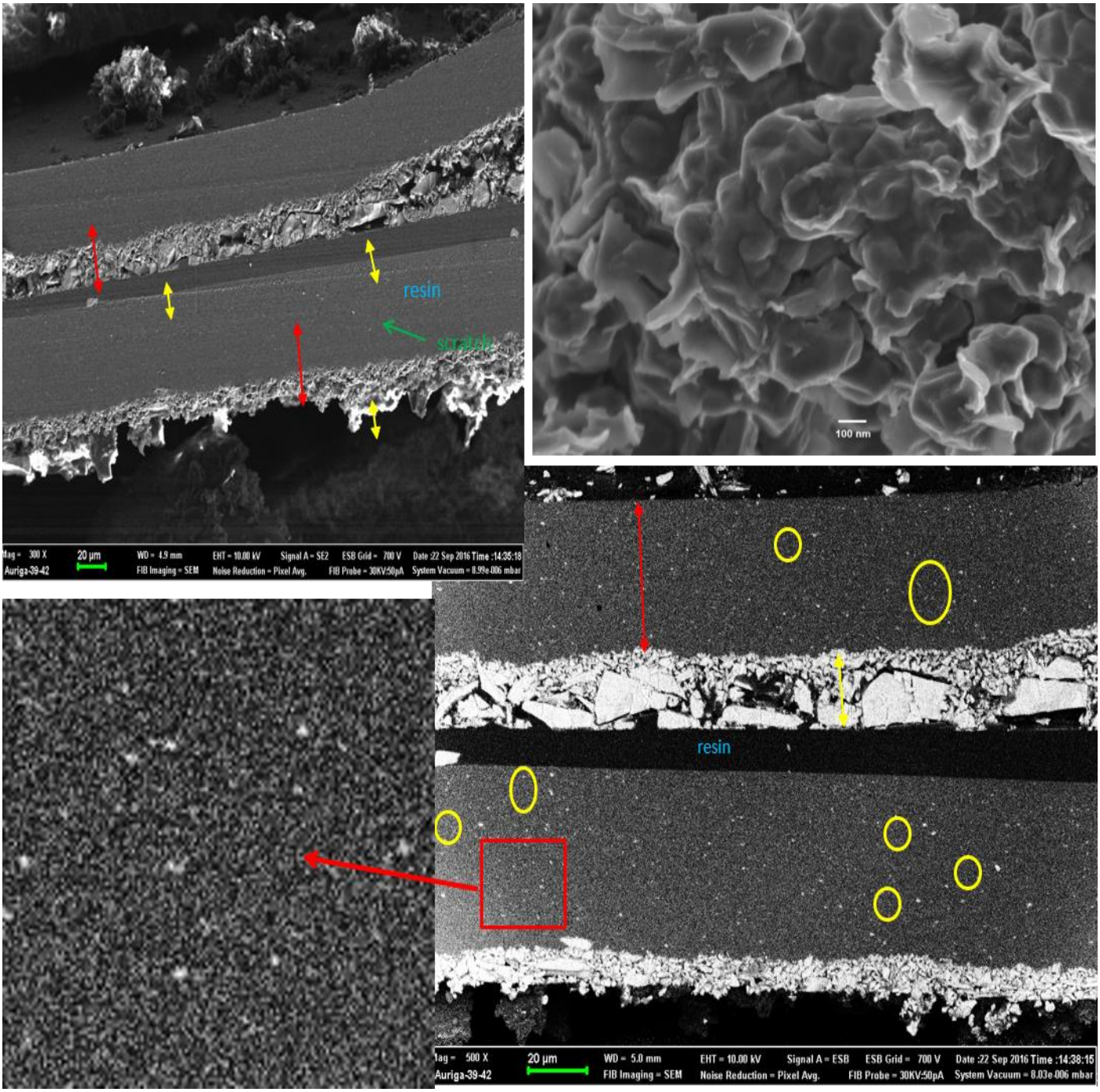

Figure 5- 11: SEM micrograph of Nafion®/ Zr-80 nanocomposite membrane, (insert) SEM micrograph of Zr-80 nanoparticles.

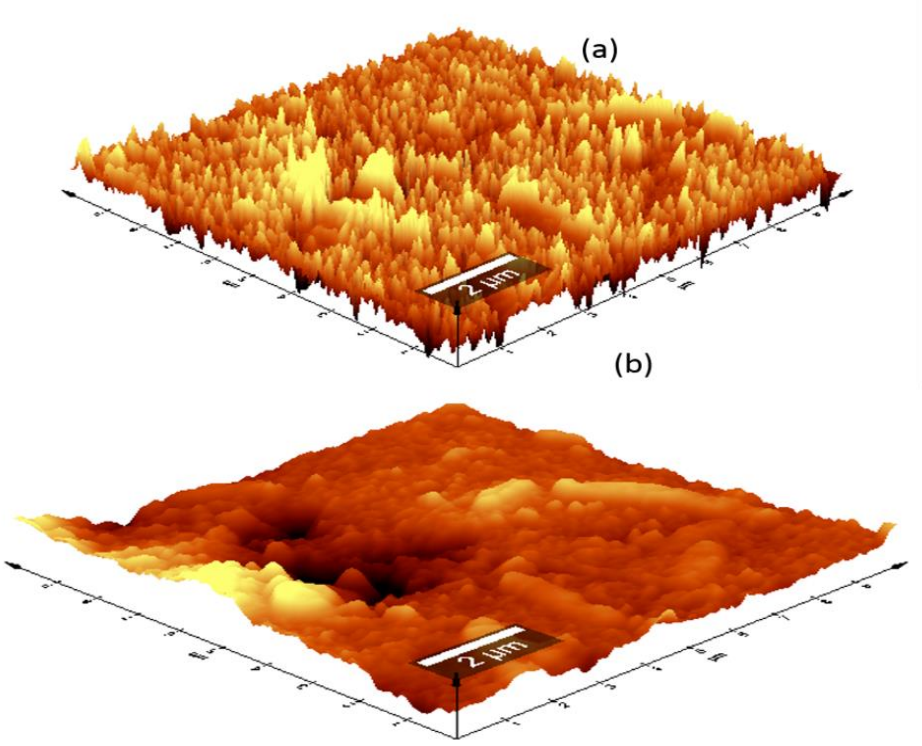

Figure 5- 12: Atomic force microscopy (AFM) (a) amplitude image (b) topography measured in tapping mode of the modified membranes.

5.7.3. Tensile test

The uniaxial force was applied on the recast Nafion® and Nafion®/ Zr-80 nanocomposite membranes. The stress-strain curve was used to determine the elastic modulus of nanocomposite membranes. As shown in Figure 5-13, the elastic modulus of elasticity of dry Nafion®/ Zr-80 nanocomposite membrane is slightly lower than that of the dry recast Nafion®. Similarly, the elastic modulus of elasticity of wet Nafion®/ Zr-80 nanocomposite membrane is lower than that of the wet recast Nafion®. This may due to poor dispersion of the inorganic filler within the polymer [67]. Figure 5-14 shows that the elastic modulus of dry recast Nafion® is 1.19 % higher than that of the dry Nafion®/ Zr-80 nanocomposite membranes. Similarly, elastic modulus of wet recast Nafion® is 31.24 % higher than the wet Nafion®/ Zr-80 nanocomposite membranes. The strength of Nafion®/ Zr-80 nanocomposite membrane is greatly affected by moisture content when compared to recast Nafion®, due to the inorganic nanofiller which acts as water storage within the membrane [44-45]. Even when the effect of moisture is felt on the recast Nafion® membrane, the effect is not as great as that of the Nafion®/ Zr-80 nanocomposite membrane. Figure 5-13(e) shows improvement in secant modulus of dry Nafion®/ Zr-80 when compared to recast membrane, due to incorporated of zirconia nanoparticles within Nafion® membrane that retains water to enhance mechanical strength of Nafion® membranes. Thus, demonstrating the close bonding between the zirconia

nanoparticles and Nafion® membrane through self-assembly. This improvement of the membrane rigidity demonstrates that the zirconia nanoparticles stabilized the structure of modified membrane and give a potential restriction to the humidity-generated stress when the membrane is used as an electrolyte membrane in the fuel cells application. Hence, it observable that the recast Nafion® membrane in wet state has higher modulus of elasticity and tensile strength when compared to Nafion®/Zr-80, due to hydrophobic nature as their tensile strength and tensile modulus increase with increasing water content in the membranes [42]. Moreover, the obtained results show that modified Nafion® nanocomposite membranes can maintain the mechanical strength when operating in higher temperature fuel cell, as their secant modulus is higher at dry state than wet state. The incorporation of ZrO_2 nanoparticles within Nafion® membrane has resulted in an increase in secant modulus [18, 19]. This may be due to the free motion within the membrane chains that was slightly restricted by the intermolecular forces between the membrane chains and the inorganic oxide nanoparticles; the secant modulus of membranes is increases.

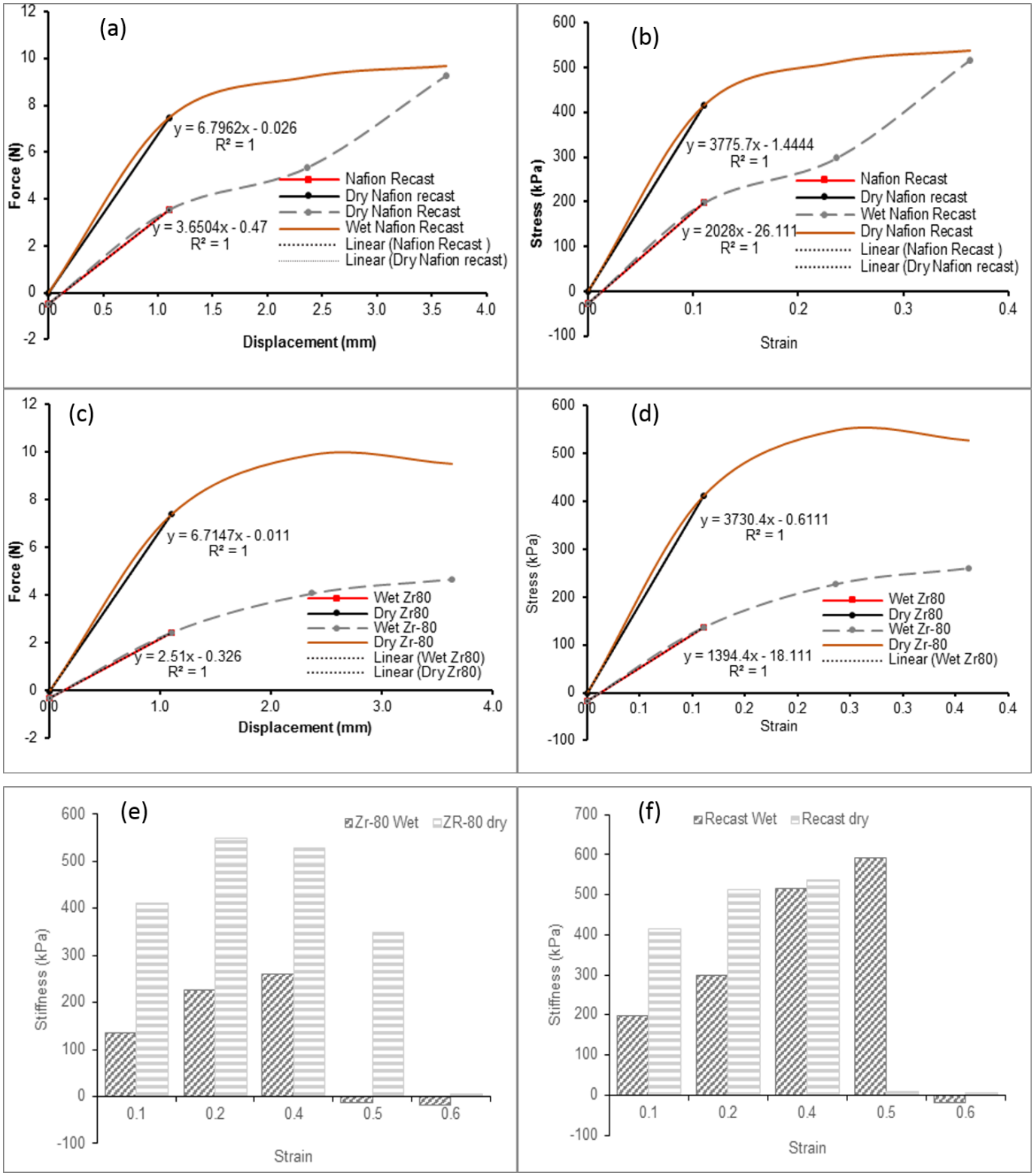

Figure 5- 13: Mechanical tensile tests results of recast Nafion® and Nafion®/ Zr-80 nano-composite membranes (a) shows the stiffness of dry and wet recast Nafion®, (b) shows the elastic modulus of dry and wet recast Nafion®, (c) shows the stiffness of dry and wet Nafion®/ Zr-80 nano-composite membrane and (d) shows the elastic modulus of dry and wet of Nafion®/ Zr-80 nano-composite membrane, Secant modulus of dry and wet (e) Nafion®/Zr-80, (f) Recast-Nafion®.

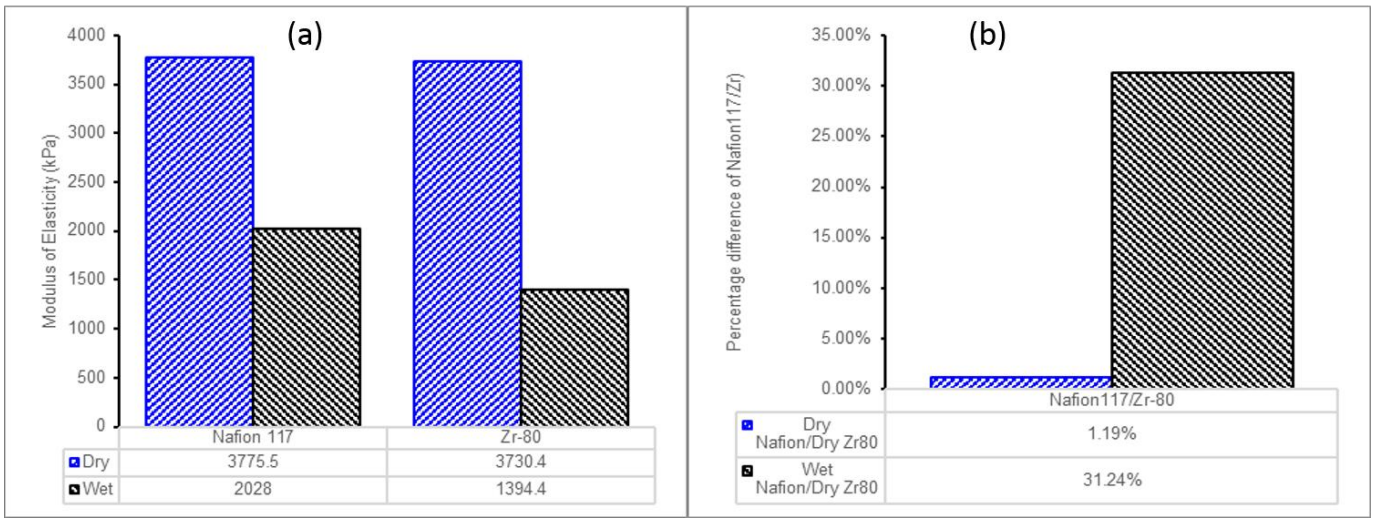

Figure 5- 14: Comparison of modulus of elasticity (a) dry an4d wet recast Nafion® and Nafion®/ Zr-80 nano-composite membranes and (b) dry/wet recast Nafion® and dry/wet Nafion®/ Zr-80 nano-composite membranes.

5.7.4. Structure analysis

The structure of zirconia nanoparticles, nano-composite membranes and recast Nafion® were measurements by X-ray diffraction (XRD) as shown in Figure 5-15(a-c). Figure 5-15(a) shows that the crystallinity of zirconia nanoparticles resembles the same diffraction patterns corresponding to (JCPDS No. 65-1022), which indicates the formation of only the pure cubic phase. With the diffraction peaks at 2θ are 30.2°, 35.2°, 50.6°, 60.2°,74.2°and 82.5° which corresponding to the planes (1 1 1), (2 0 0), (2 2 0), (3 1 1), (4 0 0), (3 3 1) [23-24]. In, corresponding to d-spacing of 0.51291 nm (a-c) and β = 90.0º, were spectra indexed as cubic phase of ZrO_2 nanoparticles. Figure 5-15(b) shows that the recast Nafion® membrane consisted of two diffractions peaks at 17.5° and 39° 2thetha which resemble the crystallinity within the per-fluorocarbon chains of the ionomer [22]. It is noticeable in Figure 5-15(c) that the ZrO_2 nanoparticles is well distributed into the moieties surface of recast Nafion® membrane, as the entire Nafion® peak at 17.5° and 39° 2thetha has been disappeared. Only observed ZrO_2 peak within the composite membrane that shows the existence of nanoparticles within the membrane as it is perfectly match with Figure 5-15(a). With the diffraction peaks at 2theta are 30.2°, 35.2°, 50.6°, 60.2°,74.2°and 82.5° which corresponding to the planes (1 1 1), (2 0 0), (2 2 0), (3 1 1), (4 0 0), (3 3 1) [23-24]. Moreover, it can be observed in Figure 5-15(c) that, by introduction the ZrO_2 nanoparticles decreases the crystallinity of Nafion® membrane [68].

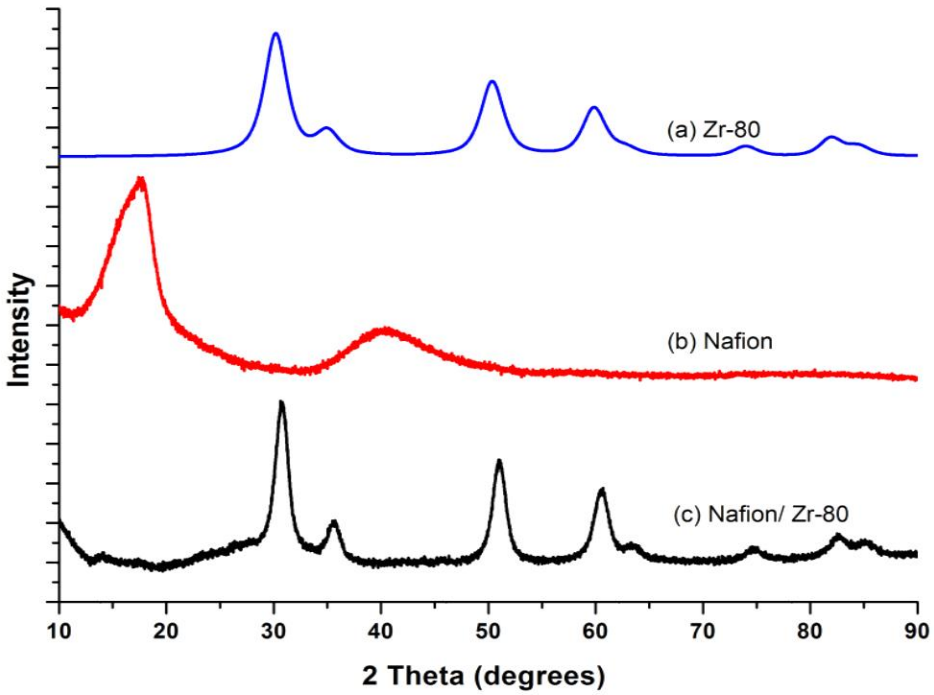

Figure 5- 15: XRD patterns of Zr-80 nanoparticles (a), recast Nafion® membrane (b) and Nafion®/ Zr-80 nanocomposite membrane (c).

5.7.5. Degradation at high temperatures

The thermal degradation of composite membrane compared to the recast Nafion® were observed under thermal gravimetric analysis (TGA) and Fourier transform infrared spectroscopy (FT-IR).

5.7.5.1. Thermo-gravimetric analysis (TGA)

The thermal degradation of nanocomposite membrane, zirconia nanoparticles compared to the recast Nafion® were observed under thermal gravimetric analysis (TGA) in Figure 5-16. Figure 5-16(a) show that Zr-80, has little loss of its original weight on heating up to 100 ˚C. This weight loss is attributed to the removal of the adsorbed water on the surface [69]. Second weight loss is between 100 °C and 900 °C corresponding to the removal of terminal hydroxyl groups bonded to the surface of zirconia [69]. Zr-80 lost only 8% of its total weight mass with less decomposition of oxide. Figure 5-16(b) shows that the modified Nafion® membrane with zirconia nanoparticles has more thermal stabilized when compared to recast Nafion® membrane that completely lose their weight, which is the same obtained by some researchers [70]. This may due to the water retention of inorganic additives within the membrane that makes

close interaction with hydrophobic backbones of Nafion® Membrane [8, 71]. Moreover, Figure 5-16(b) shows that modified nanocomposite membrane has improved thermal properties than recast Nafion® membrane as started to decompose at 530 °C, while the recast Nafion® membrane started to decompose at a lower temperature of 360 °C. As some reporters find that sulfonic acid group of pure Nafion® membrane began to be decomposed at 280 °C [72-73]. Figure 5-16(b-c), shows that all the membrane undergoes three weight loss stages, initial weight loss due to the evaporation of hydrated water, and the second weight loss due to the decomposition of the sulfonic acid groups of Nafion® membrane [25]. The third weight loss due to degradation and combustion of the polymer main chain [21, 26-27]. As expected, recast Nafion® Membrane in Figure 5-16(c) shows that it degrades faster in all stages when compared to that of modified membrane. Hence, this improvement in thermal stability shows the possibility of modified membrane to function in the high temperature PEMFCs and low relative humidity, due to the inorganic nanofiller that contributes to the water retention at high temperature [26].

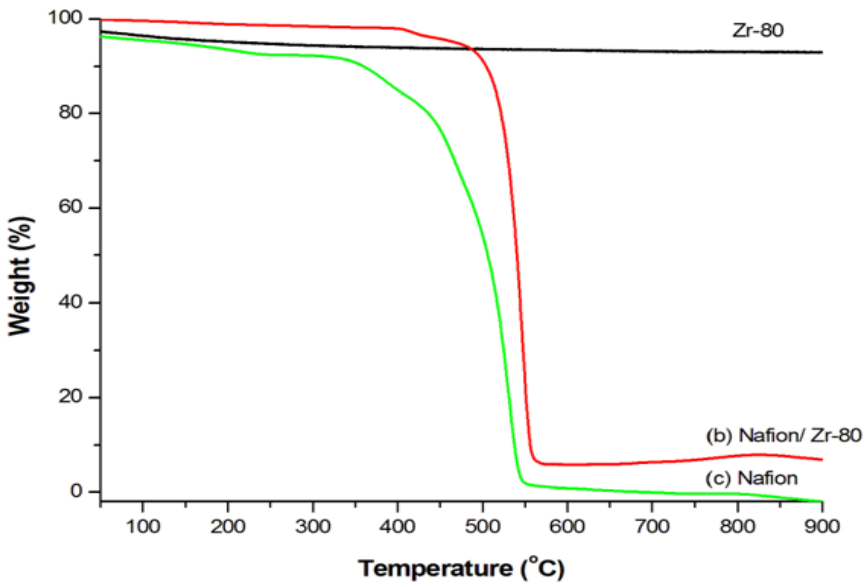

Figure 5- 16: Thermograms of Zr-80 nanoparticles (a), Nafion/ Zr-80 nano-composite membrane (b) and recast Nafion membrane (c).

5.7.5.2. FT-IR analysis

The degradation of the nanocomposite membrane, zirconia nanoparticles and recast membrane were investigated by FT-IR as shown in Figure 5-17. Figure 5-17(a), shows vibration bands at 863 cm^{-1} and 926 cm^{-1} are due to the Zr-O vibration [74], the peak at 1393 cm^{-1} and 1434 cm^{-1} are assigned to O-H bonding, the peak observed at 2346 cm^{-1} is due to the presence of inorganic ions. Figure 5-17(b) shows that the nanocomposite membrane clearly exhibited a broad peak at a wavenumber of 3480 cm^{-1} which corresponds to the

presence of bound water and the -OH functional group on the surface of the Zr nanoparticles. Due to the water that tightly bound on the surface of the Zr nanoparticles, which resulted in it being highly stable at a temperature greater than 100 °C. Figure 5-17(b) shows the vibration peak at 1016 cm^{-1} that could be attributed to vibrational mode of Zr-O and the peak at 1550 cm^{-1} due to Zr-OH bending vibrations, indicating the presence of zirconia nanoparticles within the modified Nafion membrane [75]. Figure 5-17(c) shows the O-H vibration of physically adsorbed water occurs at wavenumbers of 3451 cm^{-1} and 3456 cm^{-1} [76-77]. In Figure 5-17(b-c), shows the vibration peaks at 1195 cm^{-1} and 1198 cm^{-1} that attributed to the $-CF_2-CF_2-$ vibration and 1060 cm^{-1} attributed to $-SO_3^-$ [72, 78].

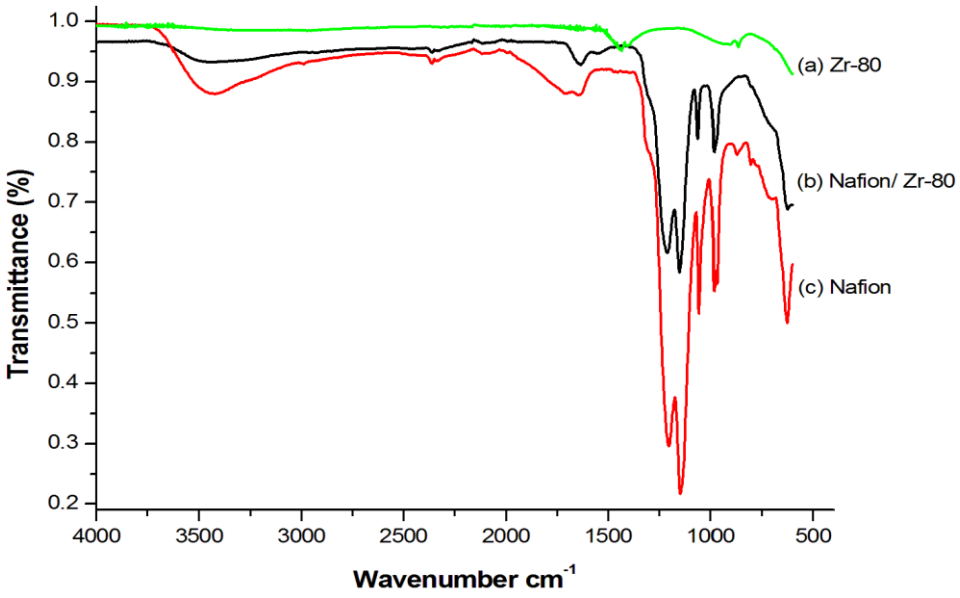

Figure 5- 17: FTIR spectra of Zr-80 nanoparticles (a), Nafion/ Zr-80 nanocomposite membrane (b) and recast Nafion membrane (c).

5.7.6. Water contact angle and water uptake measurement

One very important element that determines the performance of the PEMFC is the water-content dependence of the protonic conductivity in the ionomer membrane. The contact angle was measured to determine the effect of ZrO_2 nanoparticles in hydrophilicity and hydrophobicity of modified membranes. The digital images of water droplets at the surface area of recast Nafion® and modified membrane are presents at Figure 5-18 below. Figure 5-18(a-b) shows that the modified Nafion® membrane with Zr-80 nanoparticles acts as hydrophilic surface as the obtained contact angles less than 90° whereas the recast Nafion® membrane is hydrophobic surface since they have obtained the contact angle above 90° as indicated in Figure 5-18(c-d). Generally, the contact angles of the modified membranes were decreasing from 88° to 64° when compared with that of unmodified recast Nafion® membranes

(118° to 100°), this may due to the hydrophilicity of nanoparticles that adsorbed on the surface of membrane to introduce the hydrophilicity of modified membrane surface [79]. Contact angles below 90 ° indicate the hydrophilic character of a sample describing the water-uptake capability. Figure 5-18(d) shows that when the water droplet touches the hydrophobic recast Nafion membrane, immediately changes their morphological structure as it becomes swells within the measuring time [80]. Whereas in Figure 5-18(b) shows no swelling on the membrane, due to the incorporation of inorganic oxide nanoparticles within the membrane matrix which is anti-swelling [44-47]. Figure 5-18(e) shows the water uptake percentage of modified membrane and recast Nafion® membrane. From Figure 5-18(e), we find that the modified Nafion membrane with inorganic filler of zirconium oxide has obtained a higher water uptake of 34 % when compared to recast Nafion membrane (30%), this may be due to inorganic fillers distributed on the pores of swollen membrane to increase the hydrophilic nature of Nafion [31]. Incorporating of zirconia nanoparticles with a higher porosity increases the water retention within the nanocomposite membranes which resulted also in increasing the proton conductivity, due to the increases of exchange sites available per cluster which is an important parameter of fuel cells in order to operate on higher temperature [32].

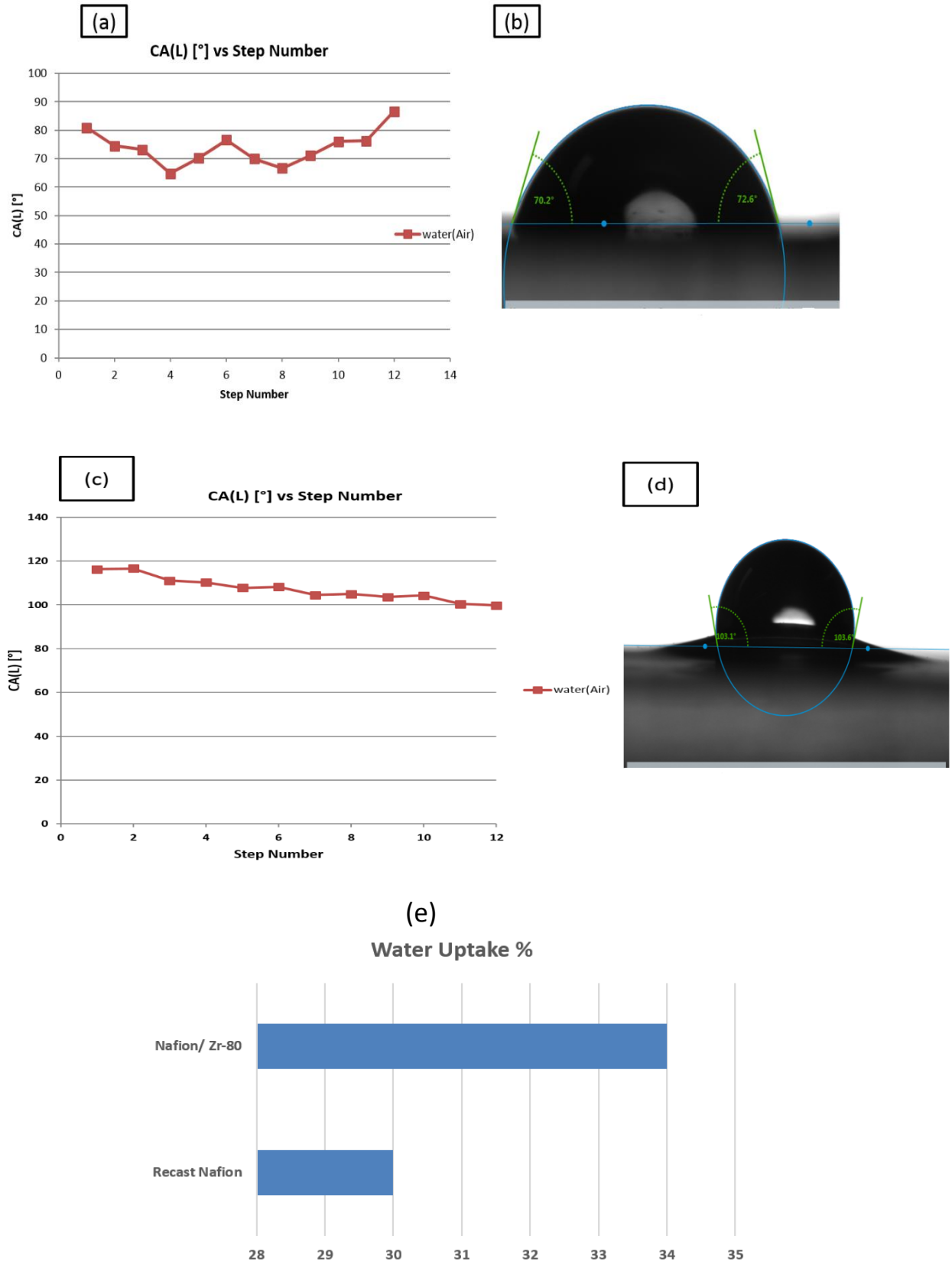

Figure 5- 18: Water contact angle of Nafion® /Zr-80 nanocomposite (a-b) and recast Nafion® membranes (c-d), Water uptake of Nafion® /Zr-80 nanocomposite and recast Nafion® membranes (e).

5.8. Conclusion

The modified membranes obtained by recast method shows decrease in water contact angle when compared to the recast Nafion® membrane. Furthermore, the water uptake of modified membrane was higher than that of recast Nafion® membrane, this may due incorporation of the inorganic nanofiller that adsorb water. XRD, AFM and SEM results show that using zirconia nanoparticles as inorganic filler improves the morphology and crystallinity of Nafion® membrane, as it was well dispersed within Nafion matrix that makes them suitable candidates for fuel cell applications. The incorporation of zirconia nanoparticles also shows the effect on hydrophilicity roughness of the membrane. The strength of Nafion®/ Zr-80 nanocomposite membrane in its wet state was greatly affected by moisture content when compared to recast Nafion® membrane. However, the obtained results show that modified Nafion® nanocomposite membranes can maintain the mechanical strength when operating in higher temperature fuel cell, as their secant modulus is higher at dry state than wet state. The incorporation of ZrO_2 nanoparticles within Nafion® membrane has resulted in an increase in secant modulus. Zirconia nanoparticles shows better improvements on thermal stability of modified membrane when compared to recast Nafion® membrane under TGA results. In addition, the membrane started decomposed at a higher temperature when compared to the pure recast Nafion® membrane.

C: Mechanical strength of Nafion®/ ZrO_2 nano-composite membrane

5.9. Introduction

Proton exchange membrane fuel cells (PEMFCs) are considered as the future alternatives or replacement of combustion fossil fuels for power generation due to their high energy-efficient and environmentally-friendly characteristics. The proton exchange membranes (PEMs) such as Nafion® membranes have high proton conductivity, high mechanical, chemical and thermal stability at temperatures below the boiling point of water [5-6]. However, this Nafion® membrane must exhibit high mechanical properties in order to perform on the methanol or hydrogen fuel cell without mechanical failure, as tough membranes improve fuel cell longevity [3-4, 6]. But the Nafion® membrane faces some challenges as the conductivity depends on the bound water within the membrane that hinders the operation in high temperatures and low relative humidity [81]. Moreover, its hydrophobic states can have effects on the mechanical properties of the membrane as it becomes swollen when in contact with water [42, 82], and also reduces the mechanical stability at elevated temperatures [83]. This due to the diminished stability of the polymer chains at high temperatures as a result of the relatively low glass transition temperature of Nafion [84-85]. Many researchers have enhanced the mechanical properties of

commercial Nafion® membrane with inorganic materials such as zirconia, silica, titanium and clay that retain water in the Nafion® matrix and enhance thermal stability over 100 ˚C in order to function at high temperatures and low relative humidity [18, 86]. By operating at high temperatures above 100 ˚C the PEMFC performance is improved. It increases the water and thermal management of the fuel cell system and there is an oxygen reduction reaction (ORR)) and carbon monoxide (CO) tolerance [48, 87-88], [48]. Furthermore, the mechanical failure of the membrane such as cracks, pinholes and tensile strength can limit its operation at fuel cell level [18, 43, 86, 89]. Using the inorganic material as a nanofiller shows an improvement of the elastic modulus on the nanocomposite membrane when compared with the commercial membrane [90]. This may be due to the water retention of inorganic material within the membrane[44-45], as incorporation of inorganic material within the Nafion® matrix increases the interaction between polymer matrix and filler materials [91]. The inorganic incorporation in organic materials improves the thermal and mechanical stability while reducing the swelling of the membrane [47]. In this work, the incorporation of zirconium oxide nanoparticles within Nafion membrane was prepared by the recast and impregnation method to enhance the mechanical strength of the electrolytes for the PEM fuel cell applications. Mechanical stress-strain properties of all prepared nanocomposite membrane were measured under tensile stress-strain tests at wet and dry conditions and compared to the commercial Nafion® 117 and plain recast membrane.

5.10. Experiment

5.10.1. Materials

Sodium hydroxide, silver nitrate, N, N-dimethylformade (Merck), Sulfuric Acid (Merck), Zirconium oxychloride hydrate (Merck), Iso-propanol (Merck) and Nafion® solution (Sigma) were obtained and used as received.

5.10.2. Synthesis of ZrO_2 nanoparticles

The ZrO_2 nanoparticles were prepared by precipitation method. Zirconium oxychloride hydrate ($ZrOCl_2 .8H_2O$) and sodium hydroxide (NaOH) were used as starting materials. 0.2M $ZrOCl_2.8H_2O$ was prepared in a 250 ml beaker and 2N NaOH solution was added dropwise with continuous stirring for 45 minutes. The obtained precipitate was divided into six parts, one part was filtered and washed several times with distilled water until chlorine ions (Cl^-) were no longer detected by the silver nitrate ($AgNO_3$). The precipitate was dried at 100 °C for 24 hours, which was calcined at 600 °C for 4 hours and labelled as Zr-0. The remaining parts of the solution were covered with a foil and put in an oven at 50 °C, 80 °C and 100 °C for 24 hours,

after which they were filtered, then washed and calcinated according to the Zr-0 procedure and then stored for analysis. Then the samples were labelled as Zr-50, Zr-80 and Zr-100 respectively.

5.10.3. Preparation of nano-composite membranes (recast method)

The nanocomposite membranes were prepared using a 5% Nafion® solution as the standard material for reference. Nafion® solution with N, N-dimethylformade **(**DMF) was mixed to replace solvents. The appropriate amount of Zr, Zr-50, Zr-80 and Zr-100 nanoparticles was added to the Nafion®/ DMF solution and stirred at room temperature for 2 hours, then ultrasonized for 30 minutes [21]. The resulting solution was poured onto a piece of flat glass and placed into an oven at 80 °C for 12 hours to remove solvent, and finally heated up to 160 °C for 30 minutes. The membranes were then removed by peeling them off from the glass plate. Before conducting any measurement, all membranes were kept in deionized water for 12 hours.

5.10.4. Preparation of nanocomposite membranes (impregnation method)

Nafion® 117 membranes were treated according to the standard procedure: 1 hour in a boiling 3% solution of hydrogen peroxide; 1 hour in boiling 0.5 M sulphuric acid; 1 hour in boiling distilled water. The nanocomposite membranes were prepared by extending the Nafion® 117 membranes over a petri dish, adding a required amount of Zr-0, Zr-50, Zr-80 and Zr-100 (5wt %) nanoparticles in a methanol solution. The nanocomposite membranes were repeatedly impregnated (up to 5 times) at room temperature [92]. In order to remove any air from the membrane pores, the sol and immersed membranes were heated up to 100 °C, then slowly cooled down to room temperature and kept in the solution for 24 hours. After drying, these membranes were stored in de-ionized water.

5.10.5. Tensile test

A Univert CellScale® Mechanical Tester with a 200 N load cell as shown in Figure 5-19 tested the tensile mechanical property. The specimens were rectangular, about 10 mm in width and about 30 mm in length. We used sandpaper to ensure adherence on the two surfaces of the clamp, which prevented the slip of specimen during the testing. The length, width and thickness of samples were measured using a Vernier caliper and recorded prior to testing. The testing area of the membrane samples was 4 mm x 10 mm in dimension. To allow for a clamping area, the samples were prepared in such a way that they were clamped on both

sides and with a testing area of 4 mm x 10 mm as shown in Figure 5-19. The thickness of the membrane was measured to be 0.18 cm. The thickness of 0.18 cm of the nanocomposite membrane was used in analyzing the stress applied to the sample. The membrane was soaked in water for 24 hours and used a wet sample. Then the membrane was dried in a vacuum oven at 80 °C for 24 hours and used as a dry sample. The tensile strength of modified Nafion® membranes was measured using the CellScale Ustretch device dried at 25 °C and wet at 34 °C and an actuator speed of 5 mm per min. The crosshead speed was set at 3 mm/min, and the load was applied until ultimate fracture of the specimen. The elastic modulus was calculated as the slope of the initial linear portion of the force-strain curve. The tensile strength was determined at the maximum point of the force-strain curve as shown in Figure 5-20.

(a) (b)

Figure 5- 19: Tensile mechanical testing of zirconia/ Nafion® Nanocomposite membrane (a) Clamp; (b) specimen- pure Nafion® membrane and Nafion®/ ZrO_2 nanocomposite membrane.

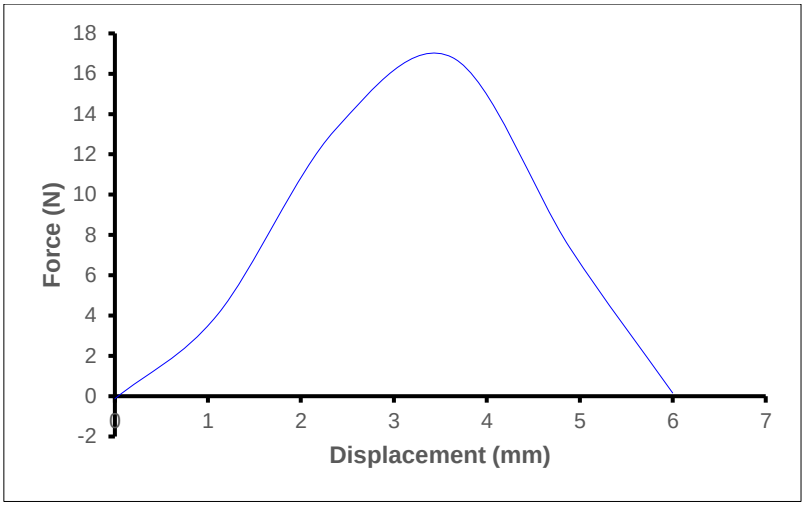

Figure 5- 20: Force and displacement curve as applied in the experiment

5.11. Results and discussion

Mechanical properties of the pure Nafion® and Nafion®/ ZrO_2 nanocomposite membrane for fuel cells play an important role in the development of durable materials. These materials are considered to be the future alternatives for the replacement of combustion fossil fuels for power generations. In this study, two methods were utilized, and mechanical tests were conducted of wet and dry plain Nafion® membranes and modified Nafion® nanocomposite membranes. Figure 5-21(a) (stress vs strain) plots the Nafion®/ Zr-0, Nafion®/ Zr-50, Nafion®/ Zr-80 and Nafion®/Zr-100 nanocomposite membrane using the impregnation method. Figure 5-21(a) shows that the Nafion®/ Zr-50, Nafion®/Zr-80 and Nafion®/Zr-100 nanocomposite membrane obtained by the impregnation method has the highest tensile stress of 2133 kPa when compared to commercial Nafion 117 (1347 kPa). The stress vs strain graph of dry ZrO_2 nanocomposite membrane using the recast method was observed and compared with recast Nafion® membranes (Figure 5-21(b)). The Nafion®/Zr-100 nanocomposite membrane showed the highest tensile stress of 662 kPa using the recasting methods when compared to recast Nafion® membrane (537 kPa). However, using the recasting methods on the dry Nafion®/ Zr-50 nanocomposite membrane obtained the lowest tensile stress of 492 kPa (see Figure 5-21(b)). This may be due to the distribution of inorganic metal within the Nafion® membrane [93]. Therefore, for both the impregnation and recasting methods of dry nanocomposite membranes, the Nafion®/ Zr-100 nanocomposite membrane has proven to have the highest tensile stress when compared to pure Nafion® membrane. This may be due to the synthesized procedure as Zr-100 nanoparticles were aged at 100 °C for 24 hours. This stabilized the high temperature cubic phase which enhanced their diffusivity, mechanical strength and ductility [94], all of which are very important in the modification of the membrane for fuel cell application. The maximum tensile stress was improved by the impregnation process (1347 kPa for the

commercial Nafion® 117 membrane) when compared to that of the recast process (537 kPa for the recast Nafion® membrane). The dry Nafion®/ Zr-100 nanocomposite prepared using the impregnation method presented a higher tensile stress of 2133 kPa compared to recast method presented a tensile stress of 662 kPa. This could be due to the addition of inorganic oxide nanoparticles that cause an increase in tensile stress to some extent [79, 93, 95]. Generally, the impregnation methods of dry nanocomposite membranes show a good tensile stress comparable to dry recast method.

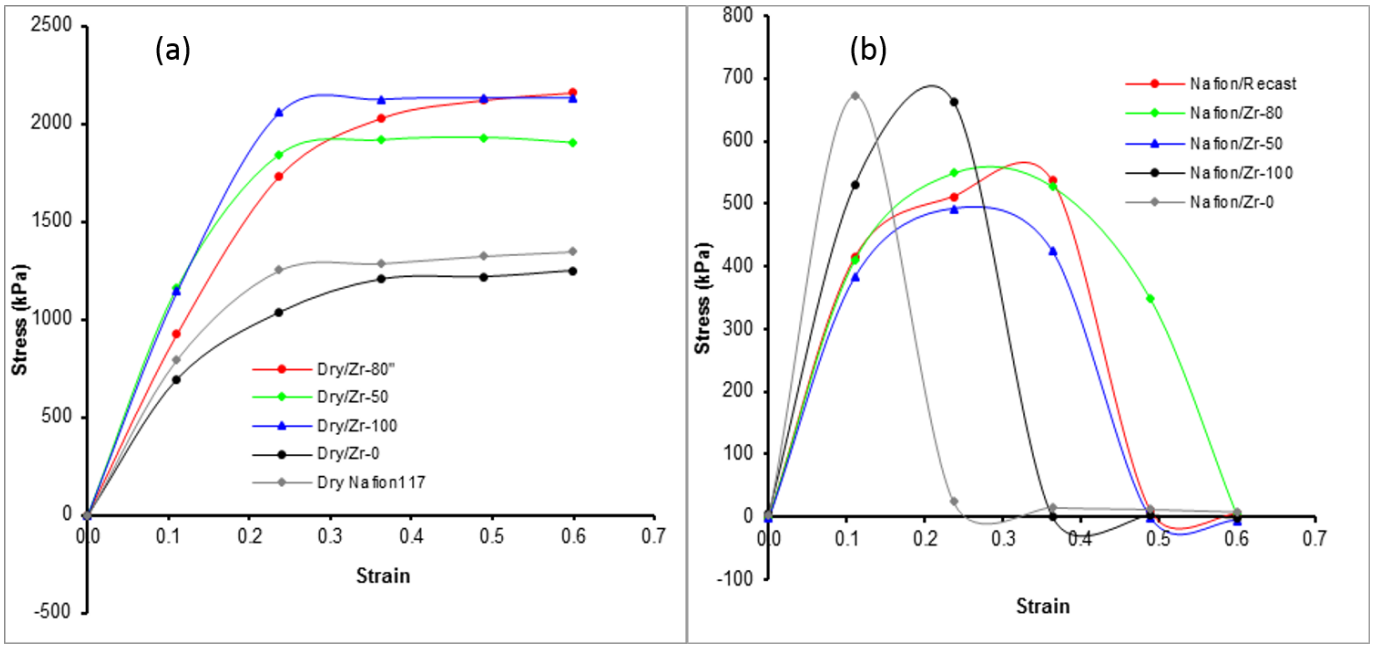

Figure 5- 21: Stress vs strain for dry membranes (a) Impregnation and (b) Recasting methods.

The wet pure Nafion® and Nafion®/ ZrO_2 nanocomposite membrane using the impregnation and recast methods are displayed in Figure 5-22. The wet commercial Nafion117 membrane shows a higher tensile stress than that with modified membrane (Figure 5-22(a)). At wet state, tensile stress of Nafion®/ Zr-0 nanocomposite membrane was higher than those of the Nafion®/Zr-50, Nafion®/Zr-80 and Nafion®/Zr-100 nanocomposite membrane using the impregnation method (Figure 5-22(a)). It clear that modification of Nafion® membrane with zirconia nanoparticles do not have impact on the tensile stress of wet membrane. Furthermore, the tensile stress of wet recast Nafion® membrane was also higher than the wet modified Nafion®/ Zr-50, Nafion®/ Zr-80 and Nafion®/ Zr-100 nanocomposite membrane (see Figure 5-22(b)). During the impregnation method of the dry nanocomposite membrane, the dry Nafion®/ Zr-0 nanocomposite membrane had the lowest tensile strength; however, when looking at the wet modified membrane, the wet Nafion®/ Zr-0 nanocomposite membrane has the highest tensile strength as shown in Figure 5-22(b). In the recasting method, the wet Nafion®/ Zr-100 nanocomposite membrane is shown to have the highest tensile strength. This result agrees

with the dry Nafion®/ Zr-100 nanocomposite membrane when using the recast method that has the highest tensile strength. The results of recasting method of wet and dry Nafion®/ ZrO_2 nanocomposite membranes clearly shows an improvement on the mechanical strength of the nanocomposite membrane, especially the Nafion®/ Zr-100 nanocomposite membrane has obtained the highest tensile strength. It has been observed that the modified Nafion® membrane with inorganic oxide nanoparticles enhances the tensile strength of membrane whereas the tensile strength of the wet modified Nafion® / Zr-50 nanocomposite membranes is lower when compared to the wet plain Nafion® membranes prepared using the recast method [39]. The results of the tensile stress of wet Nafion®/ Zr-100 nanocomposite membrane during the recast methods clearly showed an increased in the stress-strain when compared to that of commercial Nafion® 117 membrane. Therefore, it can be concluded that the recasting method has little influence on the mechanical properties of both the dry and wet Nafion®/ ZrO_2 nanocomposite membrane (see Figure 5-21(b) and 5-22(b)).

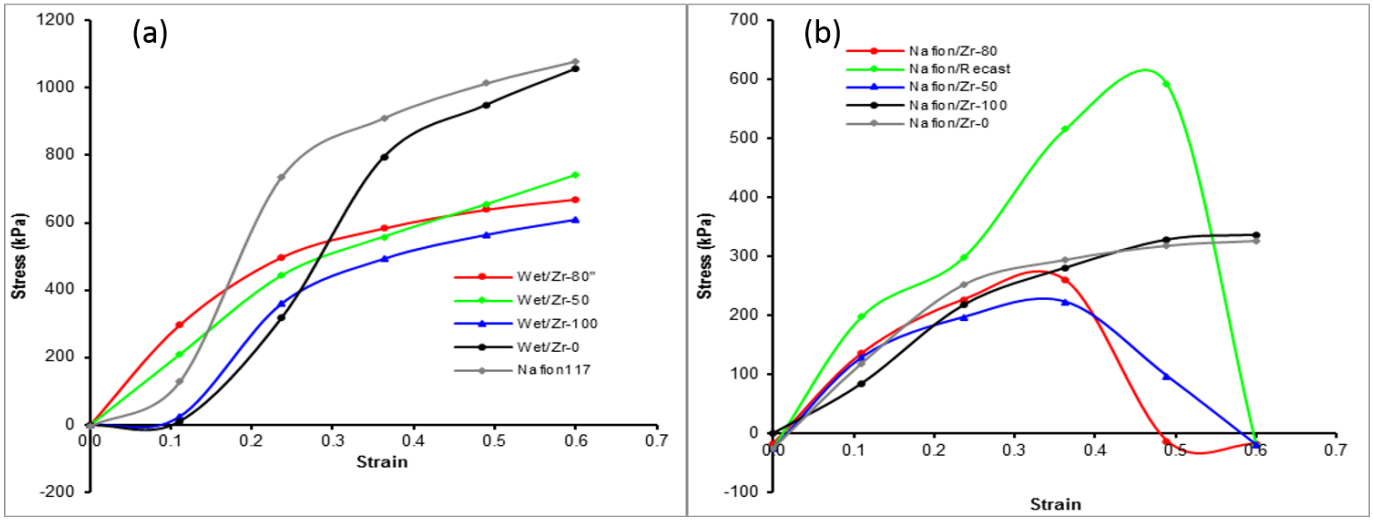

Figure 5- 22: Stress vs strain for wet nanocomposite membranes (a) Impregnation and (b) Recasting methods.

The modulus of elasticity of the Nafion®117 nanocomposite membrane in dry and wet conditions were compared with the Nafion®/ Zr-0, Nafion®/ Zr-50, Nafion® /Zr-80 and Nafion®/ Zr-100 nanocomposite membrane prepared using the impregnation method (Figure 5-23(a)). It was observed that the modulus of elasticity of dry Nafion®117 membrane is 17.1% higher than in the Zr-0/ Nafion® nanocomposite membrane. Similarly, the modulus of elasticity of dry Nafion®117 membrane is 47.2%, 38.5% and 64.3% lower than in the Nafion®/Zr-50, Nafion®/Zr-80 and Nafion®/Zr-100 nanocomposite membrane respectively. This indicates that the incorporation of the ZrO_2 nanoparticles improved the mechanical property of the Nafion® membrane in its dry states - mainly due to the interaction between the sulfonic acid groups of the Nafion® ionomer and the ZrO_2 filler. The improvement of the membrane rigidity

demonstrates that the zirconia nanoparticles stabilized the structure of the nanocomposite membrane and give a potential restriction to the humidity-generated stress when the membrane is used as an electrolyte membrane in the fuel cells. The modulus of elasticity of wet Nafion®117 membrane is 56.7%, 39.8%, 32.3% and 51.0% higher than in the Nafion®/Zr-0, Nafion®/Zr-50, Nafion®/Zr-80 and Nafion®/ Zr-100 nanocomposite membrane respectively (see Figure 5-23(a)). Hence, the modulus of elasticity of wet modified nanocomposite membrane prepared by impregnation method was much lower when compared to the dry membrane, this may due to the incorporation of inorganic nanoparticles that enhance water within the membrane [44-45]. Figure 5-23(b) shows the modulus of elasticity of dry and wet membrane prepared by recast method. The modulus of elasticity of dry membrane of recast Nafion® membrane is 60.7% and 25.9% lower than the Nafion®/ Zr-0 and Nafion®/ Zr-100, nanocomposite membrane respectively. Ironically, the modulus of elasticity of dry membrane of Nafion is 7.4% and 1.2% higher than the Nafion®/ Zr-50 and Nafion®/ Zr-80 nanocomposite membrane (see Figure 5-23). This may be due to the distribution of inorganic metal within the Nafion® membrane [93]. When comparing the wet membrane of recast Nafion® membrane, it was observed that recast Nafion® membrane is 35.3%, 30.8%, 35.3% and 62.1% higher than the Nafion®/Zr-0, Nafion®/Zr-50, Nafion®/Zr-80 and Nafion®/Zr-100 nano-composite membrane, respectively.

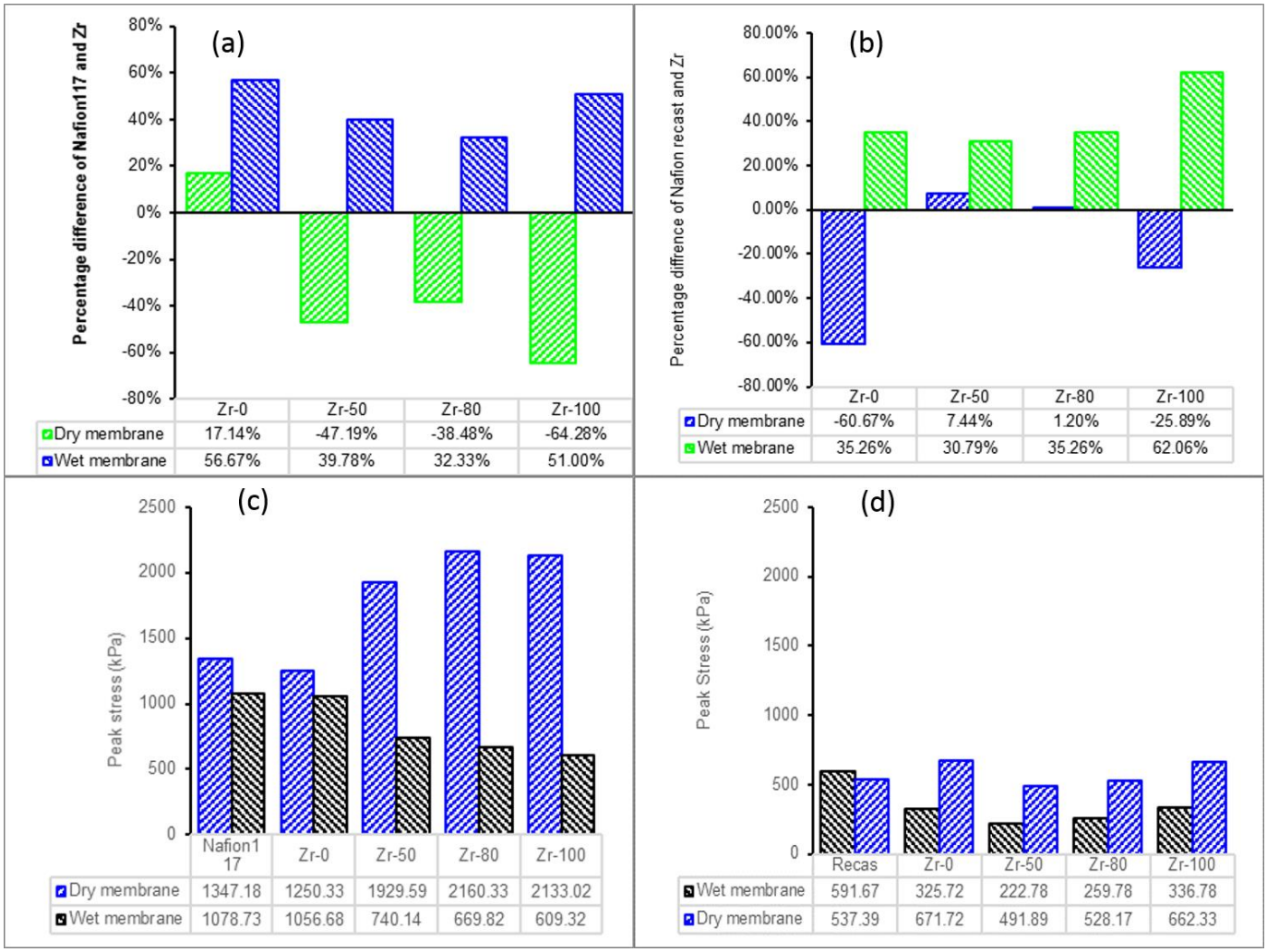

Figure 5- 23: Percentage difference of wet and dry pure Nafion® and modified membrane – samples prepared using the impregnation (a) and recast (b) method, Peak stress value-samples prepared using the impregnation (c) and recast (d) method.

The peak stress of wet and dry membranes using the impregnation and recast methods are shown in Figure 5-23(c and d). In Figure 5-23(c and d), it is clear that the impregnation method has high tensile stress when compared with recast methods. For example, Zr-0 (impregnation methods) has the highest tensile stress of 1250 kPa while Zr-0 (Recast methods) has a tensile stress of 326 kPa. The corresponding dry Nafion®/ Zr-100 nanocomposite membrane presented a tensile strength of 2133 kPa (impregnation methods) higher than 662 kPa (Recast methods) (Figure 5-23(c and d)). This could be due to the addition of inorganic oxide nanoparticles which cause an increase in tensile strength to some extent [93]. It has been observed that the modified Nafion® membrane with inorganic oxide nanoparticles enhances the tensile strength membrane [39]. In the study of the mechanical behavior of nonlinear material properties, it is vital to determine the strength of material in the elastic region. In doing so, the modulus of elasticity in a region between strain 0 and 0.23 has been identified as the elastic region. Therefore, all modulus of elasticity of dry and wet nanocomposite membranes using

impregnation and recasting methods were processed in Figure 5-24. In a region between 0 and 0.23 strain of the dry commercial Nafion®117 membrane, Nafion®/ Zr-0, Nafion®/ Zr-50, Nafion®/ Zr-80 and Nafion®/ Zr-100 nanocomposite membrane using impregnation methods, the modulus of elasticity was found to be 5266.5 kPa, 4341.2 kPa, 7730.07 kPa, 7293.2 kPa and 8651.8 kPa respectively (Figure 5-24a). Similarly, the modulus of elasticity of wet Nafion117 membrane, Nafion®/Zr-0, Nafion®/Zr-50, Nafion®/Zr-80 and Nafion®/Zr-100 nanocomposite membrane using impregnation methods in the region between 0 and 0.23 strain were also determined to be 4817.5 kPa, 2434.7 kPa, 1872.4 kPa, 2092.1 kPa and 2661.4 kPa respectively (Figure 5-24 (b)). In Figure 5-24(a), the modulus of elasticity of the dry recast Nafion® membrane, Nafion®/Zr-0, Nafion®/Zr-50, Nafion®/Zr-80 and Nafion®/Zr-100 nanocomposite membrane using recasting methods in the region between 0 and 0.23 strain were found to be 3775.7 kPa, 6066.3 kPa, 3494.9 kPa, 3730.4 kPa and 4753.4 kPa respectively. Similarly, the modulus of elasticity of wet recasting Nafion® membrane, Nafion®/Zr-0, Nafion®/Zr-50, Nafion®/Zr-80 and Nafion®/Zr-100 nanocomposite membrane using recasting methods in the region between 0 and 0.23 strain were also determined to be 2028 kPa, 1312.9 kPa, 1403.5 kPa, 1312.9 kPa and 769.42 kPa respectively (Figure 5-24b). Nevertheless, the dry nanocomposite membrane synthesised by a recast and impregnation method has a higher modulus of elasticity than that of wet nanocomposite membrane synthesised by a recast and impregnation method. This may be due to the water retention of inorganic additives within the membrane [8], as these inorganic nanomaterials act as water storage in the membrane [44-45]. The water retention ability is one of the important parameters for fuel cell applications because water is a proton-transporting medium for PEMs [8].

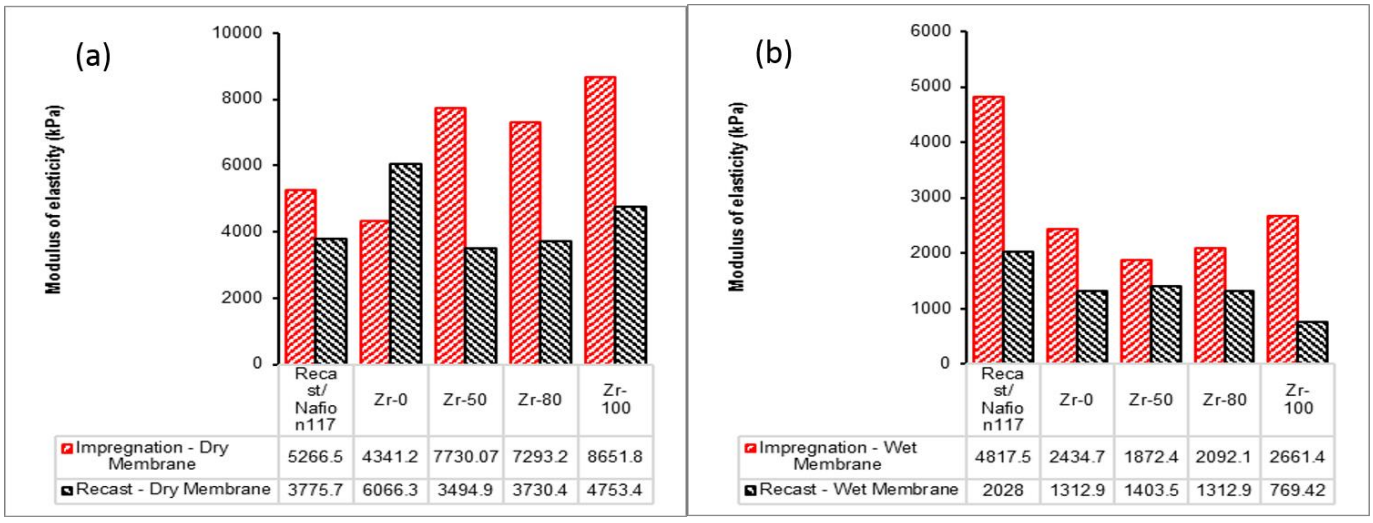

Figure 5- 24: Comparison of modulus of elasticity of impregnation and recast methods (a) dry membrane and (b) Wet membranes.

Figure 5-25 compares the stiffness of dry and wet pure Nafion® membrane, Nafion®/ Zr-0, Nafion®/ Zr-50, Nafion®/ Zr-80 and Nafion®/ Zr-100 nanocomposite membrane using impregnation and recasting methods. In a region between 0 and 0.23 strain of dry Nafion®117 membrane, Nafion®/ Zr-0, Nafion®/ Zr-50, Nafion®/ Zr-80 and Nafion®/ Zr-100 nanocomposite membrane using impregnation methods, the stiffness was found to be 11.6 N/mm, 9.6 N/mm, 17.0 N/mm, 16.1 N/mm and 19.0 N/mm respectively (Figure 5-25(a)). The Nafion®/ Zr-50, Nafion®/ Zr-80 and Nafion®/ Zr-100 nanocomposite membranes show a higher stiffness when compared to dry Nafion®117 membrane. The stiffness of wet Nafion®117 membrane, Nafion®/Zr-0, Nafion®/Zr-50, Nafion® /Zr-80 and Nafion®/ Zr-100 nanocomposite membranes using impregnation methods in the region between 0 and 0.23 strain was also determined to be 10.6 N/mm, 5.4 N/mm, 4.1 N/mm, 4.6 N/mm and 5.9 N/mm respectively Figure 5-25(b)). Similarly, in a region between 0 and 0.23 strain of dry nanocomposite membranes, recast Nafion®, Nafion®/ Zr-0, Nafion®/ Zr-50, Nafion®/ Zr-80 and Nafion®/ Zr-100 nanocomposite membrane using recasting methods, the stiffness was found to be 6.8 N/mm, 10.9 N/mm, 6.3 N/mm, 6.7 N/mm and 8.5 N/mm respectively. Furthermore, the dry Nafion®/ Zr-0 and Nafion®/ Zr-100 nanocomposite membranes also provide a higher stiffness than dry recast Nafion® membrane (Figure 5-25(a)). The stiffness of wet recast Nafion® membrane, Nafion® /Zr-0, Nafion®/ Zr-50, Nafion®/ Zr-80 and Nafion®/Zr-100 nanocomposite membrane using recasting methods in the region between 0 and 0.23 strain was also determined to be 3.7 N/mm, 2.4 N/mm, 2.5 N/mm, 2.5 N/mm and 1.4 N/mm respectively (Figure 5-25a and b). As shown in Figure 5-25(a and b), the stiffness of nanocomposite membrane improves with the addition of ZrO_2 nanoparticles with specific morphological properties within the Nafion® matrix that enhance the interaction of inorganic oxides and membrane materials resulting in superior Nafion® nanocomposite membranes [91].

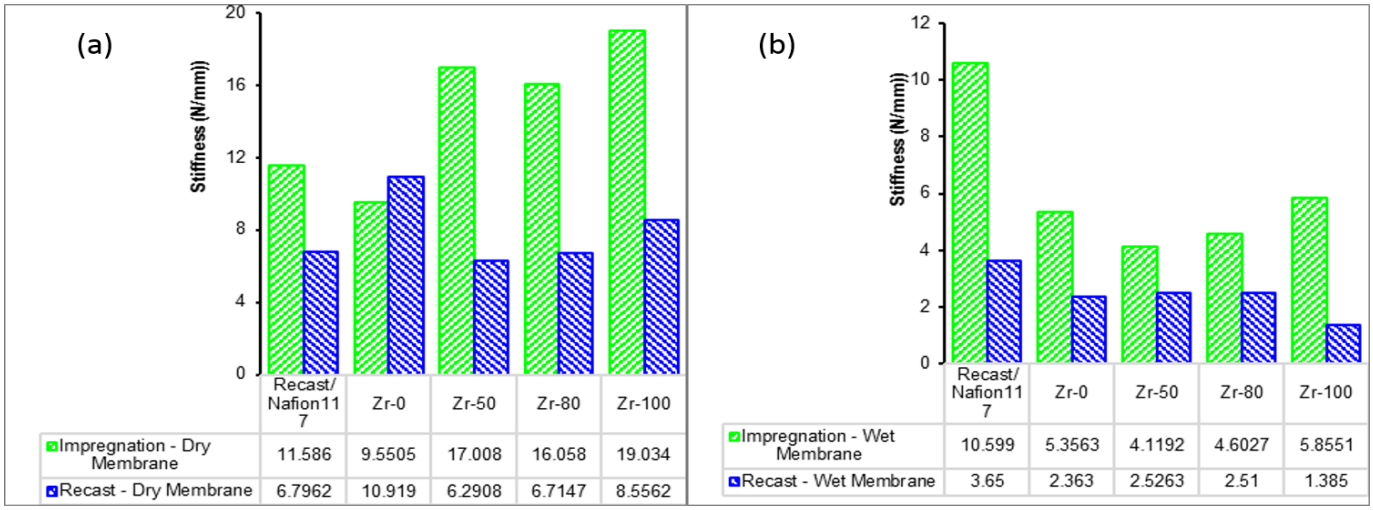

Figure 5- 25: Comparison of stiffness of impregnation and recast methods (a) dry membrane and (b) Wet membranes.

To clarify the best preparation method of nanocomposite membrane, the modulus of elasticity and stiffness in the region between 0 and 0.23 strain of dry and wet pure Nafion® membrane, Nafion®/ Zr-0, Nafion®/ Zr-50, Nafion®/ Zr-80 and Nafion® /Zr-100 nanocomposite membrane was investigated by comparing the recast methods with the impregnation method (see Figure 5-26). The modulus of elasticity of the impregnation method of dry Nafion®117, Nafion®/ Zr-50, Nafion®/ Zr-80 and Nafion®/ Zr-100 nanocomposite membranes are respectively 28.3%, 54.8%, 48.9% and 45.1% higher than in the recast dry nanocomposite membrane (Figure 5-26(a)). Similarly, the modulus of elasticity of the impregnation method of wet Nafion®117 membrane, Nafion®/ Zr-0, Nafion®/ Zr-50, Nafion®/ Zr-80 and Nafion®/ Zr-100 nanocomposite membranes are 57.9%, 46.1%, 25.0%, 37.2% and 71.1% higher than in the recast wet nanocomposite membrane respectively (Figure 5-26(a)). When comparing the stiffness in the region between 0 and 0.23 strain, it was found that using impregnation methods, the dry Nafion®117, Nafion®/ Zr-50, Nafion®/ Zr-80 and Nafion®/ Zr-100 nanocomposite membranes are respectively 41.3%, 63.0%, 58.2% and 55.1% higher than in the dry nanomembranes prepared using the recast method (Figure 5-26(b)). Similarly, when comparing the stiffness in the region between 0 and 0.23 strain, it was found that using the impregnation method, the wet Nafion®117, Nafion®/ Zr-50, Nafion®/ Zr-80 and Nafion®/Zr-100 nanocomposite membranes are respectively 65.6%, 55.9%, 38.7%, 45.5% and 76.4% higher than in the wet nanocomposites membranes prepared using the recast method (see Figure 5-26(a)). Figure 5-26(a) shows noticeably different on the modulus of elasticity, when comparing wet and dry modified membrane prepared using the impregnation and recast method, this may be due to the hygroscopic nature of zirconia nanoparticles that retain water within the membrane [44-45]. The highest obtained modulus of elasticity and stiffness of modified membrane indicates that the incorporation of zirconia nanoparticles into Nafion® 117 membrane by impregnation method have greatly effect on the mechanical strength of membrane when compared to recast method. This may be due to the casting the solution on a glass plate, which leads to poor dispersion of inorganic nanofiller in membrane.

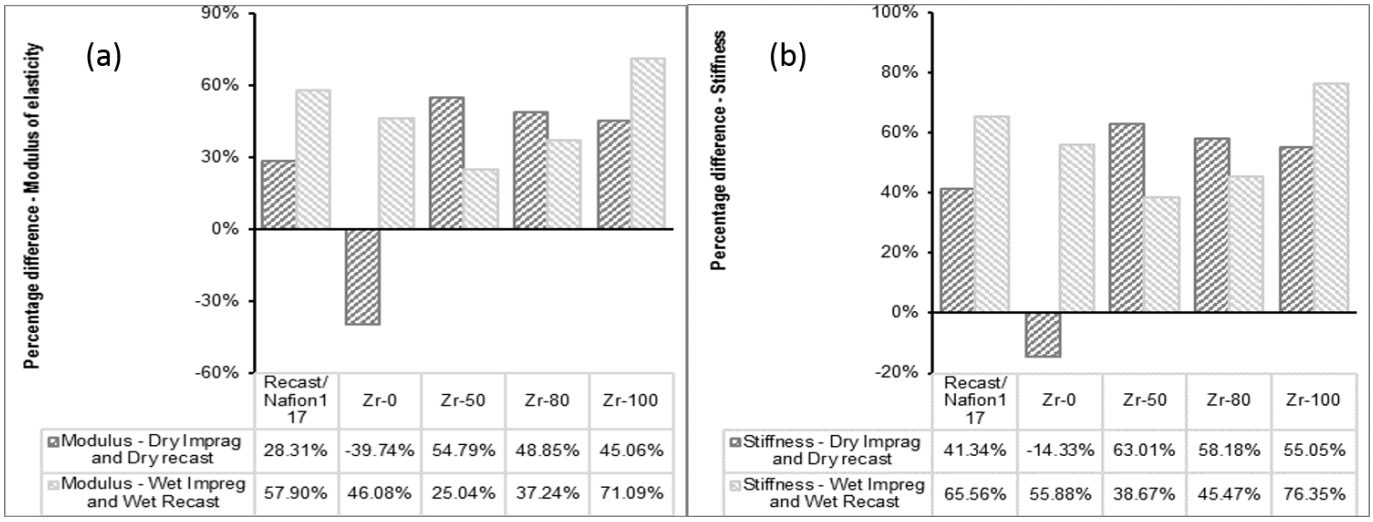

Figure 5- 26: Percentage difference of dry and wet during impregnation and recast methods (a) modulus of elasticity and (b) stiffness.

5.12. Conclusion

Preperation of modified Nafion® nano-composite membranes for fuel cell application plays an important role in the improvement of their mechanical properties. The tensile tests were performed both during dry conditions at ambient temperatures and wet conditions at 34 °C compared to the commercial Nafion® 117 and plain recast Nafion® membranes. The tensile strength of the wet modified Nafion® membranes prepared using the impregnation method is higher compared to the wet modified Nafion® membrane prepared using the recast method. The tensile strength of the dry ZrO_2 nano membrane prepared using impregnation is higher than the wet ZrO_2 nano-composite membrane prepared using impregnation methods. Due to the inorganic nanofiller that shows an improvement of the elastic modulus on the nanocomposite membrane when compared with the commercial membrane Also, the tensile strength of the dry ZrO_2 nano membrane prepared using the recast method is higher than the wet ZrO_2 nano membrane prepared using the recast method. It was found that the impregnation method obtained a highest modulus of elasticity and stiffness, indicates that the incorporation of zirconia nanoparticles into Nafion® 117 membrane by impregnation method have greatly effect on the mechanical strength of membrane when compared to recast method.

5.13. Reference

1. Tang, Y.; Karlsson, A. M.; Santare, M. H.; Gilbert, M.; Cleghorn, S.; Johnson, W. B., An experimental investigation of humidity and temperature effects on the mechanical properties of perfluorosulfonic acid membrane. *Materials Science and Engineering: A* **2006,** *425* (1), 297-304.

2. Barbir, F.; Gomez, T., Efficiency and economics of proton exchange membrane (PEM) fuel cells. *International Journal of Hydrogen Energy* **1997,** *22* (10-11), 1027-1037.
3. Hector, L. G.; Lai, Y.-H.; Tong, W.; Lukitsch, M. J., Strain accumulation in polymer electrolyte membrane and membrane electrode assembly materials during a single hydration/dehydration cycle. *Journal of Fuel Cell Science and Technology* **2007,** *4* (1), 19-28.
4. Huang, X.; Solasi, R.; Zou, Y.; Feshler, M.; Reifsnider, K.; Condit, D.; Burlatsky, S.; Madden, T., Mechanical endurance of polymer electrolyte membrane and PEM fuel cell durability. *Journal of Polymer Science Part B: Polymer Physics* **2006,** *44* (16), 2346-2357.
5. Bauer, F.; Willert-Porada, M., Characterisation of zirconium and titanium phosphates and direct methanol fuel cell (DMFC) performance of functionally graded Nafion (R) composite membranes prepared out of them. *Journal of Power Sources* **2005,** *145* (2), 101-107.
6. Dimitrova, P.; Friedrich, K.; Vogt, B.; Stimming, U., Transport properties of ionomer composite membranes for direct methanol fuel cells. *Journal of Electroanalytical Chemistry* **2002,** *532* (1), 75-83.
7. Sahu, A. K.; Ketpang, K.; Shanmugam, S.; Kwon, O.; Lee, S.; Kim, H., Sulfonated graphene–Nafion composite membranes forpolymer electrolyte fuel cells operating under reduced relative humidity. *The Journal of Physical Chemistry C* **2016,** *120* (29), 15855-15866.
8. Pan, J.; Zhang, H.; Chen, W.; Pan, M., Nafion–zirconia nanocomposite membranes formed via in situ sol–gel process. *International Journal of Hydrogen Energy* **2010,** *35* (7), 2796-2801.
9. Bauer, B.; Jones, D.; Roziere, J.; Tchicaya, L.; Alberti, G.; Casciola, M.; Massinelli, L.; Peraio, A.; Besse, S.; Ramunni, E., Electrochemical characterisation of sulfonated polyetherketone membranes. *Journal of New Materials for Electrochemical Systems* **2000,** *3* (2), 93-98.
10. Yaroslavtsev, A. B.; Nikonenko, V. V.; Zabolotsky, V. I., Ion transfer in ion-exchange and membrane materials. *Russian chemical reviews* **2003,** *72* (5), 393-421.
11. Xu, T., Ion exchange membranes: state of their development and perspective. *Journal of membrane science* **2005,** *263* (1), 1-29.
12. Yang, J.; Shen, P. K.; Varcoe, J.; Wei, Z., Nafion/polyaniline composite membranes specifically designed to allow proton exchange membrane fuel cells operation at low humidity. *Journal of Power Sources* **2009,** *189* (2), 1016-1019.
13. Muraviev, D. N.; Macanás, J.; Farre, M.; Muñoz, M.; Alegret, S., Novel routes for inter-matrix synthesis and characterization of polymer stabilized metal nanoparticles for molecular recognition devices. *Sensors and Actuators B: Chemical* **2006,** *118* (1), 408-417.

14. Huo, H.; Wang, S.; Lin, S.; Li, Y.; Li, B.; Yang, Y., Chiral zirconia nanotubes prepared through a sol–gel transcription approach. *Journal of Materials Chemistry A* **2014,** *2* (2), 333-338.
15. Yang, C.; Srinivasan, S.; Bocarsly, A.; Tulyani, S.; Benziger, J., A comparison of physical properties and fuel cell performance of Nafion and zirconium phosphate/Nafion composite membranes. *Journal of Membrane Science* **2004,** *237* (1-2), 145-161.
16. Thampan, T. M.; Jalani, N. H.; Choi, P.; Datta, R., Systematic approach to design higher temperature composite PEMs. *Journal of The Electrochemical Society* **2005,** *152* (2), A316-A325.
17. Bauer, F.; Willert-Porada, M., Zirconium phosphate Nafion® composites a microstructure-based explanation of mechanical and conductivity properties. *Solid State Ionics* **2006,** *177* (26), 2391-2396.
18. Adjemian, K.; Srinivasan, S.; Benziger, J.; Bocarsly, A., Investigation of PEMFC operation above 100 ^{o}C employing perfluorosulfonic acid silicon oxide composite membranes. *Journal of Power Sources* **2002,** *109* (2), 356-364.
19. Zhang, H.; Wu, W.; Wang, J.; Zhang, T.; Shi, B.; Liu, J.; Cao, S., Enhanced anhydrous proton conductivity of polymer electrolyte membrane enabled by facile ionic liquid-based hoping pathways. *Journal of Membrane Science* **2015,** *476*, 136-147.
20. Di Noto, V.; Negro, E.; Sanchez, J.-Y.; Iojoiu, C., Structure-relaxation interplay of a new nanostructured membrane based on tetraethylammonium trifluoromethanesulfonate ionic liquid and neutralized nafion 117 for high-temperature fuel cells. *Journal of the American Chemical Society* **2010,** *132* (7), 2183-2195.
21. Zhai, Y.; Zhang, H.; Hu, J.; Yi, B., Preparation and characterization of sulfated zirconia (SO_4^{2-}/ZrO_2)/Nafion composite membranes for PEMFC operation at high temperature/low humidity. *Journal of Membrane Science* **2006,** *280* (1), 148-155.
22. Starkweather Jr, H. W., Crystallinity in perfluorosulfonic acid ionomers and related polymers. *Macromolecules* **1982,** *15* (2), 320-323.
23. Tahmasebpour, M.; Babaluo, A.; Aghjeh, M. R., Synthesis of zirconia nanopowders from various zirconium salts via polyacrylamide gel method. *Journal of the European Ceramic Society* **2008,** *28* (4), 773-778.
24. Davar, F.; Hassankhani, A.; Loghman-Estarki, M. R., Controllable synthesis of metastable tetragonal zirconia nanocrystals using citric acid assisted sol–gel method. *Ceramics International* **2013,** *39* (3), 2933-2941.
25. Kyu, T.; Hashiyama, M.; Eisenberg, A., Dynamic mechanical studies of partially ionized and neutralized Nafion polymers. *Canadian Journal of Chemistry* **1983,** *61* (4), 680-687.
26. Adjemian, K. T.; Dominey, R.; Krishnan, L.; Ota, H.; Majsztrik, P.; Zhang, T.; Mann, J.; Kirby, B.; Gatto, L.; Velo-Simpson, M., Function and characterization of metal oxide−

nafion composite membranes for elevated-temperature H_2/O_2 PEM fuel cells. *Chemistry of Materials* **2006,** *18* (9), 2238-2248.

27. Smitha, B.; Devi, D. A.; Sridhar, S., Proton-conducting composite membranes of chitosan and sulfonated polysulfone for fuel cell application. *International Journal of Hydrogen Energy* **2008,** *33* (15), 4138-4146.
28. Deng, Q.; Wilkie, C.; Moore, R.; Mauritz, K. A., TGA–FTIR. investigation of the thermal degradation of Nafion® and Nafion®/[silicon oxide]-based nanocomposites. *Polymer* **1998,** *39* (24), 5961-5972.
29. Tang, H. L.; Pan, M., Synthesis and characterization of a self-assembled nafion/silica nanocomposite membrane for polymer electrolyte membrane fuel cells. *The Journal of Physical Chemistry C* **2008,** *112* (30), 11556-11568.
30. Mohammadi, G.; Jahanshahi, M.; Rahimpour, A., Fabrication and evaluation of Nafion nanocomposite membrane based on ZrO_2–TiO_2 binary nanoparticles as fuel cell MEA. *International Journal of Hydrogen Energy* **2013,** *38* (22), 9387-9394.
31. Savadogo, O., Emerging membrane for electrochemical systems:(I) solid polymer electrolyte membranes for fuel cell systems. *Journal of New Materials for Electrochemical Systems* **1998,** *1* (1), 47-66.
32. Zawodzinski, T. A.; Derouin, C.; Radzinski, S.; Sherman, R. J.; Smith, V. T.; Springer, T. E.; Gottesfeld, S., Water uptake by and transport through Nafion® 117 membranes. *Journal of the Electrochemical Society* **1993,** *140* (4), 1041-1047.
33. Ketpang, K.; Son, B.; Lee, D.; Shanmugam, S., Porous zirconium oxide nanotube modified Nafion composite membrane for polymer electrolyte membrane fuel cells operated under dry conditions. *Journal of Membrane Science* **2015,** *488*, 154-165.
34. Xiangguo, T.; Jicui, D.; Jing, S., Effects of different kinds of surfactants on Nafion membranes for all vanadium redox flow battery. *Journal of Solid State Electrochemistry* **2015,** *19* (4), 1091-1101.
35. Vishnyakov, V., Proton exchange membrane fuel cells. *Vacuum* **2006,** *80* (10), 1053-1065.
36. Kreuer, K., On the development of proton conducting polymer membranes for hydrogen and methanol fuel cells. *Journal of Membrane Science* **2001,** *185* (1), 29-39.
37. Gierke, T.; Munn, G.; Wilson, F., The morphology in Nafion perfluorinated membrane products, as determined by wide-and small-angle x-ray studies. *Journal of Polymer Science: Polymer Physics Edition* **1981,** *19* (11), 1687-1704.
38. Zook, L. A.; Leddy, J., Density and solubility of Nafion: recast, annealed, and commercial films. *Analytical chemistry* **1996,** *68* (21), 3793-3796.
39. Zhengbang, W.; Tang, H.; Mu, P., Self-assembly of durable Nafion/TiO_2 nanowire electrolyte membranes for elevated-temperature PEM fuel cells. *Journal of Membrane Science* **2011,** *369* (1), 250-257.

40. Sacca, A.; Gatto, I.; Carbone, A.; Pedicini, R.; Passalacqua, E., ZrO_2–Nafion composite membranes for polymer electrolyte fuel cells (PEFCs) at intermediate temperature. *Journal of Power Sources* **2006,** *163* (1), 47-51.
41. Dresch, M. A.; Isidoro, R. A.; Linardi, M.; Rey, J. F. Q.; Fonseca, F. C.; Santiago, E. I., Influence of sol–gel media on the properties of Nafion–SiO_2 hybrid electrolytes for high performance proton exchange membrane fuel cells operating at high temperature and low humidity. *Electrochimica Acta* **2013,** *94*, 353-359.
42. Satterfield, M. B.; Majsztrik, P. W.; Ota, H.; Benziger, J. B.; Bocarsly, A. B., Mechanical properties of Nafion and titania/Nafion composite membranes for polymer electrolyte membrane fuel cells. *Journal of Polymer Science Part B: Polymer Physics* **2006,** *44* (16), 2327-2345.
43. Chalkova, E.; Pague, M. B.; Fedkin, M. V.; Wesolowski, D. J.; Lvov, S. N., Nafion⁄ TiO_2 Proton conductive composite membranes for PEMFCs operating at elevated temperature and reduced relative humidity. *Journal of The Electrochemical Society* **2005,** *152* (6), A1035-A1040.
44. Brown, A. C.; Hargreaves, J. J., Sulfated metal oxide catalysts. Superactivity through superacidity? *Green Chemistry* **1999,** *1* (1), 17-20.
45. Lu, Y.; Yang, Y.; Sellinger, A.; Lu, M.; Huang, J.; Fan, H.; Haddad, R.; Lopez, G.; Burns, A. R.; Sasaki, D. Y., Self-assembly of mesoscopically ordered chromatic polydiacetylene/silica nanocomposites. *Nature* **2001,** *410* (6831), 913-917.
46. Yang, C.-C.; Li, Y. J.; Liou, T.-H., Preparation of novel poly (vinyl alcohol)/SiO_2 nanocomposite membranes by a sol–gel process and their application on alkaline DMFCs. *Desalination* **2011,** *276* (1), 366-372.
47. Zulfikar, M. A.; Mohammad, A. W.; Hilal, N., Preparation and characterization of novel porous PMMA-SiO_2 hybrid membranes. *Desalination* **2006,** *192* (1-3), 262-270.
48. Licoccia, S.; Traversa, E., Increasing the operation temperature of polymer electrolyte membranes for fuel cells: From nanocomposites to hybrids. *Journal of power sources* **2006,** *159* (1), 12-20.
49. Siddiqui, M. R. H.; Al-Wassil, A. I.; Al-Otaibi, A. M.; Mahfouz, R. M., Effects of precursor on the morphology and size of ZrO_2 nanoparticles, synthesized by sol-gel method in non-aqueous medium. *Materials Research* **2012,** *15* (6), 986-989.
50. Jalani, N. H.; Dunn, K.; Datta, R., Synthesis and characterization of Nafion®-MO_2 (M= Zr, Si, Ti) nanocomposite membranes for higher temperature PEM fuel cells. *Electrochimica Acta* **2005,** *51* (3), 553-560.
51. Lu, S.; Wang, D.; Jiang, S. P.; Xiang, Y.; Lu, J.; Zeng, J., HPW/MCM-41 phosphotungstic acid/mesoporous silica composites as novel proton-exchange membranes for elevated-temperature fuel cells. *Advanced Materials* **2010,** *22* (9), 971-976.

52. Chen, Z.; Holmberg, B.; Li, W.; Wang, X.; Deng, W.; Munoz, R.; Yan, Y., Nafion/zeolite nanocomposite membrane by in situ crystallization for a direct methanol fuel cell. *Chemistry of Materials* **2006,** *18* (24), 5669-5675.
53. Bonnet, B.; Jones, D.; Roziere, J.; Tchicaya, L.; Alberti, G.; Casciola, M.; Massinelli, L.; Bauer, B.; Peraio, A.; Ramunni, E., Hybrid organic-inorganic membranes for a medium temperature fuel cell. *Journal of New Materials for Electrochemical Systems* **2000,** *3* (2), 87-92.
54. Navarra, M.; Croce, F.; Scrosati, B., New, high temperature superacid zirconia-doped Nafion™ composite membranes. *Journal of Materials Chemistry* **2007,** *17* (30), 3210-3215.
55. Wang, K.; Chen, L.; Wu, J.; Toh, M. L.; He, C.; Yee, A. F., Epoxy nanocomposites with highly exfoliated clay: mechanical properties and fracture mechanisms. *Macromolecules* **2005,** *38* (3), 788-800.
56. Fornes, T.; Paul, D., Crystallization behavior of Nylon 6 nanocomposites. *Polymer* **2003,** *44* (14), 3945-3961.
57. Munoz, M.; Gallego, S.; Beltrán, J.; Cerdá, J., Adhesion at metal–ZrO_2 interfaces. *Surface Science Reports* **2006,** *61* (7), 303-344.
58. Grover, V.; Shukla, R.; Tyagi, A., Facile synthesis of ZrO_2 powders: control of morphology. *Scripta Materialia* **2007,** *57* (8), 699-702.
59. Li, W.; Huang, H.; Li, H.; Zhang, W.; Liu, H., Facile synthesis of pure monoclinic and tetragonal zirconia nanoparticles and their phase effects on the behavior of supported molybdena catalysts for methanol-selective oxidation. *Langmuir* **2008,** *24* (15), 8358-8366.
60. Yu, H.; Ziegler, C.; Oszcipok, M.; Zobel, M.; Hebling, C., Hydrophilicity and hydrophobicity study of catalyst layers in proton exchange membrane fuel cells. *Electrochimica Acta* **2006,** *51* (7), 1199-1207.
61. Matsui, K.; Ohgai, M., Formation mechanism of hydrous zirconia particles produced by the hydrolysis of $ZrOCl_2$ Solutions: III, kinetics study for the nucleation and crystal-growth processes of primary particles. *Journal of the American Ceramic Society* **2001,** *84* (10), 2303-2312.
62. Bauer, F.; Willert-Porada, M., Microstructural characterization of Zr-phosphate–Nafion® membranes for direct methanol fuel cell (DMFC) applications. *Journal of Membrane Science* **2004,** *233* (1), 141-149.
63. Tolba, G. M. K.; Bastaweesy, A. M.; Ashour, E. A.; Abdelmoez, W.; Khalil, K. A.; Barakat, N. A. M., Effective and highly recyclable ceramic membrane based on amorphous nanosilica for dye removal from the aqueous solutions. *Arabian Journal of Chemistry* **2016,** *9* (2), 287-296.

64. Lehmani, A.; Durand-Vidal, S.; Turq, P., Surface morphology of Nafion 117 membrane by tapping mode atomic force microscope. *Journal of Applied Polymer Science* **1998,** *68* (3), 503-508.
65. James, P.; Elliott, J.; McMaster, T.; Newton, J.; Elliott, A.; Hanna, S.; Miles, M., Hydration of Nafion® studied by AFM and X-ray scattering. *Journal of Materials Science* **2000,** *35* (20), 5111-5119.
66. Velayutham, P.; Sahu, A. K.; Parthasarathy, S., A Nafion-Ceria Composite Membrane Electrolyte for Reduced Methanol Crossover in Direct Methanol Fuel Cells. *Energies* **2017,** *10* (2), 259.
67. Realpe, A.; Mendez, N.; Acevedo, M., Proton exchange membrane from the blend of copolymers of vinyl acetate-acrylic ester and styrene-acrylic ester for power generation using fuel cell. *International Journal of Engineering and Technology* **2014,** *6* (5), 2435-2440.
68. Penkova, A. V.; Acquah, S. F.; Dmitrenko, M. E.; Sokolova, M. P.; Mikhailova, M. E.; Polyakov, E. S.; Ermakov, S. S.; Markelov, D. A.; Roizard, D., Improvement of pervaporation PVA membranes by the controlled incorporation of fullerenol nanoparticles. *Materials & Design* **2016,** *96*, 416-423.
69. Gil, E.; Mas, Á.; Lerma, C.; Vercher, J., Exposure factors influence stone deterioration by crystallization of soluble salts. *Advances in Materials Science and Engineering* **2015,** *2015*.
70. Jia, W.; Feng, K.; Tang, B.; Wu, P., β-Cyclodextrin modified silica nanoparticles for Nafion based proton exchange membranes with significantly enhanced transport properties. *Journal of Materials Chemistry A* **2015,** *3* (30), 15607-15615.
71. Devrim, Y.; Erkan, S.; Baç, N.; Eroglu, I., Improvement of PEMFC performance with Nafion/inorganic nanocomposite membrane electrode assembly prepared by ultrasonic coating technique. *International Journal of Hydrogen Energy* **2012,** *37* (21), 16748-16758.
72. Zhai, Y.; Zhang, H.; Hu, J.; Yi, B., Preparation and characterization of sulfated zirconia (SO_4^{2-}/ZrO_2)/Nafion composite membranes for PEMFC operation at high temperature/low humidity. *Journal of Membrane Science* **2006,** *280* (1), 148-155.
73. Gupta, G.; Sharma, S.; Mendes, P., Nafion-stabilised bimetallic Pt–Cr nanoparticles as electrocatalysts for proton exchange membrane fuel cells (PEMFCs). *RSC Advances* **2016,** *6* (86), 82635-82643.
74. Jansen, M.; Guenther, E., Oxide gels and ceramics prepared by a nonhydrolytic sol-gel process. *Chemistry of materials* **1995,** *7* (11), 2110-2114.
75. Sarkar, D.; Mohapatra, D.; Ray, S.; Bhattacharyya, S.; Adak, S.; Mitra, N., Synthesis and characterization of sol–gel derived ZrO_2 doped Al_2O_3 nanopowder. *Ceramics international* **2007,** *33* (7), 1275-1282.

76. Baglio, V.; Di Blasi, A.; Antonucci, V., FTIR spectroscopic investigation of inorganic fillers for composite DMFC membranes. *Electrochemistry Communications* **2003,** *5* (10), 862-866.
77. Yang, H.; Lee, D.; Park, S.; Kim, W., Preparation of Nafion/various Pt-containing SiO_2 composite membranes sulfonated via different sources of sulfonic group and their application in self-humidifying PEMFC. *Journal of Membrane Science* **2013,** *443*, 210-218.
78. Ostrowska, J.; Narebska, A., Infrared study of hydration and association of functional groups in a perfluorinated Nafion membrane, Part 1. *Colloid and Polymer Science* **1983,** *261* (2), 93-98.
79. Xuesong, Y., Preparation, Characterization and Application of a Novel PA/SIO_2 NF Membrane. *Procedia Engineering* **2012,** *44*, 2075-2078.
80. Zou, L.; Vidalis, I.; Steele, D.; Michelmore, A.; Low, S.; Verberk, J., Surface hydrophilic modification of RO membranes by plasma polymerization for low organic fouling. *Journal of Membrane Science* **2011,** *369* (1), 420-428.
81. Choi, P.; Jalani, N. H.; Thampan, T. M.; Datta, R., Consideration of thermodynamic, transport, and mechanical properties in the design of polymer electrolyte membranes for higher temperature fuel cell operation. *Journal of Polymer Science Part B: Polymer Physics* **2006,** *44* (16), 2183-2200.
82. Bauer, F.; Denneler, S.; Willert-Porada, M., Influence of temperature and humidity on the mechanical properties of Nafion® 117 polymer electrolyte membrane. *Journal of Polymer Science Part B: Polymer Physics* **2005,** *43* (7), 786-795.
83. Zhang, L.; Xu, J.; Hou, G.; Tang, H.; Deng, F., Interactions between Nafion resin and protonated dodecylamine modified montmorillonite: A solid state NMR study. *Journal of Colloid and Interface Science* **2007,** *311* (1), 38-44.
84. Savadogo, O., Emerging membranes for electrochemical systems: Part II. High temperature composite membranes for polymer electrolyte fuel cell (PEFC) applications. *Journal of Power Sources* **2004,** *127* (1), 135-161.
85. Aksoy, E. A.; Akata, B.; Bac, N.; Hasirci, N., Preparation and characterization of zeolite beta–polyurethane composite membranes. *Journal of Applied Polymer Science* **2007,** *104* (5), 3378-3387.
86. Sacca, A.; Carbone, A.; Passalacqua, E.; D'epifanio, A.; Licoccia, S.; Traversa, E.; Sala, E.; Traini, F.; Ornelas, R., Nafion–TiO_2 hybrid membranes for medium temperature polymer electrolyte fuel cells (PEFCs). *Journal of Power Sources* **2005,** *152*, 16-21.
87. Arico, A.; Baglio, V.; Di Blasi, A.; Creti, P.; Antonucci, P.; Antonucci, V., Influence of the acid–base characteristics of inorganic fillers on the high temperature performance of composite membranes in direct methanol fuel cells. *Solid State Ionics* **2003,** *161* (3-4), 251-265.

88. Li, Q.; He, R.; Jensen, J. O.; Bjerrum, N. J., Approaches and recent development of polymer electrolyte membranes for fuel cells operating above 100 °C. *Chemistry of Materials* **2003,** *15* (26), 4896-4915.
89. Liu, W.; Ruth, K.; Rusch, G., The membrane durability in PEM fuel cells. *Journal of New Materials for Electrochemical Systems* **2001,** *4* (4), 227-232.
90. Kumar, B.; Fellner, J., Polymer–ceramic composite protonic conductors. *Journal of Power Sources* **2003,** *123* (2), 132-136.
91. Wang, Z.; Tang, H.; Zhang, H.; Lei, M.; Chen, R.; Xiao, P.; Pan, M., Synthesis of Nafion/CeO 2 hybrid for chemically durable proton exchange membrane of fuel cell. *Journal of Membrane Science* **2012,** *421*, 201-210.
92. Vaivars, G.; Maxakato, N. W.; Mokrani, T.; Petrik, L.; Klavins, J.; Gericke, G.; Linkov, V., Zirconium phosphate based inorganic direct methanol fuel cell. *Mater. Sci* **2004,** *10*, 162-165.
93. Kim, B.-N.; Lee, D.-H.; Han, D.-H., Thermal, mechanical and electrical properties on the styrene-grafted and subsequently sulfonated FEP film induced by electron beam. *Polymer Degradation and Stability* **2008,** *93* (6), 1214-1221.
94. Cong, Y.; Li, B.; Yue, S.; Fan, D.; Wang, X.-j., Effect of oxygen vacancy on phase transition and photoluminescence properties of nanocrystalline zirconia synthesized by the one-pot reaction. *The Journal of Physical Chemistry C* **2009,** *113* (31), 13974-13978.
95. Zhu, Y.-F.; Shi, L.; Liang, J.; Hui, D.; Lau, K.-t., Synthesis of zirconia nanoparticles on carbon nanotubes and their potential for enhancing the fracture toughness of alumina ceramics. *Composites Part B: Engineering* **2008,** *39* (7), 1136-1141.

CHAPTER SIX

6. The methanol permeability and proton conductivity of nanocomposite membranes

This chapter presents three scientific papers summary in the following sections:
Presents the results from the paper: "**The impact of zirconia nano-rods on the methanol permeability and conductivity of Nafion®-ZrO_2 nano-composite membrane".** International Journal of Microstructure and Materials Properties13(6) (2018) 381.
Presents the results from the paper: "**Nafion®/ sulphated zirconia oxide-nanocomposite membrane: the effects of ammonia sulphate on fuel permeability**" Journal of Polymer Research 26 (2019) 108.
Presents the results from the paper: "**The proton conductivity and mechanical properties of Nafion®/ ZrP nanocomposite membrane"** Heliyon 5(8) (2019) e02240.

A: The impact of zirconia nano-rods on the methanol permeability and conductivity of Nafion®-ZrO_2 nano-composite membrane

6.1. Introduction

Methanol (MeOH) is preferred as an alternate fuel over hydrogen, due to its higher energy density at high pressures (360 atm), easy storage and transportation (liquid at room temperature)[1], availability as it is obtained from biomass (pyrolysis of timber, wood alcohol). Methanol as a liquid is a good candidate for portable generators because it is makes refuelling simple. Methanol has a simple chemical structure that can be oxidised into hydrogen in the presence of a suitable catalyst [2]. Direct methanol fuel cells (DMFCs) have high-energy efficiency and power density that make them suitable for use in mobile and portable power sources without polluting the environment [3]. A DMFC consists of a proton electrolyte membrane (PEM) sandwiched between two porous electrodes containing catalyst. Working at higher temperature above 100 °C enhances the CO tolerance, causes faster reaction kinetics and improves heat removal [4], which are essential for the life span of fuel cells. The Nafion® membrane has good chemical and mechanical properties, thermal stable and a high proton conductivity of 0.1 S/cm in a hydrated state [5-6]. At high temperature, the Nafion® membrane faces a decrease in proton conductivity, mechanical properties and cell performance as all water within the Nafion® membrane has been converted to a vapour phase. Moreover, using a Nafion® membrane above its glass transition temperature of 110 ºC [7-8], can lower the membrane's stability, performance and lifetime due to the rearrangements of polymer [9-10].

Furthermore, the changes in the thermal expansion and swelling coefficients of polymer have an effect on the mechanical properties, which leads to the deterioration and malfunction of the fuel cell [11-12]. Nevertheless, the Nafion® membrane has some major drawbacks such as fuel permeability through the membrane and poor mechanical stability in DMFCs, which result in fuel loss and poor performance [13]. When this happens, the methanol reacts at the cathode without producing electricity. This not only reduces the fuel utilisation, but also decreases the catalyst activity at the cathode, due to the cathode flooding. Intensive research efforts are focused mainly on decreasing the crossover of methanol through the polymer electrolyte membrane while maintaining good ion conductivity [14]. Nafion® membranes have been incorporated with inorganic nanofillers to enhance the proton conductivity and mechanical stability, and decrease the fuel crossover at low water content in DMFCs [15]. It has been reported in literature that the decreases in MeOH crossover due to the incorporated with zirconium or titanium phosphate [15], TiO_2 [16], SiO_2 [17], alumina silicates [18] and palladium nanoparticles [19]. The incorporation of specific morphology metal oxide within Nafion® membrane, allows the interaction of nanofiller with membrane [20]. Modification with ZrO_2 lower membrane swelling and methanol permeation [21]. This paper presents the modified Nafion® membrane with three zirconia nanoparticles Zr-50 and Zr-120 (cubic phase) and Zr-150 (monoclinic phase), which is prepared in different aging temperatures to enhance water retention, proton conductivity, mechanical and thermal properties of polymers and reduce the methanol crossover. Zr-50 and Zr-120 consists of irregular and rod-like nanostructures, Zr-150 composed of nanospheres that are useful in fuel cell electrolytes, oxygen sensors and gate dielectrics [22]. The influences of stress–strain on the mechanical strength of Nafion® 117 and the modified Nafion® membrane were also investigated.

6.2. Experimental

6.2.1. Materials

Sodium hydroxide, silver nitrate, Methanol (Merck), sulphric acid (Merck), hydrogen peroxide, zirconium oxychloride hydrate (Merck) and Nafion® 117 membrane (Sigma) were obtained and were used as received.

6.2.2. Synthesis of ZrO_2 nanoparticles

The ZrO_2 nanoparticles were prepared with the precipitation method. Zirconium oxychloride hydrate ($ZrOCl_2.8H_2O$) and sodium hydroxide (NaOH) were used as starting materials. 0.2M $ZrOCl_2.8H_2O$ was prepared in a 250 ml beaker and 2N NaOH solution was added dropwise

with continuous stirring for 45 minutes. The obtained precipitate was divided into three parts that were aged at temperatures of 50 °C, 120 °C and 150 °C for 24 hours, then filtered and washed several times with distilled water until chlorine ions (Cl^-) were not detected by the silver nitrate ($AgNO_3$). The precipitate was dried at 100 °C for 24 hours, calcined at 600 °C for four hours and labelled as Zr-50, Zr-120 and Zr-150.

6.2.3. Preparation of nanocomposite membranes (impregnation method)

Nafion® 117 membranes were treated according to the standard procedure: one hour in a boiling 3% solution of hydrogen peroxide; one hour in boiling 0.5 M sulphuric acid; one hour in boiling distilled water. The nano-composite membranes were prepared by soaking the Nafion® 117 membranes in the methanol solution in order to open the pores of membrane and then adding a required amount of Zr-50, Zr-120 and Zr-150 (5wt %) nanoparticles in the methanol solution as shown in Figure 6-1. The nanocomposite membranes were repeatedly impregnated (up to five times) at room temperature [23]. To remove any air from the membrane pores, the sol and immersed membranes were heated to 100 °C, then slowly cooled down to room temperature and kept in the solution for 24 hours. After drying, these membranes were stored in de-ionised water.

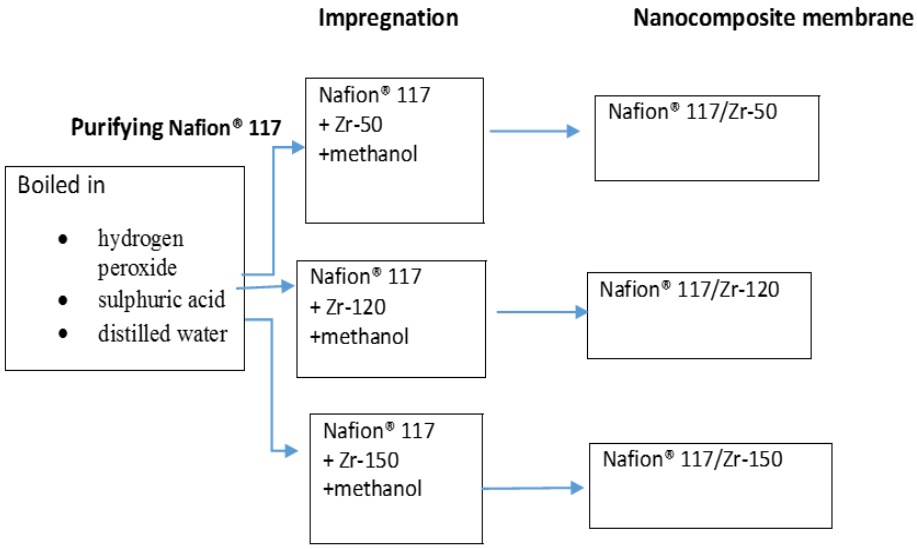

Figure 6- 1: Preparation of nanocomposite membranes.

6.3. Results and discussion

6.3.1. Structure and morphology analysis

The morphological pattern and the crystallinity degree of the nanocomposite membranes were observed under X-ray diffraction (XRD) analysis [24]. The XRD pattern of commercial Nafion® 117 compared with nanocomposite membrane is shown in Figure 6-2. It is observed from Figure 6-2(a) that the commercial Nafion® 117 membrane has two diffraction peaks at 17.5 ° and 39 ° 2θ, which can be attributed to the semi-crystallinity of the perfluorocarbon chains of the ionomer [25]. Figure 6-2(b-d) shows that when commercial Nafion® 117 membranes are impregnated with zirconia nanoparticles (Zr-50, Zr-120 and Zr-150, see insert figure), the peaks of Nafion® 117 at 17.5 ° and 39 ° decrease and the broadness increases, which indicate the amorphous nature of the membranes. The morphologies of the Nafion® 117 membrane, Nafion®/ Zr-50, Nafion®/ Zr-120, Nafion®/ Zr-150 nanocomposite membranes and their zirconia nanoparticles are shown in Figure 6-3(a-h). The Nafion® 117 membrane has a smoother external surface than the nanocomposite membranes that obtained a fractured surface as shown in Figure 6-3(a-b). The external surface of Nafion®/ Zr-50, Nafion®/ Zr-120 and Nafion®/ Zr-150 nanocomposite membranes shows well-dispersed zirconia nanoparticles with little agglomeration, which shows that the nanoparticles were successfully incorporated into the Nafion® matrix.

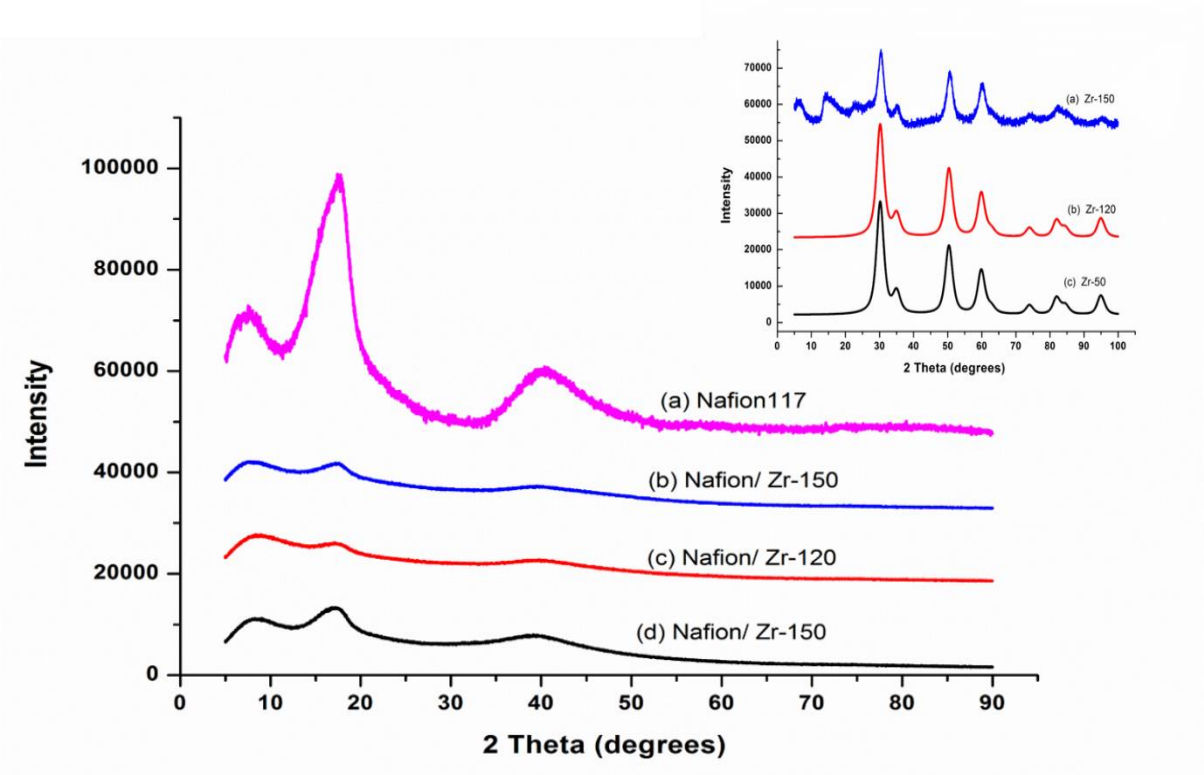

Figure 6- 2: The comparison of the XRD patterns of the (a) Nafion® 117 membrane, (b) Nafion®/ Zr-150, (c) Nafion®/ Zr-120, (d) Nafion®/ Zr 50 nanocomposite membranes and insert (XRD of (a) Zr-150, (b) Zr-120, and (c) Zr-50 nanoparticles).

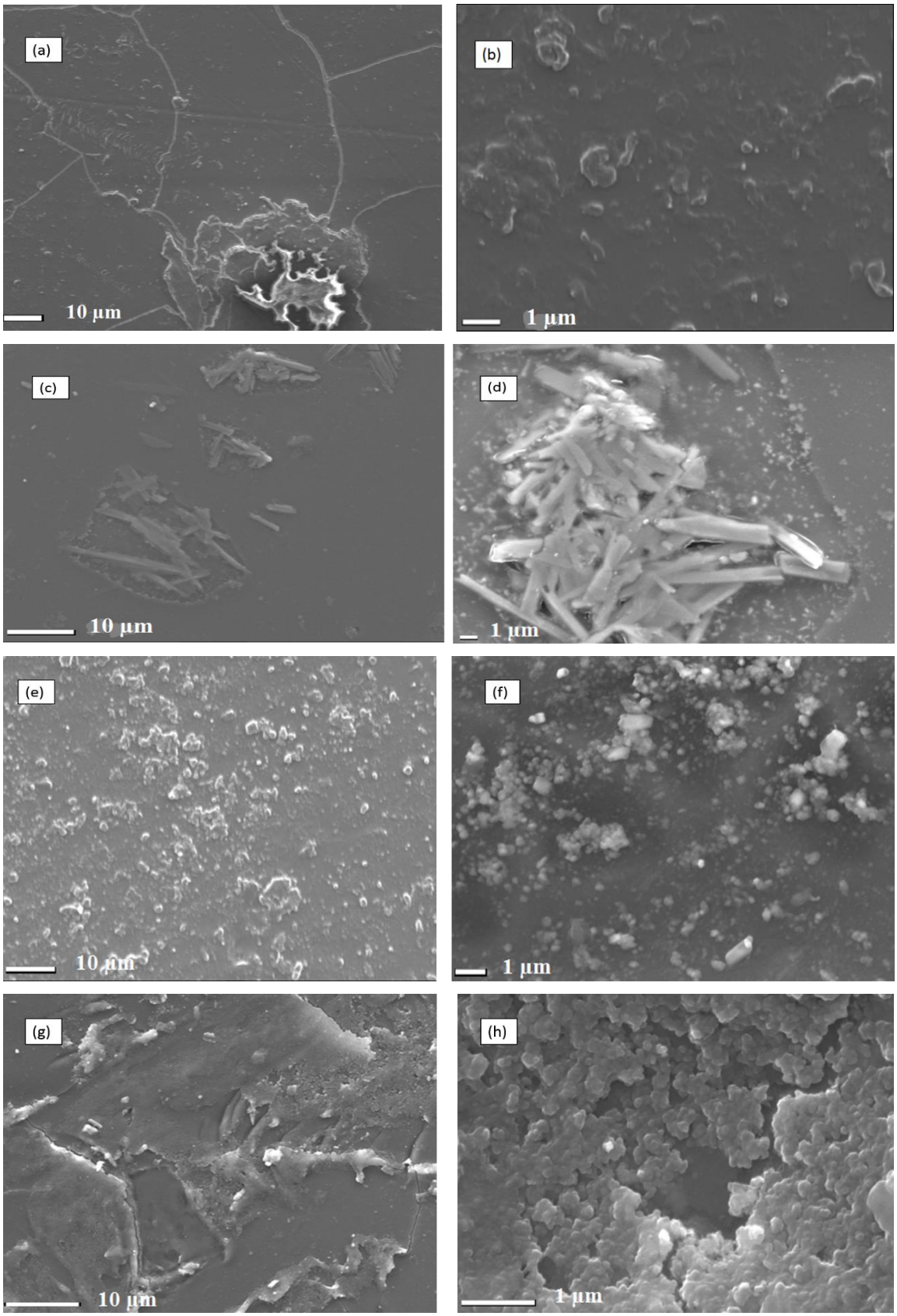

Figure 6- 3: SEM images of Nafion® 117 membrane (a) 10µm and (b) 1µm, Nafion®/ Zr-50 (c) 10µm and (d) 1µm, Nafion®/Zr-120 (e) 10µm and (f) 1µm and Nafion®/Zr-150 (g) 10µm and (h) 1µm nanocomposite membranes.

6.3.2. Degradation at high temperatures

The degradation process of the materials, as well as the weight loss percentage of Nafion® 117 and its nanocomposite membrane were determined by thermo-gravimetric analysis (TGA) and derivative thermogravimetry (DTG). Figure 6-4(a-d) shows that the Nafion®/ Zr-50, Nafion®/ Zr-120, Nafion®/ Zr-150 nanocomposite membranes as well as the Nafion® 117 membrane exhibit the three stages of weight loss up to 500 °C due to decomposition of the membrane, with a total loss of 95-100 wt. %. Figure 6-4(a) shows an initial weight loss at 100 °C corresponding to the removal of adsorbed water within the membrane. The second weight loss is due to the degradation of the sulphonic groups of the Nafion® membrane that starts at 380 °C [26]. The third weight loss at 500 °C is assigned to the degradation of the polymer main chain [27-29]. Figure 6-4(a-d) shows that the degradation of Nafion sulphonic groups starts at 380 °C in comparison with the nanocomposite membrane that shows degradation at a temperature of 510 °C due to desorption of water from membranes. Figure 6-4e (a-d) shows that the Nafion®/ Zr-50, Nafion®/ Zr-120, Nafion®/ Zr-150 nanocomposite membranes have better thermal properties than pristine Nafion® 117 membranes because their main chain starts decomposing at 510 °C, which is higher than that of the Nafion® 117 membrane (380 °C). The FTIR spectrum of the nanocomposite membrane compared with the commercial Nafion® 117 membrane is shown in Figure 6-5. Figure 6-5(a) shows that the nanocomposite membrane clearly exhibited a broad peak at a wavenumber of 3480 cm^{-1}, which corresponds to the presence of bound water and the -OH functional group on the surface of the Zr-nanoparticles [30-31]. Figure 6-5(b) shows the vibration peak at 1016 cm^{-1} and the peak at 1550 cm^{-1} in the Nafion®/ Zr-150 nanocomposite membrane due to Zr-OH bending vibrations, indicating the presence of zirconia nanoparticles within the modified Nafion® membrane [32].

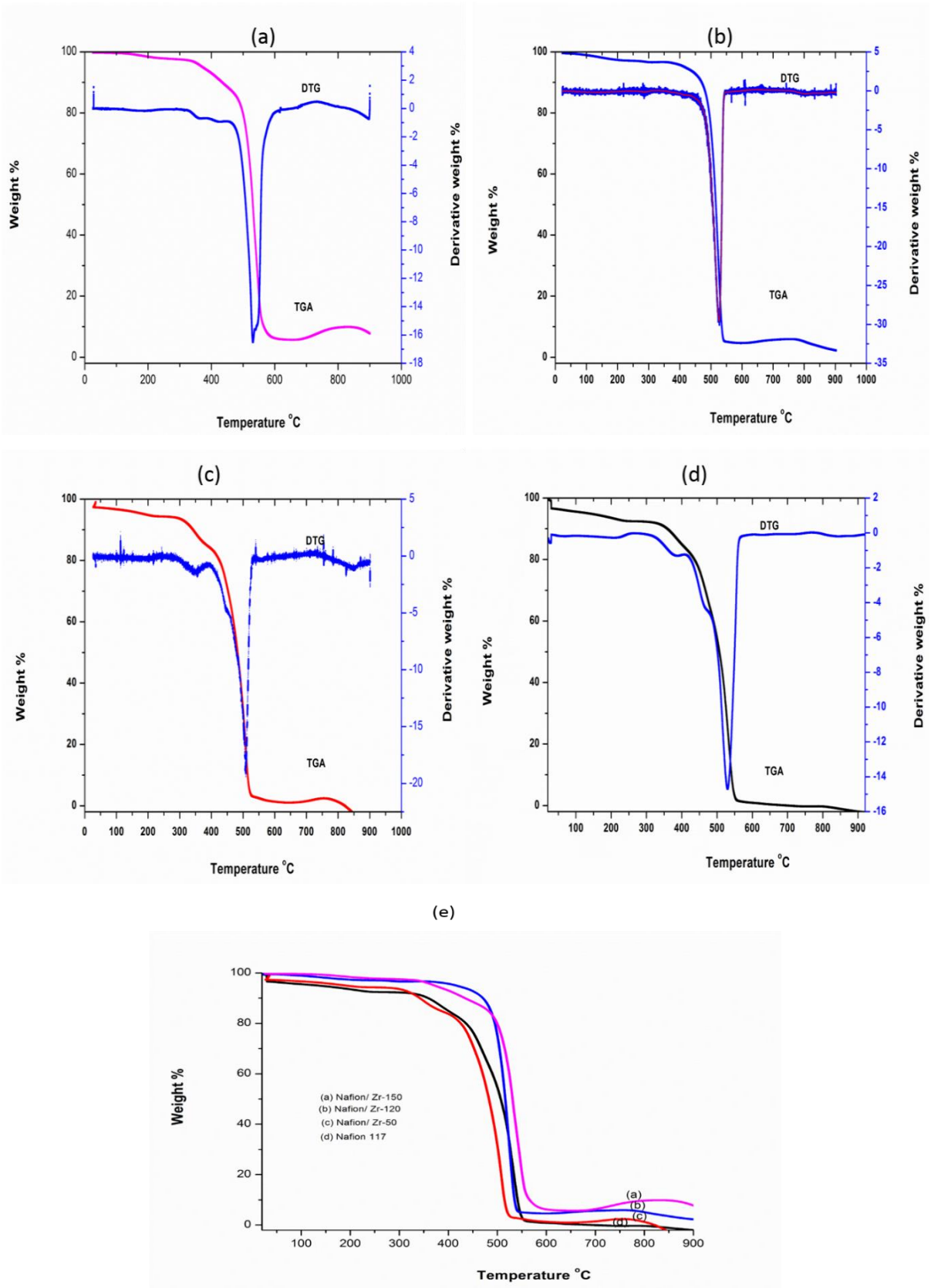

Figure 6- 4: The comparison of the TGA/ DTG curves of the (a) Nafion®/ Zr-150, (b) Nafion®/ Zr-120, (c) Nafion®/ Zr-50 nanocomposite membranes, (d) Nafion® 117 membrane and (e) the comparison of the TGA patterns of the (a) Nafion®/ Zr-150, (b) Nafion®/ Zr-120 and (c) Nafion®/ Zr 50 nanocomposite membranes and (d) Nafion® 117 membrane.

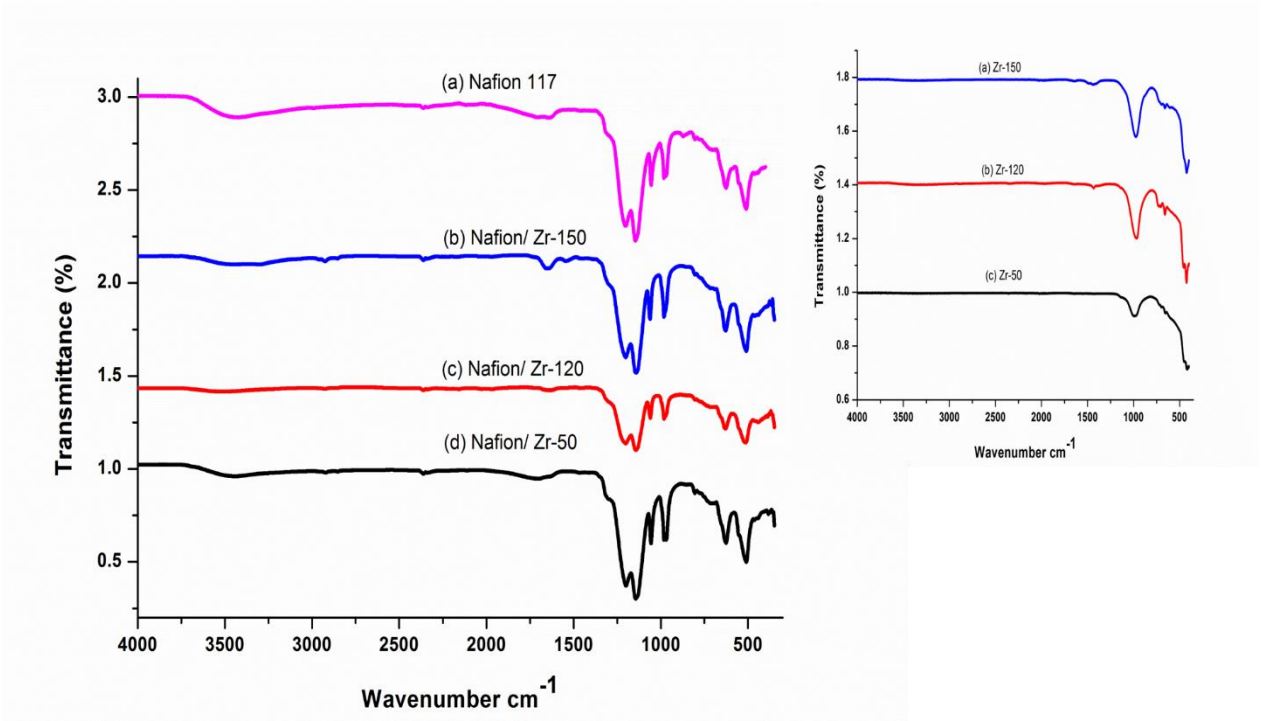

Figure 6- 5: FTIR spectra of the (a) Nafion 117 membrane, (b) Nafion/ Zr-150, (c) Nafion/ Zr-120, (d) Nafion/ Zr 50 nanocomposite membranes and insert (FTIR of (a) Zr-150, (b) Zr-120, and (c) Zr-50 nanoparticles).

6.3.3. Water contact angle measurements

The hydrophilicity of the membrane surfaces was performed with a contact-angle measurement instrument equipped with a video system. Membranes were cut into strips and mounted on glass slides for analysis. The droplet of de-ionised water (0.16 µL) was dropped onto the surface of the membranes at ambient temperature by placing the tip of the syringe close to the sample surface, and all the images were captured with a camera. The measurement was repeated ten times at different surfaces of the membranes to obtain an average value. Before the water droplet attached to the sample surface, the wetting process was recorded until no significant change at the surface was observed any longer [33]. The water contact angle of the dry commercial Nafion® 117 membrane, and the Nafion®/ Zr-50, Nafion®/ Zr-120 and Nafion®/ Zr-150 nanocomposite membranes were observed. The water droplets at the surface area of the nanocomposite membranes compared with the commercial Nafion® 117 membrane is presented in figure 6-6(a-d). The increases water contact angle is related to the hydrophobic characteristic of Nafion® 117 membrane, due to the presence of the sulphonic acid group in the hydrophilic side chain.

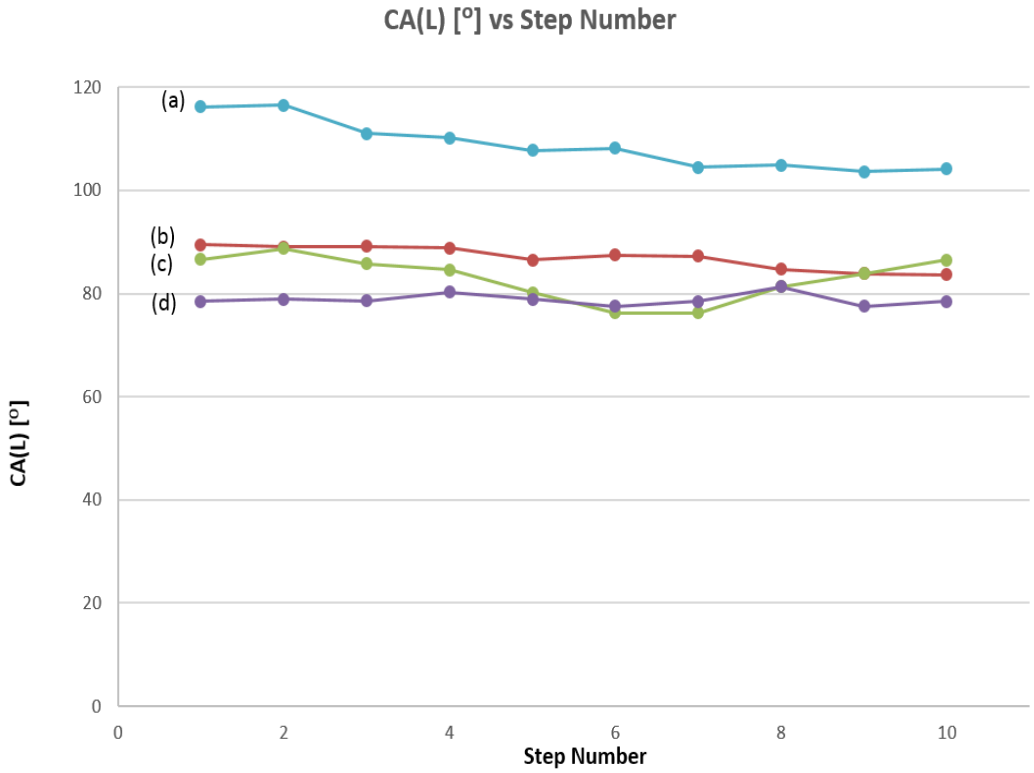

Figure 6- 6: The water contact angle of the commercial Nafion® 117 membrane (a), Nafion®/Zr-50 (b), Nafion®/Zr-120 (c) and Nafion®/Zr-150 (d) nanocomposite membranes.

6.3.4. Tensile test

The tensile mechanical property was tested with the Univert mechanical tester (CellScale) with 200 N load cell as shown in Figure 6-7. The specimens were rectangular, about 10 mm in width and about 30 mm in length. Sandpaper was adhered to the two surfaces of the clamp, which prevented the specimen from slipping during the testing. The length, width and thickness of the samples were measured with a vernier calliper and recorded prior to testing. The testing area of the membrane samples were 4 mm x 10 mm in dimension. To allow for a clamping area, the samples were prepared in such a way that they could be clamped on both sides and still allow the testing area to be 4 mm x 10 mm. The thickness of the membranes was measured to be 0.18 mm. A thickness of 0.18 mm for the nanocomposite membranes was used in analysing the stress applied to the sample. The membranes were soaked in water for 24 hours and tested as a wet test. Then the membranes were dried in a vacuum oven at 80 °C for 24 hours and tested as a dry test. The tensile strength of the modified Nafion® membranes were measured using a Ustretch device (CellScale) dried at 25 °C and wet at 34 °C and actuator speed of 5 mm/min. The crosshead speed was set as 3 mm/min, and the load was applied until the ultimate fracture of the specimen. The elastic modulus was calculated as the slope of the initial linear portion of the stress–strain curve. The tensile strength was

determined as the maximum point of the stress–strain curve. The tensile test was measured on the wet and dry commercial Nafion® 117 membrane, Nafion®/ Zr-50, Nafion®/ Zr-120 and Nafion®/ Zr-150 nanocomposite membranes. The stress vs strain of nanocomposite membranes compared to the pristine Nafion® 117 membrane as presented in Figure 6-8. Figure 6-8(a) shows that the Nafion®/ Zr-50, Nafion®/ Zr-120 and Nafion®/ Zr-150 nanocomposite membranes in their dry state obtained the highest tensile stress of 1902 kPa, 2220 kPa and 2145 kPa respectively, when compared with commercial Nafion® 117 (1347 kPa). This may be due to the distribution of inorganic metal within the Nafion® [34]. The Nafion®/ Zr-120 nanocomposite membrane showed a higher tensile stress than the commercial Nafion® 117 membrane. Figure 6-8(b) shows that the Nafion® 117 membrane, Nafion®/ Zr-50, Nafion®/ Zr-120 and Nafion®/ Zr-150 nanocomposite membranes obtained the tensile stress of 1078 kPa, 740 kPa, 1015 kPa and 855 kPa, respectively. The modulus of elasticity of the Nafion®117 nanocomposite membrane in dry and wet conditions were compared with the Nafion®/ Zr-50, Nafion®/ Zr-120 and Nafion®/ Zr-150 nanocomposite membrane as shown in Figure 6-9 and 6-10. The modulus of elasticity of dry Nafion®/Zr-50, Nafion®/Zr-120 and Nafion®/Zr-150 nanocomposite membrane is 47.2%, 65.79% and 49.32% higher than dry Nafion®117 membrane, respectively (Figure 6-9(a)).

Figure 6- 7: Tensile mechanical testing of Nafion® nanocomposite membrane.

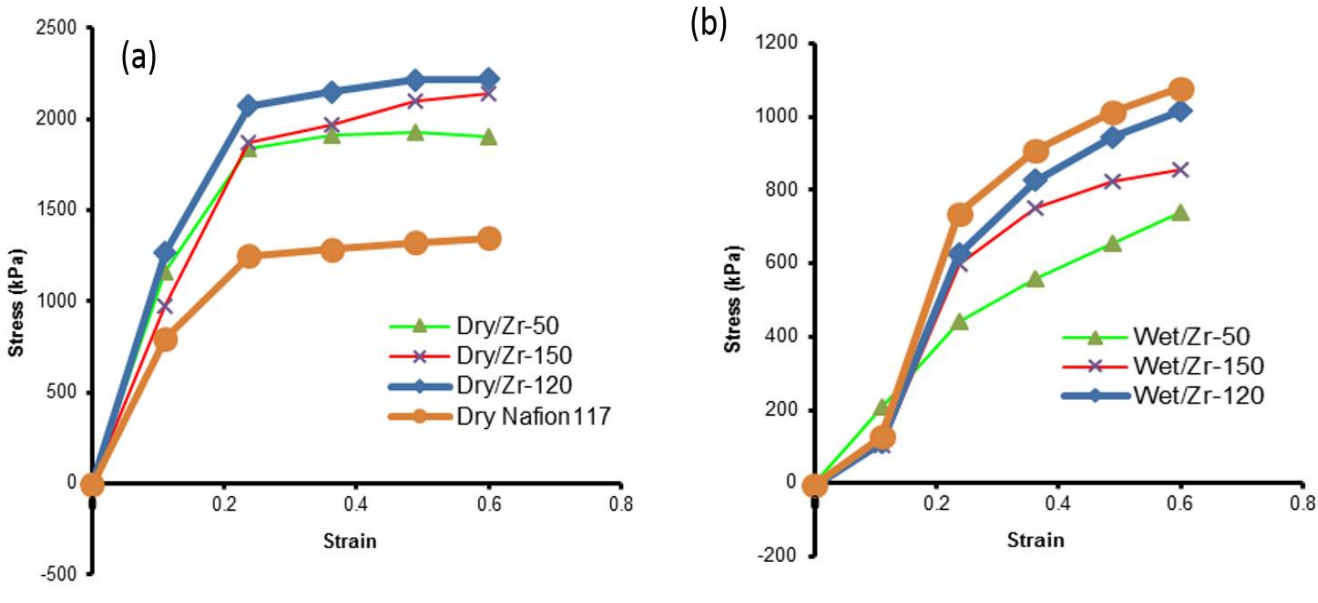

Figure 6- 8: Stress vs strain for dry (a) and wet (b) membranes (Nafion® 117 membrane, Nafion®/ Zr-50, Nafion®/ Zr-120 and Nafion®/ Zr-150 nanocomposite membranes).

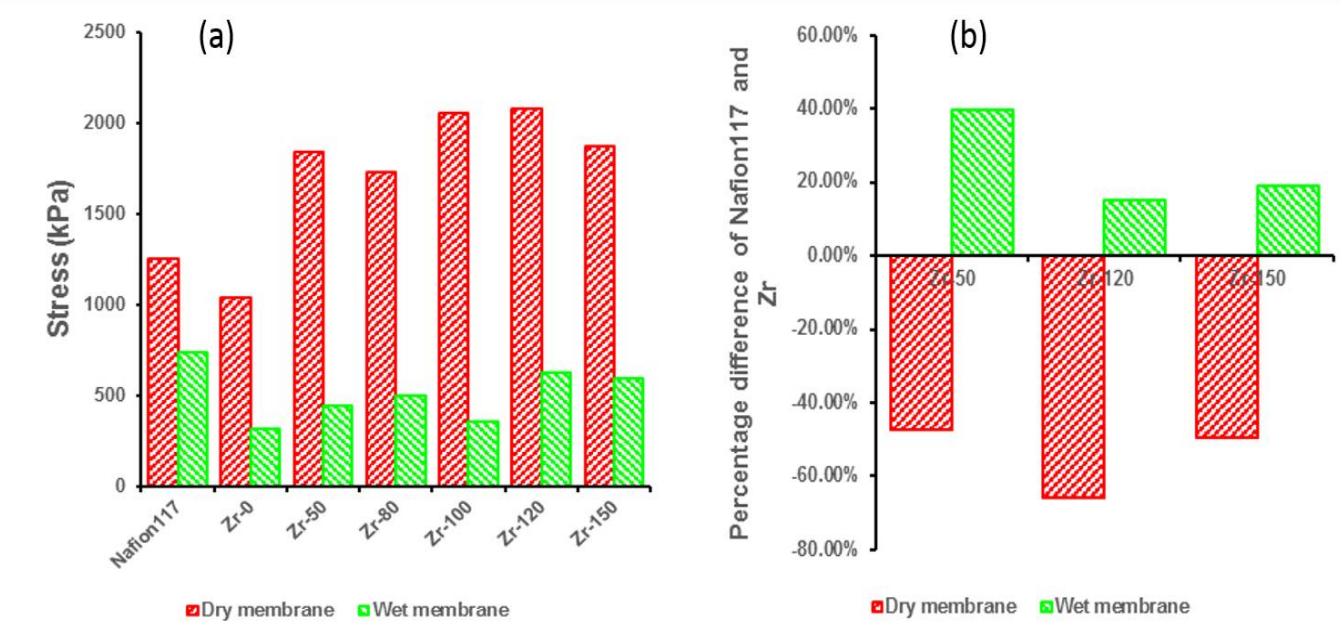

Figure 6- 9: Stress value at 0.236 strain (a), Percentage difference of wet and dry Nafion®117 membrane, Nafion®/ Zr-50, Nafion®/ Zr-120 and Nafion®/ Zr-150 nanocomposite membranes.

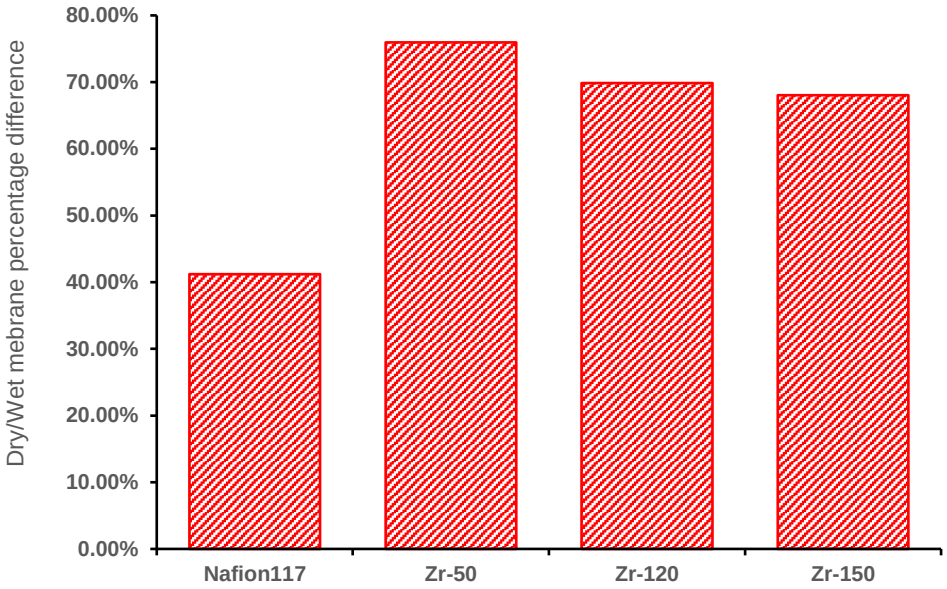

Figure 6- 10: Comparison of dry and wet membrane (stress at 0.236 strain) of Nafion®117 membrane, Nafion®/ Zr-50, Nafion®/ Zr-120 and Nafion®/ Zr-150 nanocomposite membranes.

6.3.5. Methanol permeability measurements

Methanol permeability was measured using a homemade permeation-measuring cell as shown in Figure 6-11. The O-ring and the membrane were mounted between the two compartments, and the diameter of the diffusion area was 3.5 cm. The one compartment (A) was filled with a methanol solution of 50 ml and the other compartment (B) was filled with 50 ml of distilled water as shown in Figure 6-11. The solutions were prepared in 2 M and 5 M methanol and the results collected at 30 ºC, 60 ºC and 80 ºC within three hours for comparison. The methanol concentration sensor was used to monitor the methanol concentration in compartment B. The output signal was converted by a data module and recorded by a personal computer. Methanol permeability (P) was obtained by means of the following relationship. Methanol permeability (P) was obtained by means of the following relationship [35]:

$$C_B = \frac{A\,P}{V_B\,L}\,C_A\,(t - t_O) \qquad (6\text{-}1)$$

where C_A is the initial methanol concentration in compartment A; C_B the methanol concentration in compartment B at diffusion time t; V_B the volume of distilled water in compartment B; L the thickness of the membrane; and A the effective permeating area.

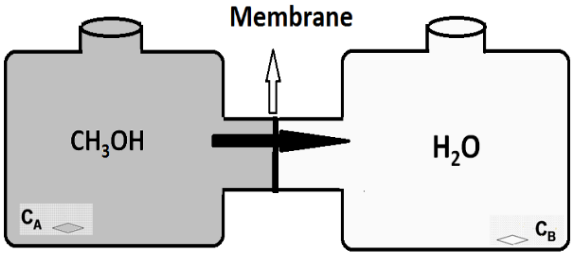

Figure 6- 11: Schematic representation of the experimental setup for the determination of the methanol permeability across the membranes.

The methanol permeability across the modified Nafion® membranes compared with the pristine Nafion® 117 was observed under different methanol concentrations (2 M and 5 M) as shown in Figure 6-12. The water bath temperature was fixed at 30 ºC, 60 ºC and 80 ºC and then the methanol samples were taken within a period of two hours. Figure 6-12(b) shows the permeation of methanol versus time. At 2 M MeOH the results showed that there was no permeation of MeOH for all the membranes at different temperature. This may due to the lower concentration of methanol solution that may reduce the methanol permeation [36-37]. Figure 6-12(a) shows that when increasing the methanol solution to 5 M, it also increased the methanol permeability. The MeOH permeability of the pristine Nafion® 117 membrane obtained a low value of 8.8 10^{-7} cm^2/s when compared with 1.77×10^{-6} cm^2/s, 1.66×10^{-6} cm^2/s and 1.22×10^{-6} cm^2/s for Nafion®/ Zr-50, Nafion®/ Zr-120, Nafion®/ Zr-150 nanocomposite membranes at a higher concentration of 5 M and a temperature of 60 ºC as shown in Figure 6-12(a). These results show that using zirconia nanoparticles as a nanofiller for the Nafion® 117 membrane has no effect on the blocking of the methanol diffusion at the lower temperature of 60 ºC, as the methanol permeability of the Nafion® 117 membrane is lower than the modified Nafion® 117 membranes [38-41]. Figure 6-12(a) shows that when the temperature was raised to 80 ºC, it obtained a methanol permeability of 2.87×10^{-6} cm^2/s, 1.88×10^{-6} cm^2/s, 1.98×10^{-6} cm^2/s and 1.98×10^{-6} cm^2/s for Nafion®/ Zr-50, Nafion®/ Zr-120, Nafion®/ Zr-150 nanocomposite membranes and Nafion® 117 at the higher concentration of 5 M. The modified Nafion®/ Zr-120 and Nafion®/ Zr-150 nanocomposite membranes have low methanol permeability due to zirconia nanoparticles that blocked the methanol crossover within the Nafion® matrix.

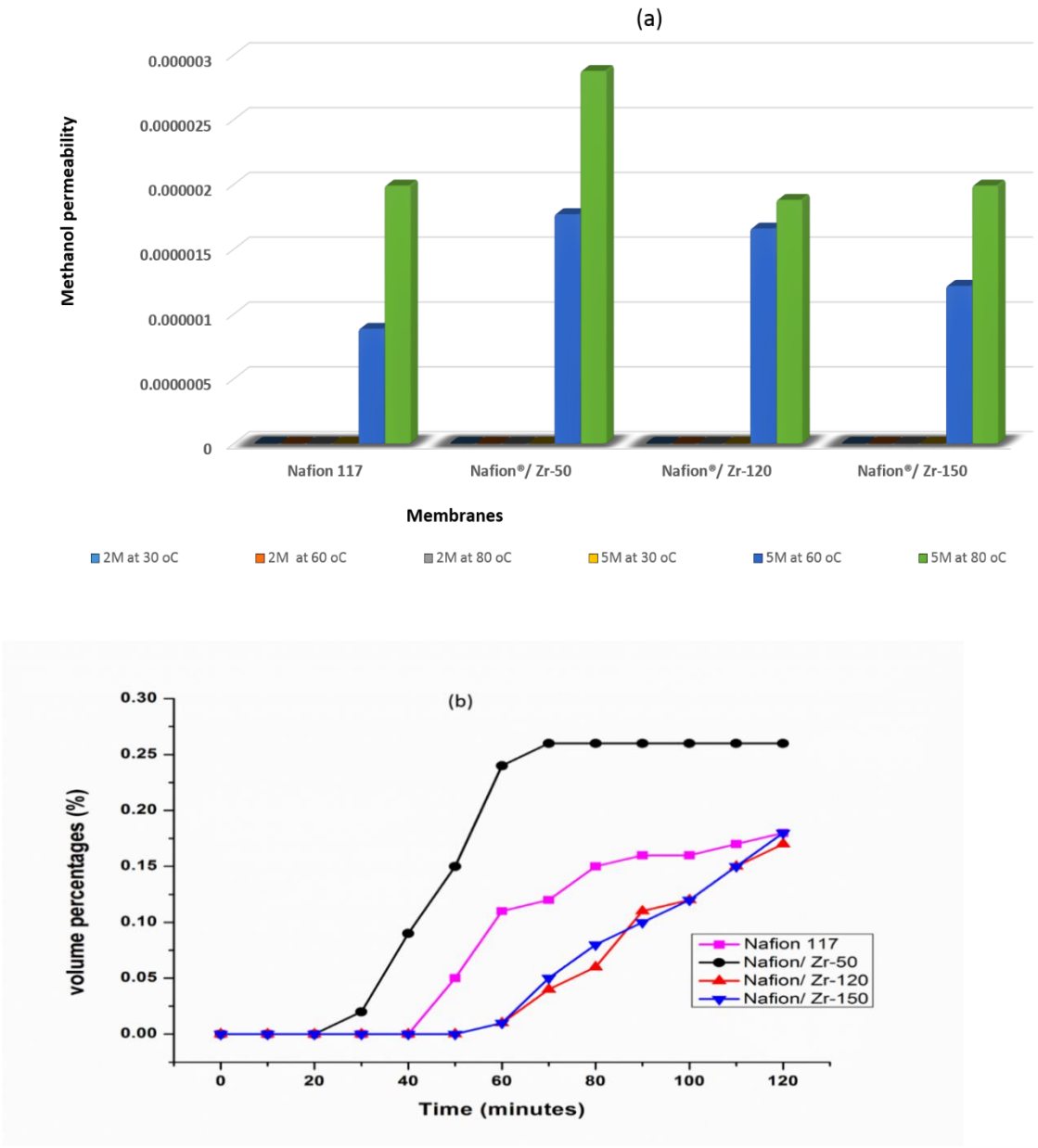

Figure 6- 12: (a) The methanol permeability (2 M and 5 M) for the Nafion ®117 membrane, Nafion®/ Zr-50, Nafion®/ Zr-120 and Nafion®/ Zr-150 nanocomposite membranes at 30 °C, 60 °C and 80 °C. and (b) Comparison of the methanol crossover (5 M concentration) of the Nafion® 117 membrane, Nafion®/ Zr-50, Nafion®/ Zr-120 and Nafion®/ Zr 150 nanocomposite membranes at 80 °C.

6.3.6. Proton conductivity measurement

The conductivities of nanocomposite membranes and commercial Nafion® membranes were measured with a four-point probe conductivity cell [42] as shown in Figure 6-13. The ionic conductivity was determined galvanostatically with a current amplitude of 0.1 mA over frequencies ranging from 1MHz to 10Hz.[43]. Using a Bode plot, the frequency region over which the impedance had a constant value was checked, and the electrical resistance was then

obtained from a Nyquist plot [44]. The ionic conductivity (k) was calculated according to the following Equation [6]:

$$K = L/RWd \qquad (6\text{-}2)$$

where R is the obtained membrane resistance; L the distance between potential-sensing electrodes (1 cm); and W and d the width (2 cm) and thickness of the membrane.

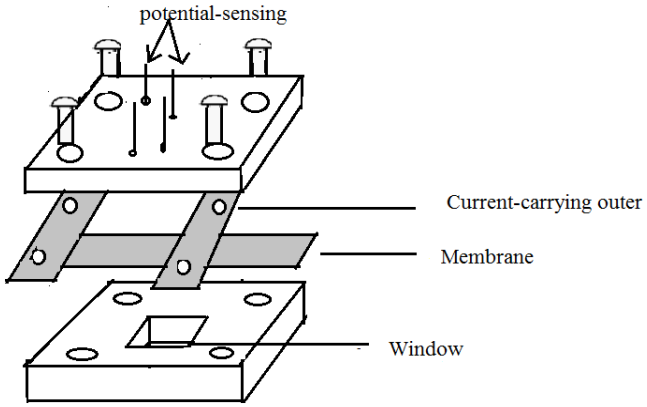

Figure 6- 13: Schematic diagram of a proton conductivity cell for the four-point-probe electrochemical impedance spectroscopy technique.

For conductivity testing, the membrane was immersed in 1 M sulphuric acid solution at room temperature for six hours. The membrane was then rinsed with deionised water several times to remove any excess H_2SO_4 and then immersed in deionised water for six hours at 60 °C. All the membranes were kept in deionised water at room temperature before conductivity testing measurement. The proton conductivity of the Nafion®/ Zr-50, Nafion®/ Zr-120, Nafion®/ Zr-150 nanocomposite membranes and the Nafion® 117 membrane was measured at ambient temperature. The proton conductivity, membrane thickness and resistance of Nafion® 117 and modified Nafion® membranes was presented in Table 6-1. Nafion®/ Zr-50 nanocomposite membranes obtained a higher proton conductivity than commercial Nafion® 117 membrane as shown in Figure 6-14(a). This may due to the lower distribution of zirconia nanorods within the Nafion matrix that act as a water reservoir. The proton conductivity of the Nafion®/ Zr-50, Nafion®/ Zr-120, Nafion®/ Zr-150 nanocomposite membranes and the Nafion® 117 membrane is 0.139 S cm^{-1}, 0.090 S cm^{-1}, 0.097 S cm^{-1} and 0.113 S cm^{-1}, respectively as shown in Figure 6-14(a). The typical complex-plane of imaginary impedance (-Z'') versus the real impendence (Z') of Nafion® 117 membrane, Nafion®/ Zr-50, Nafion®/ Zr-120 and Nafion®/ Zr-150 nanocomposite membranes are shown in Figure 6-14(b). The plots highlight the part of the electrochemical impendence spectrum (EIS) from 1MHz to 10Hz [45].

Table 6- 1: The conductivity of the, Nafion®/ Zr-50, Nafion®/ Zr-120 and Nafion®/ Zr-150 nanocomposite membranes and Nafion® 117 membrane at 25 °C

Membranes	Proton conductivity (S/cm) at 25 °C	Membrane resistances (Ohm)	Membrane thickness (cm)
Nafion 117	0.113	248	0.018
Nafion®/ Zr-50	0.139	200	0.018
Nafion®/ Zr-120	0.090	308	0.018
Nafion®/ Zr-150	0.097	285	0.018

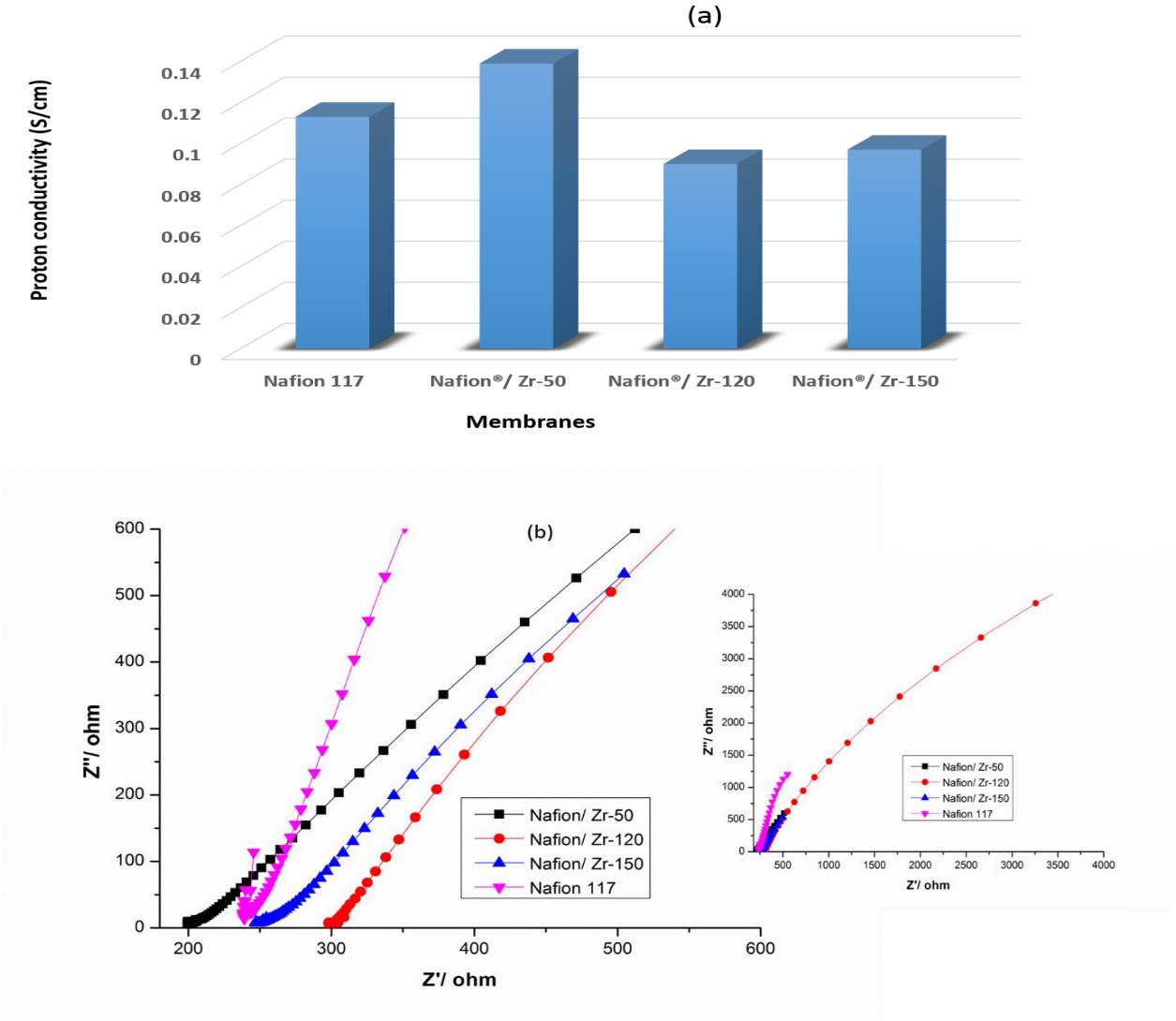

Figure 6- 14: (a) The proton conductivity of the Nafion®/ Zr-50, Nafion®/ Zr-120 and Nafion®/ Zr-150 nanocomposite membranes and Nafion® 117 membrane at 25 °C and (b) the typical complex-plane of imaginary impedance (-Z'') versus the real impendence (Z') of Nafion®/ Zr-50, Nafion®/ Zr-120 and Nafion®/ Zr-150 nanocomposite membranes at 25 °C and Nafion® 117 membrane.

6.4. Discussion

The XRD results shows a slight deviation from the main chain of Nafion® peaks at 17 °, which is more amorphous without any peak corresponding to the zirconia nanoparticles. The morphology of the Nafion®/ Zr-50 nano-composite membrane has clearly visible when compared to that commercial Nafion® 117 at 1 µm. The SEM image confirmed that the Zr-50 nanoparticles were in the form of nanorods, which may be due to the ultrasonic bath that breaks the nanoparticles into small pieces and well impregnated within the membrane matrix. All the nanocomposite membranes have impregnated with the same mass percentage of zirconia nanoparticles, but Zr-120 nanoparticles clearly show that zirconia nanoparticles in the form of nanobars have been successfully impregnated with less agglomeration due to their good compatibility. Moreover, well distribution of nanoparticles shows the microscopic porosity of membrane with inorganic nanoparticles that enhanced the water uptake of the membrane [46], which is also confirmed by the water contact angle and TGA. The SEM image Nafion®/ Zr-150 nano-composite membrane showed well distributed zirconia nanoparticles within the membrane which confirmed by TGA and FTIR.The improvement of thermal stability confirmed the presence of water retention zirconia nanoparticles within the Nafion® membrane [47], reducing the weight loss rate while also increasing the decomposition of the nano-composite membranes at high temperature. Therefore, this thermal stability improvement shows the enhanced potential of the zirconia nano-composite membrane for higher temperature operations for PEMFC applications. The DTG curves of the Nafion® 117 membrane obtained the two transition peaks that are associated with the second and third decomposition stage of a membrane. The DTG curves of the Nafion® 117 membrane show a maximum decomposition rate of 2% per °C at 380 °C. Similarly, the DTG curves of the modified Nafion® membrane appear in two peaks. The DTG curve of the Nafion®/ Zr-50 nano-composite membrane also shows the maximum decomposition rate of 2% per °C at 380 °C. The FTIR results of nanocomposite membranes clearly show a vibration peak at 1550 cm^{-1} and 1474 cm^{-1} due to Zr-OH bending vibrations, indicating the presence of zirconia nanoparticles within the modified Nafion membrane [32]. While the peak observed at 2355 cm^{-1} and 2927 cm^{-1} are due to the presence of inorganic ions. Comparison FTIR results of Nafion® 117 membrane shows the band at 3456 cm^{-1} due to O-H vibration corresponding to physically adsorbed water [48-49]. Similar vibration peaks at 1195 cm^{-1} and 1198 cm^{-1} in all the membranes were observed, which attributed to the -CF_2-CF_2- vibration and 1060 cm^{-1} attributed to -SO_3^- [50-51]. Furthermore, two major vibrational structures at 1199cm^{-1} and 1146cm^{-1} for CF_2 stretching vibration of the Nafion® backbone are shown [30] and 1065 cm^{-1} and 978 cm^{-1}, which are attributed to the stretching vibration moieties of $SO3^-$ and C-O-C, respectively [30]. In the modified Nafion® 117 membranes, the decreased in water contact angle were noticeable (from 118° to 84°), this

may be due to the hydrophilicity of zirconia nanoparticles. In addition, the decreased contact angles of nano-composite membranes (below 90°), may due to the zirconia nanoparticles that are adsorbed on the surface of the membrane to enhance the hydrophilicity [52]. Contact angles below 90 ° indicate the hydrophilic character of a material describing the water-uptake capability. The tensile results show that the nano-composite membrane in its wet state obtained a slightly lower tensile stress than the pristine Nafion® 117 membrane. This shows that the incorporation of zirconia nanoparticles within the Nafion® matrix does not have an impact on the tensile stress of the wet membrane, as the dry membrane had a higher tensile strength than the wet membrane. It has been observed that the modified Nafion® membrane with inorganic oxide nanoparticles enhances the tensile strength of the membrane. This indicates that the incorporation of the ZrO_2 nanoparticles improved the mechanical property of the Nafion® membrane in its dry states, mainly due to the interaction between the sulfonic acid groups of the Nafion® ionomer and the ZrO_2 filler. The improvement of the membrane rigidity demonstrates that the zirconia nanoparticles stabilized the structure of the nano-composite membrane, and give a potential restriction to the humidity-generated stress when the membrane is used as an electrolyte membrane in the fuel cells. The wet Nafion®117 membrane have the higher modulus of elasticity compared to wet nano-composite membrane. This show that the incorporation of zirconia nanoparticles within the Nafion® matric does not have impact on the tensile stress of wet membrane. In contrast the methanol permeability of the Nafion®/ Zr-50 nano-composite membrane is high 2.87 x 10^{-6} cm^2/s compared with the pristine Nafion® 117 membrane (1.98×10^{-6} cm^2/s) at a higher temperature of 80 ºC [53-54]. This may be because the methanol permeates through hydrophilic ionic channels, especially free water molecules. In addition, protons are transported by hopping between ionic sites due to hydrogen bonding between bound water molecules as well as through ionic channels, and it has a low concentration of zirconia nanoparticles as confirmed by TGA results. The membrane resistance of commercial Nafion® 117 membranes are higher than modified Nafion® nanocomposite membranes due to the addition of zirconia nanoparticles in Nafion® membrane that enhanced the conduction of protons. incorporating zirconia nanoparticles with a higher porosity, decrease the water contact angle within the nanocomposite membranes which resulted also in increasing the proton conductivity due to the increases of exchange sites available per cluster which is an important parameter of fuel cells in order to operate on higher temperature.

6.5. Conclusion

Nanocomposite membrane prepaid by impregnation methods shows a higher proton conductivity, decreased in water contact angle and methanol crossover, which are more

improved when compared to the commercial Nafion® 117 membrane. This may due to the addition of higher porosity zirconia nanoparticles in Nafion® membrane that decrease the water contact angle within the nanocomposite membranes, which resulted also in increasing the proton conductivity due to the increases of exchange sites available per cluster, which is an important parameter of fuel cells in order to operate on higher temperature. The TGA and DTG results of the modified Nafion® membrane shows that incorporation of zirconia nanoparticles obtained a thermal stabilised degradation even at high temperature, due to the water retained within the Nafion® membrane, which leads to fuel cell application at higher temperature. The XRD results confirmed the presents of the zirconia nanoparticle within the membrane. However, the results show no new peak, due to the incorporation of low wt.% of zirconia nanoparticles. Wherever the crystallinity not visible in XRD, the SEM image shows the present of zirconia nanoparticles within the Nafion® matrix. The FTIR results of modified Nafion® membrane also confirmed the present of zirconia nanoparticles at vibration peak at 1550 cm^{-1} and 1474 cm^{-1} due to Zr-OH bending vibrations and at 2355 cm^{-1} and 2927 cm^{-1}. The proton conductivity and the resistance of Nafion®/ Zr-50 nanocomposite membrane increased because of the incorporation of zirconia nano-rods. The decreased in high methanol concentration shows a potential application of the membrane in direct fuel cells, as the lower permeation was obtained at the higher temperature of 80 ºC. This observation shows the possibilities of modified Nafion® membrane to operate at high temperature and reduced relative humidity. The incorporation of the ZrO_2 nanoparticles improved the mechanical property of the Nafion® membrane in its dry states - mainly due to the interaction between the sulfonic acid groups of the Nafion® ionomer and the ZrO_2 filler. As tensile results show that nanocomposite membranes in their dry state obtained the highest tensile stress of 1902 kPa, 2220 kPa and 2145 kPa when compared with commercial Nafion® 117 (1347 kPa). This indicates that the improvement of the membrane rigidity demonstrates that the zirconia nanoparticles stabilized the structure of the nanocomposite membrane and give a potential restriction to the humidity-generated stress when the membrane is used as an electrolyte membrane in the fuel cells.

B: Nafion®/ Sulfated Zirconia oxide-nanocomposite membrane: The effects of ammonia sulfate on fuel permeability

6.6. Introduction

Energy production from carbon-free or low-carbon sources is one of the most pressing issues facing humanity today. Fuel cells will be the future alternative for crude oil automotive and

portable applications. Fuel cells are one of the clean energies generating electricity at low cost without polluting the environment. Direct methanol fuel cells (DMFCs) are the devices that convert liquid methanol (MeOH) into electrical energy and can be used directly in fuel cells without the need for a hydrogen-reforming process. This makes them more advantageous than proton exchange membrane (PEM) fuel cells as they use MeOH as fuel that is easily stored and transported due to their higher energy density than hydrogen. Additionally, their high energy density and environmentally friendly nature, operating at low temperature, make them preferable to use in portable applications such as laptops, computers and cellphones than rechargeable lithium-ion batteries [55]. PEMs such as Nafion® maintain higher proton conductivity and good mechanical and chemical stability and reduce gas and methanol crossover at lower temperature fuel cell application [56]. However, at higher temperatures of above 80 °C they face some challenges due to the water loss and softening of the polymer backbone, resulting in membrane shrinkage, which reduces proton conductivity while permeating the fuel to crossover [57]. This also lowers cell performance, which results in degradation due to anode dehydration [43]. Furthermore, the high methanol permeability, high production cost and complicated and time-consuming manufacturing process has limited the Nafion® membrane to function in DMFCs [58]. It is well known that working at higher temperatures is favourable for the kinetics of Pt catalyst and may improve its tolerance to contaminants [59], improves CO tolerance, facilitates heat rejection and improves water management but leads to poor mechanical stability. These limitations can be overcome through the modification of Nafion® membrane. Modification of Nafion® membrane with hydroscopic metal oxide was observed by some researchers, as it can retain water at a higher temperature [60] and enhances reaction kinetics at both electrodes. The modification of Nafion® membrane with inorganic particles such as silicon dioxide (SiO_2), titanium dioxide (TiO_2) and zirconium oxide (ZrO_2) [61] enhances the higher temperature proton conductivity, improves the operating temperature, maintains water retention and also lowers methanol permeability which is the major problem in the DMFC system, due to its hydrophilic nature [61]. The retained water within the inorganic particles does not evaporate even under dry conditions, due to electrostatic attraction within the electrical double layer [62]. The incorporation of inorganic acid such as sulfated zirconia enhances proton conductivity (14.5 mS/cm) when calcined at 300 °C, with higher ion IEC of 0.54 meq/g and increased water uptake due to the sulfate ions, which increases the sulfonic acid content within the membrane [63]. Moreover, when sulfated zirconia is incorporated in the membrane, it provides an extra proton ion within the Nafion® matrix [3]. Furthermore, the modified Nafion® membrane with S-ZrO_2 nanoparticles has less swelling, improves mechanical properties and decreases methanol permeability. Mesoporous sulfated zirconia has good potential for widening applications of zirconia-based acid materials, but the major problem still lies with its low thermal stability, leading to the collapse of the

mesoporous when the template is removed at high temperature. Under strong acidic conditions, zirconia exists mostly in cationic form rather than the polyoxo species. However, when zirconia is sulfated with ammonia sulfate, the polyoxo ions can form $[Zr(OH)_2(SO_4^{2-})x(H_2O)]n^{n(2-2x)}$ [64]. Moreover, impregnating the S-ZrO_2 nanoparticles within Nafion® membranes improves the high temperature response [8]. Zirconia oxide is the only metal oxide which possesses four chemical properties, namely acidity, basicity as well as reducing or oxidising agents [65]. The main aim of this paper is to modify Nafion® membrane with sulfated zirconia in order to obtain good chemical and thermal stability, high proton conductivity and improved water uptake of modified membrane.

6.7. Experimental

6.7.1. Materials

Sodium hydroxide pellets, silver nitrate, methanol, sulphuric acid, ammonia sulfate, zirconium oxychloride hydrate and Nafion® 117 membrane was purchased from Sigma Aldrich. All the chemicals with analytical grades were used as received, without any further purification.

6.7.2. Synthesis of ZrO_2 nanoparticles

The ZrO_2 nanoparticles were prepared by precipitation method where zirconium oxychloride hydrate ($ZrOCl_2.8H_2O$) and sodium hydroxide (NaOH) were used as starting materials. 0.2M $ZrOCl_2.8H_2O$ was prepared in a 250 ml beaker and 2N NaOH solution was added dropwise with continuous stirring for 45 minutes at room temperature (RT). Obtained precipitate was filtered and washed several times with distilled water until chlorine ions (Cl^-) were not detected by the silver nitrate ($AgNO_3$). The precipitate was dried at 100 °C for 24 hours, calcinated at 600 °C for 4 hours and then labelled as ZrO_2 [66].

6.7.3. Preparation of Sulfated zirconia oxide (S-ZrO_2) nanoparticles

Sulfated zirconia oxide (S-ZrO_2) was prepared by two methods: firstly, by vigorously stirring the dried ZrO_2 nanoparticles in 0.5 M H_2SO_4 solution for 30 minutes at room temperature. The resulting solid was filtered and dried at 100 °C for 48 hours. The dried powder was then calcined at 600 °C for 2 hours and the resulting particles were crushed with a mortar and pestle and labelled S-ZrO_2 [67]. Secondly, the ZrO_2 nanoparticles was mixed with 0.5M $(NH_4)_2SO_4$ solution for 30 minutes at room temperature. Then the particles were filtered, dried

and calcined following the above procedure and the resulting particles were crushed with a mortar and pestle and labelled S-ZrO_2 (NH_3SO_4).

6.7.4. Preparation of nanocomposite membranes (impregnation method)

6.7.5. Characterisations

The XRD analysis was performed using a Philips X-ray diffraction with Cu K radiation source. The analysed material was finely ground and homogenised and the average bulk composition was determined. Samples were scanned in continuous mode from 10°- 90° with a scanning rate of 0.026 (degrees)/1 (sec). The thermal properties of the samples and their characteristics were studied by thermogravimetric analysis (TGA) under nitrogen flow. TGA data was obtained with a PerkinElmer instrument over nitrogen and at a heating rate of 10 °C/min from 28 °C to 1 000 °C. The surface morphologies of all the membrane were studied using Scanning Electron Microscopy (SEM). Electronic techniques were based on the interaction of the sample with electrons, resulting in a secondary effect that was detected and measured. Fourier Transform Infrared (FTIR) was employed to investigate the changes in the chemical structure of the membrane.

6.7.6. Water contact angle measurements

The contact-angle instrument was used to measure the hydrophilicity of the membrane. Membranes were cut into strips and mounted on glass slides for analysis. The droplet of de-ionised water (0.16 µL) was dropped onto the surface of the membranes at ambient temperature by placing the tip of the syringe close to the sample surface, and all the images were captured with a camera. The measurement was repeated ten times at different surfaces of the membranes to obtain an average value. Before the water droplet attached to the sample surface, the wetting process was recorded until no significant change at the surface was observed any longer [33].

6.7.7. Water uptake and dimensional swelling ratio of nanocomposite nanofibers

The membranes were soaked in distilled water for one day at 30 °C, 60 °C and 80 °C. They were then removed, wiped, measured and weighed. Water uptake and swelling ratio were calculated according to the equations below:

$$\boldsymbol{W_{up}}(\%) = \frac{(\boldsymbol{m_{wet}} - \boldsymbol{m_{dry}})}{\boldsymbol{m_{dry}}} \boldsymbol{X100} \qquad (6\text{-}3)$$

$$\boldsymbol{SR}(\%) = \frac{(\boldsymbol{L_w - L_d})}{\boldsymbol{L_d}} \boldsymbol{X100} \quad (6\text{-}4)$$

Where W_{up} is the percentage of water uptake, m_{wet} is the weight of wet membrane and m_{dry} is the weight of the dried membrane, L_w is the length of the wet membrane and L_d is the length of the dried membranes.

6.7.8. Ion exchange capacity (IEC)

The ion exchange capacity (IEC) of all membranes were determined by the titration method.

$$\text{IEC} = \frac{V_{NaOH} \text{ X } C_{NaOH}}{W_{sample}} \quad (6\text{-}5)$$

Where V_{NaOH} is the titrated volume of NaOH and W_{sample} is the weight of the dry membranes.

6.7.9. Methanol permeability measurements

The methanol permeability was measured with a permeation-measuring cell designed in our lab that consisted of two compartments. The membrane was placed in the middle of two compartments, and the diameter of the diffusion area was 3.5 cm. The membrane was placed in the middle of two compartments, and the diameter of the diffusion area was 3.5 cm. The compartment (A) was filled with a methanol solution of 50 ml and compartment (B) was filled with 50 ml of distilled water. The solutions were prepared in 2 M and 5 M methanol and the results collected at 30 ºC, 60 ºC and 80 ºC within three hours for comparison. The methanol concentration sensor was used to monitor the methanol concentration in compartment B. The output signal was converted by a data module and recorded by a personal computer. Methanol permeability (P) was obtained by means of the following relationship:

$$\boldsymbol{CB} = \frac{\boldsymbol{A\,P}}{\boldsymbol{VB\,L}}\, \boldsymbol{CA}\, (\boldsymbol{t - t0}) \quad (6\text{-}6)$$

where C_A is the concentration of initial methanol in compartment A; C_B the concentration of methanol in compartment B at diffusion time t; V_B the volume of distilled water in compartment B; L the membrane thickness; and A the effective permeating area.

6.7.10. Conductivity measurement

The conductivities of all membranes were measured using a four-point probe conductivity cell. The ionic conductivity was determined galvanostatically with a current amplitude of 0.1 mA over frequencies ranging from 1MHz to 10Hz. Using a Bode plot, the frequency region over which the impedance had a constant value was checked and the electrical resistance was then obtained from a Nyquist plot [44]. The ionic conductivity (σ) was calculated according to the following equation:

$$\boldsymbol{K = L/RWd} \quad (6\text{-}7)$$

Where R is the obtained membrane resistance, L is the distance between potential-sensing electrodes (1 cm), W is the width (2 cm) of the membrane and d is the thickness of the membrane. For conductivity testing, the membrane was immersed in 1 M sulphuric acid solution for 6 hours at room temperature. The membrane was then rinsed with de-ionised water several times to remove any excess H_2SO_4 and then immersed in de-ionised water for 6 hours at 60 °C. All the membranes were kept in de-ionised water at room temperature before conductivity testing.

6.8. Results and discussion

6.8.1. Fourier transform infrared spectroscopy (FTIR) analysis

Figure 6-15 shows the FTIR analysis of the commercial Nafion® 117 membrane and nanocomposite membranes. The nanocomposite membranes show the similar bands to commercial Nafion® 117 membrane, at 1 133 cm^{-1} attributed to the CF_2 stretching vibration of the PTFE backbone [30]. The observed peaks at 1 062 cm^{-1} and 1 212 cm^{-1} were attributed to the symmetry and asymmetry stretching vibrations of $SO3^-$, the peak at 983 cm^{-1} corresponds to the C-O-C symmetry stretch and was assigned to symmetric stretching frequencies of S-O bonds [30] as shown in Figure 6-15. Furthermore, the peaks observed at 636 cm^{-1} and 515 cm^{-1} were assigned to asymmetric stretching vibrations of the Zr–O–Zr bond and Zr-O, which are the same transmittance peaks as Nafion® 117 membrane [68]. This may be due to the well-dispensed inorganic materials within the Nafion matrix. Commercial Nafion® 117 membrane shows the peak at a wave number of 3 428 cm^{-1} is attributed to O-H stretching of Zr-nanoparticles, whereas the peak was less shallow on nanocomposite membranes [31] as shown in Figure 6-15(a-c). This may be due to the inorganic materials that retain water within the membrane. Figure 6-15(a) shows the bands at 1 619 cm^{-1} was assigned to the bending

vibration mode of HOH, this may due to the coordinated molecular water associated with the sulfate group [68]. Figure 6-15(b) shows the bands at 1 442 cm^{-1} which assigned to the asymmetric or symmetric stretching vibration frequencies of S=O or S-O bonds [69]. The bands at 1 680cm^{-1} can be attributed to the stretching and bending vibrations of O–H group on the surface of the Nafion® 117 membrane as shown in Figure 6-15(c) [70].

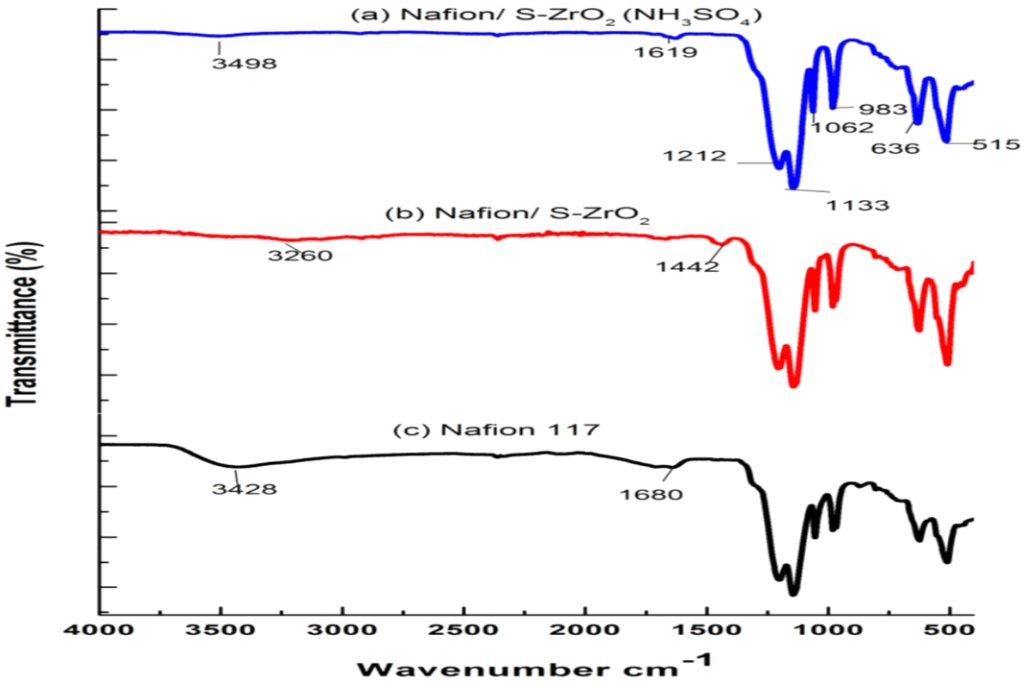

Figure 6-15: FTIR spectra of (a) Nafion®/S-ZrO_2 (NH_3SO_4), (b) Nafion®/S-ZrO_2 nanocomposite membranes and (c) Nafion® 117 membrane.

6.8.2. X-ray diffraction (XRD) analysis

The morphology and crystallinity of Nafion® membrane and nanocomposite membranes were observed under X-ray diffraction (XRD) analysis. The X-ray diffraction (XRD) pattern of the modified Nafion® and commercial Nafion® membranes was observed in Figure 6-16. Figure 6-16(a) shows that Nafion® 117 membrane has two diffraction peaks at 17.5° and 39° 2θ, which can be attributed to the semi-crystalline nature of the perfluorocarbon peak chains of the ionomer [25]. The nanocomposite membranes have no new crystallisation peak as observed in Figure 6-16(b) and (c), except a slight shift from the main chain of Nafion® peak at 17°, and was more amorphous, indicating that there is less formation of metal oxide crystalline, as confirmed by the TGA results [71]. The XRD pattern of nanocomposite membranes showed similar patterns when compared to commercial Nafion® membrane with the two diffraction peaks at Bragg angles (2θ) of 17.5° and 39°.

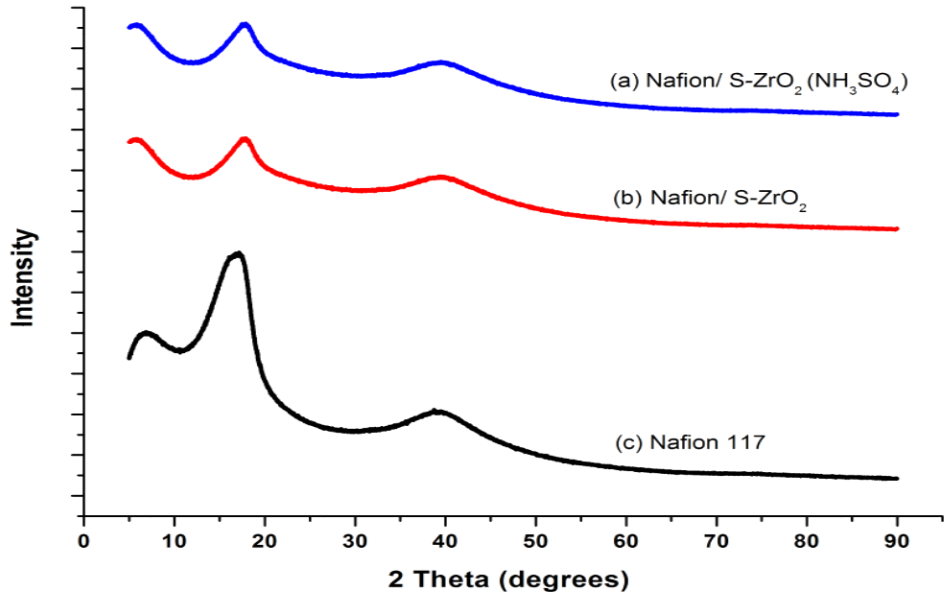

Figure 6-16: XRD patterns of (a) Nafion®/S-ZrO_2 (NH_3SO_4), (b) Nafion®/S-ZrO_2 nanocomposite membranes and (c) Nafion® 117 membrane.

6.8.3. The thermal degradation analysis (TGA) and derivative thermogravimetric (DTG) analysis

Thermal degradation analysis and derivative thermogravimetric analysis of Nafion®/S-ZrO_2 (NH_3SO_4), Nafion®/S-ZrO_2 nanocomposite membranes and Nafion® 117 membrane are shown in Figure 6-17. Figure 6-17(a-c) shows the thermal decomposition occurs in three steps. Figure 6-17(a) shows that Nafion®/S-ZrO_2 (NH_3SO_4) nanocomposite membrane has higher thermal retention as it starts to lose a little weight at a higher temperature of 250 °C, due to the to the decomposition of the sulfonic acid within the membrane [26]. There was no water loss observed. The third weight loss between 450°C and 500 °C is due to the decomposition of membrane backbone [51]. Figure 6-17(b) shows that modified Nafion® membrane with S-ZrO_2 nanoparticles obtained thermal stability at a higher temperature of 335 °C, which is better than commercial Nafion® membrane. The initial weight loss at 335 °C, due to the to the decomposition of the sulfonic acid within the membrane [26]. The initial weight loss of Nafion®/S-ZrO_2 was more improved compared to Nafion®/S-ZrO_2 (NH_3SO_4) nanocomposite membranes as shown in Figure 6-17(b). This may be due to the incorporation of S-ZrO_2 nanoparticles that enhanced water retention within the membrane, which increased to a higher temperature degradation [72] as confirmed by DTG on Figure 6-17(insert). Figure 6-17(b) shows the second weight loss of Nafion®/S-ZrO_2 nanocomposite membrane which starts to decompose at lower temperatures of 380 °C. But the third weight loss starts to degrade at the higher temperature of 570 °C, with the 5wt% of the inorganic materials remaining; this confirms the incorporation of inorganic

nanofiller within Nafion® membrane reduces the high temperature thermal degradation. This may be due to the intermolecular forces between the embedded nanoparticles and the polymer matrix. Figure 6-17b(insert) shows that the DTG curves start degradation at the higher temperature of 570 °C, due to thermal stability of the nanocomposite membrane. Figure 6-17(c) shows that the thermal decomposition of Nafion® 117 membrane also undergoes three stages of weight loss. The initial weight loss occurs at 100 °C due to removal of absorbed water within the membrane, the second weight loss occurs at 380 °C due to the decomposition of membrane, and the third weight loss occurs at 550 °C due to the degradation of polymer [73]. This is also confirmed by DTG curves in Figure 6-17(insert), which shows the degradation of polymer above 500 °C. Zheng et al. also obtained the thermal stability membranes due to the inorganic filler [74]. In conclusion, the nanocomposite membranes were more thermal stable at all stages of decomposition than commercial Nafion® 117 membrane which totally decomposed, due to the nanoparticles that improve the backbones of nanocomposite membranes. Their thermal stability above 250 °C, makes them suitable used for fuel cell application at higher temperature.

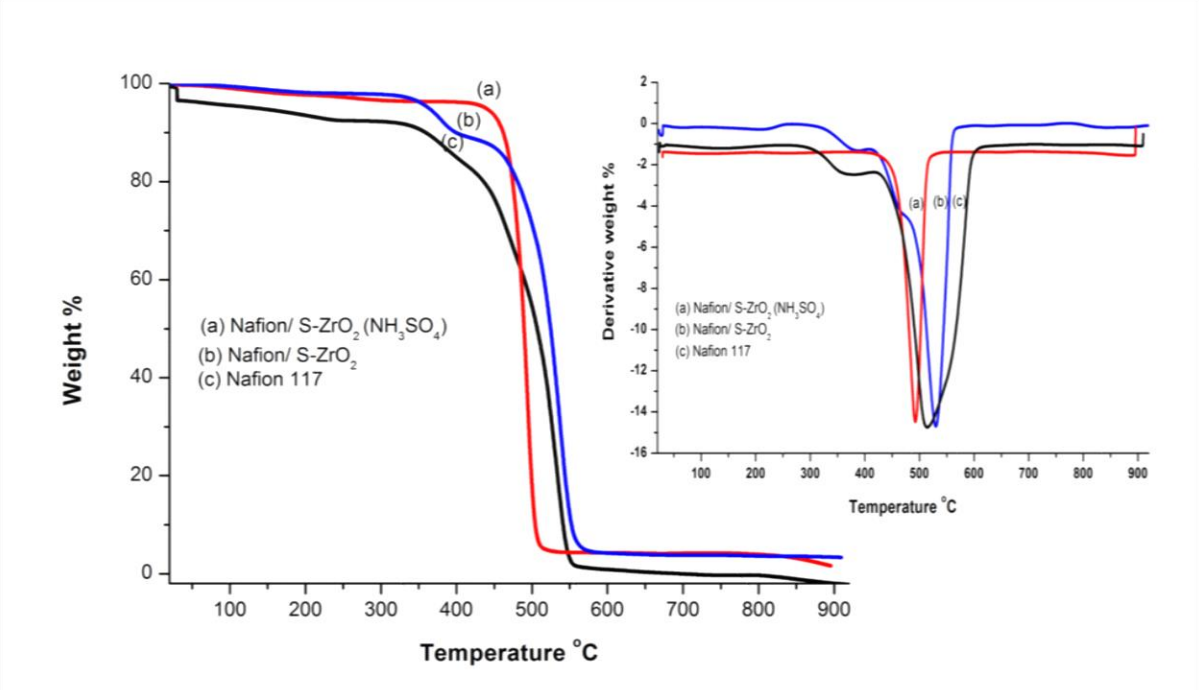

Figure 6-17: The TGA/DTG curves of (a) Nafion®/S-ZrO_2 (NH_3SO_4), (b) Nafion®/S-ZrO_2 nanocomposite membranes and (c) Nafion® 117 membrane.

6.8.4. Morphology

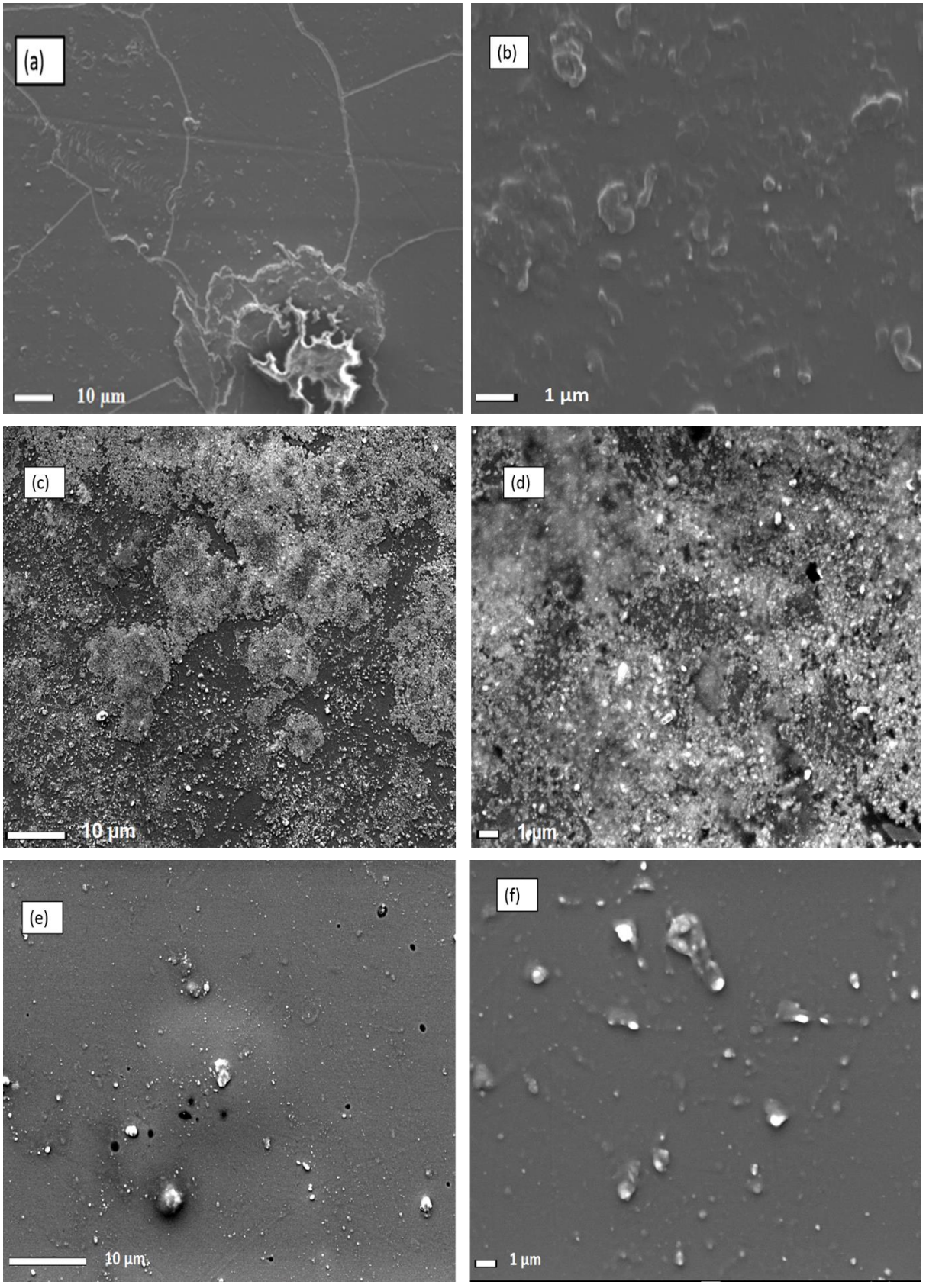

Figure 6-18: Scanning Electron Microscopy (SEM) of (a-b) Nafion®/ S-ZrO_2 (NH_3SO_4), (c-d) Nafion®/ S-ZrO_2 nanocomposite membranes and (e-f) Nafion® 117 membrane.

The surface morphology of Nafion®/S-ZrO_2 (NH_3SO_4), Nafion®/S-ZrO_2 nanocomposite membranes and Nafion® 117 membrane was observed under SEM as shown in Figure 6-18. The results in Figure 6-18(a-b) show that S-ZrO_2 (NH_3SO_4) nanoparticles were successfully impregnated within the Nafion® matrix as they cover the whole surface area of Nafion® membrane. These modified membranes show that the nanoparticles agglomerated to a high diameter of 0.5 µm and were well dispersed within the membrane. This may be due to the method of impregnation, which was repeated five times to ensure that the nanoparticles were successfully impregnated. However, when Nafion® membrane was impregnated with S-ZrO_2 the nanoparticles showed less agglomeration with irregular shape which were well distributed within the membrane as shown in Figure 6-18(c-d). This nanocomposite membrane shows a spongy surface, which endures some holes due to the high magnification. This spongy surface may be due to the good adsorption within the sulfated zirconia as confirmed by higher uptake when compared to commercial Nafion® 117 membrane. Figure 6-18(e-f) shows that commercial Nafion® membrane has a smooth surface without any cracks or holes.

6.8.5. Atomic force microscopy (AFM) analysis

Atomic force microscopy (AFM) was used to measure the roughness of nanocomposite membranes as shown in Figure 6-19. Figure 6-19(a-b) and (c-d) show the amplitude and topography images of Nafion®/S-ZrO_2 (NH_3SO_4) and Nafion®/S-ZrO_2 nanocomposite membranes. The surface roughness of Nafion®/S-ZrO_2 (NH_3SO_4) and Nafion®/S-ZrO_2 nanocomposite membranes was 41.46 nm and 6.59 nm, respectively, which may be due to impregnating S-ZrO_2 nanoparticles in Nafion® membrane. Figure 6-19(c) shows the amplitude image; significant changes are clearly seen due to the incorporation of S-ZrO_2 (NH_3SO_4), which is well interacted with Nafion® membrane [75]. The increased roughness on modified Nafion® nanocomposite membranes improves the contact between the electrodes [76]. Figure 6-19(d) shows that Nafion®/S-ZrO_2 nanocomposite membrane was less rough in the topography images.

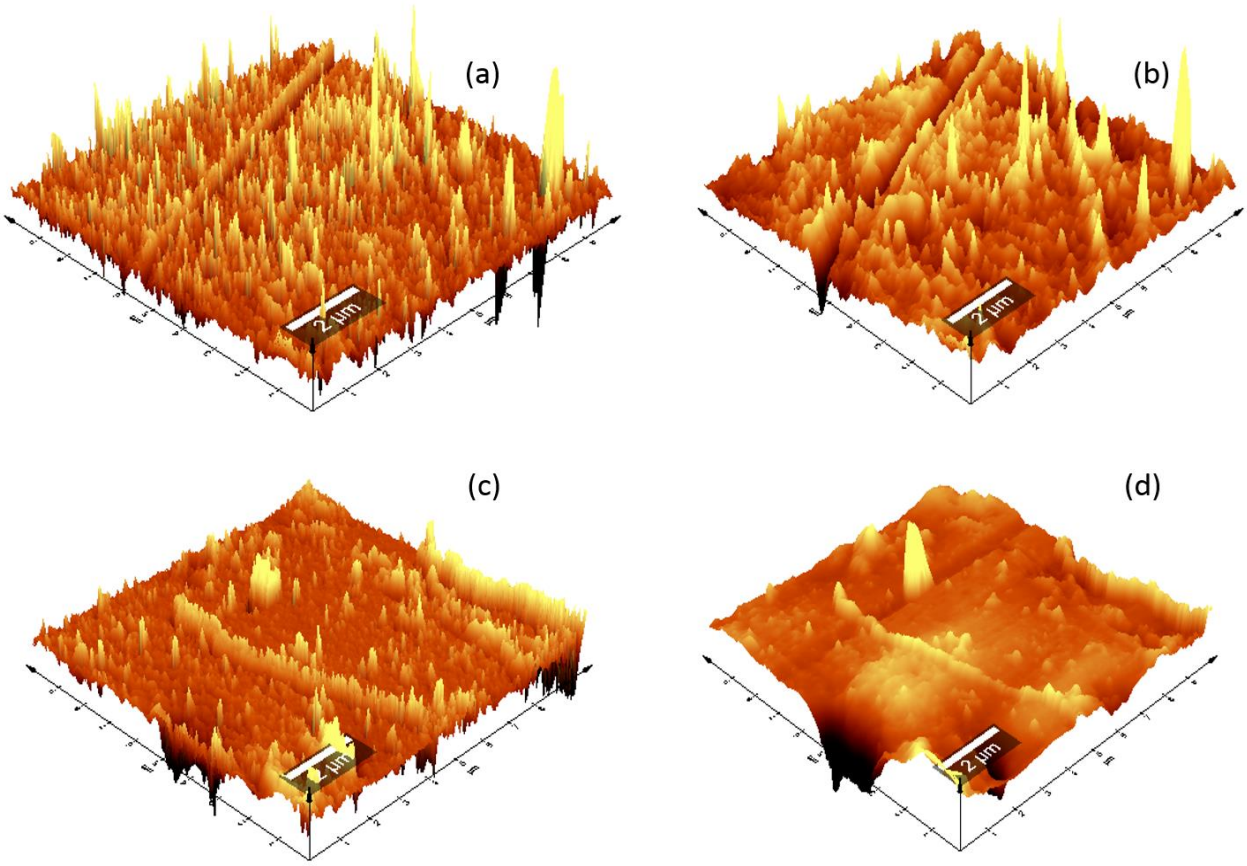

Figure 6- 19: AFM (a-b) amplitude image of Nafion®/S-ZrO_2 (NH_3SO_4) and Nafion®/S-ZrO_2 nanocomposite membranes and (c-d) topography amplitude image of Nafion®/S-ZrO_2 (NH_3SO_4) and Nafion®/S-ZrO_2 nanocomposite membranes.

6.8.6. Water contact angle, water uptake and swelling ratio measurement

Retention of water within the membrane matrix is very important in fuel cell application as it allows the protons ion movement that promotes protonic conductivity of the membrane. This water retention was measured by contact angle as shown in Figure 6-20A. Commercial Nafion® 117 membrane obtained a contact angle greater than 90 °, due to its hydrophobic nature as shown in Figure 6-20A(a) [77]. Figure 6-20A(b) shows that the contact angles of Nafion®/S-ZrO_2 nanocomposite membranes was not constant on one part which is greater than 90 °, whereas the other part was more improved (98 °- 66 °). This may be due to the poor distribution of nanoparticles within the membrane as confirmed by SEM results. Figure 6-20A(c) shows that Nafion®/S-ZrO_2 (NH_3SO_4) nanocomposite membranes obtain contact angles less than 90 ° between 80° - 68°, due to the incorporation of inorganic material that retains water due to its hydrophilic character [58]. Furthermore, the modified membranes show that impregnating inorganic material introduces hydrophilicity in the Nafion® membrane surface. Figure 6-20B and Table 6-2 shows the water uptake of Nafion®/S-ZrO_2, Nafion®/S-ZrO_2 (NH_3SO_4) nanocomposite membranes and commercial Nafion® 117 at 30 °C, 60 °C and

80 °C. As indicated in Figure 6-20B, the water uptake of all the membranes increases with the increase in temperature. Nafion®/S-ZrO_2 (NH_3SO_4) and Nafion®/S-ZrO_2 nanocomposite membranes obtain a higher water uptake (40%, 44%, 47% and 33%, 40%, 44%, respectively) than commercial Nafion® 117 (30%, 32%, 34%) at 30 °C, 60 °C and 80 °C; this may be due to good distribution of hygroscopic S-ZrO_2 nanoparticles that retain water within the membrane matrix as presented in the SEM results. The reason for this may be the impregnation of sulfated zirconia nanoparticles, which introduce the additional acid sites for absorption of water. Moreover, the impregnation of nanoparticles makes clusters in the pore of Nafion® membrane, which results in the higher water uptake of the nanocomposite membrane. The modified membrane with S-ZrO_2 (NH_3SO_4) nanoparticles showed increased water uptake at a higher temperature than modified with S-ZrO_2 nanoparticles as shown in Figure 6-20B. This may be due to the hydrophilic nature of sulfated nanoparticles which increases the surface area and acidity of the nanoparticles that are impregnated within the membranes [78]. The swelling ratio of membranes is an important parameter for proton conductivity, but their dimensional stability must be balanced. since excessive absorbed water often results in serious swelling and loss in mechanical properties [79]. Figure 6-20C shows that the dimensional swelling ratio of all the nanocomposite membranes increases as the temperature increases, which may be due to the water absorption ability in the nanoparticles within the Nafion® membrane pores. As shown in Figure 6-20C, the dimensional swelling ratio for commercial Nafion® 117 membrane was slightly lower than nanocomposite membranes at different temperatures, this may due to the incorporating the nanoparticles within the Nafion matrix that lowers the compatibility and shape-stability of the membrane and thus elevates the swelling ratio of the membrane. These results showed that nanocomposite membranes have dimensional stability. The IEC was used to detect the free sulfonic acid group in the membranes. Figure 6-20D shows that the ion exchange capacity of Nafion®/S-ZrO_2 and Nafion®/S-ZrO_2 (NH_3SO_4) nanocomposite membranes was 1.2 meq-g^{-1} and 1.3 meq-g^{-1}, respectively, which is higher than that of commercial Nafion® 117 (0.93 meq-g^{-1}) [80]. As expected, the incorporation of sulfated zirconia increases the acidic site in the membranes, as the nanocomposite membranes improves in IEC when compared with commercial Nafion® 117 membrane.

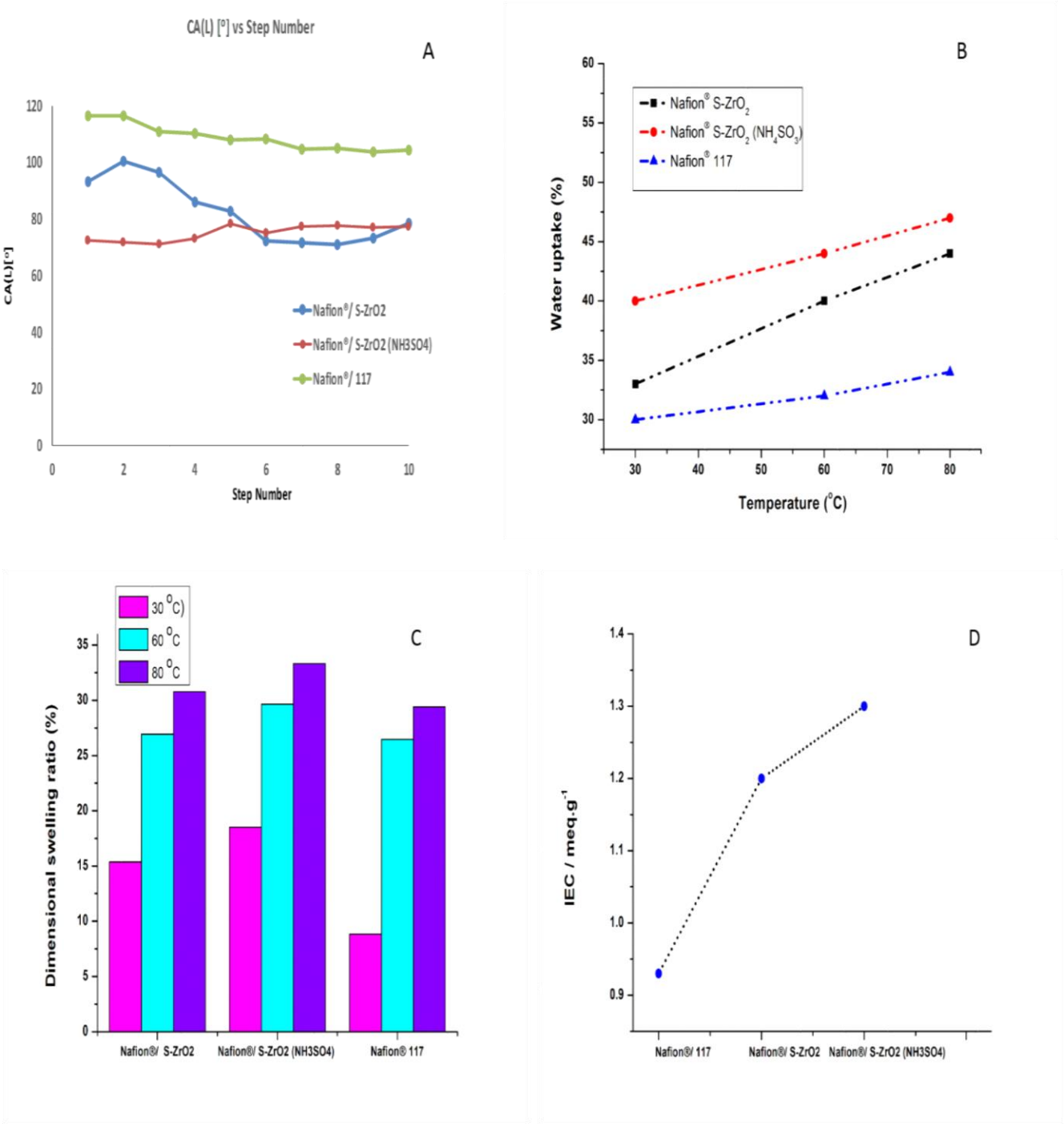

Figure 6- 20: Water contact angle of (A) (a) Nafion® 117 membrane, (b) Nafion®/S-ZrO_2 and (c) Nafion®/S-ZrO_2 (NH_3SO_4) nanocomposite membranes, water uptake (B), linear expansion (C) and IEC (D) of Nafion® 117 membrane, Nafion®/S-ZrO_2 and Nafion®/S-ZrO_2 (NH_3SO_4) nanocomposite membranes.

Table 6- 2: IEC and proton conductivity of Nafion® 117 membrane, Nafion®/S-ZrO_2 and Nafion®/S-ZrO_2 nanocomposite membranes

Membranes	Nafion® 117	Nafion®/S-ZrO_2	Nafion®/S-ZrO_2 (NH_3SO_4)
IEC (meq/g)	0.93	1.2	1.3
Proton conductivity (S/cm) at 25 ºC	0.113	0.146	7.891
Membrane resistances (Ohm)	248	199	3.6840
Membrane thickness (cm)	0.0183	0.0172	0.0172
Water uptake % (30 ˚C)	30	33	40
Water uptake % (60 ˚C)	32	40	44
Water uptake % (80 ˚C)	34	44	47

6.8.7. Methanol permeability

The reduced or low methanol crossover is the major key of DMFC applications, as the methanol crossover can lower the fuel efficiency. The methanol crossover of Nafion® 117 membrane, Nafion®/S-ZrO_2 and Nafion®/S-ZrO_2 (NH_3SO_4) nanocomposite membranes was measured at 30 ˚C, 60 ˚C and 80 ˚C using 2 M and 5 M methanol solution as shown in Figure 6-21. The nanocomposite membranes showed no methanol crossover at a higher concentration of 5 M methanol (60 °C) compared to 8.84 x 10^{-7} cm^2/s for commercial Nafion® 117 membrane as shown in Figure 6-21. This may be due to the impregnation of S-ZrO_2 and S-ZrO_2 (NH_3SO_4) nanoparticles into Nafion® membrane, which reduced the permeation of methanol. Moreover, the well-dispersed nanoparticles may reduce methanol crossover by blocking the methanol from migrating through the membrane [81]. At lower concentration of 2 M methanol, there was no methanol crossover observed for all membranes at different temperatures [82]. The methanol crossover of nanocomposite membranes decreases with the addition of S-ZrO_2 and S-ZrO_2 (NH_3SO_4) nanoparticles, due to the more compact structure. Nafion®/S-ZrO_2 (NH_3SO_4) nanocomposite membranes shows the lower methanol crossover of 1.50 x10^{-7} cm^2/s), that those of Nafion®/S-ZrO_2 nanocomposite membranes (1.31 x 10^{-7} cm^2/s) and commercial Nafion® 117 (1.99 x 10^{-6} cm^2/s). Figure 6-21 (b) shows the selectivity of Nafion® 117 membrane and modified membranes. Selectivity is the ratio of proton conductivity to methanol permeability [83]. Nafion®/S-ZrO_2 (NH_3SO_4) and Nafion/S-ZrO_2 nanocomposite membrane obtained the highest selectivity of 5.24 x 10^7 Ss cm^{-3} and 1.12 x 10^7 Ss cm^{-3}, which is much higher than that of Nafion® 117 (5.68 x 10^4 Ss cm^{-3}) as shown in Figure 6-21 (b). This conclude that nanocomposite membranes, can be suitable use in DMFC.

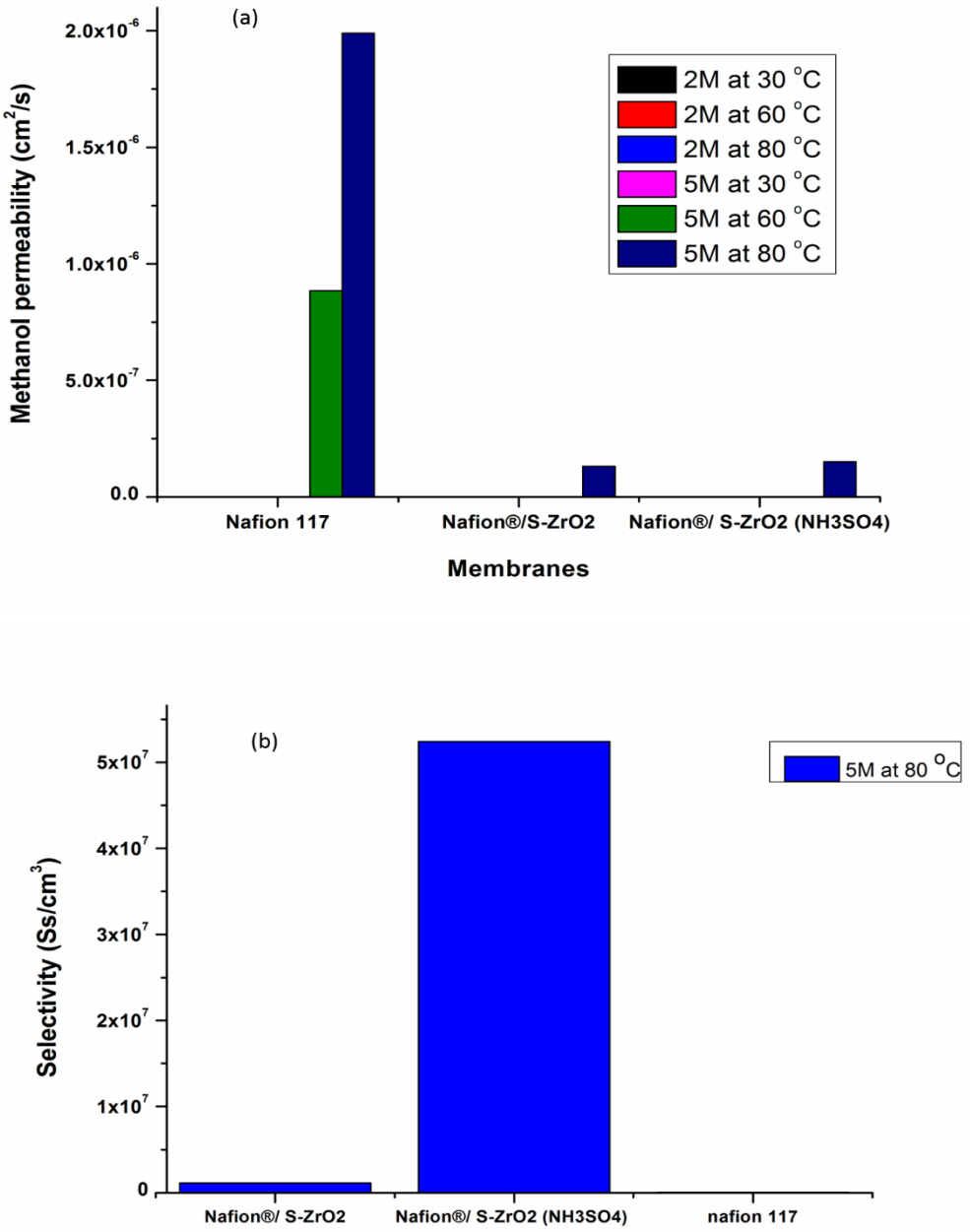

Figure 6- 21: (a) Comparison of methanol crossover (5 M and 2 M concentration) of Nafion® 117 membrane, Nafion®/S-ZrO_2 and Nafion®/S-ZrO_2 (NH_3SO_4) nanocomposite membranes at 30 ˚C, 60 ˚C and 80 ˚C, (b) selectivity ratio of Nafion® 117 membrane, Nafion®/S-ZrO_2 and Nafion®/S-ZrO_2 (NH_3SO_4) nanocomposite membranes at 80 ˚C.

6.8.8. Proton conductivity

The proton conductivity of nanocomposite and commercial membranes is presented in Figure 6-22(a) and Table 6-2. Nafion®/S-ZrO_2 (NH_3SO_4) and Nafion®/S-ZrO_2 nanocomposite membranes show higher proton conductivities of 7.89 S/cm and 0.146 S/cm than Nafion® 117 membrane (0.113 S/cm). The proton conductivity of Nafion®/S-ZrO_2 (NH_3SO_4) nanocomposite

membranes is higher than that of Nafion®/S-ZrO_2 nanocomposite membranes as shown in Figure 6-22(a). This may be due to the incorporation of sulfated zirconia ((S-ZrO_2 (NH_3SO_4)) which enhanced the proton conductivity of Nafion® membrane. Moreover, the proton conductivity of the nanocomposite membranes was enhanced by sulfating zirconia nanoparticles with $(NH_4)_2SO_4$ acid which promotes the migration of sulphonated groups to form cluster aggregates via the strong electrostatic interactions of the Na^+ counter ions. Table 6-2 shows that the proton conductivity of Nafion®/S-ZrO_2 nanocomposite membranes was slightly higher than Nafion® 117 membrane. This may be due to incorporating sulfated zirconia nanoparticles in the membrane, which increases the acid sites and provides extra water within the membrane as was confirmed by the water uptake and TGA results.

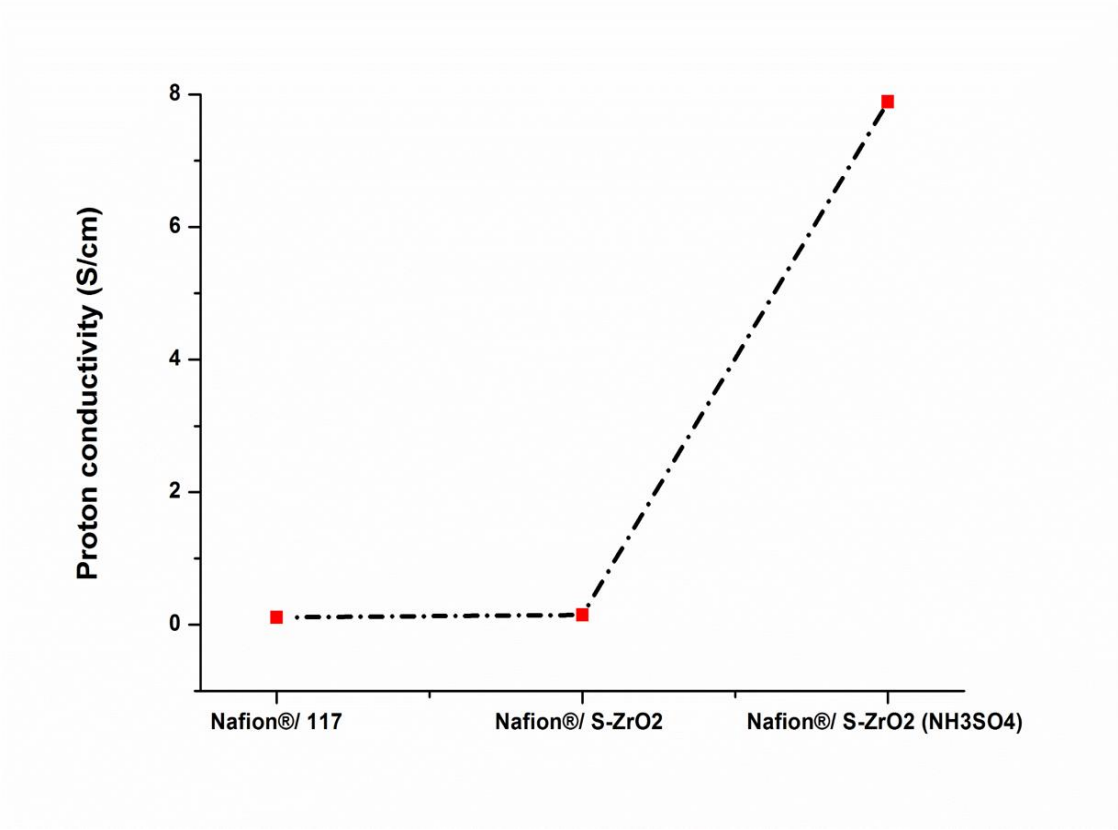

Figure 6- 22: proton conductivity of Nafion® 117 membrane, Nafion®/S-ZrO_2 and Nafion®/S-ZrO_2 nanocomposite membranes.

6.9. Conclusion

The XRD shows that nanocomposite membranes have no new crystallisation peak, except a slight shift from the main chain of Nafion® peak at 17°, and is more amorphous, indicating that there is less formation of metal oxide crystalline. The Nafion®/ S-ZrO_2 (NH_3SO_4) nanocomposite membrane shows higher thermal retention as it starts to lose a little weight at 250 °C, due to the decomposition of the sulphonic acid within the membrane. There was no water loss observed. Modified Nafion® membrane with sulfated zirconia oxide improves the proton conductivity, IEC and membrane swelling, while it prevents the methanol from crossing over. The water uptake was more improved at a higher temperature of 80 °C in nanocomposite membranes. Nafion®/ S-ZrO_2 (NH_3SO_4) nanocomposite membrane shows low fuel crossover at 80 °C and a higher methanol concentration of 5 M. The higher selectivity ratio shows that the synthesised nanocomposite membranes can be used as electrolytes for fuel cell application. Nafion®/ S-ZrO_2 (NH_3SO_4) and Nafion®/ S-ZrO_2 nanocomposite membranes show higher proton conductivities of 7.89 S/cm and 0.146 S/cm than Nafion® 117 membrane (0.113 S/cm). The proton conductivity of Nafion®/S-ZrO_2 (NH_3SO_4) is greater than Nafion®/S-ZrO_2 nanocomposite membranes. This may be due to the incorporation of sulfated zirconia ((S-ZrO_2 (NH_3SO_4)) which enhances the proton conductivity of Nafion® membrane. The higher conductivity can be due to the NH_3SO_4 acid that does not leach out. The membrane resistance of Nafion®/S-ZrO_2 (NH_3SO_4) nanocomposite membrane was lower than that of Nafion® 117 membrane and Nafion®/S-ZrO_2 nanocomposite membrane. This confirms that the lower the resistance, the higher the conductivity. The incorporation of S-ZrO_2 (NH_3SO_4) nanoparticles lowers the resistance of Nafion® membrane. The conclusion is that the sulfated zirconia with NH_3SO_4 acid is suitable as an inorganic filler of Nafion® membrane, due to its higher acidic value which allows the ions movement without reducing the hydration of the membrane but while reducing the methanol crossover.

C: The proton conductivity and mechanical properties of Nafion®/ ZrP nanocomposite membrane

6.10. Introduction

Fuel cell is an electrochemical device, which directly converts chemical energy into an electrical energy by using various fuels such as hydrogen, methanol, ethanol, methylene blue, glucose and natural gas in a reaction with an oxidant (oxygen). DMFCs only utilise methanol as fuel. Nafion® membranes have high proton conductivity, mechanical and chemical stability in its hydrated state and lower temperature, which make them a promising fuel cell electrolyte for transport, portable and stationary application [84-85]. However, at lower relative humidity and higher temperature, Nafion® membranes faces some challenges of higher permeation of methanol and dramatically drops of protons conduction due to their dependence on hydration [49]. That methanol fuel, which crossover through the membrane reduced cell voltage at higher current and oxidised at the cathode [18]. The researches prompt a research on the reduction of methanol crossover and improves the fuel cell performance by modified membrane with hygroscopic oxides or inorganic acids in nanometre-range, which retain water. This hygroscopic inorganic acids such as zirconium phosphate (ZrP) has been used to modify the Nafion® membrane due to their hydrophilic nature, proton conducting material, very low in toxic, inexpensive, not soluble in water and stable in a hydrogen/oxygen atmosphere [15, 86]. Modified Nafion® membrane with ZrP nanofiller found to have a reduced methanol permeability, enhanced proton conductivity and higher power density due to good water retention capabilities and high proton mobility on the surface of ZrP particles [53]. Costamagna et al. obtained stable behaviour on Nafion®/ zirconium phosphate membranes with the electronic current of 1500 mA/cm^2 while compared with Nafion® membrane that sustain an irreversible degradation with the electronic current of 250 mA/cm^2 produced at 0.45 V and 130°C temperature [87-88]. Similarly, Alberti et al. obtained the higher conductivity at 140 °C and 90% relative humidity when modified Nafion® membrane with 10wt% zirconium phosphate compared to pure recast Nafion® membrane [89-90]. Moreover, the modified Nafion® membrane with ZrP obtained a higher proton conductivity and decreased methanol permeability at a higher temperature of 150 °C [46]. Modified Nafion® membrane with ZrP nanoparticles obtained an improvement on the tensile modulus, stiffness and exhibit better fuel cell performance compared to commercial Nafion® 117 membrane under high temperature and low RH conditions [53]. The aim of this work was to synthesis the modified Nafion® 117 membrane by

acidic zirconia that enhance the mechanical strength, water uptake, proton conductivity and reduce the methanol permeability. The stress-strain of Nafion® 117 membrane and Nafion®/ ZrP nanocomposite membrane were observed under 10 mm/s, 20 mm/s, 30 mm/s, 40 mm/s and 50 mm/s.

6.11. Experimental

6.11.1. Materials

Hydrogen peroxide (Merck), Zirconium oxychloride hydrate (Merck), phosphoric acid (Sigma), Sulfuric acid (Merck) and Nafion 117 membrane (Sigma) were used as received.

6.11.2. Synthesis of zirconia phosphates (ZrP)

The zirconia phosphates (ZrP) nanoparticles was prepared by adding 120 mL of 0.4 M $ZrOCl_2 \cdot 8H_2O$ aqueous solution in 6 M solution of phosphoric acid (H_3PO_4) and stirred for 30 minutes. The solution was then refluxed at 80 ºC for further 24 hours while stirring. The obtained material was then centrifuged and washed extensively with distilled water up to pH 3 and dried at 80 ºC and then calcinated it at 600 ºC for two hours.

6.11.3. Preparation of nanocomposite membranes (impregnation method)

Nafion® 117 membranes were treated according to the standard procedure one hour in a boiling 3% solution of hydrogen peroxide; one hour in boiling 0.5 M sulphuric acid; one hour in boiling distilled water [91]. The nanocomposite membranes were prepared by soaking the Nafion® 117 membrane in the methanol solution in order to open the pores of membrane and followed by adding the required amount of ZrP (2.5wt %, 5wt %, 7.5wt %) nanoparticles in methanol solution. The nanocomposite membranes were repeatedly impregnated (up to five times) at room temperature [23]. The air from the nanocomposite membrane pores was removed by heating the solution for 2 hours up to 100 °C, then slowly cooled down to room temperature and kept in solution for further 24 hours. After drying, thicknesses of the nanocomposite membranes were measured with digital micrometre (0.18 mm). Each thickness was measured in the average of 3-7 reading at different position of membrane and was repeated twice on each membrane to obtain the average value.

6.11.4. Characterisations

The X-ray diffraction (XRD) analysis was performed through X-ray diffraction with Cu K radiation source and the samples were scanned in a continuous mode from 10°–90°. The thermal properties and the characteristics of the samples were studied by thermal gravimetric analysis (TGA) under nitrogen flow. TGA data was obtained using TGA instrument (PerkinElmer) over nitrogen and at a heating rate of 10° C/min from 28° C to 1000° C. the surface morphologies of all the membrane were studied using Scanning Electron Microscopy (SEM). Fourier-transform infrared spectroscopy (FTIR) was employed to investigate the changes in the chemical structure of the membrane.

6.11.5. Tensile test

The uniaxial mechanical properties of nanocomposite membranes and recast membrane were captured by using a uniaxial testing system. The length, width and thickness of samples were measured by using a Vernier caliper and recorded prior to testing. The testing area of the membrane samples were 4 mm x 10 mm in dimension. To allow a clamping area, the sample was prepared in such a way that they will be clamped both sides and still allow the testing area to be 4 mm x10 mm. The length, width and thickness of samples were measured with a Vernier caliper and recorded prior to testing. The thickness of 0.18 mm of the nanocomposite membranes was used to analyse the stress applied to the sample. The tensile strength of modified Nafion® membranes were measured by using a CellScale Ustretch device at 25 °C at the actuator speed of 10 mm/s, 20 mm/s, 30 mm/s, 40 mm/s and 50 mm/s.

6.11.6. Water uptake (WU) and swelling ratio (SR)

The membranes were soaked in distilled water for one day at 30 ºC, 60 ºC and 80 ºC temperature. Then was removed, wiped, measured and weighed. Water uptake and dimensional swelling ratio were calculated according to the equations below:

$$\boldsymbol{W_{up}}(\%) = \frac{(\boldsymbol{m_{wet}} - \boldsymbol{m_{dry}})}{\boldsymbol{m_{dry}}} \boldsymbol{X100} \qquad (6\text{-}8)$$

$$\boldsymbol{SR}(\%) = \frac{(\boldsymbol{L_w} - \boldsymbol{L_d})}{\boldsymbol{L_d}} \boldsymbol{X100} \qquad (6\text{-}9)$$

Where W_{up} is the percentage of water uptake, m_{wet} is the weight of wet membrane and m_{dry} is the weight of the dried membrane, L_w is the length of the wet membrane and L_d is the length of the dried membranes.

6.11.7. Ion exchange capacity (IEC)

Ion exchange capacity (IEC) of nanocomposite membranes and commercial Nafion® 117 membrane was determined by titration method:

$$\mathbf{IEC} = \frac{\mathbf{V_{NaOH}\ X\ C_{NaOH}}}{\mathbf{W_{sample}}} \qquad (6\text{-}10)$$

Where V_{NaOH} is the titrated volume of NaOH and W_{sample} is the weight of the dry membranes.

6.11.8. Methanol permeability measurements

The methanol permeability was measured with a permeation-measuring cell designed in our lab that consisted of two compartments. The membrane was placed in the middle of two compartments, and the diameter of the diffusion area was 3.5 cm. The membrane was placed in the middle of two compartments, and the diameter of the diffusion area was 3.5 cm. The compartment (A) was filled with a methanol solution of 50 ml and compartment (B) was filled with 50 ml of distilled water. The solutions were prepared in 2 M and 5 M methanol and the results collected at 30 ºC, 60 ºC and 80 ºC within three hours for comparison. The methanol concentration sensor was used to monitor the methanol concentration in compartment B. The output signal was converted by a data module and recorded by a personal computer. Methanol permeability (P) was obtained by means of the following relationship:

$$\mathbf{CB} = \frac{\mathbf{A\ P}}{\mathbf{VB\ L}}\ \mathbf{CA}\ (\mathbf{t} - \mathbf{t0}) \qquad (6\text{-}11)$$

where C_A is the concentration of initial methanol in compartment A; C_B the concentration of methanol in compartment B at diffusion time t; V_B the volume of distilled water in compartment B; L the membrane thickness; and A the effective permeating area.

6.11.9. Conductivity measurement

The conductivities of all membranes were measured using a four-point probe conductivity cell. The ionic conductivity was determined galvanostatically with a current amplitude of 0.1 mA over frequencies ranging from 1MHz to 10Hz. Using a Bode plot, the frequency region over which the impedance had a constant value was checked and the electrical resistance was then obtained from a Nyquist plot [44]. The ionic conductivity (σ) was calculated according to the following equation:

$$\sigma = \mathrm{L}/\mathrm{RS} \qquad (6\text{-}12)$$

where R is the obtained membrane resistance, L is the thickness of membrane and S is the membrane area normal to the current flow.

6.12. Results and discussion

6.12.1. Fourier Transform Infrared (FTIR) analysis

Zirconia phosphate (ZrP) nanoparticles were successfully impregnated within the Nafion® matrix and the structural combination was confirmed by FTIR spectroscopy as indicated in Figure 6-23. Figure 6-23 shows the spectra of Nafion®/ ZrP nanocomposite membranes and commercial Nafion® 117 membrane in the range of 400-4000 cm^{-1}. The band at 3456 cm^{-1} in Figure 6-23(a-d) shows the O-H stretching vibration corresponding to physically adsorbed water [48-49] and 1630 cm^{-1} due to O-H bending vibration. It was observed that the ZrP bands at 797 cm^{-1}, 509 cm^{-1} and 446 cm^{-1} corresponds to stretching peaks of Zr–O and $P–O_4$ as indicated in Figure 6-23(a-c) [92]. Figure 6-23(b) shows the vibration peak at 1016 cm^{-1} and the peak at 1550 cm^{-1} due to Zr-OH bending vibrations, indicating the presence of zirconia nanoparticles within the modified Nafion® membrane [32]. The stretch vibrations between 2925 and 2865 cm^{-1}, are attributed to the C–H stretching of the modified Nafion® in Figure 6-23(a-b) [93]. The band at 1060 cm^{-1}, due to symmetric S-O stretching as shown in Figure 6-23(a-d) [94]. Figure 6-23(a-d) shows the band at 1145 cm^{-1}, due to symmetric C-F stretching and a band at 1201 cm^{-1}, due to asymmetric C-F stretching [30, 94]. The peaks observed at 976 cm^{-1} in Figure 6-23(a-d) attributed to the C-O-C stretching [94]. The band at 512 cm^{-1} is attributed to symmetric O-S-O bending and the band at 632 cm^{-1} is assigned to the stretching of C-S groups [94]

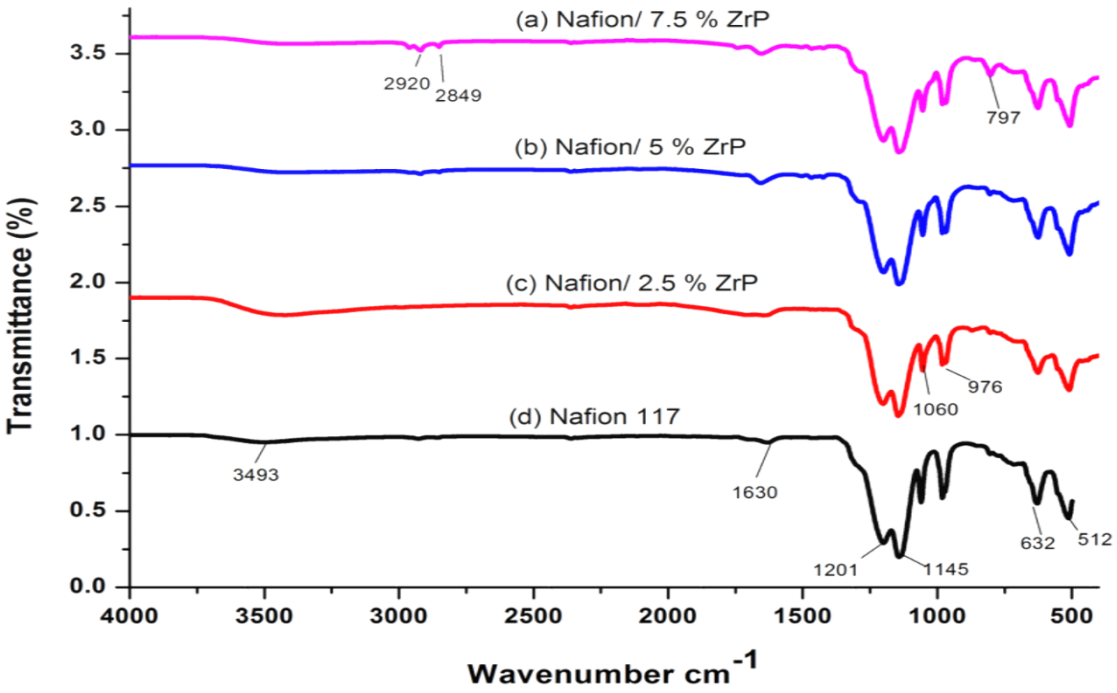

Figure 6- 23: FTIR spectra of (a) Nafion®/ 7.5% ZrP, (b) Nafion®/ 5% ZrP, (c) Nafion®/ 2.5% ZrP nanocomposite membrane and (d) Nafion® 117 membrane.

6.12.2. Scanning electron microscopy (SEM)

Figure 6-24 shows SEM surface morphologies of the Nafion® 117 membrane and Nafion®/ ZrP nanocomposite membranes. Figure 6-24(a) shows the plain Nafion® 117 membrane, which is dark in colour without nanoparticles. The SEM image of Nafion®/ 7.5% ZrP nanocomposite membrane in Figure 6-24(b) shows ZrP nanoparticles are well distributed within the membrane matrix with less agglomeration. When 5% of ZrP is added in Nafion® membrane, the nanoparticle is well distributed within the membrane matrix as shown in Figure 6-24(c). This SEM image in Figure 6-24(c) shows that ZrP nanoparticles within the membrane are uniform in shape but less visible than when 7.5% ZrP is added. Figure 6-24(d) shows the addition of 2.5% ZrP nanoparticles obtained the well distributed within the membrane matrix but with less visible when compared to the higher percentages added in the membrane. Figure 6-24(e-f) shows the SEM image of ZrP nanoparticles in 1µm and 100 nm, respectively. ZrP nanoparticles agglomerated together in the spherical shape with particle sizes around 100 nm as observed in Figure 6-24(e-f). In conclusion, the results show that, when 7.5% ZrP nanoparticles has been used as nanofiller, ZrP is well distributed within the membrane matrix and well visible.

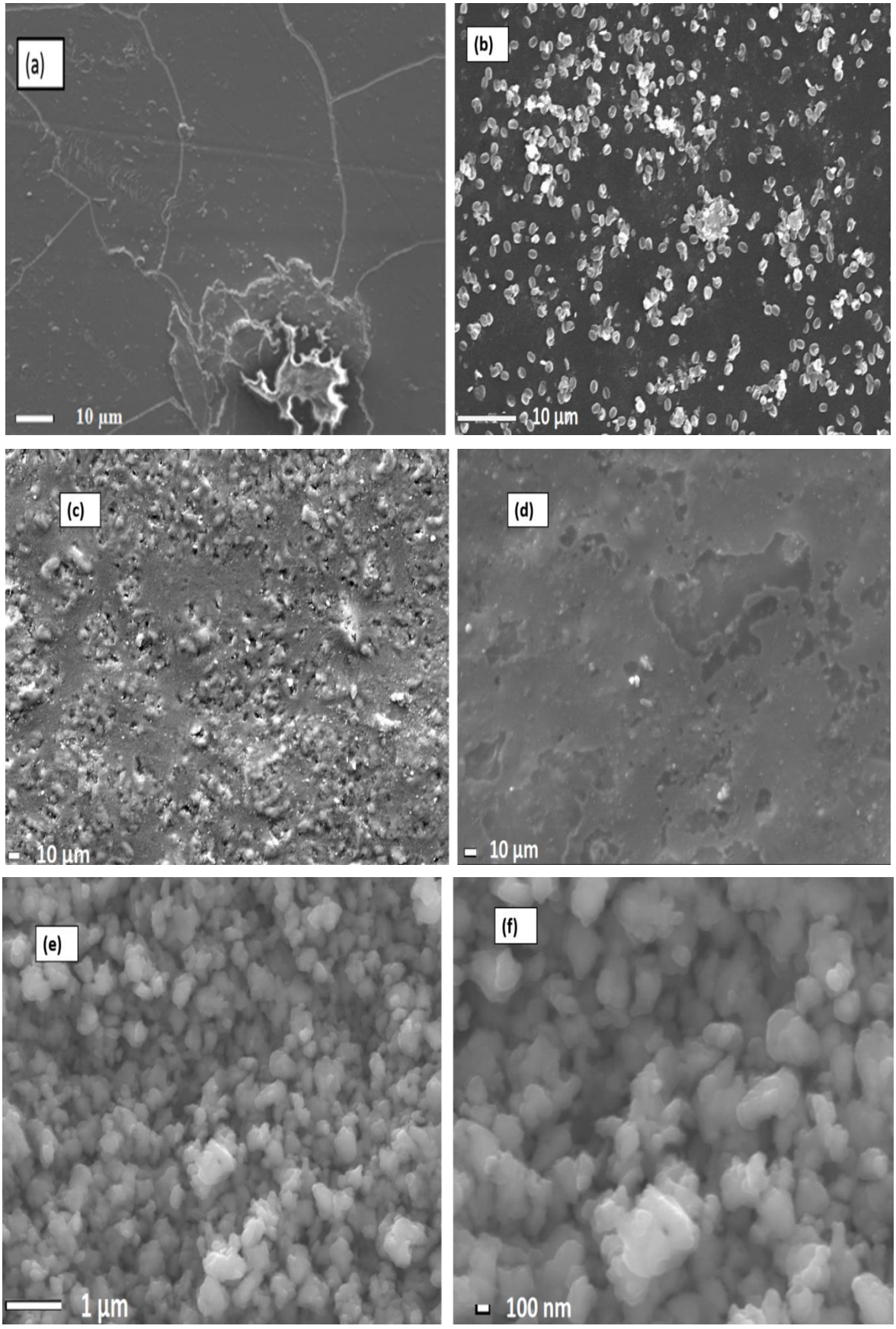

Figure 6- 24: **(a)** SEM micrograph of (a) Nafion® 117 membrane, (b) Nafion®/ 7.5% ZrP, (c) Nafion®/ 5% ZrP, (d) Nafion®/ 2.5% ZrP nanocomposite membranes and (e-f) ZrP nanoparticles (1 µm and 100 nm).

6.12.3. Structure analysis

The X-ray diffraction (XRD) pattern of the modified Nafion® and commercial membranes were observed as shown in Figure 6-25. As shown in Figure 6-25(d), Nafion® 117 membrane has two diffraction peaks at 17.5° and 39° 2θ, which can be attributed to semi crystalline of the perfluorocarbon chains of the ionomer [25]. Figure 6-25(a-c) shows that modified Nafion® 117 membrane with ZrP nanoparticles has a little effect on the crystallinity as it reassembles the same peaks with Nafion® 117 membrane at 17.5° and 39° 2θ. Nevertheless, with a slight shift from the main chain of Nafion® peak at 17 ° and more amorphous indicating that there is a less formation of metal oxide crystalline, as confirmed by TGA and SEM results [71].

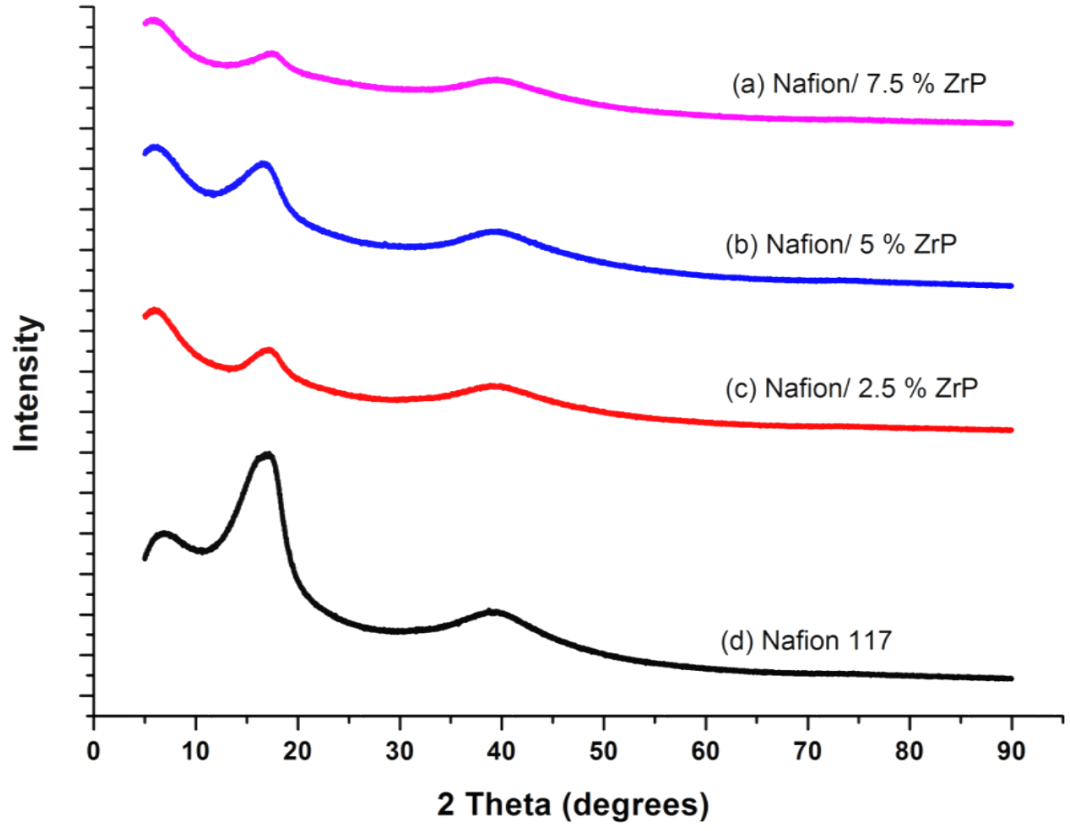

Figure 6- 25: XRD patterns of (a) Nafion®/ 7.5% ZrP, (b) Nafion®/ 5% ZrP, (c) Nafion®/ 2.5% ZrP nanocomposite membrane and (d) Nafion® 117 membrane.

6.12.4. Thermo-gravimetric analysis (TGA)

The thermal degradation of nanocomposite membranes compared to the recast Nafion® were observed under thermal gravimetric analysis (TGA) and derivative thermogravimetric (DTG) as indicated in Figure 6-26 below. In Figure 6-26, it was observed that the membrane

undergoes three weight-loss stages. The commercial Nafion® 117 membrane starts to lose weight at lower temperature of 100 °C that corresponding to the adsorption of water bonded to the sulfonic groups as shown in Figure 6-26 [73]. The second weight loss is attributed to the degradation of the sulfonic groups of Nafion® membrane that starts at 380 ˚C [26]. The third weight loss was assigned to degradation of the polymer backbone chain [29]. However, Nafion®/ 7.5 wt% ZrP nanocomposite membrane starts to lose weight at temperature of 150 ˚C that corresponds to the adsorption of water bonded to the sulfonic groups. The second weight loss is attributed to the decomposition of the sulfonic acid groups of Nafion® membrane that starts at 490 °C as shown in Figure 6-26(b) [26]. The modified Nafion® /7.5 wt% ZrP membrane showed improved thermal degradation at high temperature of 490 °C that may be due to the nature of inorganic filler whereas the commercial Nafion® 117 starts to decompose at 380 ˚C [95]. The third weight loss was assigned to degradation of the polymer main chain [29]. The Nafion®/ 7.5%wt ZrP, Nafion®/ 5%wt ZrP and Nafion®/ 2.5%wt ZrP nanocomposite membranes showed thermal stability up to 340 °C whereas Nafion® 117 membrane showed a thermal stability up to 240 °C as shown in Figure 6-26 (DTG insert). This may be due to the presence of water retention zirconia nanoparticles within Nafion® membrane [47], which reduce the weight loss rate while also increasing the decomposition temperature of the nanocomposites in high temperature. The thermal stability improvement shows that the enhanced potential of the zirconia nanocomposite membrane for higher temperature operations for PEMFC applications. The DTG curves (insert graph) of Nafion® 117 membranes showed two peaks of decomposition, similarly, the DTG curves of the modified Nafion® membrane with 5% ZrP and 2.5% ZrP nanoparticles also showed two peaks, as appeared in Figure 6-26(insert), with the decomposition rate of 5% per °C at 380 °C. The modified Nafion® membrane with 7.5% ZrP nanoparticle showed a higher thermal stability than the commercial Nafion® 117 as shown in Figure 6-26 (insert), which makes them suitable to be used in fuel cell application.

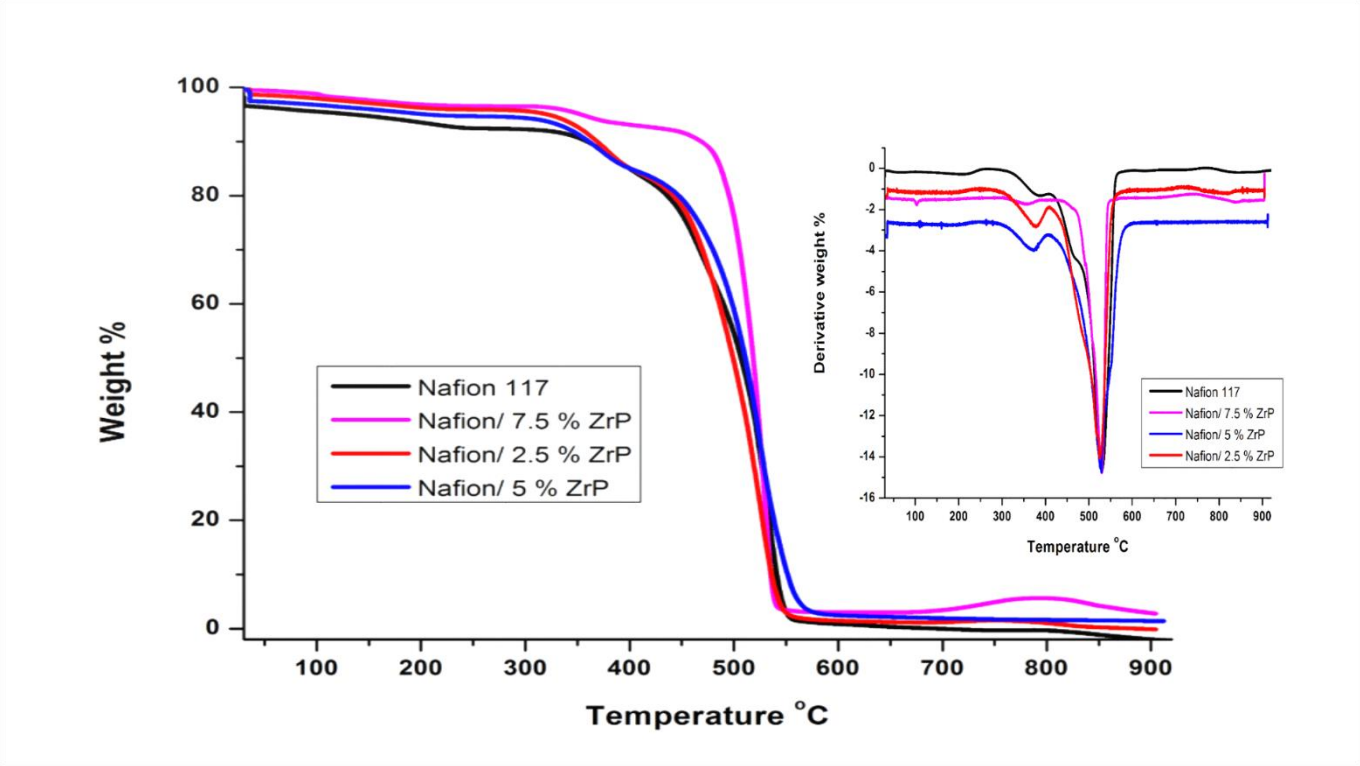

Figure 6- 26: The comparison of the TGA/ DTG curves of Nafion®/ 7.5% ZrP, Nafion®/ 5% ZrP, Nafion®/ 2.5% ZrP nanocomposite membrane and Nafion® 117 membrane.

6.12.5. Tensile test

Figure 6-27 shows the stress-strain curves of the commercial Nafion® 117 membrane compared with Nafion®/ 2.5% ZrP, Nafion®/ 5% ZrP and Nafion®/ 7.5% ZrP nanocomposite membrane at 10 mm/s, 20 mm/s, 30 mm/s, 40 mm/s and 50 mm/s. The stress rate of 10 mm/s, 20 mm/s, 30 mm/s, 40 mm/s and 50 mm/s show the elasticity and flexibility of the commercial Nafion® membrane at 0.6 stress versus strain as shown in Figure 6-27(a). Figure 6-27(b-c) shows that when increasing the strain rate to 50mm/s decreases the tensile stress, whereas when the strain rate decreases to 30mm/s increasing the tensile stress to 1737 kPa and 1790 kPa, respectively, this may due to the percentage of ZrP nanoparticles deposited in the membrane. The stress-strain of 10 mm/s, 20 mm/s and 40 mm/s were merely affected by varying the strain rate values, as there was no difference on their tensile strain. Furthermore, the stress-strain of the Nafion®/ 7.5 ZrP nanocomposite membranes were higher than Nafion® 117 membrane at a strain rate of 50 mm/s were 1737 kPa and 947 kPa, respectively as shown in Figure 6-27(d). Whereas some of the strain rate of nanocomposites membrane shows a lower strain of 3.7 and 4.9, but with a higher stress than commercial Nafion® 117 membrane, which may be due to compatibility of nanoparticles within the Nafion® matrix. Moreover, the stress-strain of the nanocomposite membrane were higher than Nafion® 117 membrane. Generally, the results showed that the modification of Nafion® membrane with zirconia

phosphates has an impact on the tensile strength of the membrane, which is good properties for DMFC [96]. However, the stress-strain of modified membrane with the higher percentage of ZrP nanoparticles is not compactible for the lower stress rate as it reduces the elasticity and mechanical properties, which shows the elastic in the entire stress rate as shown in Figure 6-27(d). This may due to the high percentages of ZrP nanoparticles introduced within the Nafion® matrix that can cause the brittle fracture in the modified membrane.

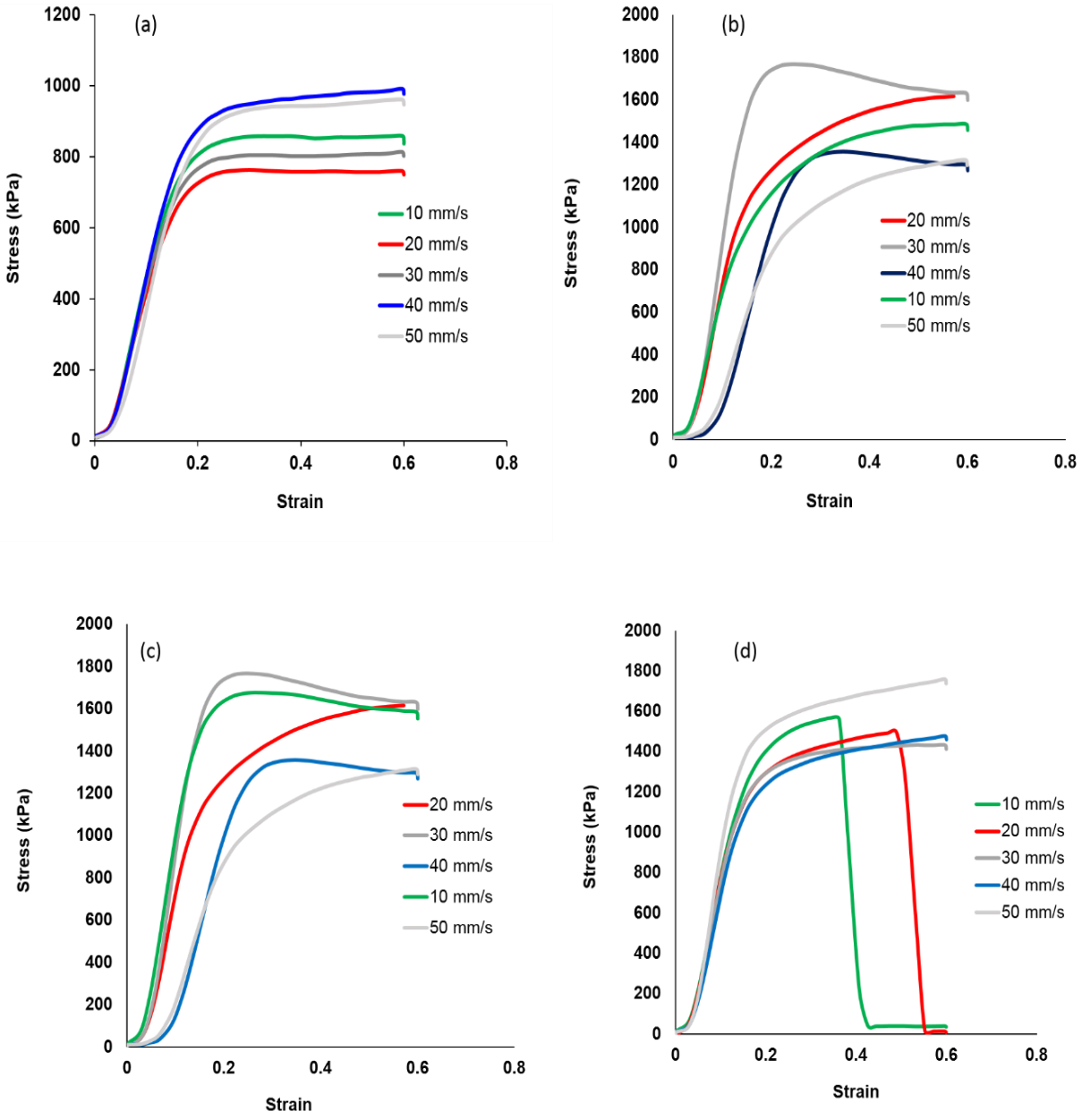

Figure 6- 27: Mechanical tensile tests results of (a) Nafion® 117 membrane, (b) Nafion®/ 2.5% ZrP, (c) Nafion®/ 5% ZrP and (d) Nafion®/ 7.5% ZrP nanocomposite membranes shows stress versus strain ratio curve.

6.12.6. Methanol permeability

Figure 6-28 presented the methanol permeability of composited Nafion® membranes with 2.5% ZrP, 5% ZrP and 7.5% ZrP nanoparticles compared to commercial Nafion® membrane is presented in Figure 6-28. Figure 6-28(a) shows that the methanol permeability of nanocomposite membrane was lower than that of commercial Nafion® membrane; this may be due to ZrP nanoparticles added to Nafion® membrane that improve the barrier properties of Nafion® membrane towards methanol. Table 6-3 shows the methanol permeability measured at different temperatures of 30 °C, 60 °C and 80 °C and methanol concentration of 2 M and 5 M. As we know, the decrease of the methanol concentration can reduce the methanol crossover [97], which is due to the decreased concentration gradient. Therefore, we also used a higher concentration of 5 M methanol solution. Figure 6-28(a) shows that the methanol permeability of Nafion®/ ZrP nanocomposite membranes measured at 60 °C were 0 cm^2/s (no crossover) when compared to 8.84 10^{-7} cm^2/s of commercial Nafion® 117 membrane. Figure 6-28(a) shows that the methanol permeability of modified and unmodified Nafion® membranes increases as the temperature increases. The results show that Nafion®/ ZrP nanocomposite membranes obtain a lower methanol permeation when the temperature rise to 80 °C, which indicate that there is more water permeation at high temperature than methanol. This temperature rise leads to a strong rise of the methanol permeation in commercial Nafion® 117 membrane. The methanol permeability for Nafion®/ 2.5% ZrP Nafion®/ 5% ZrP and Nafion®/ 7.5% ZrP nanocomposite membranes and Nafion® 117 membranes are 1.66×10^{-6} cm^2/s, 1.55×10^{-6} cm^2/s, 1.42×10^{-6} cm^2/s and 1.99×10^{-6} cm^2/s, respectively as shown in table 6-3. The modified Nafion® membrane with ZrP nanoparticles shows a slight decrease of methanol permeability when compared to Nafion® 117 membrane, due to zirconia phosphates nanoparticles that blocked the methanol crossover within the Nafion® matrix. The results show that the methanol permeation in the nanocomposite membranes decrease with the amount of ZrP nanoparticles added. Moreover, the modified Nafion® nanocomposite membranes seem to be the promising electrolytes for fuel cell application when compared with the commercial Nafion® 117 membrane.

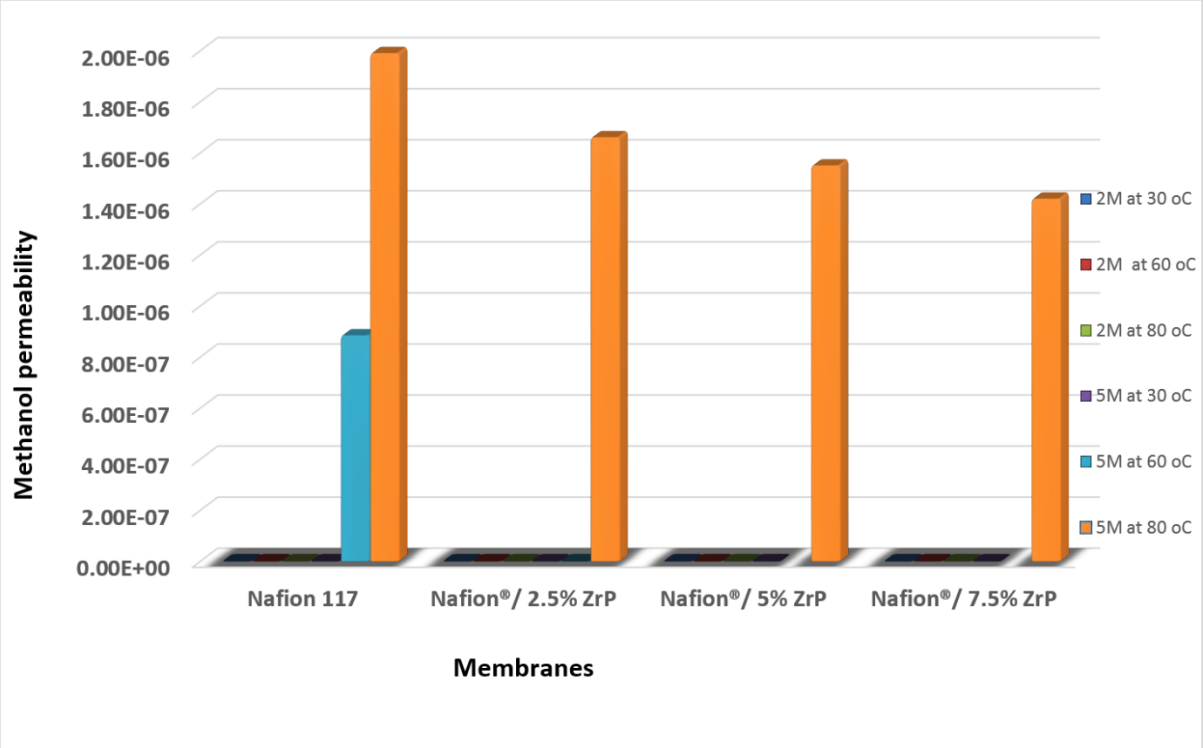

Figure 6- 28: Comparison of methanol crossover (5M and 2M concentration) of Nafion® 117 membrane, Nafion®/ 2.5% ZrP, Nafion®/ 5% ZrP and Nafion®/ 7.5% ZrP nanocomposite membranes at 30 °C, 60 °C and 80 °C.

Table 6- 3: The methanol permeability for Nafion® 117 membrane, Nafion®/ 2.5% ZrP, Nafion®/ 5% ZrP and Nafion®/ 7.5% ZrP nanocomposite membranes at 30 °C, 60 °C and 80 °C

Methanol solutions	**2M**	**2M**	**2M**	**5M**	**5M**	**5M**
Temperature	**30 °C**	**60 °C**	**80 °C**	**30 °C**	**60 °C**	**80 °C**
Nafion 117	-	-	-	-	8.84E-07	$1.99E^{-06}$
Nafion®/ 2.5% ZrP	0	0	0	0	0	$1.66E^{-06}$
Nafion®/ 5% ZrP	0	0	0	0	0	$1.55E^{-06}$
Nafion®/ 7.5% ZrP	0	0	0	0	0	$1.42E^{-06}$

6.12.7. Water uptake, dimensional swelling ratio, Ion exchange capacity and proton conductivity measurement

Figure 6-29(a) shows the water uptake of commercial Nafion® 117 membrane, Nafion®/ 2.5%, ZrP Nafion®/ 5% ZrP, and Nafion®/ 7.5% ZrP nanocomposite membranes. The effect of ZrP nanofiller in the water uptake of nanocomposite membranes were observed. The nanocomposite membrane shows the higher water-uptake whereas the commercial Nafion® 117 membrane has obtained the lower water uptake as indicated in Figure 6-29(a). The Nafion®/ 2.5% ZrP, Nafion®/ 5% ZrP and Nafion®/ 7.5% ZrP nanocomposite membranes obtained a higher water uptake of 41 %, 49 % and 53 % when compared to Nafion® 117 membrane (34%) at 80 °C, which may be due to inorganic fillers distributed on the pores of swollen membrane to increase the hydrophilic nature of Nafion® [58]. Incorporating of zirconia phosphates nanoparticles increases the water retention within the nanocomposite membranes which resulted also in increasing the proton conductivity due to the increases of exchange sites available per cluster which is an important parameter of fuel cells in order to operate on higher temperature [85]. Generally, the water uptake of the nanocomposite membranes increases with the increases of ZrP weight content within Nafion® 117 membranes, which may be due to the hydrophilicity of nanoparticles that adsorbed on the surface of membrane to introduce the hydrophilicity of modified membrane surface. The dimensional swelling ratio at 30 °C, 60 °C and 80 °C shows a slightly increased with the increases in wt% of ZrP nanoparticles within the membrane as shown in Figure 6-29(b). However, when Nafion®/ 7.5% ZrP nanocomposite membrane soaked at higher temperature of 80 °C obtain a higher dimensional swelling ratio of 44%, this may due to the absorbed water within the membrane matrix.

The Ion exchange capacity (IEC) and proton conductivity of Nafion® 117 membrane, Nafion®/ 2.5% ZrP, Nafion®/ 5% ZrP and Nafion®/ 7.5% ZrP nanocomposite membranes are shown in Table 6-4. The proton conductivity of the Nafion®/ 7.5% ZrP and Nafion®/ 5% ZrP nanocomposite membranes (0.011 S cm^{-1} and 0.013 S cm^{-1}) at 30 ^{o}C were slightly lower than Nafion® 117 membrane (0.015 S cm^{-1}) as shown in Figure 6-29(d) and Table 6-4, this may be due to inorganic particles within the Nafion® matrix. The results show that introducing the zirconia phosphate nanoparticles in the membrane decreases the proton conductivity at lower temperature [73, 98]. Whereas the water uptake of the modified Nafion® membrane was higher than unmodified Nafion® membrane as shown in Figure 6-29(a). The conductivity at 80 °C and 70% RH, found to be higher than that measured at 30°C and 60°C, due to the increases of temperature, which increases the conductivity as shown in Table 6-4 and Figure 6-29(d) [99]. The results in Table 6-4 and Figure 6-29(c) shows that nanocomposites membranes obtained a higher IEC value of 1.42 meg. g^{-1}, 1.46 meg. g^{-1} and 1.68 meg. g^{-1}, respectively when

compared to 0.93 meg. g^{-1} of commercial Nafion® membrane. These may due to the incorporation of Zrp nanoparticles, which increased the membrane acid property for providing new strong acid site. The results in Figure 6-29(c) shows that the IEC of the nanocomposites increases with the increases in wt.% of ZrP nanoparticles within the membrane.

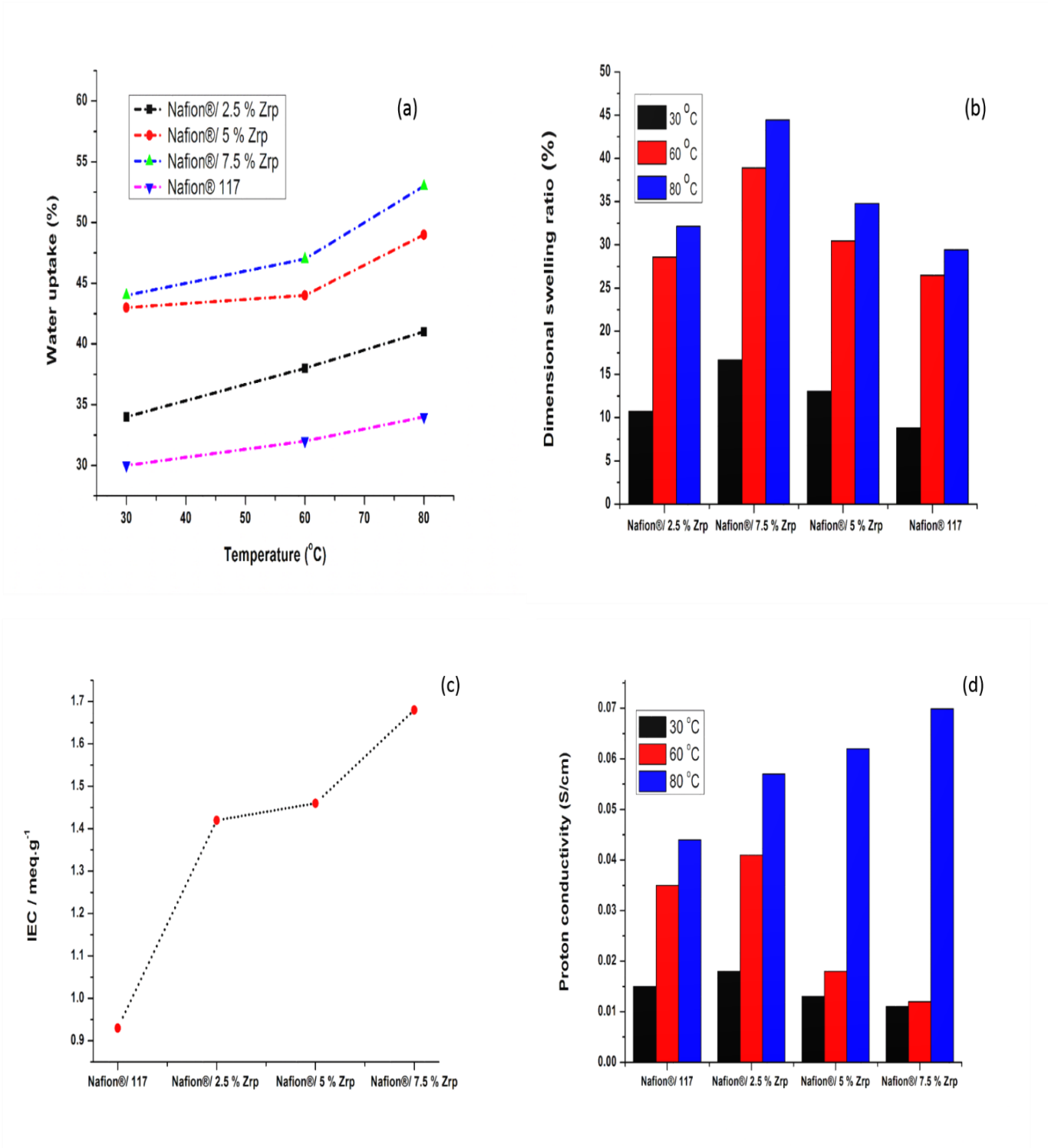

Figure 6- 29: Water uptake (a), linear expansion (b), Ion exchange capacity (c) and proton conductivity measurement(d) of Nafion®/ 2.5% ZrP, Nafion®/ 5% ZrP, Nafion®/ 7.5% ZrP nanocomposite membranes and Nafion® 117 membranes.

Table 6- 4: The IEC and proton conductivity of Nafion® 117 membrane, Nafion®/ 2.5% ZrP, Nafion®/ 5% ZrP and Nafion®/ 7.5% ZrP nanocomposite membranes at 30 °C, 60 °C and 80°C at 70% RH

Membranes	**Proton conductivity (S/cm) at 30 °C**	**Proton conductivity (S/cm) at 60 °C**	**Proton conductivity (S/cm) at 80 °C**	**IEC**
Nafion® 117	0.015	0.035	0.044	0.93
Nafion®/ 2.5 % ZrP	0.018	0.041	0.057	1.42
Nafion®/ 5 % ZrP	0. 013	0.018	0.062	1.46
Nafion®/ 7.5 % ZrP	0.011	0.012	0.0699	1.68

6.13. Conclusion

The preparation of the Nafion/ ZrP nanocomposite membrane with higher proton conductivity and reduced methanol permeability was successfully achieved by the impregnation method. The thermal stability of the nanocomposite membrane started to decompose at high temperature of 450 ºC that may be due to the nature of an inorganic filler. When compared to the commercial Nafion® 117 that starts to decompose at lower temperature of 380 ºC, which makes them possible to be used for fuel cell application. Moreover, the water uptake, IEC, swelling ratio of nanocomposite membranes were higher than Nafion® 117 membrane at 80 ºC. The results show the decrease of methanol permeability of modified Nafion® membrane at higher temperature of 80 ºC and 5 M methanol concentration compared to Nafion® 117 membrane. The higher temperature conductivity on the nanocomposite membranes obtained an enhanced proton conductivity than commercial Nafion® membrane, due to the incoporation of metal oxide materials within the membranes. The higher proton conductivity resistance and reduced methanol permeability of modified membrane also confirmed the suitability used in fuel cell. SEM and FTIR results show the presence of ZrP nanoparticles within the Nafion matrix that also enhanced the water uptake.

6.14. References

1. Jorissen, L.; Gogel, V.; Kerres, J.; Garche, J., New membranes for direct methanol fuel cells. *Journal of Power Sources* **2002,** *105* (2), 165-171.
2. Kundu, P.; Sharma, V.; Shul, Y. G., Composites of proton-conducting polymer electrolyte membrane in direct methanol fuel cells. *Critical Reviews in Solid State and Materials Sciences* **2007,** *32* (1-2), 51-66.
3. Okamoto, K.-i.; Yin, Y.; Yamada, O.; Islam, M. N.; Honda, T.; Mishima, T.; Suto, Y.; Tanaka, K.; Kita, H., Methanol permeability and proton conductivity of sulfonated co-polyimide membranes. *Journal of Membrane Science* **2005,** *258* (1), 115-122.
4. Malhotra, S.; Datta, R., Membrane-supported nonvolatile acidic electrolytes allow higher temperature operation of proton-exchange membrane fuel cells. *Journal of The Electrochemical Society* **1997,** *144* (2), L23-L26.
5. Zawodzinski Jr, T. A.; Neeman, M.; Sillerud, L. O.; Gottesfeld, S., Determination of water diffusion coefficients in perfluorosulfonate ionomeric membranes. *The Journal of Physical Chemistry* **1991,** *95* (15), 6040-6044.
6. Sone, Y.; Ekdunge, P.; Simonsson, D., Proton conductivity of Nafion 117 as measured by a four-electrode AC impedance method. *Journal of The Electrochemical Society* **1996,** *143* (4), 1254-1259.
7. Escoubes, M.; Pineri, M.; Robens, E., Application of coupled thermal analysis techniques to thermodynamic studies of water interactions with a compressible ionic polymer matrix. *Thermochimica Acta* **1984,** *82* (1), 149-160.
8. Pineri, M., Microstructure of organic ionic membranes. ACS Publications: 1986.
9. Yeo, S. C.; Eisenberg, A., Physical properties and supermolecular structure of perfluorinated ion-containing (Nafion) polymers. *Journal of Applied Polymer Science* **1977,** *21* (4), 875-898.
10. Hinatsu, J. T.; Mizuhata, M.; Takenaka, H., Water uptake of perfluorosulfonic acid membranes from liquid water and water vapor. *Journal of the Electrochemical Society* **1994,** *141* (6), 1493-1498.
11. Tang, Y.; Karlsson, A. M.; Santare, M. H.; Gilbert, M.; Cleghorn, S.; Johnson, W. B., An experimental investigation of humidity and temperature effects on the mechanical properties of perfluorosulfonic acid membrane. *Materials Science and Engineering: A* **2006,** *425* (1), 297-304.
12. Klose, C.; Breitwieser, M.; Vierrath, S.; Klingele, M.; Cho, H.; Büchler, A.; Kerres, J.; Thiele, S., Electrospun sulfonated poly (ether ketone) nanofibers as proton conductive

reinforcement for durable Nafion composite membranes. *Journal of Power Sources* **2017,** *361*, 237-242.

13. Silva, R.; Passerini, S.; Pozio, A., Solution-cast Nafion®/montmorillonite composite membrane with low methanol permeability. *Electrochimica Acta* **2005,** *50* (13), 2639-2645.
14. Heitner-Wirguin, C., Recent advances in perfluorinated ionomer membranes: structure, properties and applications. *Journal of Membrane Science* **1996,** *120* (1), 1-33.
15. Bauer, F.; Willert-Porada, M., Characterisation of zirconium and titanium phosphates and direct methanol fuel cell (DMFC) performance of functionally graded Nafion (R) composite membranes prepared out of them. *Journal of Power Sources* **2005,** *145* (2), 101-107.
16. Baglio, V.; Di Blasi, A.; Aricò, A. S.; Antonucci, V.; Antonucci, P. L.; Trakanprapai, C.; Esposito, V.; Licoccia, S.; Traversa, E., Composite mesoporous titania Nafion-based membranes for direct methanol fuel cell operation at high temperature. *Journal of the Electrochemical Society* **2005,** *152* (7), A1373-A1377.
17. Zhang, Y.; Cai, W.; Si, F.; Ge, J.; Liang, L.; Liu, C.; Xing, W., A modified Nafion membrane with extremely low methanol permeability via surface coating of sulfonated organic silica. *Chemical Communications* **2012,** *48* (23), 2870-2872.
18. Meenakshi, S.; Sahu, A.; Bhat, S.; Sridhar, P.; Pitchumani, S.; Shukla, A., Mesostructured-aluminosilicate-Nafion hybrid membranes for direct methanol fuel cells. *Electrochimica Acta* **2013,** *89*, 35-44.
19. Tang, H.; Pan, M.; Jiang, S.; Wan, Z.; Yuan, R., Self-assembling multi-layer Pd nanoparticles onto Nafion™ membrane to reduce methanol crossover. *Colloids and Surfaces A: Physicochemical and Engineering Aspects* **2005,** *262* (1), 65-70.
20. Wang, Z.; Tang, H.; Zhang, H.; Lei, M.; Chen, R.; Xiao, P.; Pan, M., Synthesis of Nafion/CeO 2 hybrid for chemically durable proton exchange membrane of fuel cell. *Journal of Membrane Science* **2012,** *421*, 201-210.
21. Silva, V.; Ruffmann, B.; Silva, H.; Gallego, Y.; Mendes, A.; Madeira, L.; Nunes, S., Proton electrolyte membrane properties and direct methanol fuel cell performance: I. Characterization of hybrid sulfonated poly (ether ether ketone)/zirconium oxide membranes. *Journal of Power Sources* **2005,** *140* (1), 34-40.
22. Noh, H.-J.; Seo, D.-S.; Kim, H.; Lee, J.-K., Synthesis and crystallization of anisotropic shaped ZrO_2 nanocrystalline powders by hydrothermal process. *Materials Letters* **2003,** *57* (16), 2425-2431.
23. Vaivars, G.; Maxakato, N. W.; Mokrani, T.; Petrik, L.; Klavins, J.; Gericke, G.; Linkov, V., Zirconium phosphate based inorganic direct methanol fuel cell. *Mater. Sci* **2004,** *10*, 162-165.

24. Xu, W.; Lu, T.; Liu, C.; Xing, W., Low methanol permeable composite Nafion/silica/PWA membranes for low temperature direct methanol fuel cells. *Electrochimica Acta* **2005,** *50* (16), 3280-3285.
25. Starkweather Jr, H. W., Crystallinity in perfluorosulfonic acid ionomers and related polymers. *Macromolecules* **1982,** *15* (2), 320-323.
26. Kyu, T.; Hashiyama, M.; Eisenberg, A., Dynamic mechanical studies of partially ionized and neutralized Nafion polymers. *Canadian Journal of Chemistry* **1983,** *61* (4), 680-687.
27. Zhai, Y.; Zhang, H.; Hu, J.; Yi, B., Preparation and characterization of sulfated zirconia (SO_4^{2-}/ZrO_2)/Nafion composite membranes for PEMFC operation at high temperature/low humidity. *Journal of Membrane Science* **2006,** *280* (1), 148-155.
28. Adjemian, K. T.; Dominey, R.; Krishnan, L.; Ota, H.; Majsztrik, P.; Zhang, T.; Mann, J.; Kirby, B.; Gatto, L.; Velo-Simpson, M., Function and characterization of metal oxide− Nafion composite membranes for elevated-temperature H_2/O_2 PEM fuel cells. *Chemistry of Materials* **2006,** *18* (9), 2238-2248.
29. Smitha, B.; Devi, D. A.; Sridhar, S., Proton-conducting composite membranes of chitosan and sulfonated polysulfone for fuel cell application. *International Journal of Hydrogen Energy* **2008,** *33* (15), 4138-4146.
30. Di Noto, V.; Gliubizzi, R.; Negro, E.; Pace, G., Effect of SiO_2 on relaxation phenomena and mechanism of ion conductivity of [Nafion/$(SiO_2)_x$] composite membranes. *The Journal of Physical Chemistry B* **2006,** *110* (49), 24972-24986.
31. Stevens, W. J.; Meynen, V.; Bruijn, E.; Lebedev, O. I.; Van Tendeloo, G.; Cool, P.; Vansant, E. F., Mesoporous material formed by acidic hydrothermal assembly of silicalite-1 precursor nanoparticles in the absence of meso-templates. *Microporous and Mesoporous Materials* **2008,** *110* (1), 77-85.
32. Sarkar, D.; Mohapatra, D.; Ray, S.; Bhattacharyya, S.; Adak, S.; Mitra, N., Synthesis and characterization of sol–gel derived ZrO_2 doped Al_2O_3 nanopowder. *Ceramics International* **2007,** *33* (7), 1275-1282.
33. Yu, H.; Ziegler, C.; Oszcipok, M.; Zobel, M.; Hebling, C., Hydrophilicity and hydrophobicity study of catalyst layers in proton exchange membrane fuel cells. *Electrochimica Acta* **2006,** *51* (7), 1199-1207.
34. Kim, B.-N.; Lee, D.-H.; Han, D.-H., Thermal, mechanical and electrical properties on the styrene-grafted and subsequently sulfonated FEP film induced by electron beam. *Polymer Degradation and Stability* **2008,** *93* (6), 1214-1221.
35. Fu, R.-Q.; Woo, J.-J.; Seo, S.-J.; Lee, J.-S.; Moon, S.-H., Covalent organic/inorganic hybrid proton-conductive membrane with semi-interpenetrating polymer network: preparation and characterizations. *Journal of Power Sources* **2008,** *179* (2), 458-466.

36. Yang, T., Composite membrane of sulfonated poly (ether ether ketone) and sulfated poly (vinyl alcohol) for use in direct methanol fuel cells. *Journal of Membrane Science* **2009,** *342* (1), 221-226.
37. Verbrugge, M. W., Methanol diffusion in perfluorinated ion-exchange membranes. *Journal of The Electrochemical Society* **1989,** *136* (2), 417-423.
38. DeLuca, N. W.; Elabd, Y. A., Nafion®/poly (vinyl alcohol) blends: effect of composition and annealing temperature on transport properties. *Journal of Membrane Science* **2006,** *282* (1), 217-224.
39. Mukoma, P.; Jooste, B.; Vosloo, H., A comparison of methanol permeability in Chitosan and Nafion 117 membranes at high to medium methanol concentrations. *Journal of Membrane Science* **2004,** *243* (1), 293-299.
40. Yamazaki, Y., Application of MEMS technology to micro fuel cells. *Electrochimica Acta* **2004,** *50* (2), 663-666.
41. Tsai, J.-C.; Cheng, H.-P.; Kuo, J.-F.; Huang, Y.-H.; Chen, C.-Y., Blended Nafion®/SPEEK direct methanol fuel cell membranes for reduced methanol permeability. *Journal of Power Sources* **2009,** *189* (2), 958-965.
42. Jannasch, P., Recent developments in high-temperature proton conducting polymer electrolyte membranes. *Current Opinion in Colloid & Interface Science* **2003,** *8* (1), 96-102.
43. Zhengbang, W.; Tang, H.; Mu, P., Self-assembly of durable Nafion/TiO_2 nanowire electrolyte membranes for elevated-temperature PEM fuel cells. *Journal of Membrane Science* **2011,** *369* (1), 250-257.
44. Wu, L.; Zhou, G.; Liu, X.; Zhang, Z.; Li, C.; Xu, T., Environmentally friendly synthesis of alkaline anion exchange membrane for fuel cells via a solvent-free strategy. *Journal of Membrane Science* **2011,** *371* (1), 155-162.
45. Gardner, C.; Anantaraman, A., Measurement of membrane conductivities using an open-ended coaxial probe. *Journal of Electroanalytical Chemistry* **1995,** *395* (1-2), 67-73.
46. Bauer, F.; Willert-Porada, M., Microstructural characterization of Zr-phosphate–Nafion® membranes for direct methanol fuel cell (DMFC) applications. *Journal of Membrane Science* **2004,** *233* (1), 141-149.
47. Deng, Q.; Wilkie, C.; Moore, R.; Mauritz, K. A., TGA–FTi. r. investigation of the thermal degradation of Nafion® and Nafion®/[silicon oxide]-based nanocomposites. *Polymer* **1998,** *39* (24), 5961-5972.
48. Baglio, V.; Di Blasi, A.; Antonucci, V., FTIR spectroscopic investigation of inorganic fillers for composite DMFC membranes. *Electrochemistry Communications* **2003,** *5* (10), 862-866.

49. Yang, H.; Lee, D.; Park, S.; Kim, W., Preparation of Nafion/various Pt-containing SiO_2 composite membranes sulfonated via different sources of sulfonic group and their application in self-humidifying PEMFC. *Journal of Membrane Science* **2013,** *443*, 210-218.
50. Ostrowska, J.; Narebska, A., Infrared study of hydration and association of functional groups in a perfluorinated Nafion membrane, Part 1. *Colloid and Polymer Science* **1983,** *261* (2), 93-98.
51. Zhai, Y.; Zhang, H.; Hu, J.; Yi, B., Preparation and characterization of sulfated zirconia (SO_4^{2-}/ZrO_2)/Nafion composite membranes for PEMFC operation at high temperature/low humidity. *Journal of Membrane Science* **2006,** *280* (1-2), 148-155.
52. Xuesong, Y., Preparation, Characterization and Application of a Novel PA/SIO_2 NF Membrane. *Procedia Engineering* **2012,** *44*, 2075-2078.
53. Yang, C.; Srinivasan, S.; Arico, A.; Cretı, P.; Baglio, V.; Antonucci, V., Composite Nafion/zirconium phosphate membranes for direct methanol fuel cell operation at high temperature. *Electrochemical and Solid-State Letters* **2001,** *4* (4), A31-A34.
54. Huang, Y.; Chuang, L.; Kannan, A.; Lin, C., Proton-conducting membranes with high selectivity from cross-linked poly (vinyl alcohol) and poly (vinyl pyrrolidone) for direct methanol fuel cell applications. *Journal of Power Sources* **2009,** *186* (1), 22-28.
55. Service, R. F., Fuel cells. Shrinking fuel cells promise power in your pocket. *Science (New York, NY)* **2002,** *296* (5571), 1222.
56. Savadogo, O., Emerging membranes for electrochemical systems: Part II. High temperature composite membranes for polymer electrolyte fuel cell (PEFC) applications. *Journal of Power Sources* **2004,** *127* (1), 135-161.
57. Santiago, E.; Isidoro, R.; Dresch, M.; Matos, B.; Linardi, M.; Fonseca, F., Nafion–TiO 2 hybrid electrolytes for stable operation of PEM fuel cells at high temperature. *Electrochimica Acta* **2009,** *54* (16), 4111-4117.
58. Savadogo, O., Emerging membrane for electrochemical systems:(I) solid polymer electrolyte membranes for fuel cell systems. *Journal of New Materials for Electrochemical Systems* **1998,** *1* (1), 47-66.
59. Kong, X., Characterization of proton exchange materials for fuel cells by solid state nuclear magnetic resonance. **2010**.
60. Ghassemzadeh, L.; Pace, G.; Di Noto, V.; Müller, K., Effect of SiO_2 on the dynamics of proton conducting [Nafion/(SiO_2) X] composite membranes: a solid-state 19 F NMR study. *Physical Chemistry Chemical Physics* **2011,** *13* (20), 9327-9334.
61. Xu, W.; Lu, T.; Liu, C.; Xing, W., Low methanol permeable composite Nafion/silica/PWA membranes for low temperature direct methanol fuel cells. *Electrochimica Acta* **2005,** *50* (16-17), 3280-3285.

62. Zhang, H.; Shen, P. K., Recent development of polymer electrolyte membranes for fuel cells. *Chemical Reviews* **2012,** *112* (5), 2780-2832.
63. Navarra, M.; Abbati, C.; Scrosati, B., Properties and fuel cell performance of a Nafion-based, sulfated zirconia-added, composite membrane. *Journal of Power Sources* **2008,** *183* (1), 109-113.
64. Chen, X.-R.; Ju, Y.-H.; Mou, C.-Y., Direct synthesis of mesoporous sulfated silica-zirconia catalysts with high catalytic activity for biodiesel via esterification. *The Journal of Physical Chemistry C* **2007,** *111* (50), 18731-18737.
65. Mercera, P.; Van Ommen, J.; Doesburg, E.; Burggraaf, A.; Ross, J., Influence of ethanol washing of the hydrous precursor on the textural and structural properties of zirconia. *Journal of materials science* **1992,** *27* (18), 4890-4898.
66. Sigwadi, R.; Dhlamini, S.; Mokrani, T.; Nonjola, P., Effect of Synthesis Temperature on Particles Size and Morphology of Zirconium Oxide Nanoparticle. *Journal of Nano Research* **2017,** *50*, 8-31.
67. Sigwadi, R. A.; Mavundla, S. E.; Moloto, N.; Mokrani, T., Synthesis of zirconia-based solid acid nanoparticles for fuel cell application. *Journal of Energy in Southern Africa* **2016,** *27* (2), 60-67.
68. Sarkar, D.; Mohapatra, D.; Ray, S.; Bhattacharyya, S.; Adak, S.; Mitra, N., Synthesis and characterization of sol–gel derived ZrO_2 doped Al_2O_3 nanopowder. *Ceramics International* **2007,** *33* (7), 1275-1282.
69. Kinumoto, T.; Inaba, M.; Nakayama, Y.; Ogata, K.; Umebayashi, R.; Tasaka, A.; Iriyama, Y.; Abe, T.; Ogumi, Z., Durability of perfluorinated ionomer membrane against hydrogen peroxide. *Journal of Power Sources* **2006,** *158* (2), 1222-1228.
70. Li, L.; Pan, Y.; Chen, L.; Li, G., One-dimensional α-MnO_2: trapping chemistry of tunnel structures, structural stability, and magnetic transitions. *Journal of Solid State Chemistry* **2007,** *180* (10), 2896-2904.
71. Li, K.; Ye, G.; Pan, J.; Zhang, H.; Pan, M., Self-assembled Nafion®/metal oxide nanoparticles hybrid proton exchange membranes. *Journal of Membrane Science* **2010,** *347* (1-2), 26-31.
72. Jalani, N. H.; Dunn, K.; Datta, R., Synthesis and characterization of Nafion®-MO_2 (M= Zr, Si, Ti) nanocomposite membranes for higher temperature PEM fuel cells. *Electrochimica Acta* **2005,** *51* (3), 553-560.
73. Sigwadi, R.; Ṋemavhola, F.; Dhlamini, S.; Mokrani, T., Mechanical strength of Nafion®/ZrO_2 nano-composite membrane. *International Journal of Manufacturing, Materials, and Mechanical Engineering (IJMMME)* **2018,** *8* (1), 54-65.

74. Zheng, H.; Mathe, M., Enhanced conductivity and stability of composite membranes based on poly (2, 5-benzimidazole) and zirconium oxide nanoparticles for fuel cells. *Journal of Power Sources* **2011,** *196* (3), 894-898.
75. James, P.; Elliott, J.; McMaster, T.; Newton, J.; Elliott, A.; Hanna, S.; Miles, M., Hydration of Nafion® studied by AFM and X-ray scattering. *Journal of Materials Science* **2000,** *35* (20), 5111-5119.
76. Velayutham, P.; Sahu, A. K.; Parthasarathy, S., A Nafion-ceria composite membrane electrolyte for reduced methanol crossover in direct methanol fuel cells. *Energies* **2017,** *10* (2), 259.
77. Sigwadi, R.; Dhlamini, M.; Mokrani, T.; Ṋemavhola, F., Wettability and mechanical strength of modified Nafion® nanocomposite membrane for fuel cell. *Digest Journal of Nanomaterials & Biostructures (DJNB)* **2017,** *12* (4).
78. D'Epifanio, A.; Navarra, M. A.; Weise, F. C.; Mecheri, B.; Farrington, J.; Licoccia, S.; Greenbaum, S., Composite Nafion/sulfated zirconia membranes: effect of the filler surface properties on proton transport characteristics. *Chemistry of Materials* **2009,** *22* (3), 813-821.
79. Zheng, J.; Bi, W.; Dong, X.; Zhu, J.; Mao, H.; Li, S.; Zhang, S., High performance tetra-sulfonated poly (p-phenylene-co-aryl ether ketone) membranes with microblock moieties for passive direct methanol fuel cells. *Journal of Membrane Science* **2016,** *517*, 47-56.
80. Zhao, D.; Yi, B.; Zhang, H.; Yu, H., $MnO_2/SiO_2–SO_3H$ nanocomposite as hydrogen peroxide scavenger for durability improvement in proton exchange membranes. *Journal of Membrane Science* **2010,** *346* (1), 143-151.
81. Chien, H.-C.; Tsai, L.-D.; Huang, C.-P.; Kang, C.-y.; Lin, J.-N.; Chang, F.-C., Sulfonated graphene oxide/Nafion composite membranes for high-performance direct methanol fuel cells. *International Journal of Hydrogen Energy* **2013,** *38* (31), 13792-13801.
82. Hudiono, Y.; Choi, S.; Shu, S.; Koros, W. J.; Tsapatsis, M.; Nair, S., Porous layered oxide/Nafion® nanocomposite membranes for direct methanol fuel cell applications. *Microporous and Mesoporous Materials* **2009,** *118* (1-3), 427-434.
83. Lee, C. H.; Hwang, S. Y.; Sohn, J. Y.; Park, H. B.; Kim, J. Y.; Lee, Y. M., Water-stable crosslinked sulfonated polyimide–silica nanocomposite containing interpenetrating polymer network. *Journal of Power sources* **2006,** *163* (1), 339-348.
84. Kreuer, K., Hydrocarbon membranes. *Handbook of fuel cells* **2003**.
85. Zawodzinski, T. A.; Derouin, C.; Radzinski, S.; Sherman, R. J.; Smith, V. T.; Springer, T. E.; Gottesfeld, S., Water uptake by and transport through Nafion® 117 membranes. *Journal of the Electrochemical Society* **1993,** *140* (4), 1041-1047.
86. Yang, C., Performance of Nafion/zirconium phosphate composite membranes in PEM fuel cells. *Department of Mechanical Engineering* **2003**.

87. Winter, M.; Besenhard, J. O., Electrochemical lithiation of tin and tin-based intermetallics and composites. *Electrochimica Acta* **1999,** *45* (1), 31-50.
88. Costamagna, P.; Yang, C.; Bocarsly, A.; Srinivasan, S., Nafion® 115/zirconium phosphate composite membranes for operation of PEMFCs above 100 °C. *Electrochimica acta* **2002,** *47* (7), 1023-1033.
89. Alberti, G.; Casciola, M., Solid state protonic conductors, present main applications and future prospects. *Solid State Ionics* **2001,** *145* (1), 3-16.
90. Alberti, G.; Casciola, M.; Capitani, D.; Donnadio, A.; Narducci, R.; Pica, M.; Sganappa, M., Novel Nafion–zirconium phosphate nanocomposite membranes with enhanced stability of proton conductivity at medium temperature and high relative humidity. *Electrochimica Acta* **2007,** *52* (28), 8125-8132.
91. Yang C., S. S., Bocarsly A B., Tulyani S., Benziger J B., A comparison of physical properties and fuel cell performance of Nafion and zirconium phosphate/Nafion composite membranes. *Journal of Membrane Science* **2004,** *237* (1-2), 145-161.
92. Horsley, S.; Nowell, D.; Stewart, D., The infrared and Raman spectra of α-zirconium phosphate. *Spectrochimica Acta Part A: Molecular Spectroscopy* **1974,** *30* (2), 535-541.
93. Salavati-Niasari, M.; Dadkhah, M.; Davar, F., Pure cubic ZrO_2 nanoparticles by thermolysis of a new precursor. *Polyhedron* **2009,** *28* (14), 3005-3009.
94. Laporta, M.; Pegoraro, M.; Zanderighi, L., Perfluorosulfonated membrane (Nafion): FT-IR study of the state of water with increasing humidity. *Physical Chemistry Chemical Physics* **1999,** *1* (19), 4619-4628.
95. Devrim, Y.; Erkan, S.; Baç, N.; Eroglu, I., Improvement of PEMFC performance with Nafion/inorganic nanocomposite membrane electrode assembly prepared by ultrasonic coating technique. *International Journal of Hydrogen Energy* **2012,** *37* (21), 16748-16758.
96. Xing, P.; Robertson, G. P.; Guiver, M. D.; Mikhailenko, S. D.; Kaliaguine, S., Synthesis and characterization of poly (aryl ether ketone) copolymers containing (hexafluoroisopropylidene)-diphenol moiety as proton exchange membrane materials. *Polymer* **2005,** *46* (10), 3257-3263.
97. Yang, T., Composite membrane of sulfonated poly (ether ether ketone) and sulfated poly (vinyl alcohol) for use in direct methanol fuel cells. *Journal of Membrane Science* **2009,** *342* (1-2), 221-226.
98. Sigwadi, R. Zirconia based/Nafion coposite membranes for fuel cell applications. 2013.
99. Ahmad, A.; Isa, K. M.; Osman, Z., Conductivity and structural studies of plasticized polyacrylonitrile (PAN)-lithium triflate polymer electrolyte films. *Sains Malaysiana* **2011,** *40* (7), 691-694.

CHAPTER SEVEN

7. Nafion® membranes reinforced with PAN/Zr nanofibers for direct methanol fuel cell application

This chapter presents a summary of a scientific paper that presented the results from the paper: "**Nafion® membranes reinforced with PAN/Zr nanofibers for direct methanol fuel cell application"**

7.1. Introduction

All around the world, our sources of transportation rely on petroleum-based fuels which emit poisonous gases, such as CO_2, that pollute our environment [1]. Proton exchange membrane fuel cells (PEMFCs) have been considered as an alternate to our petroleum-fuelled transportation due to them having fewer or no CO_2 emissions [2]. Fuel cells generate energy by converting chemical energy directly into electricity without releasing poisonous gases such as SO_x and NO_x, thus making them environmentally friendly. When compared to competing technologies, direct methanol fuel cells (DMFCs) have higher energy efficiency, reduced weight, low gas emissions, and are more easily transported due to the fuel being stored in liquid form [3]. Nevertheless, their drawbacks – methanol permeability and low performance – limit their commercialization and operations in fuel cell [4]. Perfluorinated membranes, such as Nafion®, are currently used as electrolyte in fuel cells, due to their higher proton conductivity as well as chemical and mechanical stability, which makes them promising polymer at low temperature fuel cell operation [5-6]. However, Nafion® membranes do face some challenges such as losing water at higher temperatures and this limits their use to polymer electrolyte membrane (PEM) fuel cells and to applications involving higher methanol crossover when used in DMFCs which reduce the active site on the cathode catalyst**.** The high cost of fabricating methanol crossovers prompted the researchers to initiate some research on blending Nafion® with ionic conductivity membranes such as polyvinyl alcohol (PVA) and polyacrylonitrile (PAN) without affecting or reducing their durability and mechanical strength [7]. PAN membrane has good mechanical strength and high ionic conductivity [8]. Moreover, PAN is easily mixed with other polymers due to its property of good solvent resistance [9]. Electrospun PAN nanofibers have been found to have multifaceted applications [10], such as electrode materials in supercapacitors and fuel cells [11], and they also have good mechanical properties [9]. The blending of PAN nanofibers into Nafion® membrane has reduced the use of Nafion® solution, thereby reduce costly problems. At the same time, the use of Nafion® membrane improves methanol crossover and proton conductivity, which influence fuel cell

efficiency and long-term stability. These effects may be due to the low thermal plasticity of PAN polymer [12]. Nafion® membranes incorporated with metal oxides such as ZrO_2, zeolite, TiO_2 and SiO_2 shows improvement on the mechanical strength and proton conductivity while maintaining its water management [13]. In addition, the water within the modified membrane does not evaporate, which increases the proton migration within the membrane [14]. ZrO_2 maintains a high melting point and has both outstanding chemical stability and excellent mechanical properties [15]. Nevertheless, the performance of nanocomposite membranes does not improve under conditions of high humidity. This may be due to their spherical phase which aggregate, thus preventing sufficient water diffusion through the membrane [16]. To reduce the agglomeration of ZrO_2 nanoparticles and improve water diffusion, ZrO_2 was electrospun with PAN solution to obtain a 1D morphology. In comparison, graphene flakes (GO) were added to a Nafion® solution blended with PAN/ Zr nanofibers to increase proton conductivity and retain water within the Nafion® nanocomposite membrane, this may be due to the graphene monolayer, which is highly permeable to protons [17]. The aim of this work is to produce nanocomposite membranes that will sustain good chemical and mechanical properties, higher proton conductivity and fuel cell efficiency in direct methanol fuel cells while reducing methanol permeability.

7.2. Experimental

7.2.1. Materials

Nafion® solution D521 was purchased from Ion Power. Polyacrylonitrile (PAN) (Sigma-Aldrich), Sodium hydroxide (Merck), phosphoric acid (Merck), Sulfuric Acid (Merck), zirconium acetylacetonate (Merck), Potassium hydroxide (KOH) (Merck), N, N-Dimethylformamide (DMF) (Merck), methanol (Merck), and graphene flakes (Sigma-Aldrich), were obtained and were used as received.

.

7.2.2. Preparation of electrospinning solutions

PAN/Zr nanofiber solutions were obtained by adding PAN (1g) and 0.3-wt% zirconium acetylacetonate to a DMF (6g) solution and the solution was stirred magnetically for 3 hours at 80 °C [18]. The solution was then fed through a capillary tip with a diameter of 1.25 mm using a 10 mL syringe. A voltage of 15 kV and a syringe pump were used to feed the electrospinning solution at a constant rate of 0.5 mL/h. The distance between the nozzle and the collector was set at 10 cm. The collector plate was covered with aluminium foil to gather the resultant fibres at a specified distance.

7.2.3. Preparation of nanocomposite membranes

The Nafion®-PAN/Zr nanofiber membranes were obtained using the casting method. 30 ml of Nafion® solution was mixed with 60 ml of N, N-dimethylformamide and the solution was stirred magnetically for 30 minutes. The the solution was then divided into four equal parts. A quarter of the solution was recast onto a glass plate and each of the remaining quarters of the solution were continuously stirred with 5wt% of PAN/ Zr nanofibers; 5wt% of PAN/ Zr nanofibers with 0.01g GO; and 5wt% of PAN/ Zr nanofibers with 0.01 wt% of phosphoric acid respectively for 1 hour and then placed in an ultrasonic bath for 30 minutes. The separated solutions were dried in an oven overnight at 80 ^{o}C, and then heated at 160 ^{o}C for 30 minutes. The recast membranes were labelled as recast Nafion®, Nafion®-PAN/Zr nanofiber, Nafion®-PAN/ZrGO nanofiber and Nafion®-PAN/ZrP nanofiber membranes. Membranes were washed with deionized water before characterisation.

7.2.4. Characterisations

The X-ray diffraction (XRD) analysis was performed through X-ray diffraction with Cu K radiation source and the samples were scanned in a continuous mode from 10°–90° with a scanning rate of 0.026 (degree) / 1 (sec). The thermal properties and the characteristics of the samples were studied by thermal gravimetric analysis (TGA) under nitrogen flow. TGA data was obtained using TGA instrument (PerkinElmer) over nitrogen and at a heating rate of 10° C/min from 28° C to 1000° C. the surface morphologies of all the membrane were studied using Scanning Electron Microscopy (SEM). Fourier-transform infrared spectroscopy (FTIR) was employed to investigate the changes in the chemical structure of the membrane.

7.2.5. Water Uptake (WU), swelling ratio (SR) and hydration number (λ) of membranes

The membranes were soaked in distilled water for one day at 30^{o} C, 60^{o} C and 80^{o} C. They were then removed from the water, wiped, measured and weighed. Water uptake and dimensional swelling ratios were calculated according to the equations below:

$$\mathbf{W_{up}}(\%) = \frac{(\mathbf{m_{wet} - m_{dry}})}{\mathbf{m_{dry}}}\mathbf{x100} \quad (7\text{-}1)$$

and

$$\mathbf{SR}(\%) = \frac{(\mathbf{L_w - L_d})}{\mathbf{L_d}}\mathbf{x100} \quad (7\text{-}2)$$

W_{up} is the percentage of water uptake, m_{wet} is the weight of wet membrane and m_{dry} is the weight of the dried membrane, SR is the percentage of swelling ratio, L_w is the length of the wet membrane and L_d is the length of the dried membranes.

Hydration number (λ)

The hydration number (λ) is one of the most important parameters for conductivity. It is defined as the number of water molecules per conducting functional group (sulfonic acid group). The hydration number (λ) was calculated according to the equation below [19]:

$$\lambda = \frac{\mathbf{WU}}{\mathbf{IECx\ 100x18}} \qquad (7\text{-}3)$$

7.2.6. Ion exchange capacity

The ion exchange capacity (IEC) of all membranes were determined by the titration method.

$$\mathbf{IEC} = \frac{\mathbf{V_{NaOH}\ X\ C_{NaOH}}}{\mathbf{W_{sample}}} \qquad (7\text{-}4)$$

where V_{NaOH} is the titrated volume of NaOH and W_{sample} is the weight of the dry membranes.

7.2.7. Methanol permeability measurements

The methanol permeability was measured with a permeation-measuring cell designed in our lab that consisted of two compartments. The membrane were placed in the middle of two compartments, and the diameter of the diffusion area was 3.5 cm. One of the compartments (A) was filled with 50 mL of methanol solution and the other compartment (B) was filled with 50 mL of distilled water. The solutions were prepared in 2M and 5M methanol and the results were collected at 30 ºC, 60 ºC and 80 ºC for comparison. The methanol concentration in compartment B was monitored with a methanol concentration sensor. The output signal was converted using a data module and recorded on a personal computer. Methanol permeability (P) was obtained by means of the following relationship:

$$\mathbf{CB} = \frac{\mathbf{A\ P}}{\mathbf{VB\ L}}\ \mathbf{CA}\ (\mathbf{t} - \mathbf{t0}) \qquad (7\text{-}5)$$

where C_A is the concentration of initial methanol in compartment A; C_B the concentration of methanol in compartment B at diffusion time t; V_B the volume of distilled water in compartment B; L the membrane thickness; and A the effective permeating area.

7.2.8. Conductivity measurement

The conductivities of all membranes were measured using a four-point probe conductivity cell. The ionic conductivity was determined galvanostatically with a current amplitude of 0.1 mA over frequencies ranging from 1MHz to 10Hz. Using a Bode plot, the frequency region over which the impedance had a constant value was checked and the electrical resistance was then obtained from a Nyquist plot [20]. The ionic conductivity (σ) was calculated according to the following equation:

$$K = L/RWd \tag{7-6}$$

where R is the obtained membrane resistance, L is the distance between potential-sensing electrodes (1 cm), and W and d are the width (2 cm) and thickness of the membrane. For conductivity testing, the membrane was immersed in 1 M sulfuric acid solution for six hours at room temperature. The membrane was then rinsed with deionised water several times to remove any excess H_2SO_4 and then immersed in deionised water for six hours at 60 ˚C. All the membranes were kept in deionised water at room temperature before measuring of conductivity.

7.2.9. Preparation of membrane electrode assembly (MEA) and fuel cell testing

The MEA was prepared by using 20% Pt Vulcan XC-72R in Nafion® solutions for ink preparation and Pt in Carbon cloth. The prepared ink was brushed onto the carbon cloth on the cathode side. The 2 $mgcm^{-2}$ of catalyst was loaded onto the anode and cathodes of the Nafion®-PAN/Zr nanofiber, the Nafion®-PAN/ZrP nanofiber and the Nafion®- PAN/ZrGO nanofiber membranes without hot pressing, resulting in assembly membrane electrode assemblies (MEAs). The membrane assemblies thus obtained were tested at galvanostatically in open air to measure their cell potential as a function of current density. It was passed on 2 M of methanol solution mixed with 2 M of Potassium hydroxide (KOH).

7.3. Results and discussion

7.3.1. Scanning electron microscopy (SEM)

The morphologies of PAN/Zr nanofibers are shown in Figure 7-1(a& b). The obtained nanofibers were well arranged on top of each other with their diameters ranging between 300 and 500 nm, without any zirconia nanoparticles being agglomerated within the nanofibers, as shown in Figure 7-1(a& b). This shows that the zirconia nanoparticles were well mixed within the PAN solution and that DMF is a suitable solution for the blending of polymer with metal oxide. Moreover, the PAN/Zr nanofibers show a smooth and uniform arrangement of nanofibers on the 1 µm and 100 nm scale bar as shown in Figure 7-1(a& b). Figure 7-2 presents the SEM images of recast Nafion® membrane, Nafion®-PAN/Zr nanofiber, Nafion®-PAN/ZrP nanofiber and Nafion®-PAN/ZrGO nanofiber nanocomposite membranes. The SEM image in Figure 7-2(a& b) shows that the recast Nafion® membrane obtained a smooth surface without any pinholes or cracks. It can be seen in Figure 7-2(c& d) that nanofibers were successfully incorporated within the Nafion® membrane, as the nanofibers are well dispersed, without any porosity and having strong interaction between membrane with less agglomeration. This may be due to the magnetic stirring breaking the nanofibers into small pieces and allowed them to be well blended with the Nafion® solution as observed in Figure 7-2(c-d). It can be observed in Figure 7-2(e-f) that the addition of phosphoric acid has an effect on the dispersement of the nanofibers. When phosphoric acid is mixed with Nafion® and PAN/Zr nanofibers, they form an aggregation with nanofibers not being traceable and only sphere-like shapes being observable. Furthermore, this spherical shape resulted in poor distribution of nanofibers within the Nafion® membrane, as observable in Figure 7-2(e-f), due to the nanofibers agglomerating in the spherical shape mentioned earlier and that, therefore, were not easily well distributed within the Nafion® matrix, as well as to the addition of phosphoric acid which reduces the sizes of PAN/Zr nanofibers within the Nafion® membrane. Further addition of GO, as seen in Figure 7-2(g-h), shows that the nanofibers were invisible within the membrane. This may be due to the thorough blending of GO with nanofibers within the Nafion® matrix. This indicates that the incorporation of PAN nanofibers and GO improves the dispersity within the Nafion® membrane [21]. As all the Nafion® pores within the membrane are well covered, though with more agglomeration as observed in Figure 7-2(g), this may be due to the method of incorporation of GO nanoparticles. Furthermore, the SEM images of Nafion®-PAN/ZrGO show that the nanofiber membranes were well covered in the Nafion® matrix when compared to the Nafion®-PAN/ZrP nanofiber membrane. It was observable that blending the non-beaded and well-arranged nanofibers increases the dispersity within the membrane matrix, as shown in Figure 7-2. In generally, the SEM images of nanocomposite membranes show that the nanofibers were agglomerated within the Nafion® membrane.

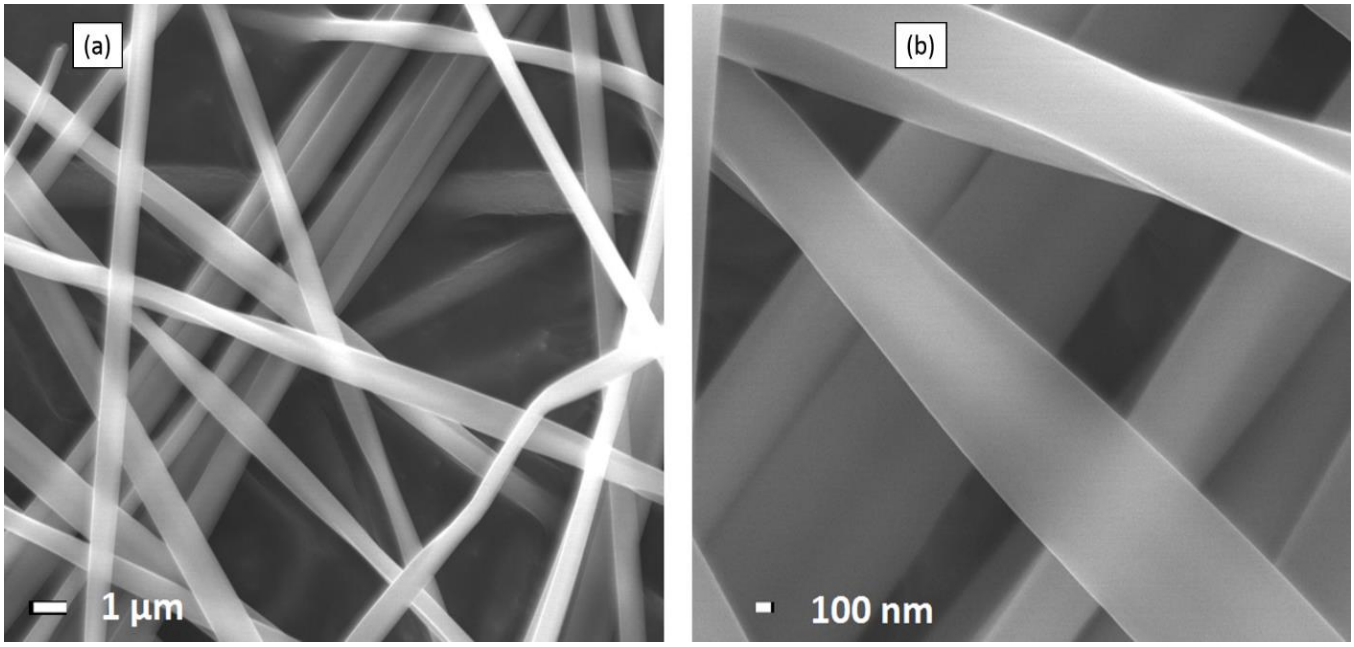

Figure 7- 1: SEM images of electrospun PAN/Zr nanofibers.

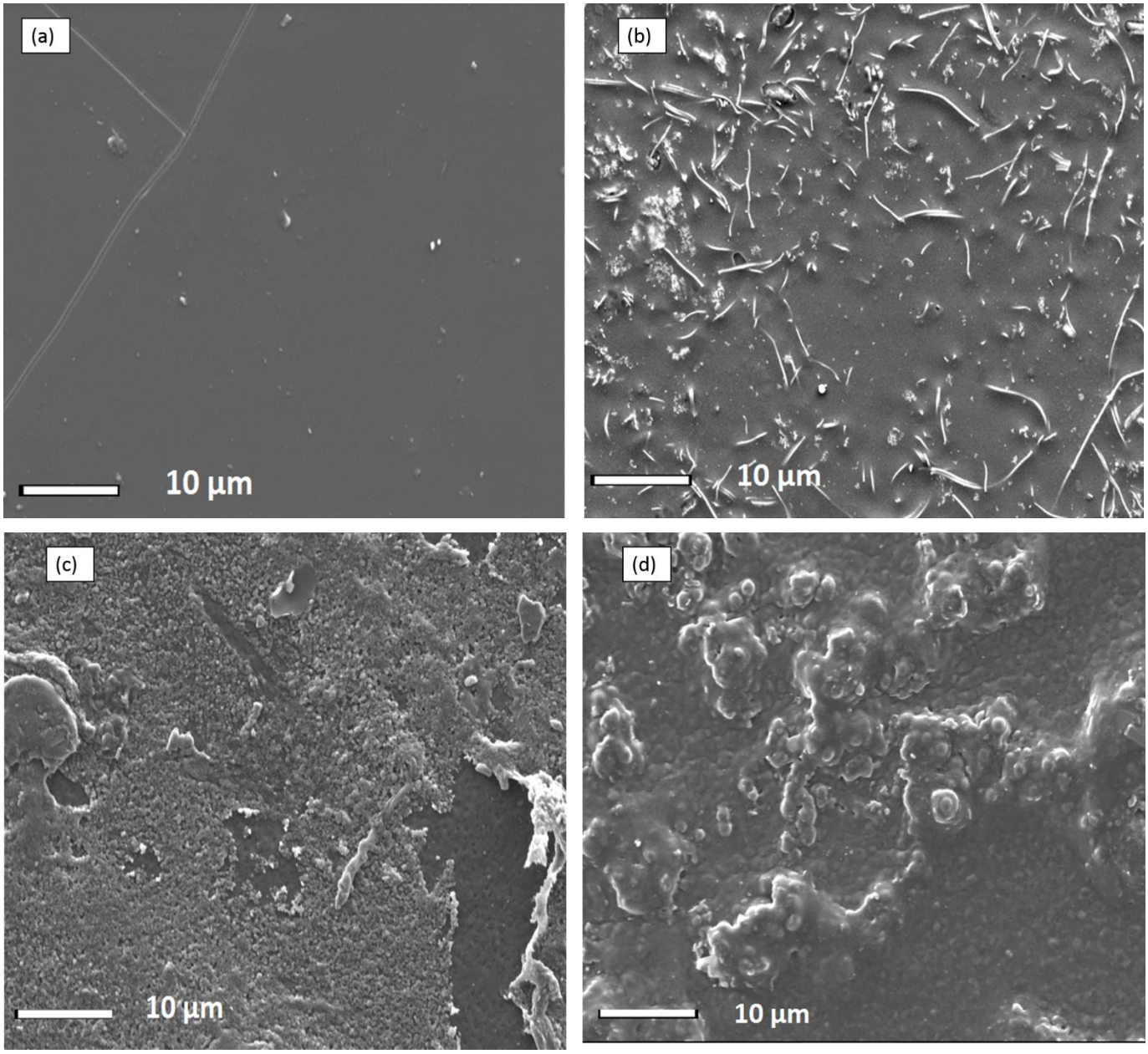

Figure 7- 2: Scanning Electron Microscopy (SEM) (a) SEM micrographs of recast Nafion® membrane, (b) Nafion®-PAN/Zr nanofiber, (c) Nafion®-PAN/ZrP nanofiber and (d) Nafion®-PAN/ZrGO nanofiber membranes**.**

7.3.2. Fourier transform infrared spectroscopy (FTIR)

Figure 7-3 shows the FTIR results of Nafion®-PAN/ZrGO nanofiber, Nafion®-PAN/ZrP nanofiber, Nafion®-PAN/Zr nanofiber nanocomposite membranes and recast Nafion® membrane. The FTIR results of nanocomposite membranes shows that the bending vibration peak at 1465 cm^{-1} can be assigned to vibrations of the C-H of PAN, as shown in Figure 7-3(a-c) [20]. Figure 7-3(a-d) shows that the PAN nanofibers are well blended with the Nafion® membrane as the samples show the stretching peaks at 1207 cm^{-1} and 1140 cm^{-1}, which can

be assigned to the stretching modes of C–F [22] and the strong peaks at 1051 cm^{-1} and 972 cm^{-1} which can be assigned to the stretching modes of S–O and C–O–C. Figure 7-3(a-c) shows the new peak at 438 cm^{-1}, due to vibration of the Zr-O group, while the peak observed at 2335 cm^{-1} is due to the presence of inorganic ions [23] . Therefore, the appearance of Zr-O groups at the nanocomposite membrane confirms the presence of zirconia nanoparticles within the electrospun nanofibers.

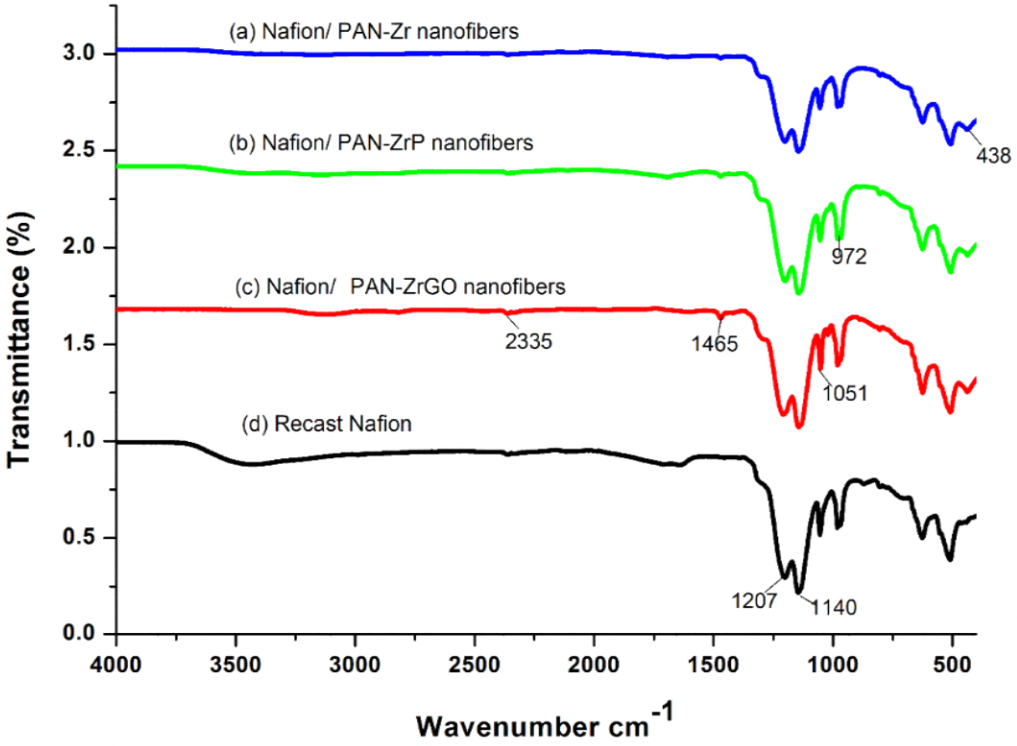

Figure 7- 3: FTIR spectra of (a) Nafion®-PAN/Zr nanofibers, (b) Nafion®-PAN/ZrP nanofibers, (c) Nafion®-PAN/ZrGO nanofibers membranes and (d) recast Nafion® membrane.

7.3.3. The X-ray diffraction (XRD) analysis

Figure 7-4 shows the crystal structures of recast Nafion® membrane, Nafion®-PAN/Zr nanofiber, Nafion®-PAN/ZrGO nanofiber and Nafion®-PAN/ZrP nanofiber membranes. The membranes present only two strong peaks, at 2θ = 17 ° and 2θ = 39 °, that show the X-ray reflections of Nafion® membrane which are attributed to the semi-crystallinity of the perfluorocarbon chains of the ionomer as shown in Figure 7-4 [24]. However, the peak at 2theta = 17 ° is also assigned to crystal planes of electrospun PAN [25], indicating that the Nafion® /PAN membranes are well-blended. The XRD results of Nafion®-PAN/Zr nanofiber membrane in Figure 7-4(a) shows the amorphous phase, without peak so as to represent the zirconia nanoparticles within the membrane. Nevertheless, the XRD peaks at 2θ = 17 ° and 2θ = 39 °

decrease while the broadness increases, which indicates the amorphous nature of the membranes. This may be due to the PAN/Zr nanofibers incorporated in Nafion® membrane as confirmed by the SEM results. Figure 7-4(b) also shows that the membranes were amorphous, as no new crystalline peaks were obtained, but with a reduced peak at 2θ = 17 ° and 2θ = 39 °. This may be due to the incorporation of PAN/Zr nanofibers that have an effect on the crystalline structure of the Nafion® membrane. The XRD results of Nafion®-PAN/ZrGO nanofiber nanocomposite membrane in Figure 7-4(c) show the presence of a weak peak at 2θ= 11° due to the added GO in the membrane [26] and weak peaks at 2θ= 9° and 2θ= 28° due to crystalline peaks of zirconia oxide which was electrospun with the PAN solution. This peak confirms the presence of GO within the Nafion® membrane. The recast Nafion® membrane shows two strong peaks at 2θ = 17 ° and 2θ = 39 °, which are attributed to the semi-crystallinity of the perfluorocarbon chains of the ionomer as shown in Figure 7-4(d) [24]. In conclusion, the XRD results show that the incorporation of PAN/Zr nanofibers into Nafion® membrane has little effect on their structure as the membranes remained amorphous.

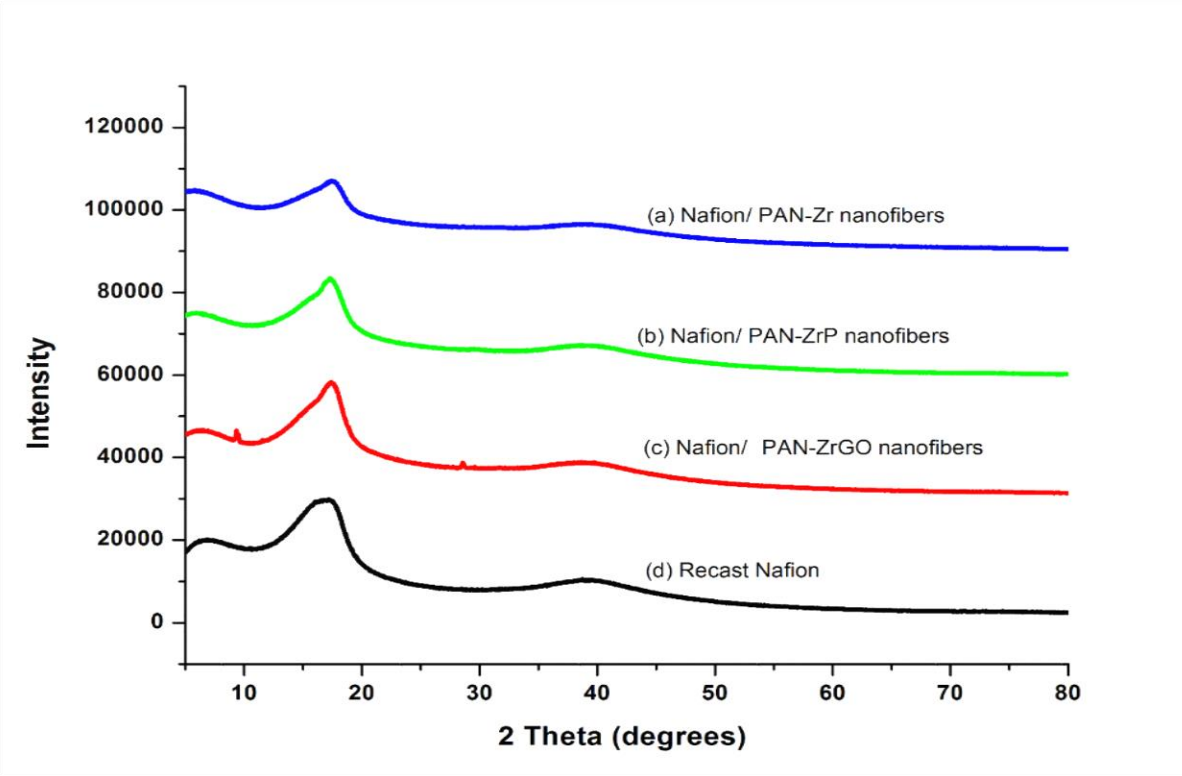

Figure 7- 4: The XRD results of the (a) Nafion®-PAN/Zr nanofibers, (b) Nafion®-PAN/ZrP nanofibers, (c) Nafion®-PAN/ZrGO nanofibers membranes and (d) recast Nafion® membrane.

7.3.4. Thermo-gravimetric analysis (TGA) and derivative thermo-gravimetric (DTG)

The thermal degradation of the Nafion®-PAN/Zr nanofiber, Nafion®-PAN/ZrP nanofiber, Nafion®-PAN/ZrGO nanofiber membranes and recast Nafion® membrane were observed

under TGA and DTG as shown in Figure 7-5. The TGA results of Nafion®-PAN/ZrGO nanofiber membranes shows two stages of the weight loss process. The initial weight loss, at 360° C, is related to the degradation of the sulphuric groups of the Nafion® membrane and the cyclization of nitrile groups in the PAN nanofibers [27]. The second weight loss at 550-680° C is due to the degradation of the polymer main chain of PAN nanofibers and Nafion® membrane [28-29]. It was observed that no weight loss occurred below 360° C, which confirms that no water was removed from the membrane. This may be due to the strong interaction between GO, nanofibers and polymer, as confirmed by the SEM results, which causes the nanocomposite membrane to be thermally stable at higher temperatures [30]. TGA results show that there is an increase of the bound water within the Nafion® membrane, due to the incorporation of inorganic filler and PAN nanofibers in comparison with the recast Nafion® membrane. Furthermore, PAN has a higher thermal stability at a higher temperature of 130° C [31]. Figure 7-5 shows that the TGA curves of Nafion®-PAN/ZrP nanofiber, Nafion®-PAN/Zr nanofiber membranes and recast Nafion® membrane, undergo three stages of weight loss and that their degradation started at almost the same temperature of 380 °C. TGA curves of Nafion®-PAN/Zr nanofiber and Nafion®-PAN/ZrP nanofiber membranes shows the initial weight loss at 150 °C due to the evaporation of adsorption water, as shown in Figure 7-5. The second weight loss, at 380 °C, was due to the degradation of the sulphuric groups of the Nafion® membrane and the cyclization of nitrile groups in the PAN nanofibers [27]. Furthermore, the degradation of nanocomposite membranes was higher than for the recast Nafion® at 380 °C. The nanocomposite membrane, with the phosphoric acid added, showed a slightly smaller mass loss at around 360 °C than did the recast Nafion® membrane. The initial weight loss of the recast Nafion® membrane at 100 °C was due to the removal of adsorption water (which can be attributed to the loss of water tightly bound to the hygroscopic sulfonic acid groups). The second weight loss at 380 °C was due to the degradation of the sulphuric groups of the Nafion® membrane [27]. The third weight loss at 550° C was due to the degradation of the polymer main chain [32]. Above a temperature of 650 °C, the recast Nafion® membrane was totally burnt, while the Nafion®-PAN/ZrP nanofiber, Nafion®-PAN/ZrGO nanofiber and Nafion®-PAN/Zr nanofiber nanocomposite membranes had 99%, 93.8% and 78.8%, respectively, of mass weight percent remaining. It may be concluded from this that all the composite membranes are suitable for use in high-temperature PEM fuel cells as they start to lose water at only above 150 °C and their backbones are more thermally stable than recast Nafion® membrane. Due to the addition of inorganic filler and PAN nanofibers that increase the bound water within the Nafion® membrane, PAN nanofibers have higher thermal stability at a higher temperature of 130 °C [31].

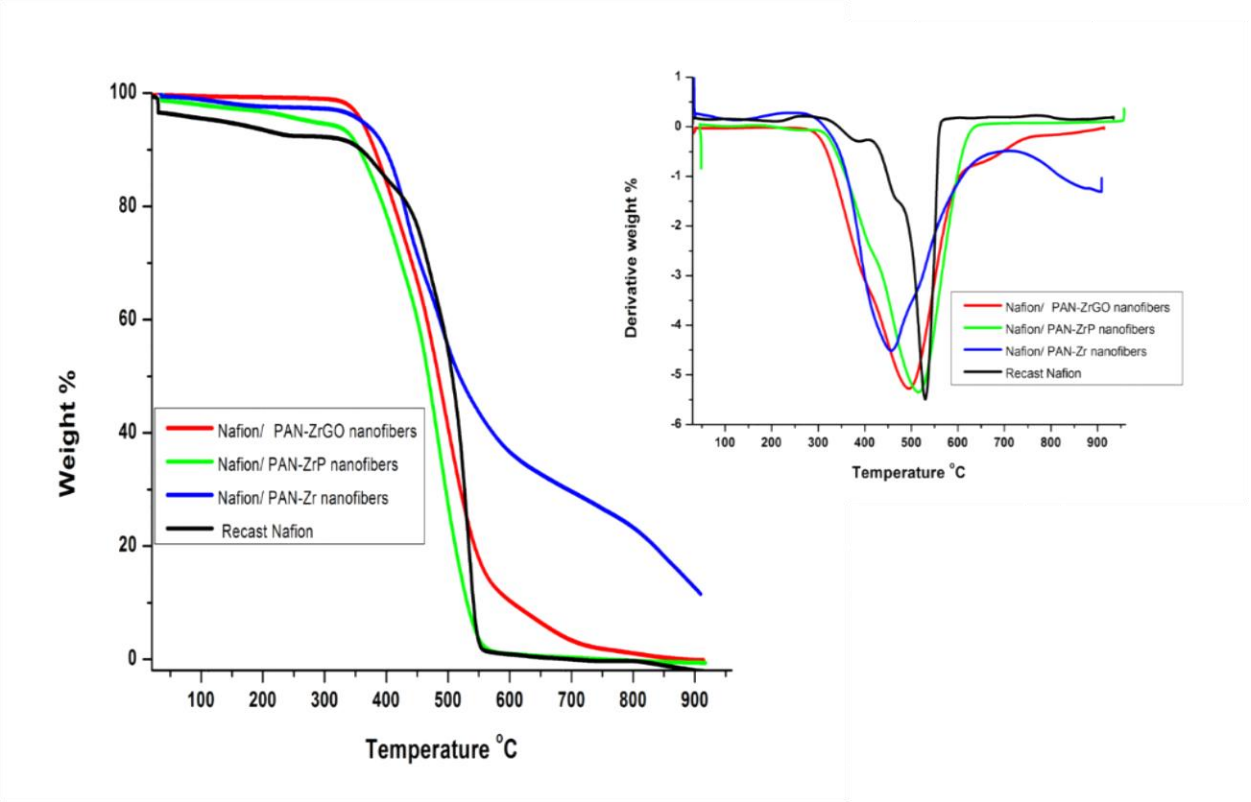

Figure 7- 5: Thermalgravimetric analysis (TGA) and Derivative thermogravimetric of Nafion®-PAN/ZrGO nanofibers, Nafion®-PAN/ZrP nanofibers, Nafion®-PAN/Zr nanofibers nanocomposite membranes and recast Nafion® membrane.

7.3.5. Water uptake (WU), Ion exchange capacity (IEC), swelling ratio (SR) and hydration number (λ) of membranes

The impact of PAN/Zr nanofibers in nanocomposite membrane were observed according to water uptake (WU), ion exchange capacity (IEC), swelling ratio (SR) and hydration number (λ) compared with recast Nafion® membrane. The higher water uptake of the nanocomposite membrane at the higher temperature sustained the proton conductivity of the membrane [33]. The results for the nanocomposite membranes showed that a higher water uptake was obtained for high temperatures than was the case for the recast Nafion® membrane, this is due to the incorporating of metal oxide within the electrospun PAN nanofibers that retain water within the membrane as shown in Figure 7-6(a) and Table 7-1. The results presented in Figure 7-6(a), show that the Nafion®-PAN/Zr nanofiber membrane obtained a higher water-uptake. This may be due to the thorough blending of PAN/Zr nanofibers and their good distribution within the Nafion® matrix, as confirmed by the SEM results. Furthermore, zirconia nanoparticles increase the water retention within the nanocomposite membranes due to their higher porosity which also resulted in an increase of proton conductivity due to the increases of exchange sites available per cluster which is an important parameter of fuel cells in order

to operate at higher temperatures [34-35]. Nafion®-PAN/Zr nanofiber, Nafion®-PAN/ZrGO nanofiber and Nafion®-PAN/ZrP nanofiber membranes obtained a higher water uptake of 49 %, 42 % and 37% at 80 °C when compared to that of recast Nafion® membrane (32 %). This may be due to the incorporation of inorganic materials that retain water within the membrane [36]. This water uptake of recast Nafion® membrane was higher than that obtained by Gosalawit et al. [37]. The higher water uptake on the nanocomposite membrane was due to the hydrophilic nature of the acidic inorganic additives within the pores of the Nafion® membrane and the increased acidity and surface areas of nanoparticles. In addition, the results showed that, for each membrane, the water uptake increases with the temperature. The swelling ratio increases with the increase in temperature in the membrane as presented in Table 7-1 and Figure 7-6(b). The blending of PAN nanocomposite nanofibers obtained a slight increase of the dimensional swelling ratio at higher temperatures due to the incorporation of zirconia nanoparticles, which are good for water retention. In Figure 7-6(c) and Table 7-1 the Nafion®-PAN/Zr nanofiber, Nafion®-PAN/ZrGO nanofiber and Nafion®-PAN/ZrP nanofiber nanocomposite membranes obtained a higher IEC of 1.4 meq/g, 1.2 meq/g and 1.1 meq/g, which is higher than that of recast Nafion® membrane (0.95 meq/g) [38]. This may be due to the incorporation of metal oxide that increase the acidic site within the Nafion® matrix and also increases the sulfonate ions (SO_3H) of the Nafion® membrane [38-39]. Moreover, the incorporation of GO nanosheet was found to enhance the IEC, due to the hydroxyl and carboxyl groups. In conclusion, this nanocomposite membrane obtained a higher water uptake and IEC that enhanced the proton conductivity, thus making them suitable for use in fuel cell performance under hot and dry conditions [40]. Water retention within the membrane promotes the proton transporting within PEMs [41]. As shown in Figure 7-6(d), the hydration number (λ) rise as the temperature increases. The results showed that the hydration number of recast Nafion® membrane was lower than that of nanocomposite membranes, these may due to hydrophobic nature of the membrane. These increases in the levels of bound water may be due to the incorporation of zirconium oxide nanoparticles within the nanofibers. These nanoparticles consist of hydroxyl groups which are responsible for the water adsorption and retention capability [42]. Furthermore, the incorporation of thermally treated PAN reduces the swelling of membranes in water, as the swelling ratio decreases with increase of PAN content in blended membranes [43] and also increases the proton conductivity of blended membranes.

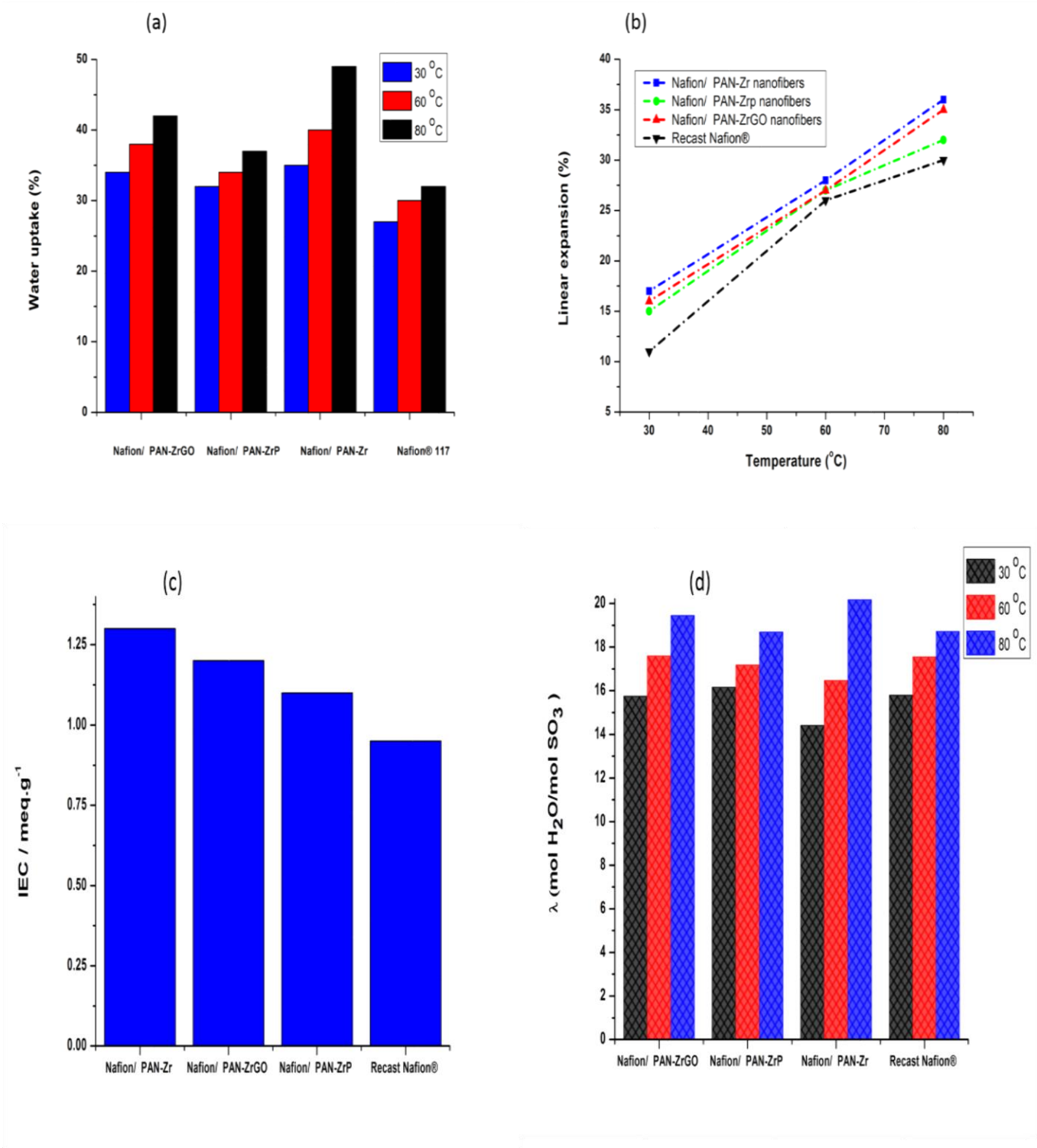

Figure 7- 6: The Water uptake (a), swelling ratio (b), Ion exchange capacity (c) and hydration number (λ) (d) measurements of Nafion®-PAN/Zr nanofibers, Nafion®-PAN/ZrP nanofibers, Nafion®-PAN/ZrGO nanofibers membranes and recast Nafion® membrane.

Table 7- 1: The IEC, swelling ratio and Water uptake of Nafion®-PAN/Zr nanofibers, Nafion®-PAN/ZrP nanofibers, Nafion®-PAN/ZrGO nanofibers membranes and recast Nafion® membrane

Membranes	IEC (meq. g^{-1})	Swelling Ratio			Water Uptake		
		30° C	60° C	80° C	30° C	60° C	80° C
Nafion®/ PAN-Zr nanofibers	1.3	17	23	30	35	40	49
Nafion®/ PAN-ZrP nanofibers	1.1	15	22	30	32	34	37
Nafion®/ PAN-ZrGO nanofibers	1.2	20	25	30	34	38	42
Recast Nafion®	0.95	9	26	29	27	30	32

7.3.6. Methanol permeability and selectivity ratio

The Nafion® membrane was blended with polyacrylonitrile (PAN) nanofibers in order to reduce the methanol permeability, as PAN has reduced methanol crossover in comparison with Nafion® membrane [44]. In order to observe the effects of blended PAN nanofibers within the Nafion® matrix, the methanol permeability at temperature ranges of 30 °C to 80 °C were observed over the sampling time period of two hours. The methanol permeability was measured at 30 °C, 60 °C and 80 °C using 2 M methanol solution showed no permeability of methanol, even at 30 °C, 60 °C using 5 M, there was no methanol crossover within the membranes. The results showed an improved permeability at a low concentration of 2 M methanol, as there was no methanol crossover in any of the membranes [45]. Figure 7-7(a) shows that the methanol permeability of nanocomposite membrane is lower than recast Nafion® membrane, as observed by other research. The methanol permeability of blended Nafion®-PAN membranes was stable for up to 80 minutes longer than that of recast Nafion® membrane. Figure 7-7(a) shows that PAN/Zr nanofiber membrane obtained a lower methanol permeability than recast Nafion®. This may be due to the incorporation of PAN nanofibers that block the methanol crossover through the membrane and the incorporation of metal oxide that can act as a barrier to methanol within Nafion® membrane, as they are well distributed within Nafion® membrane as confirm by SEM images [46]. In addition, the decrease in methanol permeability may due to the very low permeation of water and methanol through PAN polymer or nanofibers [44]. Table 7-2 shows that the methanol permeability of Nafion®-PAN/Zr nanofiber, Nafion®-PAN/ZrP nanofiber and Nafion®-PAN/ZrGO nanofiber membranes are 5.46 x 10^{-8} cm^2/s, 9.58 x 10^{-8} cm^2/s and to 4.37 x 10^{-7} cm^2/s, respectively, which represents an improvement when compared to that of recast Nafion® membrane (9.12 x 10^{-7} cm^2/s). These results make the blended Nafion® with PAN nanofibers suitable for use in DMFC applications.

However, Nafion®-PAN/ZrGO nanofiber membranes show a slightly reduced of methanol permeability when compared to Nafion® membrane, this may be due to the poor distribution of PAN nanofibers and GO within the Nafion® matrix that allows water and methanol to flow across the membrane. The selectivity of Nafion®-PAN/Zr nanofiber, Nafion®-PAN/ZrP nanofiber, Nafion®-PAN/ZrGO nanofiber membranes and recast Nafion® membrane are shown in Figure 7-7(b). Selectivity was obtained by dividing the proton conductivity by the methanol permeability value [30]. The higher selectivity ratio of membranes represents good fuel cell performance [47]. Figure 7-7 and Table 7-2 shows that Nafion®-PAN/Zr nanofiber, Nafion®-PAN/ZrP nanofiber, Nafion®-PAN/ZrGO nanocomposite membrane obtained a higher selectivity ratio of 3.37 x 10^7 Ss $cm^{-3,}$ 2.82 x 10^6 Ss cm^{-3} and 1.05 x 10^6 Ss cm^{-3} respectively, when compared to 2.74 x 10^5 Ss cm^{-3} of recast Nafion® membrane. Furthermore, the Nafion®-PAN/Zr nanofiber nanocomposite membrane shows higher selectivity than that of the recast Nafion® membrane and this may be due to the higher proton conductivity and lower methanol crossover that shows the effects of PAN nanofibers within the membrane as shown in Figure 7-7(b). These increase in the selectivity ratio show the ability of the membranes to be used as electrolyte in DMFCs.

Table 7- 2: The conductivity, Methanol permeability and Selectivity ratio of Nafion®-PAN/Zr nanofibers, Nafion®-PAN/ZrP nanofibers, Nafion®-PAN/ZrGO nanofibers membranes and recast Nafion® membrane

Membrane	**Conductivity (S/cm)**	**Methanol permeability ($cm^2.s^{-1}$)**	**Selectivity ratio (Ss/ $cm^2.s^{-1}$)**
Nafion®/ PAN-Zr nanofibers	1.84	5.46492E-08	3.37E+07
Nafion®/ PAN-ZrP nanofibers	0.27	9.57897E-08	2.82E+06
Nafion®/ PAN-ZrGO nanofibers	0.46	4.37194E-07	1.05E+06
Recast Nafion	0.25	9.11844E-07	2.74E+05

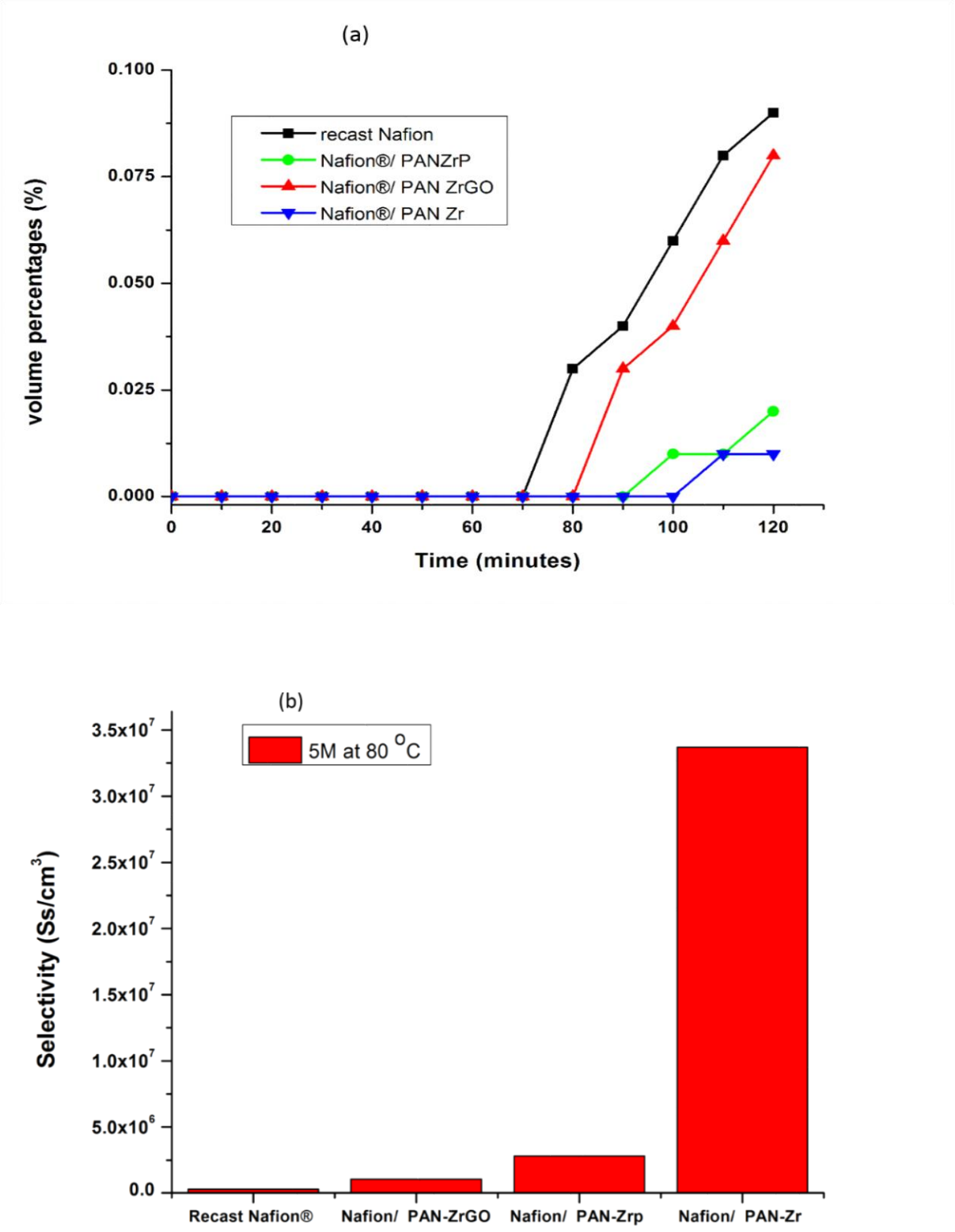

Figure 7- 7: Comparison of the methanol crossover (a) and selectivity (5 M concentration) (b) of the Nafion®-PAN/Zr nanofibers, Nafion®-PAN/ZrP nanofibers, Nafion®-PAN/ZrGO nanofibers membranes and recast Nafion® membrane at 80 °C.

7.3.7. Proton conductivity

The conductivity of nanocomposite membrane compared with that of recast Nafion® membrane is presented in Figure 7-8 and Table 7-2. The proton conductivity of Nafion®-PAN/Zr nanofiber, Nafion®-PAN/ZrP nanofiber, Nafion®-PAN/ZrGO nanofiber nanocomposite membranes and recast Nafion® membrane were 1.84 S/cm, 0.27 S/cm, 0.46 S/cm and 0.25 S/cm, respectively. These results indicated that blending Nafion® membrane with PAN/Zr nanofibers exhibits a higher proton conductivity of 1.84 S/cm compared with recast Nafion® membrane (0.25 S/cm) as shown in Table 7-2. Moreover, Nafion®-PAN/ZrP nanofiber and Nafion®-PAN/ZrGO nanofiber nanocomposite membranes obtained a lower proton conductivity than PAN/Zr nanofiber nanocomposite membrane. These may be due to the addition of phosphoric acid and GO that make a cluster within the membrane due to agglomeration [48], as observed under SEM results. In general, nanocomposite membranes obtained a higher proton conductivity when compared to the recast Nafion® membrane. These increase in proton conductivity may be due to the incorporation of electrospun PAN/Zr within the membrane as ZrO_2 nanoparticles retain water within the membranes [41]. This is also confirmed by the higher water uptake obtained, a factor that creates a proton channel through the membrane [41]. This higher proton conductivity is in agreement with the higher water uptake and IEC obtained above and which make the membranes suitable for use in fuel cell applications. Furthermore, the addition of GO sheets within the membrane increases the proton conductivity, due to the OH and COOH bond that retains a certain amount of bound water [49].

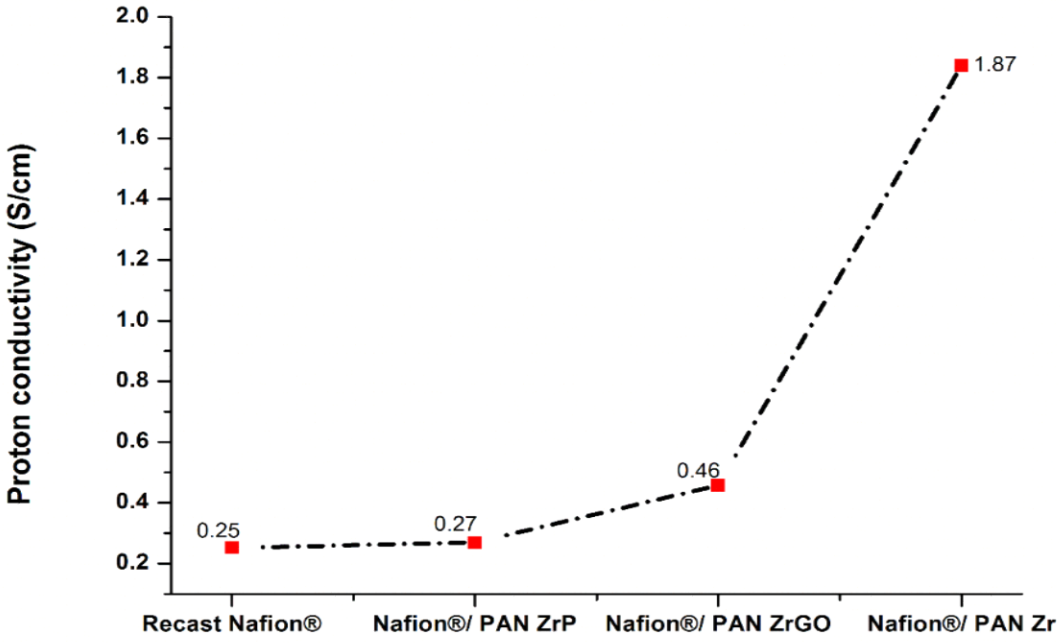

Figure 7- 8: Proton conductivity measurement of Nafion®-PAN/Zr nanofibers, Nafion®-PAN/ZrP nanofibers, Nafion®-PAN/ZrGO nanofibers membranes and recast Nafion® membrane.

7.3.8. Fuel cell performances

Figure 7-9 shows the power density and cell voltage curves of DMFCs using 2 M methanol/ 2 M KOH as a fuel. The Nafion®-PAN/Zr nanofiber, Nafion®-PAN/ZrGO nanofiber and Nafion®-PAN/ZrP nanofiber membranes in Figure 7-9(a) show a high-power density performance of 68.7 mW cm^{-2} at current density of 250 mA cm^{-2}, 75.9 mW cm^{-2} at current density of 250 mA cm^{-2} and 43.9 mW cm^{-2} current density of 200 mA cm^{-2}, compared to the 18.0 mW cm^{-2} of pristine Nafion® membrane obtained by Yuan et al. All obtained results show an improvement in cell performance at high current densities and at room temperature. However, the introduction of phosphoric acid slightly lowers the power density performance at lower temperature. Figure 7-9(b) shows that the cell voltage results of nanocomposite membranes (0.66, 0.69 and 0.61 V) were slightly higher than that of Nafion® 212 membrane (0.6 V) at the same operating temperature [50]. However, Nafion®-PAN/ZrGO nanofiber membranes obtained the highest cell voltage and this may be due to the incorporation of GO that enhances the water content within the membrane, which promotes mass transport and thus improves the fuel cell performance. Furthermore, the higher fuel cell performance could be due to the presence of hydroxyl, carboxylic, and epoxy groups in the hydrophilic region of GO that

enhance proton conductivity as the proton conductivity of the electrolyte plays a big role in fuel cell performance [51]. The Nafion®-PAN/Zr nanofiber membrane obtained the highest power density performance of 47.6 mW cm^{-2} at current density of 350 mA cm^{-2} when compared with Nafion®-PAN/ZrGO nanofiber and Nafion®-PAN/ZrP nanofiber membranes which, starting at a 300 mA cm^{-2} current density, saw their power density reduced to 32.1 mW cm^{-2} and 17.3 mW cm^{-2}. When Nafion® membrane was incorporated with composited PAN nanofibers, fuel cell performance improved when compared with the results when employing recast Nafion® membrane. This may be due to the nanofibers reducing the methanol crossover at higher concentrations of 5M methanol. Moreover, the incorporation of a graphene oxide on the composited membrane increases fuel cell efficiencies at a higher current density of 250 mA cm^{-2}, which shows more improvement than pristine Nafion® membrane. However, it can be seen that Nafion®-PAN/ZrGO nanofiber membranes successfully block the methanol crossover up to 250 mA cm^{-2}, with a sharp decrease in fuel cell efficiency at a high current density of 250 mA cm^{-2}. It is expected that the performance of a DMFC could be improved by using a lower concentration of GO to reduce agglomeration within the membranes.

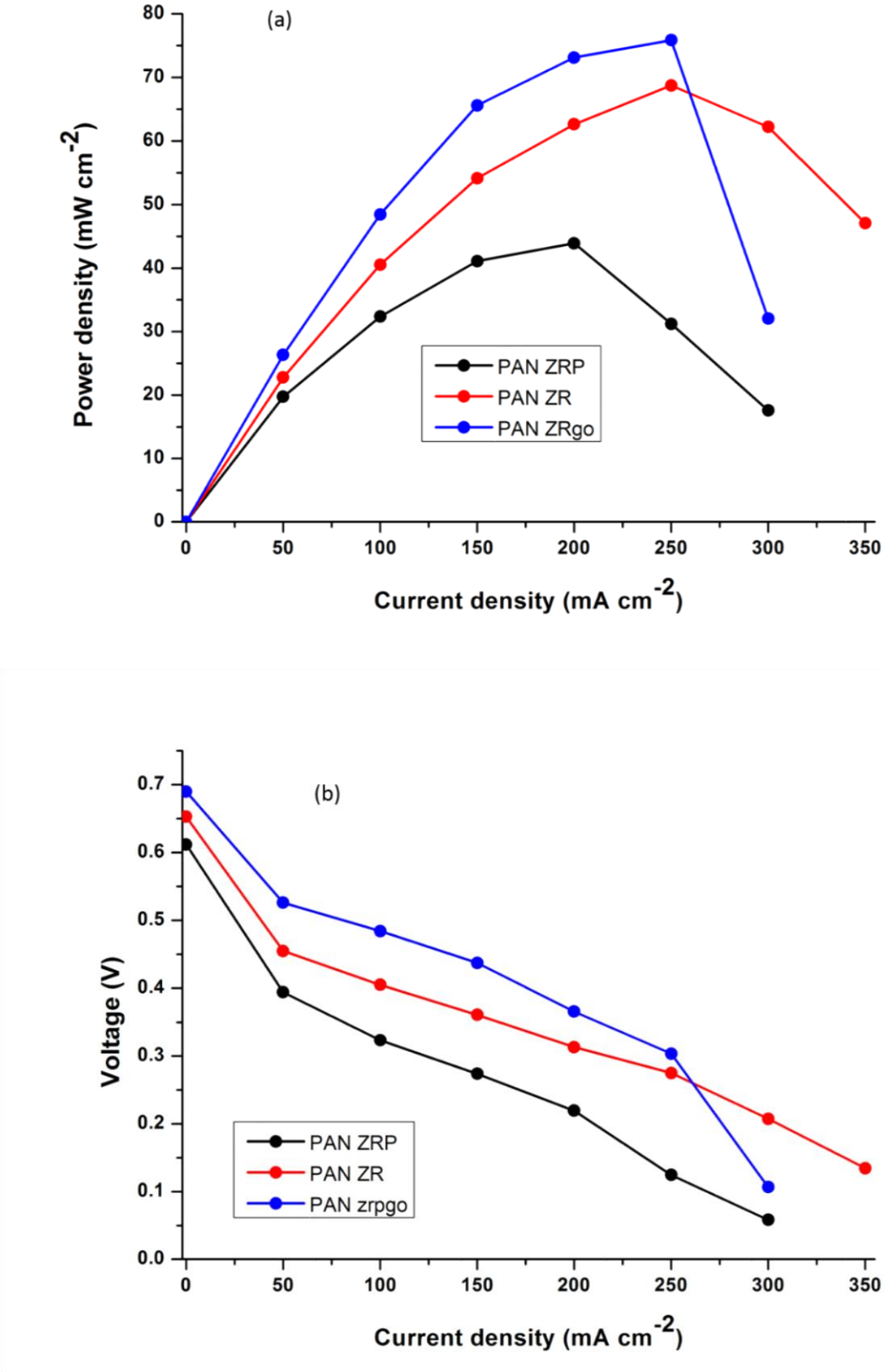

Figure 7- 9: DMFC polarization of Nafion®-PAN/ZrP, Nafion®-PAN/Zr nanofibers and Nafion®-PAN/ZrGO nanofibers membranes obtained in passive environment at room temperature.

7.4. Conclusion

The PAN/Zr nanofibers electrospan at 15kV and distance of 10 cm were well arranged next to each other and with diameters ranging between 300 and 500 nm, without any zirconia nanoparticles observed within the nanofibers. The PAN/Zr nanofibers were successfully blended with Nafion® membrane using the recast method. The results of nanocomposite membranes obtained a higher water uptake than that of the recast Nafion® membrane, due to the incorporating of metal oxide within the electrospan PAN nanofibers that retain water within the membrane. The results showed Nafion®-PAN/Zr nanofiber, Nafion®-PAN/ZrGO nanofiber and Nafion®-PAN/ZrP nanofiber membranes as obtaining a higher water uptake of 49 %, 42 % and 37% at 80 °C when comparing to the uptake of recast Nafion® membrane (32 %). The results also confirm that the blending of PAN/Zr nanofibers obtained a stable dimensional swelling ratio, due to the incorporation of zirconia nanoparticles, which is good for water retention. Moreover, this dimensional swelling ratio of membranes increases along with increases in temperature. Furthermore, the results show that the nanocomposite membranes obtain a higher λ bound water than recast Nafion® membrane – possibly due to the incorporation of zirconium oxide nanoparticles within the nanofibers, which consists of hydroxyl groups which are responsible for the water adsorption and retention capability. In addition, the Nafion®-PAN/Zr nanofiber, Nafion®-PAN/ZrGO nanofiber and Nafion®-PAN/ZrP nanofiber nanocomposite membranes show a higher IEC of 1.4 meq/g, 1.2 meq/g and 1.1 meq/g, compared to 0.95 meq/g of recast Nafion® membrane. These nanocomposite membranes also exhibited a higher proton conductivity and lower methanol crossover of 1.84 S/cm and 5.46 x 10^{-8} cm^2/s respectively. The fuel cell efficiency of nanocomposite membranes showed additional improvement when operated on 2M of MEOH and KOH concentrations. In summary, the incorporation of Nafion® membrane by PAN/Zr shows an enhancement in water uptake, lowers methanol crossover, increases proton conductivity and provides higher fuel cell efficiencies. The Nafion®-PAN/ZrGO nanofiber membrane caused a sharp decrease in fuel cell efficiency at a high current density of 250 mA cm^{-2}, but this was much better than that of recast Nafion® membrane. It can be concluded that the incorporation of PAN/Zr in the form of nanofibers improves their dispersity within the membranes and that this gives them the potential to improve the DMFCs performance at a higher concentration of 2M.

7.5. References

1. Melaina, M.; Webster, K., Role of fuel carbon intensity in achieving 2050 greenhouse gas reduction goals within the light-duty vehicle sector. ACS Publications: 2011.
2. Debe, M. K., Electrocatalyst approaches and challenges for automotive fuel cells. *Nature* **2012,** *486* (7401), 43.

3. Zheng, J.; Bi, W.; Dong, X.; Zhu, J.; Mao, H.; Li, S.; Zhang, S., High performance tetra-sulfonated poly (p-phenylene-co-aryl ether ketone) membranes with microblock moieties for passive direct methanol fuel cells. *Journal of Membrane Science* **2016,** *517*, 47-56.
4. Neburchilov, V.; Martin, J.; Wang, H.; Zhang, J., A review of polymer electrolyte membranes for direct methanol fuel cells. *Journal of Power Sources* **2007,** *169* (2), 221-238.
5. Rajeswari, N.; Selvasekarapandian, S.; Karthikeyan, S.; Prabu, M.; Hirankumar, G.; Nithya, H.; Sanjeeviraja, C., Conductivity and dielectric properties of polyvinyl alcohol–polyvinylpyrrolidone poly blend film using non-aqueous medium. *Journal of Non-Crystalline Solids* **2011,** *357* (22-23), 3751-3756.
6. Zhang, H.; Shen, P. K., A brief consideration about the structural evolution of perfluorosulfonic-acid ionomer membranes. *International Journal of Hydrogen Energy* **2012,** *37* (5), 4657-4664.
7. Subramania, A.; Sundaram, N. K.; Kumar, G. V.; Vasudevan, T., New polymer electrolyte based on (PVA–PAN) blend for Li-ion battery applications. *Ionics* **2006,** *12* (2), 175-178.
8. Gopalan, A. I.; Santhosh, P.; Manesh, K. M.; Nho, J. H.; Kim, S. H.; Hwang, C.-G.; Lee, K.-P., Development of electrospun PVdF–PAN membrane-based polymer electrolytes for lithium batteries. *Journal of Membrane Science* **2008,** *325* (2), 683-690.
9. Nie, G.; Li, Z.; Lu, X.; Lei, J.; Zhang, C.; Wang, C., Fabrication of polyacrylonitrile/CuS composite nanofibers and their recycled application in catalysis for dye degradation. *Applied Surface Science* **2013,** *284*, 595-600.
10. Sahay, R.; Kumar, P. S.; Sridhar, R.; Sundaramurthy, J.; Venugopal, J.; Mhaisalkar, S. G.; Ramakrishna, S., Electrospun composite nanofibers and their multifaceted applications. *Journal of Materials Chemistry* **2012,** *22* (26), 12953-12971.
11. Kim, C.; Choi, Y.-O.; Lee, W.-J.; Yang, K.-S., Supercapacitor performances of activated carbon fiber webs prepared by electrospinning of PMDA-ODA poly (amic acid) solutions. *Electrochimica Acta* **2004,** *50* (2-3), 883-887.
12. Nataraj, S.; Yang, K.; Aminabhavi, T., Polyacrylonitrile-based nanofibers—A state-of-the-art review. *Progress in Polymer Science* **2012,** *37* (3), 487-513.
13. Sacca, A.; Gatto, I.; Carbone, A.; Pedicini, R.; Passalacqua, E., ZrO 2–Nafion composite membranes for polymer electrolyte fuel cells (PEFCs) at intermediate temperature. *Journal of Power Sources* **2006,** *163* (1), 47-51.
14. Zhang, H.; Shen, P. K., Recent development of polymer electrolyte membranes for fuel cells. *Chemical Reviews* **2012,** *112* (5), 2780-2832.
15. Lu, J.; Zang, J.; Wang, Y.; Xu, Y.; Xu, X., Preparation and characterization of Zirconia-coated nanodiamonds as a Pt catalyst support for methanol electro-oxidation. *Nanomaterials* **2016,** *6* (12), 234.

16. Mohammadi, G.; Jahanshahi, M.; Rahimpour, A., Fabrication and evaluation of Nafion nanocomposite membrane based on ZrO_2–TiO_2 binary nanoparticles as fuel cell MEA. *International Journal of Hydrogen Energy* **2013,** *38* (22), 9387-9394.
17. Hu, S.; Lozada-Hidalgo, M.; Wang, F.; Mishchenko, A.; Schedin, F.; Nair, R.; Hill, E.; Boukhvalov, D.; Katsnelson, M.; Dryfe, R., Proton transport through one-atom-thick crystals. *Nature* **2014,** *516* (7530), 227.
18. Pilehrood, M. K.; Heikkilä, P.; Harlin, A., Preparation of carbon nanotube embedded in polyacrylonitrile (pan) nanofibre composites by electrospinning process. *AUTEX Research Journal* **2012,** *12* (1), 1-6.
19. Yang, A. C.; Narimani, R.; Zhang, Z.; Frisken, B. J.; Holdcroft, S., Controlling crystallinity in graft ionomers, and its effect on morphology, water sorption, and proton conductivity of graft ionomer membranes. *Chemistry of Materials* **2013,** *25* (9), 1935-1946.
20. Wu, L.; Zhou, G.; Liu, X.; Zhang, Z.; Li, C.; Xu, T., Environmentally friendly synthesis of alkaline anion exchange membrane for fuel cells via a solvent-free strategy. *Journal of Membrane Science* **2011,** *371* (1), 155-162.
21. Chien, H.-C.; Tsai, L.-D.; Huang, C.-P.; Kang, C.-y.; Lin, J.-N.; Chang, F.-C., Sulfonated graphene oxide/Nafion composite membranes for high-performance direct methanol fuel cells. *International Journal of Hydrogen Energy* **2013,** *38* (31), 13792-13801.
22. Harmer, M. A.; Farneth, W. E.; Sun, Q., High surface area nafion resin/silica nanocomposites: a new class of solid acid catalyst. *Journal of the American Chemical Society* **1996,** *118* (33), 7708-7715.
23. Hao, Y.; Li, J.; Yang, X.; Wang, X.; Lu, L., Preparation of ZrO_2–Al_2O_3 composite membranes by sol–gel process and their characterization. *Materials Science and Engineering: A* **2004,** *367* (1-2), 243-247.
24. Starkweather Jr, H. W., Crystallinity in perfluorosulfonic acid ionomers and related polymers. *Macromolecules* **1982,** *15* (2), 320-323.
25. Mathur, R.; Bahl, O.; Mittal, J.; Nagpal, K., Structure of thermally stabilized PAN fibers. *Carbon* **1991,** *29* (7), 1059-1061.
26. Gu, H.; Huang, Y.; Zuo, L.; Fan, W.; Liu, T., Graphene sheets wrapped carbon nanofibers as a highly conductive three-dimensional framework for perpendicularly anchoring of MoS2: Advanced electrocatalysts for hydrogen evolution reaction. *Electrochimica Acta* **2016,** *219*, 604-613.
27. Kyu, T.; Hashiyama, M.; Eisenberg, A., Dynamic mechanical studies of partially ionized and neutralized Nafion polymers. *Canadian Journal of Chemistry* **1983,** *61* (4), 680-687.
28. Xiao, S.; Lv, H.; Tong, Y.; Xu, L.; Chen, B., Thermal behavior and kinetics during the stabilization of polyacrylonitrile precursor in inert gas. *Journal of Applied Polymer Science* **2011,** *122* (1), 480-488.

29. Chen, J.; Asano, M.; Yamaki, T.; Yoshida, M., Preparation and characterization of chemically stable polymer electrolyte membranes by radiation-induced graft copolymerization of four monomers into ETFE films. *Journal of Membrane Science* **2006,** *269* (1-2), 194-204.
30. Chen, J.; Guo, Q.; Li, D.; Tong, J.; Li, X., Properties improvement of SPEEK based proton exchange membranes by doping of ionic liquids and Y_2O_3. *Progress in Natural Science: Materials International* **2012,** *22* (1), 26-30.
31. Lim, J. W.; Lee, J.-M.; Yun, S.-M.; Park, B.-J.; Lee, Y.-S., Hydrophilic modification of polyacrylonitrile membranes by oxyfluorination. *Journal of Industrial and Engineering Chemistry* **2009,** *15* (6), 876-882.
32. Smitha, B.; Devi, D. A.; Sridhar, S., Proton-conducting composite membranes of chitosan and sulfonated polysulfone for fuel cell application. *International Journal of Hydrogen Energy* **2008,** *33* (15), 4138-4146.
33. Yuan, J.; Zhou, G.; Pu, H., Preparation and properties of Nafion®/hollow silica spheres composite membranes. *Journal of Membrane Science* **2008,** *325* (2), 742-748.
34. Zawodzinski, T. A.; Derouin, C.; Radzinski, S.; Sherman, R. J.; Smith, V. T.; Springer, T. E.; Gottesfeld, S., Water uptake by and transport through Nafion® 117 membranes. *Journal of the Electrochemical Society* **1993,** *140* (4), 1041-1047.
35. Paturzo, L.; Basile, A.; Iulianelli, A.; Jansen, J. C.; Gatto, I.; Passalacqua, E., High temperature proton exchange membrane fuel cell using a sulfonated membrane obtained via H_2SO_4 treatment of PEEK-WC. *Catalysis Today* **2005,** *104* (2-4), 213-218.
36. Gosalawit, R.; Chirachanchai, S.; Manuspiya, H.; Traversa, E., Krytox-Silica–Nafion® composite membrane: A hybrid system for maintaining proton conductivity in a wide range of operating temperatures. *Catalysis Today* **2006,** *118* (1-2), 259-265.
37. Gosalawit, R.; Chirachanchai, S.; Shishatskiy, S.; Nunes, S. P., Krytox–montmorillonite–Nafion® nanocomposite membrane for effective methanol crossover reduction in DMFCs. *Solid State Ionics* **2007,** *178* (29-30), 1627-1635.
38. Chen, T.-Y.; Leddy, J., Ion exchange capacity of Nafion and Nafion composites. *Langmuir* **2000,** *16* (6), 2866-2871.
39. Arico, A.; Baglio, V.; Di Blasi, A.; Creti, P.; Antonucci, P.; Antonucci, V., Influence of the acid–base characteristics of inorganic fillers on the high temperature performance of composite membranes in direct methanol fuel cells. *Solid State Ionics* **2003,** *161* (3-4), 251-265.
40. Jalani, N. H.; Dunn, K.; Datta, R., Synthesis and characterization of Nafion®-MO_2 (M= Zr, Si, Ti) nanocomposite membranes for higher temperature PEM fuel cells. *Electrochimica Acta* **2005,** *51* (3), 553-560.

41. Li, K.; Ye, G.; Pan, J.; Zhang, H.; Pan, M., Self-assembled Nafion®/metal oxide nanoparticles hybrid proton exchange membranes. *Journal of Membrane Science* **2010,** *347* (1-2), 26-31.
42. Baglio, V.; Di Blasi, A.; Antonucci, V., FTIR spectroscopic investigation of inorganic fillers [pfor composite DMFC membranes. *Electrochemistry Communications* **2003,** *5* (10), 862-866.
43. Wang, J.; Yue, Z.; Economy, J., Preparation of proton-conducting composite membranes from sulfonated poly (ether ether ketone) and polyacrylonitrile. *Journal of membrane science* **2007,** *291* (1), 210-219.
44. Carter, R.; Wycisk, R.; Yoo, H.; Pintauro, P., Blended polyphosphazene/polyacrylonitrile membranes for direct methanol fuel cells. *Electrochemical and solid-state Letters* **2002,** *5* (9), A195-A197.
45. Hudiono, Y.; Choi, S.; Shu, S.; Koros, W. J.; Tsapatsis, M.; Nair, S., Porous layered oxide/Nafion® nanocomposite membranes for direct methanol fuel cell applications. *Microporous and Mesoporous Materials* **2009,** *118* (1-3), 427-434.
46. Dutta, K.; Das, S.; Kundu, P. P., Partially sulfonated polyaniline induced high ion-exchange capacity and selectivity of Nafion membrane for application in direct methanol fuel cells. *Journal of Membrane Science* **2015,** *473*, 94-101.
47. Sung, K. A.; Oh, K.-H.; Kim, W.-K.; Choo, M.-J.; Nam, K.-W.; Park, J.-K., Proton exchange membrane using imidazole-functionalized silica to enhance proton conductivity at lower humidity. *Electrochemical and Solid-State Letters* **2011,** *14* (10), B114-B116.
48. Devrim, Y.; Devrim, H., PEM fuel cell short stack performances of silica doped nanocomposite membranes. *International Journal of Hydrogen Energy* **2015,** *40* (24), 7870-7878.
49. Nicotera, I.; Simari, C.; Coppola, L.; Zygouri, P.; Gournis, D.; Brutti, S.; Minuto, F. D.; Aricò, A.; Sebastian, D.; Baglio, V., Sulfonated graphene oxide platelets in Nafion nanocomposite membrane: advantages for application in direct methanol fuel cells. *The Journal of Physical Chemistry C* **2014,** *118* (42), 24357-24368.
50. Cai, Z.; Li, L.; Su, L.; Zhang, Y., Supercritical carbon dioxide treated Nafion 212 commercial membranes for direct methanol fuel cells. *Electrochemistry Communications* **2012,** *14* (1), 9-12.
51. Cao, Y.-C.; Xu, C.; Wu, X.; Wang, X.; Xing, L.; Scott, K., A poly (ethylene oxide)/graphene oxide electrolyte membrane for low temperature polymer fuel cells. *Journal of Power Sources* **2011,** *196* (20), 8377-8382.

CHAPTER EIGHT

8. Conclusion and recommendations

8.1. Conclusion

The purpose of this research was to modify the state of art Nafion® membrane in order to enhance their proton conductivity and reduces their methanol permeability at lower humidity by reducing the diameter of the pores and ensures their hydration. The inorganic materials were added to organic proton conduction membranes in order to develop a new characteristic of the Nafion membrane. Furthermore, zirconia nanoparticles were impregnated with sulfuric acid and phosphoric acid to enhance the acid site of nanocomposite membrane. The composited membranes were prepared using recast and impregnation method. The structure and morphologies, water retention, thermal and mechanical properties, methanol permeability, proton conductivity and fuel cell efficiency of the modified membrane were studied.

A simple precipitate method was used to synthesis a high surface area of zirconium oxide with a high temperature phase (cubic), stabilised at a low calcination temperature of 600 °C. The modified membranes obtained by recast method shows decrease in water contact angle when compared to the recast Nafion® membrane. Furthermore, the water uptake of modified membrane was higher than that of recast Nafion® membrane, this may be due to the incorporation of the inorganic nanofiller that adsorb water. XRD, AFM and SEM results show that using zirconia nanoparticles as inorganic filler improves the morphology and crystallinity of Nafion® membrane, as it was well dispersed within Nafion matrix that makes them suitable candidates for fuel cell applications. The incorporation of zirconia nanoparticles also shows the effect on hydrophilicity roughness of the membrane. Nanocomposite membrane prepared by impregnation methods shows a higher proton conductivity, decreased in water contact angle and methanol crossover, which are more improved when compared to the commercial Nafion® 117 membrane. This may be due to the addition of higher porosity zirconia nanoparticles in Nafion® membrane that decrease the water contact angle within the nanocomposite membranes, which resulted also in increasing the proton conductivity due to the increase of exchange sites available per cluster, which is an important parameter of fuel cells in order to operate at higher temperature. The TGA and DTG results of the modified Nafion® membrane show that incorporation of zirconia nanoparticles obtained a thermal stabilised degradation even at high temperature, due to the water retained within the Nafion® membrane, which leads to fuel cell application at higher temperature. This observation shows

the possibilities of modified Nafion® membrane to operate at high temperature and reduced relative humidity. This indicates that the improvement of the membrane rigidity demonstrates that the zirconia nanoparticles stabilized the structure of the nanocomposite membrane and give a potential restriction to the humidity-generated stress when the membrane is used as an electrolyte membrane in the fuel cells.

The incorporation of sulfated zirconia oxide within Nafion® membrane improves the proton conductivity, IEC and membrane swelling, while it prevents the methanol from crossing over. The water uptake was more improved at a higher temperature of 80 °C in nanocomposite membranes. Nafion®/ S-ZrO_2 (NH_3SO_4) nanocomposite membrane shows low fuel crossover at 80 °C and a higher methanol concentration of 5 M. The membrane resistance of Nafion®/S-ZrO_2 (NH_3SO_4) nanocomposite membrane was lower than that of Nafion® 117 membrane and Nafion®/S-ZrO_2 nanocomposite membrane. This confirms that the lower the resistance, the higher the conductivity. The conclusion is that the sulfated zirconia with NH_3SO_4 acid is suitable as an inorganic filler of Nafion® membrane, due to its higher acidic value which allows the ions movement without reducing the hydration of the membrane but while reducing the methanol crossover.

The preparation of the Nafion/ ZrP nanocomposite membrane with low methanol permeability and good proton conductivity was successfully achieved by the impregnation method. Moreover, the IEC, Linear expansion and water uptake of modified Nafion® membrane was higher than Nafion® 117 membrane at higher temperature of 80 °C. The results show the decrease of methanol permeability of modified Nafion® membrane at higher temperature of 80 °C and 5 M methanol concentration compared to Nafion® 117 membrane. The higher temperature conductivity on the nanocomposite membranes obtains an enhanced proton conductivity than commercial Nafion® membrane, due to the addition of inorganic materials within the membranes. The lower methanol permeation and high proton conductivity resistance of modified membrane also confirm their suitability for use in fuel cell.

The electrospan nanofibers were successfully blended with Nafion® membrane using the recast method. The results of nanocomposite membranes obtained a higher water uptake and IEC than that of the recast Nafion® membrane, due to the incorporating of metal oxide within the electrospan PAN nanofibers that retain water within the membrane. These nanocomposite membranes also exhibited a higher proton conductivity and lower methanol crossover. The fuel cell efficiency of nanocomposite membranes showed additional improvement when operated on 2M of MEOH and KOH concentrations. In summary, the incorporation of Nafion® membrane by PAN/Zr shows an enhancement in water uptake, lowers methanol crossover, increases proton conductivity and provides higher fuel cell efficiencies. The Nafion®-PAN/ZrGO nanofiber membrane caused a sharp decrease in fuel cell efficiency at a high current density, but this was much better than that of recast Nafion® membrane. It can be

concluded that the incorporation of PAN/Zr in the form of nanofibers improves their dispersity within the membranes and that this gives them the potential to improve the DMFCs performance at a higher concentration of 2M.

8.2. Recommendations for future work

- Investigate the effect of the incorporated sulfated zirconia oxide within Nafion® membrane on the high temperature proton conductivity and DMFCs performance.
- To study the fuel cell efficiency of Nafion®/ ZrP nanocomposite membranes at higher temperature and higher concentrations (4M of MEOH and KOH).
- To determine the minimum addition of GO within the membrane, to reduce agglomeration.
- To electrospin GO with PAN nanofibers, to improves their dispersity within the membranes and increases the power density of DMFC above 300 mW/cm^2 at temperature of 80 °C.
- To study the effect of PAN carbon nanofibers in the methanol crossover, proton conductivity and DMFC efficiency.
- To investigate the effect of electrospan phosphated PAN/Zr nanofibers in proton conductivity, methanol permeation and DMFCs performance.
- Study the effect of composited membranes in the life cycle and polymer degradation.